MID MIOCENE ORBITAL CLIMATE VARIABILITY AND BIOTIC RESPONSE IN THE PACIFIC OCEAN

by

Lyndsey Rowena Fox

Submitted in accordance with the requirements for the degree of Doctor of Philosophy

The University of Leeds
School of Earth and Environment

September 2014

For my parents

"I don't pretend we have all the answers.

But the questions are certainly worth thinking about…"

- Arthur C. Clarke

DECLARATION

The candidate confirms that the work submitted is her own, except where work which has formed part of jointly authored publications has been included. The contribution of the candidate and the other authors to this work has been explicitly indicated below.

Chapter 3 includes research and figures published in:

Fox, L.R., Wade, B.S., 2013. Systematic Taxonomy of early–middle Miocene planktonic foraminifera from the equatorial Pacific Ocean: Integrated Ocean Drilling Program, Site U1338. The Journal of Foraminiferal Research 43, 374-405.

All research and figures from this publication are solely the work of the candidate, second author B. S. Wade provided editorial comments.

The candidate confirms that appropriate credit has been given within the thesis where reference has been made to the work of others.

ACKNOWLEDGEMENTS

There are a number of people who have had a substantial impact on both me and my work during the course of my PhD whom I would like to thank...

First of all, my amazing primary supervisor Professor Bridget Wade, who has always been incredibly enthusiastic and encouraging in all aspects of my PhD. I feel truly privileged to have been Bridget's student and could not imagine a better supervisor and mentor during her time at Leeds.

I am indebted to Ann Holbourn and Wolfgang Kuhnt for trusting me with such vast amounts of irreplaceable IODP material. They were excellent and generous hosts during my visits to Kiel, and an abundant source of knowledge. Their boundless enthusiasm for a huge range of topics was inspiring. Thanks also to Marcus Regenberg at Kiel for patiently teaching me the ropes in the Mg/Ca lab, and measuring out the hydrazine for me...

Heartfelt thanks to my secondary supervisor Alan Haywood, for taking me under his wing during the crucial final months of write up, and also to Graeme Swindles who was extremely generous with his time, and spent many hours discussing the intricacies of wavelet analysis and MatLab with me. I thank Richard Walshaw at the University of Leeds for assistance with the Scanning Electron Microscope, and Hilary Sloane at the British Geological Survey for her patient assistance with hundreds upon hundreds of stable isotope analyses.

I also feel it necessary to thank the following artists for providing the soundtrack to the past 4 years: Abba, The XX, Arcade Fire, The National, St. Vincent, Beirut, Stars, The Flaming Lips, Elbow, Radiohead, and above all; the genius that is Kate Bush.

In no particular order, special thanks to the Geobabes (Becky O'Salvage, Katie Farrell, Laura Gregory, Jo Hamlyn, Hollie Romain and Sarah Southern), Jen Stuart, David Collings, Andy Merritt, Thomas Swinscoe, Graham McLeod, and Tom Fletcher for making my time in Leeds so memorable. Also to Alison Balcombe for always only being a phone call away, and providing me with some much needed perspective. It wouldn't have been the same without you guys. A very special thank you to my own personal hero: James Witts, for being the voice of reason and for always being ready with a cup of tea. The words on page 232 are dedicated to you all.

Acknowledgements

My Nan and Gramps also deserve a special mention for helping to keep my car running these past 4 years and for all the times they have fed me.

Lastly, I would like to give an immeasurable thank you to three people, without whom I simply would not have been able to complete my thesis. Firstly, Sandra Karl…

Ich bin Dir so unendlich dankbar für all Deine Unterstützung und den Glauben an mich in all den Momenten, in denen ich an mir gezweifelt habe. Vielen Dank, dass Du immer für mich da warst und immer ein offenes Ohr für mich mit all meinen Problemchen und Glücksmomenten hattest. Du bist völlig verrückt, aber ich liebe Dich!

...and finally: Mummy and Daddy, thank you for *absolutely everything* over the past 27 years. You are the most amazing and wonderful parents*, and really, this thesis belongs to you.

*I promise to put you both in a nice care home.

ABSTRACT

During the Miocene, the Earth's climate transitioned from an extended phase of global warmth (Miocene climatic optimum) into a colder mode with the establishment of a permanent and stable East Antarctic Ice Sheet (EAIS). The mechanisms which drove this extreme climate shift are still poorly understood, because continuous, well-dated Miocene sedimentary archives are still scarce. Reliable sea surface temperature estimates are crucial to any reconstruction and modelling of past ocean salinity and density, water column stratification, thermohaline circulation, and ice volume. Despite extensive studies of benthic foraminifera, existing planktonic foraminiferal records for this interval are extremely scarce and of low resolution. Consequently, the impact of global warming and cooling on tropical surface waters and the propagation of orbital cycles in the Earth System are unknown.

The overarching aim of this thesis is to investigate the nature and variability of early-middle Miocene climate and the relationship to orbital variations in solar insolation, in order to better understand the extent and magnitude of the global middle Miocene Climate Transition (MMCT) and the subsequent cooling/EAIS events. Furthermore, this study aims to investigate changes in the thermal structure of the Pacific Ocean during the development of MMCT to examine Pacific Ocean circulation across the middle Miocene climatic events.

This is achieved through high resolution planktonic foraminiferal stable isotope analysis, spectral analysis and wavelet transform analysis. The first ever high-resolution (3 kyr) astronomically-tuned record of $\delta^{18}O$ and $\delta^{13}C$ from planktonic foraminifera for the eastern equatorial Pacific Ocean (15.56–13.35 Myr) is presented here. These data provide vital new information on sea surface temperatures and primary productivity changes at the tropics during the middle Miocene, at a resolution not achieved in any previous study, which sheds new light on the extent and magnitude of the MMCT and associated carbon-isotope excursion. In order to assess the reliability of these new records this thesis also goes on to document the taxonomy and palaeobiology of Miocene tropical planktonic foraminifera and their response to times of climatic stress. Finally the data from Site U1338 is compared to Site 1146 in the western equatorial Pacific Ocean, to reconstruct bottom and surface water conditions and changes in ocean dynamics across the equatorial Pacific during this highly complex interval of climate history.

CONTENTS PAGE

LIST OF TABLES PAGE

LIST OF FIGURES PAGE

LIST OF PLATES

34X-2, 78–80cm, 5 *Globigerinoides trilobus*, U1338A-42X-CC. *6 Globigerinoides diminitus*, U1338B-41H-4, 30–32cm.

PLATE 11, Figure 1 *Globigerinoides* aff. *G. grilli*, U1338B-42H-2, 40–42cm. 2 *Globorotaloides* cf. *G. hexagonus*, U1338B-41H-3, 30–32cm. 3 *Globoturborotalita* sp., U1338A-40X-2, 78–80cm. 4 *''Dentoglobigerina'' venezuelana*, U1338B-41H-4, 30–32cm.

PLATE 12, Figure 1. *Paragoborotalia continuosa*, U1338B-41H-4, 30–32cm. 2 *Tenuitella munda* U1338B-38H-5, 20–22cm. 3–6 *Globorotaloides* sp., U1338B-38H-4, 0–2 cm.

PLATE 13, Figures 1–5. *Paragloborotalia siakensis*, U1338C-37H-4, 130–132cm. 6 *Fohsella peripheroronda*, U1338A-38X-CC.

PLATE 14, Figures 1, 2, 4–6 *Globorotalia praemenardii*, U1338C-35H-5, 90–92cm. 3 *Fohsella peripheroacuta* U1338B-36H-2, 30–32cm.

PLATE 15, Figures. 1–5 *Praeorbulina circularis*, U1338B-42H-2, 40–42 cm. 6–8 *Sphaeroidinellopsis disjuncta*, U1338C-35H-5, 90–92 cm.

PLATE 16. *Globorotalia praemenardii*, U1338B-36H-2, 30–32 cm; test broken to reveal wall structure.

PLATE 17. *Sphaeroidinellopsis disjuncta*, U1338C-35H-5, 90–92 cm; test broken to reveal internal wall structure.

PLATE 18. *Globigerinoides subquadratus*, U1338B-42H-2, 40–42 cm; test broken to reveal wall structure.

PLATE 19. *Paragloborotalia siakensis*, U1338C-37H-4, 130–132 cm; test broken to reveal internal wall structure.

PLATE 20, Planktonic foraminifera from the Cipero Formation, Trinidad. 1 *Catapsydrax dissimilis*, 2 Catapsydrax sp., 3 *Dentoglobigerina tripartita*, 4 *Dentoglobigerina* sp., 5 *Paragloborotalia* sp., 6 *Globigerinoides subquadratus*, 7 *Paragloborotalia siakensis*, 8 *Paragloborotalia* sp.

PLATE 21. Planktonic foraminifera from the Brasso Formation, Trinidad. 1 *Globigerinoides* sp., 2 *Paragloborotalia* sp., 3 *Paragloborotalia* sp., 4

Sphearoidinellopsis disjuncta, 5 *Praeorbulina* sp., 6 *Globigerinoides subquadratus*, 7 *Turborotalita* sp.

PLATE 22. *Dentooglobigerina* sp. from the Cipero Fm; test broken to reveal internal wall structure.

PLATE 23. *Dentooglobigerina* sp. from the Brasso Fm; test broken to reveal internal wall structure.

LIST OF APPENDICES

List of Acronyms

AABW - Antarctic Bottom Water

$CaCO_3$ - Calcium carbonate

CAS - Central American Seaway

CM – Carbon Maxima

CPDW - Circumpolar Deep Water

DIC - Dissolved Inorganic Carbon

DSDP - Deep Sea Drilling Project

EAIS - East Antarctic Ice Sheet

EEP - Eastern Equatorial Pacific

ENSO - El Nino and the Southern Oscillation

EUC - Equatorial Undercurrent

HO – Highest Occurrence

(I)ODP - (Integrated) Ocean Drilling Program

ITCZ - Inter-tropical Convergence Zone

LO – Lowest Occurrence

MMCO - Middle Miocene Climate Optimum

MMCT - Middle Miocene Climatic Transition

NADW - North Atlantic deep water

NCW - Northern Component Water

NEC - North Equatorial Currents

NECC - North Equatorial Counter-current

NRM - Natural remnant magnetisation

pCO_2 - atmospheric partial pressure of carbon dioxide

PCW - Pacific Central Water

SEC - South Equatorial Currents

SEM – Scanning electron microscope

SST - Sea Surface Temperature

TISW - Tethyan-Indian Saline Water

TOC - Total Organic Carbon

WEP - Western Equatorial Pacific

WPWP - West Pacific Warm Pool

XCB – Extended Core Barrel

1. Introduction

1.1 Rationale

Despite recent advances in our understanding of Miocene climate some fairly significant gaps persist. Reliable seawater temperature estimates are crucial to any reconstruction and modelling of past ocean salinity and density, water column stratification, thermohaline circulation, and ice volume (Bemis et al., 1998). A primary measure of (past) ocean water temperatures lies in the chemical analysis of calcite shells of marine organisms called foraminifera. Foraminifera are single-celled protists that secrete calcium carbonate shells; the chemistry of these calcite shells provides information about the chemical and physical conditions in which they grew (Murray, 1995).

This thesis applies a range of geochemical palaeoceanographic proxies to planktonic foraminifera of middle Miocene age (15.6–13.3 Ma) including stable isotope and trace metal analysis. The ratio of oxygen isotopes ($\delta^{18}O$) in biogenic calcite is perhaps the best established geochemical proxy for quantifying climate change throughout the Cenozoic and is utilised in the following chapters to investigate changes in sea surface temperatures and global ice volume at a resolution never approached before. There are many detailed benthic foraminiferal isotope records for the Miocene (Billups and Schrag, 2002; Holbourn et al., 2007; Lear et al., 2010) which provide insight to deep water conditions and high latitudes. However, research into the planktonic foraminiferal isotope record and conditions at the tropics over this interval are extremely scarce. Existing records are of low resolution with samples representing time intervals of $2x10^5$and $5x10^5$ years (e.g., Gasperi & Kennett 1993). Therefore at present we cannot ascertain whether deep ocean and surface ocean waters warmed at the same rate or magnitude which is critical to understanding forcing and feedback in the Earth system.

The sediments recovered by Integrated Ocean Drilling Program (IODP) Expedition 320/321 at Site U1338 provide the opportunity to document climate variability from a planktonic foraminiferal perspective in the early to middle Miocene for the first time at an eastern equatorial Pacific Site. The aim of this study is threefold; firstly to produce the first ever detailed multispecies record of planktonic foraminiferal geochemistry in the early to middle Miocene and provide constraints on the surface to benthic $\delta^{13}C$ and $\delta^{18}O$ gradient through a major climatic cooling interval. Secondly, to investigate the influence of orbital variations on Miocene climate through a combination of spectral and wavelet analyses, and thirdly, to examine planktonic foraminiferal evolution during times of climatic stress.

1.2 Biological characteristics of the foraminifera

Foraminifera are an important order of unicellular protists, which secrete calcium carbonate shells and inhabit marine environments from tropical to polar latitudes (Bé, 1977; Hemleben et al., 1989). Foraminifera differ from other eukaryotes because they possess granular and reticulose (netlike) pseudopodia; fibrillar extensions used for feeding which emanate from the ectoplasm that engulfs the test.

The planktonic taxa are members of the zooplankton and live free-floating in the water column, with the greatest concentration of species and individuals in the upper 100-150 m. Many species living within the photic zone host photosynthesising algal symbionts (Hemleben et al, 1989), whilst others predate on larval arthropods and other plankton. Those specialised for living at depth typically graze on sinking phytodetritus.

The tests, which can have one or more chambers, have very diverse morphologies with varying degrees of ornamentation. Traditionally, classification of foraminifera has been based primarily on characteristics of the shell or test. Wall composition and structure, chamber shape and arrangement, the shape and position of any apertures, surface ornamentation and other morphologic features of the shell are all used to define taxonomic groups of foraminifera (Hemleben et al., 1989).

1.3 The use of planktonic foraminifera as indicators of past environmental conditions and climatic change

When planktonic foraminifera die their calcitic shells slowly sink in the water column forming a component of “marine snow” (Bishop et al., 1977; Wefer et al., 1982), which settles on the seabed forming a layer of sediment in which the shells eventually become fossilised. The steady accumulation of such sediments, particularly in stable settings, makes it common for millions of years of evolutionary history to be captured in a single location and for morphospecies to be preserved continuously throughout their existence (Aze et al., 2011). It is this continuous and exceptional fossil record that has afforded planktonic foraminifera great utility in reconstructing past climate, ecological conditions and geological history (Berger, 1979; Boersma et al., 1987; CLIMAP, 1976; Ruddiman et al., 1986; Vincent et al., 1981).

Planktonic foraminifera have often been used as biostratigraphic markers (Leckie et al., 1993; Wade et al., 2011) or to provide geochemical proxies of oceanic and atmospheric temperatures and chemistry. Shell chemical composition, particularly stable isotopes (e.g. the ratio of $^{18}O/^{16}O$), is also widely employed to estimate water temperatures where the planktonic foraminifers grew (Anderson and Arthur, 1983; Berger, 1979; Hemleben, 1989; Vincent et al., 1981). When calcification of foraminiferal shells occurs the relative amounts of the two isotopes incorporated is dependent on temperature, and thus the ratio of the common isotope ^{16}O to the heavier isotope ^{18}O may be used to estimate the water temperature at the time that the calcite of the shell was deposited. Carbon isotopic records are also of interest in palaeoclimatology because they provide information on water mass movement, palaeoproductivity and the temperature dependent air-sea exchange of CO_2 (ventilation) (Lynch-Stieglitz et al., 1995). The $\delta^{13}C$ in marine calcite is controlled by the dissolved inorganic carbon (DIC) of the seawater from which it precipitates (Keith and Webber, 1964). Stable isotope and trace metal analysis of foraminiferal calcite has been used in the construction of long-term climate records that highlight important periods in the development of Earth's climate system, such as the onset of glaciation at the Eocene-Oligocene transition approximately 34 Ma (Coxall et al., 2005).

1.4 Miocene biotic and climatic changes

1.4.1 Continental configuration and Orography

By the Middle to Late Miocene the continental distributions were largely similar to the present day with the following exceptions; North and South America remained separated until the Pliocene, the Arctic Circle had greater landmass and the Paratethys Sea was still present in Europe. There was also more land in Southeast Asia, and in southern South America a seaway was present until ~9 Ma (Aceñolaza and Sprechmann, 2002; Markwick, 2007; Potter and Szarmari, 2009).

All of the world's major mountain ranges uplifted during the Middle Miocene with intensification after 10 Ma (Pound et al., 2012). The Tibetan Plateau and the Himalayas experienced rapid uplift during the Middle and Late Miocene as suggested by a dramatic increase in sedimentation into the Indian Ocean after 15 Ma (Potter and Szarmari, 2009; Rea, 1992). The mean maximum altitude of the region at 15 Ma is estimated to be between 3775 m and 6570 m (Currie et al., 2005; Spicer et al., 2003). Between 16 and 14 Ma the alps reached 1600 to 3000 m above sea level and rose steadily to 2500–3500 m at around 8 Ma (Jiménez-Moreno et al., 2008; Kuhlemann et al., 2001). The Andes are also estimated to have had a steady uplift of 0.2–0.3 mm/year from around 1800 m at 10.7 Ma (Gregory-Wodzicki, 2000).

1.4.2 Ocean circulation during the middle Miocene

Plate tectonic developments during the Miocene gave rise to the modern oceanic currents. During the Paleogene, ocean circulation was dominated by a circum-equatorial current (Potter and Szatmari, 2009). Restriction of the Indonesian Gateway between Borneo and New Guinea, which connected the Pacific to the Indian Ocean, began during the latest Oligocene (~25 Ma) when the Australian tectonic plate collided with south east Asia (Hall et al., 2011). Benthic foraminiferal isotope records from the western Pacific, South China Sea and eastern Indian Ocean indicate this was closed to deep water exchange between the Pacific and Indian Oceans, and deep water movement along the circum-equatorial current was restricted by the end of the early Miocene (~15.97 Ma) (Kuhnt et al., 2004; Potter and Szarmari, 2009).

During the middle Miocene the connection between the Mediterranean Sea with the Indian Ocean was intermittent until the Arabian plate–Eurasian plate collision caused complete closure at 11–10 Ma (Allen and Armstrong, 2008; Potter and Szarmari, 2009; Rögl, 1999). Finally, collision of North and South America at 12.8 Ma (Coates et al., 2004) resulted in the shallowing of the Central American Seaway (CAS) and restricted exchange between the Atlantic and Pacific Oceans until its final closure at 3.5–2.7 Ma (Coates et al., 2004; Coates and Obando, 1996; Webb, 2006). This final closure shut down global equatorial flow and initiated the modern Gulf Stream current. In sum, the closure of low latitude gateways produced steeper pole-to-equator gradients leading to the world's present “conveyor belt” system of oceanic circulation (Potter and Szatmari, 2009).

1.4.3 Miocene vegetation

In the terrestrial record palaeobotanical changes from ~16 Ma to ~7 Ma and the expansion of grasslands are correlated to a drying of continental interiors and a global cooling of the planet, linked to falling atmospheric CO_2 concentrations (Favre et al., 2007; Pound et al., 2012; Utescher et al., 2007). At ~16 Ma there is evidence for a warm biome distribution with greatly reduced desert regions, boreal – temperate mixed forests at the high northern latitudes, extensive subtropical to warm temperate mixed forests in the middle latitudes and tundra on Antarctica (Pound et al., 2012; Wolfe, 1985).

Continental climates underwent major changes in the middle Miocene and by ~13.8 Ma vegetation was no longer present on Antarctica (Wolfe, 1985). The warm temperate evergreen broadleaf and mixed forests were partly replaced by cooler and drier temperate biomes, suggesting significant cooling had occurred. During the late Miocene boreal forests and dryer vegetation types continued to expand, and major deserts began to appear. Increased aridity is inferred at this time for mid-latitude continental regions including Australia (Robert et al., 1986; Stein and Robert, 1986), Africa (Retallack, 1992), North America and South America (Pascual and Jaureguizar, 1990) which may have fostered the development of grasses and the consequent evolution of grassland- adapted biota (Pound et al., 2012).

1.5 Climate events

The middle Miocene represents a time of major changes in the evolution of the Earth's climate with major uplift of modern mountain chains, the origin of modern ocean currents, the overall cooling trend of the global climate and the reduction in atmospheric CO_2 levels (Beerling, 2011; Potter and Szarmari, 2009; Zachos et al., 2008). The Earth's climate changed from the warm Miocene Climate Optimum (17–15 Ma) to an interval of global climatic cooling between ~15 Ma and 13.7 Ma with an associated increase in the latitudinal temperature gradient. The rapid expansion of the East Antarctic Ice Sheet (EAIS) around 13.8 Ma, referred to as the Mi3 event in oxygen isotope records (Miller et al., 1991), is one of the major cooling steps in Cenozoic climate (Abels et al., 2005; Flower and Kennett, 1994; Holbourn et al., 2005; 2007; Shackleton and Kennett, 1975; Shevenell et al., 2004; Woodruff and Savin, 1991; Zachos et al., 2001).

The cause of the middle Miocene cooling has been attributed to increased burial of organic carbon (e.g., Vincent and Berger, 1985) and weathering of silicate rocks due to uplift in the Himalayan-Tibetan region (e.g., Raymo and Ruddiman, 1992); both leading to the withdrawal of CO_2 from the atmosphere and hence a reduction of the greenhouse capacity. However, existing CO_2 reconstructions based on different proxies do not show convincing evidence for lower atmospheric CO_2 values after or during middle Miocene cooling (Badger et al., 2013; Foster et al., 2012; Pagani et al., 1999;

Pearson and Palmer, 2000; Royer et al., 2001). Further, changes in ocean circulation patterns, for example, due to tectonic closure of basins, may have increased moisture transport or reduced heat transport to the Antarctic region (Shevenell et al., 2004). Additionally, orbital parameters may have played an important role in Cenozoic climate change by punctuating longer-term trends or by positive feedback mechanisms that pushed climate into a new state. The sequence of climate events and the processes which drove this profound climate transition are still poorly understood, because continuous, well-dated Miocene sedimentary archives and records of sea surface conditions are still extremely scarce.

1.5.1 The Mid Miocene Climate Optimum

The Middle Miocene Climate Optimum (MMCO) occurred at approximately 17 - 15 Ma and was the warmest interval of the Neogene punctuating the overall cooling trend that has characterised the last 50 million years (Fig.1.1). The MMCO is associated with rapid global sea-level fluctuations during an interval of high eustatic levels (Haq et al., 1987), terrestrial and marine faunal changes, and plate tectonic activity affecting global ocean currents. Flower and Kennett (1994) estimate that the MMCO was associated with a mid-latitude warming of about 6°C relative to the present. The warming of the climate during this period is suggested to be driven by tectonic and physical oceanographic changes rather than changes in CO_2 (Holbourn et al., 2014; Shevenell et al., 2004).

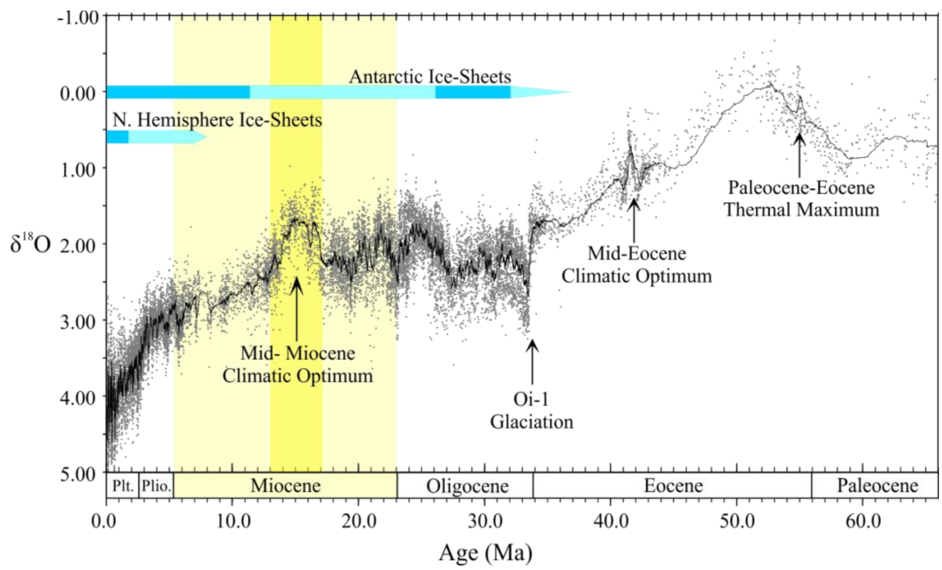

Figure 1. 1. Updated stacked deep-sea benthic foraminiferal oxygen isotope curve for 0–65 Ma. Updated from Zachos et al. (2008) and converted into Gradstein timescale (Gradstein et al., 2012).

1.5.2 Middle Miocene Climate Transition

The Antarctic ice sheets are a major component of the Earth's climate system, strongly influencing ocean and atmospheric circulation. The expansion of the East Antarctic Ice Sheet (EAIS) and transition into cooler climates at around 13.9 Ma marks the Middle Miocene Climatic Transition (MMCT) which led to major environmental changes (e.g., Flower and Kennett, 1994; Zachos et al. 2001; Shevenell and Kennett, 2004).

During the early to middle Miocene, benthic foraminiferal oxygen isotope records reveal several prominent positive excursions (Fig. 1.1) (Miller et al., 1991; 1996; Woodruff and Savin, 1991) which reflect brief periods of increased glaciations. The Mi3a and Mi3b events defined by Miller et al. (1991) and Woodruff and Savin (1991), together mark the major shift in $\delta^{18}O$ between ~14.1 and ~13.7 Ma (Abels et al., 2005; Holbourn et al., 2005; Tian et al., 2013). However, because the $\delta^{18}O$ of foraminiferal calcite ($CaCO_3$) is a function of both seawater $\delta^{18}O$ ($\delta^{18}O_{sw}$) and the temperature of the waters in which the foraminifers calcify, fundamental questions remain concerning the magnitude and phasing of middle Miocene Antarctic ice growth and global cooling (Shevenell et al., 2008). The benthic foraminiferal carbon isotope record displays a shift to heavier $\delta^{13}C$ values (the CM6 event) coincident with the Mi3b event (Holbourn et al., 2014; Woodruff and Savin, 1991).

The MMCT has been linked to variations in atmospheric CO_2, the global carbon cycle, opening and closure of oceanic gateways and uplift of mountain ranges (Hay et al., 2002; Vincent and Berger, 1985), but to date no clear consensus on the exact cause has been reached. A further mechanism to explain the MMCT is a favourable orbital configuration (Holbourn et al., 2005; 2007). Like other major Cenozoic climate shifts the timing of the major cooling step is supposedly controlled by long-period orbital forcing (Abels et al., 2005; Holbourn et al., 2007). Minima in the amplitude variation of Earth’s tilt (obliquity) and minima in the ellipsoidal shape of the Earth’s orbit around the sun (eccentricity), which modulates the amplitude of climatic precession (the rotational movement of the Earth’s axis relative to the elliptical orbit), might have suppressed summer insolation maxima for a prolonged interval of time, thereby favouring ice sheet growth. However, orbital forcing alone cannot explain the long-term cooling trend from the MMCO onwards.

1.5.3 The Monterey Carbon Excursion

The long-lasting positive "Monterey carbon-isotope excursion" between ~17 and 13.5 Ma (Vincent and Berger, 1985) is a prominent feature in Miocene oceanic stable isotope records (Fig. 1. 2) (Woodruff and Savin, 1991). Bulk carbonate and benthic foraminiferal stable isotope records reveal that this prolonged $\delta^{13}C$ excursion is characterised by low-frequency fluctuations (~ 1‰) which appear to approximate long (400 kyr) eccentricity cycles (Holbourn et al., 2007; Woodruff and Savin, 1991). The apparent co-variance between $\delta^{13}C$ and $\delta^{18}O$ together with the large sedimentary deposits of organic rich carbon along the circum-Pacific margins and the phosphatic deposits of the south eastern U.S (Compton et al., 1990; 1993) gave support to the hypothesis that increased burial rates of organic carbon led to atmospheric CO_2 drawdown and global cooling in the middle Miocene via a series of positive feedback mechanisms (Flower and Kennett, 1993; Vincent and Berger, 1985) as the largest carbon isotope maxima ("CM6"(Woodruff and Savin, 1991)) immediately follows the major ice expansion event of the middle Miocene ("Mi-3";(Miller et al., 1991)). The "Monterey Excursion" has also been linked to the tectonic uplift of the Himalaya mountain range and Tibetan Plateau as a result of enhanced chemical weathering of silicate minerals. This hypothesis is based on the monotonically increasing trend in the marine $^{87}Sr/^{86}Sr$ record through the Neogene, and increased marine productivity due to excess influx of nutrients into oceans and the subsequent organic carbon burial (Raymo and Ruddiman, 1992; Raymo, 1994; Raymo et al., 1988).

Alternatively, it has been suggested that carbon isotope maxima associated with glacial transitions may be evidence of a negative feedback in the climate system (Shevenell et al., 2008). Under this scenario, ice sheet expansion blankets an area of silicate basement that was previously a sink for atmospheric CO_2 via silicate weathering (Pagani et al., 1999; Shevenell et al., 2008; Tian et al., 2009). Thus, resulting in a positive carbon isotope excursion by lowering buried organic matter $\delta^{13}C$ values through increased photosynthetic isotopic fractionation due to higher concentrations of dissolved carbon dioxide. However, these scenarios involve opposite changes in atmospheric CO_2 concentration.

While an alkenone based CO_2 record displays little variation through this interval (Pagani et al., 2009), boron isotope ratios and a leaf stomatal record do point to a decrease in CO_2 at the MMCT (Badger et al., 2013; Kürschner and Kvacek, 2009;

Pearson and Palmer, 2000). pCO_2 levels for the middle Miocene are discussed further in the following section.

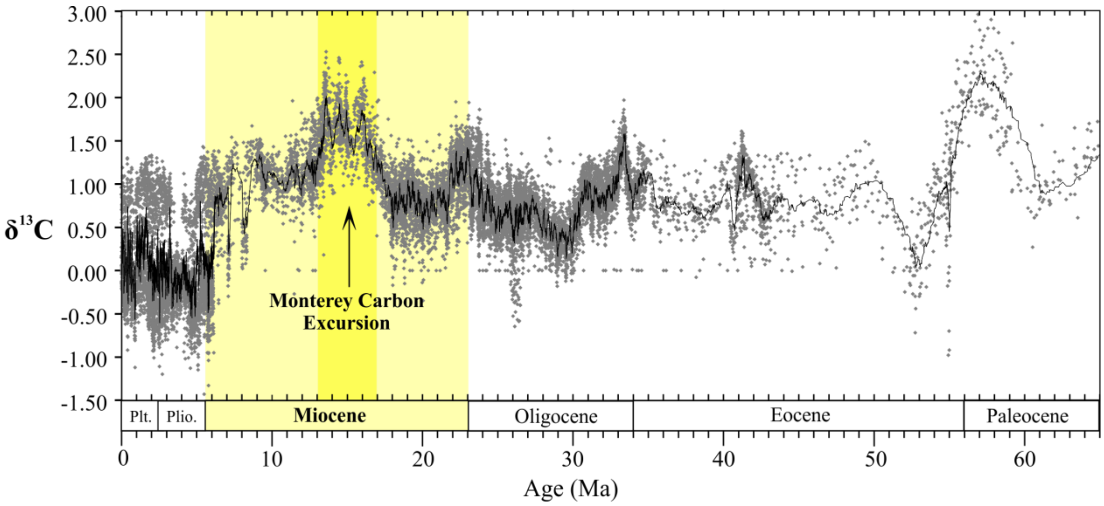

Figure 1. 2. Updated Cenozoic stacked deep-sea benthic foraminiferal carbon isotope curve for 0–65 Ma. Updated from Zachos et al. (2008) and converted into the Gradstein timescale. (Gradstein et al., 2012).

1.6 Mechanisms for Miocene cooling

1.6.1 Atmospheric *p*CO2

Miocene pCO_2 levels have been reconstructed using numerous techniques and each differs in both atmospheric concentration and in trend through time. Estimates of Middle Miocene pCO_2 based on alkenones (Pagani et al., 2005), boron isotopes (Pearson and Palmer, 2000), the B/Ca ratio of planktonic foraminifera (Tripati et al., 2009), pedogenic carbonates (Ekart et al., 1999; Retallack, 2009) and stomatal indices (Beerling et al., 2009; 2008; Stults et al., 2011; Wagner et al., 1996) range from glacial levels to nearly twice the modern value (Henrot et al., 2010).

On the basis of stomatal indices from fossil leaves, Royer et al. (2001) and Kürschner et al. (2008) estimate mean mid-Miocene atmospheric pCO_2 concentrations ranging from 270 to 564 ppmv with a peak at ~16 Ma of between 460 and 564 ppmv. In contrast, reconstructions based on marine pCO_2 proxy records indicate much lower values through the middle Miocene. For example, the alkenone based reconstructions place atmospheric pCO_2 levels between 190 and 360 ppmv reaching a peak at around 6–7 Ma of approximately 360 ppmv, while atmospheric pCO_2 concentrations reconstructed from boron isotopic ratios of planktonic foraminiferal shells show a range from 137 to 305 ppmv with a peak in pCO_2 at ~16 Ma and ~6 Ma (Pearson and Palmer, 2000). The B/Ca ratio of planktonic foraminifera shows a peak of 433 ppmv at 15 Ma which then drops to concentrations of between 206 and 304 ppmv by 10 Ma (Tripati et al., 2009).

A number of models have attempted to test the sensitivity of the climate system to changes in the atmospheric CO_2 level and other variables during the Miocene. These models show that an increase in pCO_2 levels results in greater warming at high latitudes (Henrot et al., 2010; Tong et al., 2009; You, 2010). Simulations run by Henrot et al. (2010) revealed that a warmer climate at both high and low latitudes during the middle Miocene can only be achieved with CO_2 levels higher than present, and that warm and humid conditions might have been maintained and intensified by changes in vegetation cover (Henrot et al., 2010). Modelling experiments by You (2010) over the MMCO showed that northern and southern polar temperatures are driven by different mechanisms. The model also supports the hypothesis that higher than modern CO_2 levels were necessary to cause the global temperature rise during the MMCO.

Overall, the time scales on which CO_2 drawdown and climate change occurred, as well as the locations of major carbon sinks in the Miocene, remain unclear (Holbourn et al., 2013). The low CO_2 estimates have led to disagreements over how much Miocene climate was influenced by this greenhouse gas and raises the possibility of a CO_2-temperature decoupling during other times in Earth history (Kürschner et al., 2008; Mosbrugger et al., 2005; Pagani et al., 2005; Shevenell et al., 2004).

1.6.2 Ocean Circulation

In the absence of pCO_2 control on the middle Miocene global climate variability, changes in oceanic heat and atmospheric water vapour transport driven by changes in ocean gateway configurations are considered to have played important roles (Pagani et al., 1999; Zachos et al., 2001).

Changes in ocean circulation patterns are considered to be an important factor in controlling the global climate and have been hypothesised as another potential cause of middle Miocene cooling and Antarctic Ice Sheet growth. In 1980, Schnitker argued that subsidence of Iceland/the Faeroe Ridge accelerated Antarctic cryosphere expansion by increasing moisture flux to Antarctica via increased production and circum-Antarctic upwelling of warm, saline Northern Component Water (NCW; Analogous to North Atlantic Deep Water). It has also been suggested that closure of the Indonesian Seaway in the western equatorial Pacific triggered intensification of gyral circulation and western boundary currents resulting in northward migration of tropical planktonic foraminiferal assemblages into the north-west Pacific in the middle Miocene (Kennett et al., 1985), although the timing of such events is ambiguous.

Alternatively, Woodruff and Savin (1989, 1991) suggested that, prior to 14 Ma, global thermohaline circulation was controlled by influx of relatively warm, Tethyan-Indian Saline Water to the Indian Ocean, transporting heat from low-latitudes to the Southern Ocean intermediate waters. They proposed that the closure of the Tethys seaway, linking the Atlantic and the Indian Ocean, could have decreased meridional heat transport to high southern latitudes. Thus, allowing cooling of Antarctic surface waters and expansion of the EAIS (Flower and Kennett, 1995; Ramsay et al., 1998). However, a direct relationship between the MMCT and the closure of the Tethys seaway has so far not been proven (e.g. Hüsing, 2008; Smart et al., 2007).

The lack of datable sediments and complex processes involved in the convergence of the Eurasian and Arabian plates have complicated attempts to date the closure accurately, and the precise timing of the closure of the Tethys seaway remains elusive. Estimates range from the late Oligocene to the late Miocene, however, mammal migrations from ~18 Ma onwards suggest that the connection was closed well before the onset of the MMCT (Rögl, 1999; Wessels, 2009). An alternative group of hypotheses focuses on orbital variations as drivers of climatic change.

1.6.3 Milankovitch cycles

The external insolation forcing controlled by the shape of the Earth's orbit (eccentricity) (Fig. 1.3), the tilt of its axis (obliquity) (Fig. 1.4) and the direction of its axis (precession) (Fig 1.5) has played an important role in regulating global climate changes. These orbital perturbations are named after the Serbian mathematician, Mulitin Milankovitch, who used them to explain the advance and retreat of polar ice caps.

A few studies have revealed the astronomical imprints from the obliquity (40 kyr) and eccentricity (100 kyr and 400 kyr) cycles in the middle Miocene deep sea benthic foraminiferal $\delta^{18}O$ and $\delta^{13}C$ (Holbourn et al., 2005, 2007, 2013; Shevenell et al., 2004; Tian et al., 2013). Some modelling results also highlight the dominant long eccentricity (400 kyr) forcing on the middle Miocene climate change (DeConto and Pollard, 2003; Ma et al., 2011). However, prior to this study, astronomical cyclicity had not been examined in Miocene planktonic foraminiferal records from the open ocean, thus, demonstrating this study's original contribution to our understanding of Miocene climate.

1.6.3.1 Eccentricity

Eccentricity *e* is a measure of how elliptical an orbit is (Milankovitch, 1941). It is the only orbital parameter that controls the total amount of solar radiation received by the Earth when averaged over the course of one year. A planet's closest approach to the sun is called the perihelion (p) and the furthest distance is the aphelion (a) (Fig. 1.3). The eccentricity is a measure of how different these are;

Eq.1.1

$$e = (a\text{-}p) / (a+p)$$

When $e = 0$, the orbit is circular. As e gets close to 1, the orbit becomes more elongated. The eccentricity for the orbit of the Earth varies from a minimum of $e = 0.0005$ to a maximum of $e = 0.0607$. The larger the eccentricity, the greater the difference in solar radiation that reaches the Earth at the perihelion versus aphelion. At its current value of e = 0.017, given by the astronomical calculation of Laskar *et al.* (2004), this difference is 6.7%. It is thought that, over the long term, the changes in eccentricity can affect the Earth's climate through modulation of the precession cycle.

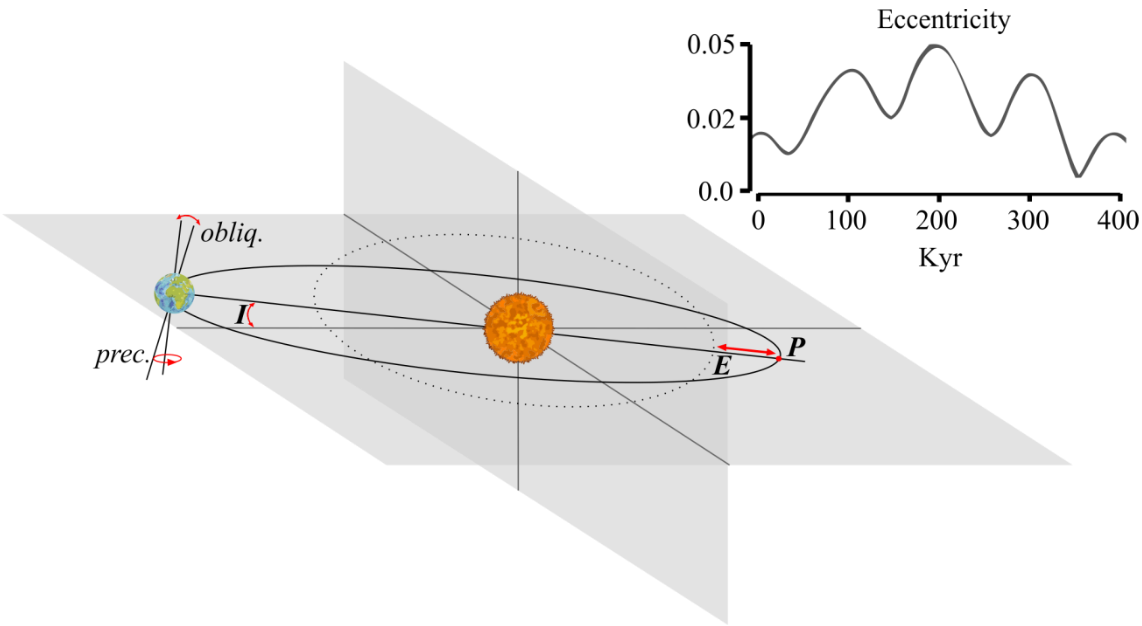

Figure 1. 3. The orbit of the Earth is shown here in a simplified perspective drawing. The horizontal grey plane contains the Earth's orbital plane at an arbitrary date and comprises the reference plane. Abbreviations are: *prec.*, general precession (wobble) of the Earth's rotational axis; *obliq.*, obliquity of the Earth's axis (tilt); *I*, inclination of the plane of the Earth's orbit relative to the reference frame; *P*, point of perihelion. Inset: Earth's orbital eccentricity from 0–400kyr.

The eccentricity of the Earth's orbit follows a long 400,000 year cycle, with additional "short" eccentricity cycles with periods clustered around ~96 and ~127 kyr. These arise mainly from the interactions of the planets Venus and Jupiter due to their close approach and large mass, respectively. This component is called the "long" eccentricity cycle, and of all of Earth's orbital frequencies it is considered to be the most stable.

1.6.3.2 Obliquity

Obliquity refers to the tilt of the Earth's axis relative to the plane of its orbit, which follows a ~40,000 year cycle (Berger, 1988). The obliquity varies from a minimum of 22.1 degrees to a maximum of 24.5 degrees (Fig. 1. 4). The present day obliquity is approximately 23.45 degrees. The main climatic effect of variations in the Earth's obliquity is its control of the seasonal contrast. While the total annual energy received on Earth is not affected, the obliquity controls the distribution of heat as a function of latitude and is strongest at high latitudes.

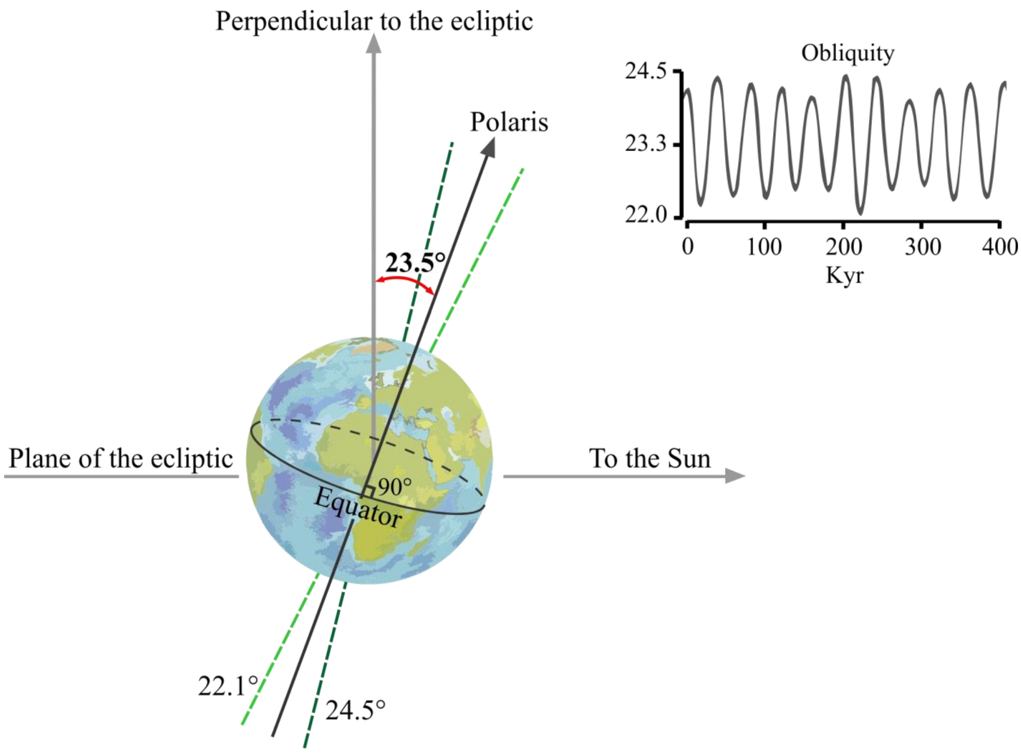

Figure 1. 4. Schematic diagram of the 22.1–24.5° range of the Earth's obliquity (not to scale). Inset: Earth's obliquity from 0–400kyr.

1.6.3.3 Precession

The precession of the equinoxes occurs as a result of the torque exerted on the solid Earth, which has the shape of an oblate spheroid, by the moon and the sun. Of the secular motions associated with the Earth's orbit, the interpretation of precession is the most complex. Precession changes the direction of tilt of the Earth’s axis relative to its aphelion and perihelion (Fig. 1. 5). Currently the Northern Hemisphere experiences winter when the Earth is closest to the sun, as opposed to 13,000 years ago when winter occurred in the Northern Hemisphere when it was furthest from the sun. Since most of the Earth’s land mass is in the Northern hemisphere, these changes are believed to have an effect on the accumulation of ice and snow at the poles and may play a role in the Earth’s long term climatic cycles and ice ages (Berger, 1988).

With respect to the stars, the precessional movement of the Earth’s spin axis traces out a cone with a period of ~25.8 kyr. However, due to the precession of the perihelion within the orbital plane, the period of precession, measured with respect to the Sun and the seasons, is shorter. The motion of the perihelion is not steady but caused by a superposition of the different frequencies. For this reason the precession of the equinoxes with respect to the orbital plane lurches with a superposition of three periods around ~19 kyr, 22 kyr and 24 kyr.

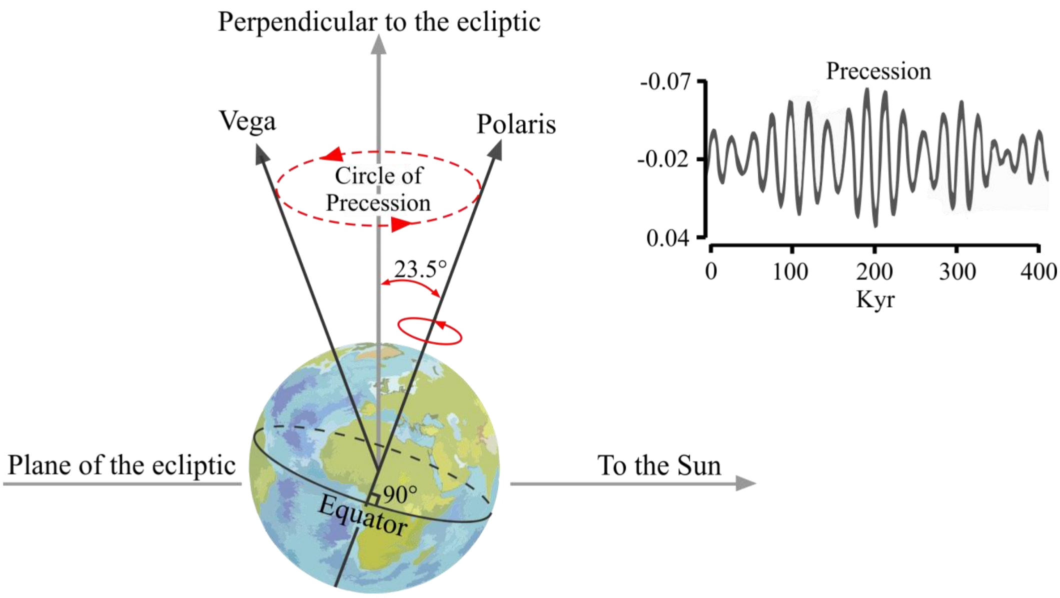

Figure 1. 5. Schematic diagram of procession of the equinoxes (not to scale). Inset: Earth’s precession from 0–400 kyr.

Recent research by Holbourn et al. (2013) describes three distinct climate phases with different imprints of orbital variations in the middle Miocene benthic foraminiferal stable isotope records of the West Pacific Ocean (Sites 1146 and 1237 $\delta^{18}O$, $\delta^{13}C$; 1237 XRF Fe, fraction 63µm). Firstly, during the MMCO (prior to 14.7 Ma) benthic foraminiferal oxygen isotope records are characterised by minimum ice volume and prominent 100 and 400 kyr variability. Then prior to the MMCT (14.7 to 13.9 Ma), 40 kyr obliquity cycles dominate the isotope records and appear to be driving long term cooling. Finally, after 13.9 Ma the Earth enters "Ice house" conditions (Holbourn et al., 2005) with distinct 100 kyr variability and improved ventilation of the deep Pacific. The benthic foraminiferal carbon data consists overall of nine 400 kyr cycles over the "Monterey" carbon-isotope excursion (16.9–13.5 Ma) which show high coherence with the long eccentricity period. Superposed on these low-frequency variations are 100 kyr oscillations which closely track the amplitude modulation of the short eccentricity period. These results suggest that eccentricity was driving middle Miocene climate evolution through the modulation of long-term carbon budgets, and that obliquity-paced changes in high-latitude seasonality created favourable conditions for ice growth and hence global cooling.

1.7 Aims of this study

The overarching aim of this thesis is to investigate the nature and variability of early-middle Miocene climate and the relationship to orbital variations in solar insolation, in order to better understand the extent and magnitude of the global MMCT and the subsequent cooling/EAIS events.

Furthermore, this study aims to investigate changes in the thermal structure of the Pacific Ocean during the development of MMCT to examine Pacific Ocean circulation across the middle Miocene climatic events. This is achieved through high resolution planktonic foraminiferal stable isotope analysis, spectral analysis and wavelet transform analysis. In order to assess the reliability of these new records this thesis also goes on to document the taxonomy and palaeobiology of Miocene tropical planktonic foraminifera and their response to times of climatic stress.

1.8 Thesis layout

Chapter 1: Sets out the current understanding of both the proxies and the climatic events that are the focus of this study.

Chapter 2: Includes detailed explanations of the core material, sample selection, geochemical analyses, numerical analyses, and also cleaning methods in order to avoid any undue repetition in the following Chapters.

Chapter 3: Presents an overview of the planktonic foraminiferal taxonomy of Site U1338, and includes 20 plates of high resolution scanning electron microscope images. The taxonomy of planktonic foraminifera is the foundation for understanding palaeoclimate proxy measurements. To reconstruct Miocene palaeoclimate records with any certainty, planktonic foraminifera must be studied at the species level. In this section the preservation of the foraminifera and their suitability for geochemical analysis are discussed.

Key questions addressed:

> *(Q. 1) What is the state of planktonic foraminiferal preservation at Site U1338?*

Chapter 4: Presents a high resolution (3 kyr) planktonic foraminiferal $\delta^{18}O$ and $\delta^{13}C$ record spanning the period of 15.6–13.3 Ma from IODP Site U1338 in the eastern equatorial Pacific Ocean, in addition to the first planktonic foraminiferal record of trace metal ratios for this interval. Separation of the components of the $\delta^{18}O$ signal is required to improve understanding of the processes and feedbacks involved in this dynamic climate reorganization. Therefore, in this chapter Mg/Ca ratios are used as a palaeotemperature proxy to provide an independent temperature record necessary to reveal the ice volume component of the middle Miocene $\delta^{18}O$ signal.

This Chapter further investigates the Middle Miocene astronomical imprints in the planktonic foraminiferal isotopic records and develops the discussions on the impact of orbital forcing on Miocene ice sheet expansion.

Key questions addressed:

> *(Q. 2) How does the timing and magnitude of stable isotope events in the planktonic foraminiferal record compare with the deep ocean?*
>
> *(Q. 3) Were fluctuations in tropical surface water conditions driven by orbital forcing?*

Chapter 5: Examines the bioevents over the middle Miocene climate transition, paying particular attention to changes in coiling direction in *Paragloborotalia siakensis*, its use as a biostratigraphic tool and the timing of this event in relation to changing surface water conditions in the Miocene Equatorial Pacific Ocean. This chapter presents multispecies stable isotope and Mg/Ca results, and investigates the palaeoecology of several species of planktonic foraminifera.

Key questions addressed:

> *(Q. 4) What is the biotic response to inferred major shifts in ice volume during the middle Miocene?*
>
> *(Q. 5) What are the key bioevents during the middle Miocene?*

Chapter 6: Examines changes at Site U1338 in the context of the global ocean, discusses the data in terms of implications for the global climate across the MMCT, and goes on to question the validity of the “Permanent El Nino” hypothesis (Watanabe et al., 2011). The planktonic and benthic (Holbourn et al., 2013) $\delta^{18}O$ and $\delta^{13}C$ records of IODP Site U1338 are compared with previously published records from ODP Site 1146 from the South China Sea (Holbourn et al., 2007). Their significance within the context of palaeoclimate research is discussed and a new model for middle Miocene Pacific Ocean dynamics is proposed.

Key questions addressed:

> *(Q. 6) To what extent was there and east west temperature contrast in the Miocene equatorial Pacific Ocean?*
> *(Q. 7) What are the implications of east-west temperature contrasts across the equatorial Pacific Ocean?*

Chapter 7: Summarises the key conclusions from this research and identifies future work.

2. Methodology

In the course of this PhD I have used a number of different analytical methods. Some of these techniques are applicable to more than one science chapter, while others are only relevant to one. To avoid undue repetition between chapters all of the analytical methods are presented here.

2.1 Site locations

2.1.1 IODP Site U1338

This study is based on Miocene marine sediments recovered at IODP Site U1338 (2°30.4699N, 117°58.1789W, 4200 m water depth) in the equatorial Pacific Ocean (Fig. 2.1). Four holes (A–D) were drilled at Site U1338 on 18 Ma crust using the APC/XCB coring systems. A 415 m thick succession of biogenic carbonate sediments of early Miocene–Recent age was recovered with high sedimentation rates averaging 30 m/Myr (Lyle et al., 2009). The sediments are divided into four major lithological units; Unit I (~50 m mcd (meters composite depth); middle Pliocene to Pleistocene) consists of an alternating sequence of multi-coloured nannofossil ooze, diatom nannofossil ooze, and radiolarian nannofossil ooze; Unit II (~194m thick; upper Miocene to middle Pliocene) is mainly composed of light green and light grey nannofossil ooze with varying amounts of diatoms and radiolarians; Unit III (~171m thick; lower to upper Miocene) predominantly consists of white, pale yellow, and very pale brown nannofossil ooze and chalk, with generally low but sometimes common abundances of siliceous microfossils. Unit IV is composed of lower Miocene aphanitic basalt.

2.1.2 ODP Site 1146

In Chapter 7 the results of this study are compared to data collected by Holbourn et al. (2007) from Miocene marine sediments recovered at ODP Site 1146 (19° 27.40′N, 116° 16.37′E; water depth: 2092 m, Fig. 2.1) in order to examine palaeoceanographic changes across the Pacific ocean. Detailed site locations, core recovery and lithological descriptions can be found in Wang et al. (2000).

Coring with the Extended Core Barrel (XCB) system at Site 1146 recovered a continuous Miocene sequence of carbonate-rich hemipelagic sediments, which grade from unlithified green nannofossil clay in the lower Miocene to light brownish grey foraminifers and nannofossil clay in the upper Miocene (Wang et al., 2000).

Foraminifers and nannofossil clays were sampled at ~10 cm intervals (~4 kyr time resolution) in Hole 1146A (463.05–568.47 m below seafloor).

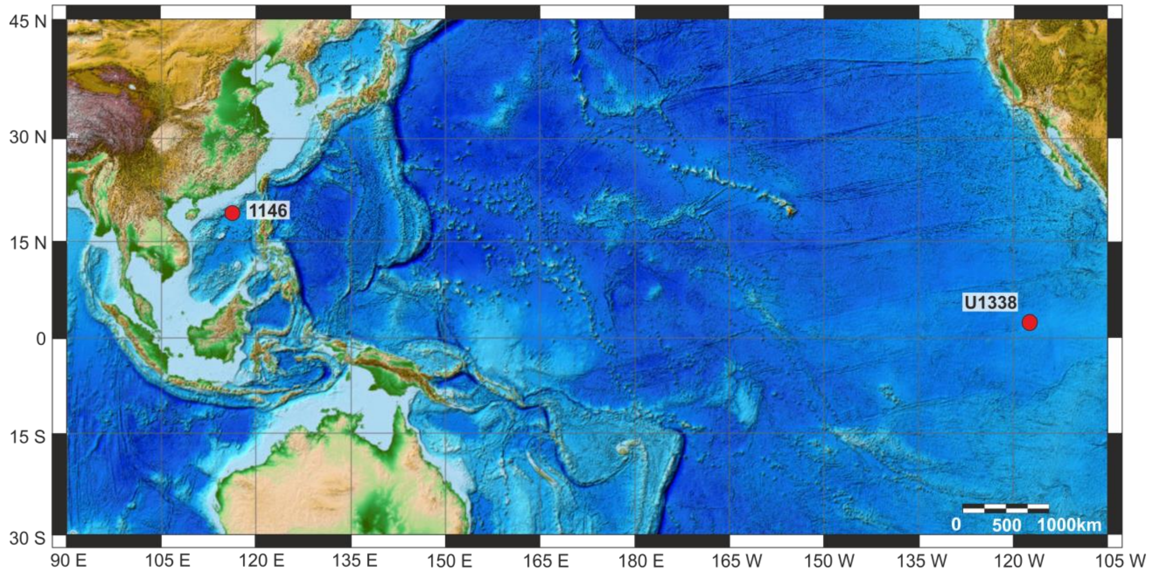

Figure 2. 1 Map showing location of Integrated Ocean Drilling Program Site U1338 and ODP Site 1146. Map adapted from NOAA, larger version can be viewed in Appendix B.

2.2 Sampling Strategy

The samples used in this research are taken from an 80 m section of lower–middle Miocene sediments from 350–430 m composite depth (mcd) (Fig. 2. 2), following the shipboard splice of the B hole and the C Hole cores to ensure a complete and continuous sedimentary record. The transition from ooze to chalk occurs at 378 mcd. Core sample notation follows the standard IODP format, with designation for site, hole, core number, section number and centimetre interval.

2.3 Sample preparation

Sediment volumes of ~10 cc were collected at 10 cm intervals and washed with distilled/tap water over a 63 µm sieve; the residues were dried in an oven at 40°C. All samples (Appendix A, Table 1) were examined under a binocular light microscope. Species identifications of the planktonic foraminifera were generally made on the 315–250 µm and 250–150 µm size fractions. The 150–63 µm fraction was scanned for distinctive taxa.

Selected specimens were mounted on SEM stubs, coated with gold, and inspected in a FEI Quanta 650 SEM at the University of Leeds, UK. After imaging their external surfaces at low and high resolution, several tests were broken using moderate pressure under a glass slide, and the fragments were used for the investigation of internal surfaces and test walls in cross-section.

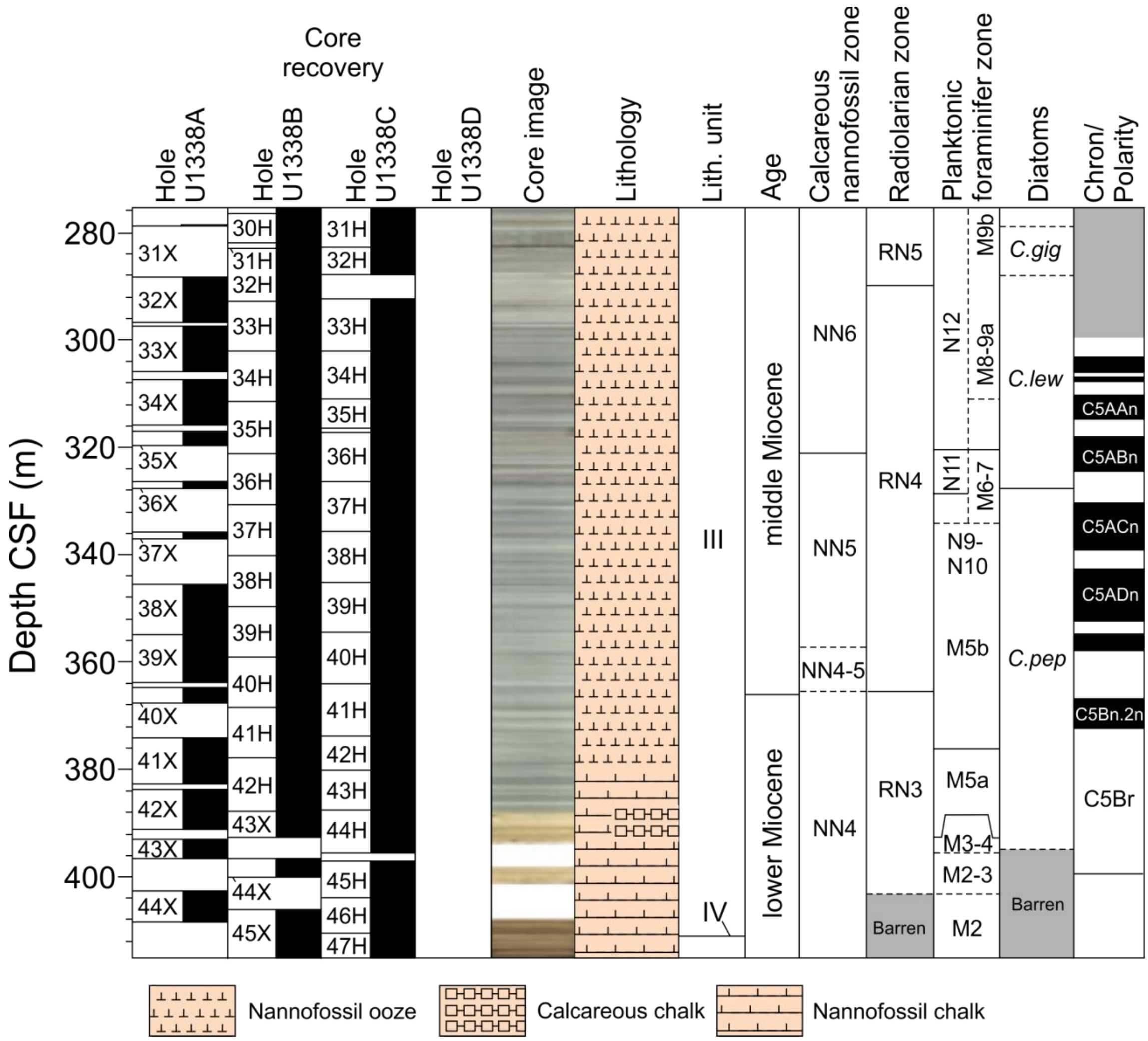

Figure 2. 2. Shipboard Lithostratigraphy summary, Site U1338. Biostratigraphic zones mainly based on Hole U1338A. Magnetostratigraphy represents a spliced record from all holes and is plotted relative to Core Composite depth below Sea Floor (CCSF-B) depth (Lyle et al., 2009).

2.4 Age model

The age model for the depth interval 350–425 mcd from the spliced section of Site U1338 was developed by Holbourn et al. (2014), by correlating the benthic foraminiferal $\delta^{18}O$ record to computed variations of the Earth's orbit (Laskar et al. 2004). An eccentricity-tilt-precession composite was constructed as a tuning target, with no phase shift and with equal weight of eccentricity and obliquity and only 1/3 precession. The $\delta^{18}O$ minima were correlated to eccentricity-tilt-precession maxima, following a minimal tuning approach to preserve original spectral characteristics and avoid artificial changes in sedimentation rates (Muller and MacDonald, 2002).

Astronomical tuning depends on an initial age model that constrains the time interval of the depth profile. The initial age model of Site U1338 is derived from planktonic foraminiferal datum events, nannofossil datum events, radiolarian datum events, and magnetostratigraphic events (Fig. 2. 2) (Lyle et al., 2009). Palaeomagnetic data from shipboard measurements of the natural remnant magnetisation (NRM) of the core archive-half sections shows the studied interval extends from Chron C5AAr (13.36 Ma) to Chron C5Br (~15.2 Ma), however magnetostratgraphy below 400 mcd is unreliable (Pälike et al., 2010). This interval belongs to planktonic foraminiferal Zones N12–N5 of Kennett and Srinivasan (1983) and M9–M2 of Wade et al., (2011). The planktonic foraminiferal biostratigraphic zonation is discussed further in Chapter 5.

The results of this study are plotted against the Holbourn et al., 2014 age model, as this allows direct comparison between the planktonic and benthic data sets, and the independently tuned Site U1338 isotope data correlate well with astronomically tuned $\delta^{18}O$ and $\delta^{13}C$ records from the southeast and northwest subtropical Pacific (Holbourn et al., 2007).

2.5 Stable isotope mass spectrometry

In Chapters 4 and 6, long term stable isotope records are reported across the middle Miocene (15.6–13.3 Ma). This section addresses the systematics of oxygen and carbon stable isotopes and how they were measured.

2.5.1 Oxygen isotope systematics

Oxygen has three stable isotopes: ^{16}O (99.76%), ^{17}O (0.04%) and ^{18}O (0.20%) that occur naturally in Earth’s water and air. These isotopes share identical chemical characteristics as they contain the same number and arrangement of protons and electrons. However, they exhibit differing chemical-physical properties due to their difference in mass (due to varying numbers of neutrons) (Craig, 1957).

Molecules consisting of light isotopes react more easily than those consisting of heavy isotopes. This is because the energy of a bond formed between lighter isotopes is weaker compared to heavier isotopes of the same element, and is therefore more likely to break when energy is applied. Seawater $\delta^{18}O$ is directly linked with the hydrological cycle, consisting of evaporation atmospheric vapour transport and return of freshwater to the ocean via precipitation and runoff, or ice sheet melting (Ruddiman, 2001).

When seawater evaporates, the water vapour is enriched in ^{16}O and the water left behind becomes enriched in ^{18}O, this partitioning of isotopes between substances is called "fractionation". The abundance of ^{18}O compared to ^{16}O is displayed in a ratio of the two isotopes and expressed as the following:

Eq. 2.1

$$\delta^{18}O = \left(\frac{\left(\frac{^{18}O}{^{16}O}\right) sample \left(\frac{^{18}O}{^{16}O}\right) standard}{\left(\frac{^{18}O}{^{16}O}\right) standard} \right) * 1000$$

The oxygen isotope composition of foraminiferal calcite ($\delta^{18}O_{carb}$) reflects the isotopic composition of the seawater at the time of calcification, which is primarily influenced by the ambient water temperature, global ice volume and local salinity (Craig, 1965).

2.5.2 Oxygen isotope palaeothermometry

Temperature and $\delta^{18}O$ have an inverse relationship where a change in temperature of 1ºC will give a ~0.23‰ change in the $\delta^{18}O$ of the biogenic calcite (Bemis et al., 1998; Epstein and Mayeda, 1953). The relationship between temperature and the oxygen isotope composition of carbonate was first empirically derived by McCrea (1950):

Eq. 2.2

$$T(°C) = a + b(\delta^{18}O_{carb} - \delta^{18}O_{sw}) + c(\delta^{18}O_{carb} - \delta^{18}O_{sw})^2$$

Where T is temperature, $\delta^{18}O_{carb}$ the oxygen isotopic composition of the solid carbonate, $\delta^{18}O_{sw}$ the oxygen isotopic composition of the seawater in which the carbonate precipitated, and *a*, *b* and *c* empirically derived constants. These constants have been subsequently revised based on laboratory studies of biologically and inorganically precipitated $CaCO_3$ (Bemis et al., 1998; Craig, 1965; Epstein and Mayeda, 1953; Erez and Luz, 1983; Kim and O'Neil, 1997; O'Neil et al., 1969). The quadratic fit is based on theoretical predictions of the nature of isotopic fractionation at low vs. high temperatures. Though, linear (c=0) and quadratic (c≠0) fits have proven to fit experimental data equally well at warm oceanic temperatures, within a precision of 0.2°C (Erez and Luz, 1983). Standard errors of various palaeo-temperature equations are estimated to be ±0.4-0.7ºC (Ruddiman, 2001). However, during times of changing ice volume $\delta^{18}O_{sw}$ cannot easily be estimated, and an independent proxy is required for either temperature or ice volume in order to deconvolve the $\delta^{18}O$ signal. Mg/Ca palaeothermometry provides one such method to test the accuracy of reconstructions (e.g. Lear et al., 2000).

Planktonic foraminifera are known to be highly susceptible to post-depositional diagenetic alteration, which can significantly alter the geochemistry of the tests, and in turn, stable isotope measurements. In this study, a detailed analysis of the state of preservation and degree of recrystallization was conducted on Site U1338 planktonic foraminifera prior to geochemical analyses. This study found the state of preservation to be generally excellent, the results are discussed in detail in Chapter 3.

2.5.3 Carbon isotopes systematics

There are two stable isotopes of carbon, namely ^{12}C (98.9%) and ^{13}C (1.1%). As with oxygen, the carbon isotope ratio ($\delta^{13}C$) is calculated according to Equation 2.3 and reported against the VPDB standard as permil (‰). Carbon isotopic records from carbonates are of interest in palaeoclimatology because they provide information on how the carbon cycle functions (Emiliani, 1955).

The $\delta^{13}C$ in marine calcite is controlled by the dissolved inorganic carbon (DIC) of the sea water from which it precipitates (equation 2.4). The biological carbon pump redistributes DIC and nutrients within the ocean via the phytoplankton, which preferentially use ^{12}C opposed to the heavier ^{13}C during photosynthesis (Park and Epstein, 1960; Wefer et al., 1999). This fractionation leaves the surrounding water enriched in ^{13}C and the organic matter enriched in ^{12}C. As this material falls through the water column it is remineralised and leaves the deeper waters enriched in ^{12}C relative to the depleted waters in the photic zone. As a result, surface waters tend to have high ^{13}C values, whereas deep waters are generally low in ^{13}C. Therefore, during periods of high-productivity in the ocean surface waters, the ^{13}C gradient from surface to deep increases.

Eq. 2.3

$$\delta^{13}C = \left(\frac{\left(\frac{^{13}C}{^{12}C}\right) sample \left(\frac{^{13}C}{^{12}C}\right) standard}{\left(\frac{^{13}C}{^{12}C}\right) standard} \right) * 1000$$

Eq. 2.4

$$DIC = CO_2(aq) + H_2CO_3 + HCO_3^- + CO_3^{2-}$$

2.5.4 Mass spectrometry

At the outset, $\delta^{18}O$ and $\delta^{13}C$ was measured on 10 to 12 shells of *G. subquadratus* from the >250 and >150 μm size fraction from 350 mcd until its extinction at 390 mcd. Analyses then continue with *Globigerinoides* spp until 425 mcd. In few samples, where foraminiferal density was low, only 5–7 specimens were analysed. Analyses were made with a VG Optima mass spectrometer at the British Geological Survey (BGS), Keyworth, UK. When picking shells care was taken to exclude individuals with visible signs of dissolution such as broken or missing chambers and/or fragile shells, although preservation of specimens was generally excellent (Fox and Wade, 2013). The standard deviation of external measurements is ±0.07‰ and ±0.05‰ for $\delta^{18}O$ and $\delta^{13}C$ respectively. To examine the reproducibility of the results duplicate measurements were made on 35 samples (5%), which indicate mean reproducibility better than ±0.12‰ and ±0.14‰ for $\delta^{18}O$ and $\delta^{13}C$, respectively. All isotope data are reported as per mil on the VPDB scale by reference to an internal laboratory working standard Keyworth carbonate marble (KCM). Reproducibility was further estimated from repeat measurements of KCM and was <0.1‰. All taxa and isotopic measurements for the U1338 samples are listed in Appendix A.

2.6 Trace metal/calcium ratio proxies in planktonic foraminifera

2.6.1 Mg/Ca

The elemental ratio of Mg to Ca in foraminiferal calcite is commonly used as a proxy for determining past ocean temperatures (Badger et al., 2013; Elderfield and Ganssen, 2000; Evans and Müller, 2012; Lear et al., 2000; Nürnberg et al., 1996; Rosenthal et al., 1997). The incorporation of Mg^{2+} into the calcite lattice of $CaCO_3$ (by substituting for the Ca^{2+} ion) is temperature dependent, i.e., requires energy in the form of heat for the reaction to proceed. Therefore with increasing water temperature, Mg content in calcite also increases (Chilingar, 1962; Katz, 1973). The temperature sensitivity of Mg uptake in foraminiferal calcite is in the order of 9% increase per 1°C rise in temperature (Elderfield and Ganssen, 2000; Lea et al., 1999; Nürnberg et al., 1996), but only 3% per 1°C increase in inorganic carbonate (Katz, 1973).

Since the $\delta^{18}O$ value of planktonic foraminiferal calcite is controlled by both sea surface temperature and the isotopic composition of the ambient seawater ($\delta^{18}O_{sw}$) (Rohling and Cooke, 2003), Mg/Ca in the same biotic carrier can be used to subtract the temperature effect on $\delta^{18}O$ in order to gain information on past sea water $\delta^{18}O$, which is directly related to variables like salinity and global continental ice volume (Elderfield and Ganssen, 2000; Groeneveld et al., 2008; Lear et al., 2000; Rosenthal et al., 2000).

2.6.2 Sr/Ca

Sr/Ca measurements are routinely obtained as a bi-product of Mg/Ca analysis and can be used to reconstruct long term changes in seawater Sr/Ca, reflecting relative changes in contributions from continental and hydrothermal sources (Graham et al., 1982; Lear et al., 2003), although other environmental factors such as seawater temperature, dissolution may also be important (Elderfield and Ganssen, 2000; Stoll and Schrag, 1998; Stoll et al., 1999).

2.6.3 Trace element cleaning procedure

We selected 25–35 specimens of *Globigerinoides quadrilobatus* (350–500 μg) from the 250–315 μm size fraction; the same species and size fraction as used for $\delta^{18}O$ analysis, to minimize size-related intraspecific elemental variation (Elderfield et al., 2002). The tests were gently crushed between two glass plates in order to open all chambers, and subsequently cleaned according to the protocol of Martin and Lea (2002) to remove clays. The foraminiferal fragments were rinsed 5 times with ultrapure water and twice with methanol, including ultrasonic treatment after each rinse.

For the removal of metal oxides, a cleaning solution was prepared consisting of 750 μl Hydrazine, 15 ml NH_4OH and 15 ml ammonium citrate. 100 μL of this solution was added to each vial, which were then placed in a hot water bath for 30 minutes briefly flipping and ultrasonicating every 2 minutes. The samples were then rinsed 3 times with ultrapure water. Next, in order to remove any organic matter, 250 μL of a

$NaOH/H_2O_2$ reagent (30 mL NaOH (analytical grade); 100 µL H_2O_2) was added, and the vials were placed in a hot water bath for 10 minutes briefly flipping and ultrasonicating twice. Remaining oxidizing solution was removed by three rinsing steps with ultrapure water. After transferring the samples into clean vials, a weak acid leach with 250 µL 0.001 M nitric acid (HNO_3, sub-boiled distilled) was applied with 30 seconds ultrasonic treatment, followed by two rinses with ultrapure water.

Finally, the samples were dissolved in 500 µL of 0.1 HNO_3, ultrasonicated for 25 minutes and then placed in a centrifuge for 2 minutes at 13.4 rpm. Samples were checked for smectite or ash and 400 uL of the supernatant was transferred to polypropylene tubes. Samples were finally diluted with 0.1 HNO_3 as follows:

If sample weight between:	Add:	Dilution factor
0.100-0.200mg	1200 µl HNO_3	3
0.200-0.500mg	1600 µl HNO_3	5
0.500-0.700mg	2000 µl HNO_3	6

Samples were measured on an ICP-AES device at Christian-Albrechts-Universität zu Kiel, Germany. Analytical error for Mg was ~0.45%, for Ca ~0.15%; Spectro CirosCCDSOP at fG, Kiel: Analytical error for Mg/Ca was ~0.1%). Replicate Mg/Ca measurements revealed an average standard deviation of ~0.1 mmol/mol and ~ 0.08 mol/mol, respectively (Appendix A, Table 2; Regenberg et al., 2006). Adequate cleaning is indicated by very low Fe/Ca and Mn/Ca ratios (Appendix B, Fig. 2).

The conversion of foraminiferal Mg/Ca ratios into SSTs was carried out by applying the multispecies calibration equation of Anand et al. (2003):

Eq. 2.5

$$SST = (log\ (Mg/Ca) - log\ 0.38) / 0.09$$

2.6.4 Uncertainties in Mg/Ca ratio analysis

The largest uncertainty in estimating Miocene palaeotemperature using Mg/Ca, relates to temporal variations in seawater Mg/Ca (Billups and Schrag, 2002; Lear et al., 2000). Hydrothermal alteration of basalts, variations in continental weathering rates, and changes in $CaCO_3$ sedimentation, all have the potential to alter seawater Mg/Ca (Lear et al., 2000; Lear et al., 2010), hence the long term evolution of Mg/Ca in seawater is poorly understood. Recent reconstructions based on modelling experiments and low resolution analyses of evaporite fluid inclusions have produced vastly differing results (Sime et al., 2007). However, oceanic Mg^{2+} and Ca^{2+} have long residence times of 13 Ma and 1 Ma respectively (Broecker et al., 1982), which suggests that while absolute values of SST's may be affected by changing water Mg/Ca, the magnitude of temperature change across rapid (<1 Ma) climate transitions should remain unchanged (Lear et al., 2010). Therefore, due to the limitations of current Mg/Ca_{sw} reconstructions, uncorrected SST values are presented in this study. The interpretations and conclusions are based on relatively short-term changes in planktonic $\delta^{18}O$ and SST, which occur on suborbital to orbital timescales and are beyond the temporal variability of $Mg/Ca_{sw.}$

Additionally, diagenetic alteration of foraminiferal tests after they have settled on the seafloor can significantly alter the Mg/Ca signature and palaeotemperature estimates (Barker et al., 2003; Lorens et al., 1977; Regenberg et al., 2007). The Mg/Ca values obtained from Site U1338 do not appear to be significantly altered by dissolution and the data appear to represent a primary signal. This is supported by the excellent preservation of the foraminifera as illustrated in Chapter 3, owing to the high clay content of the sediments from which the foraminifera were recovered, which helped to reduce the corrosiveness of pore waters and prevented post deposition diagenesis. Secondly, Middle Miocene Mg/Ca values and temperature estimates are realistic, when compared to present day.

2.7 Spectral analysis

In order to detect cyclic patterns in the isotope record and distinguish them from background noise, spectral analysis was carried out on the $\delta^{18}O$ and $\delta^{13}C$ records to test the palaeoclimatic series in the frequency domain. The Lomb-Scargle Fourier transform method (Lomb, 1976; Scargle, 1982) was initially used because the stable isotope record contains unevenly spaced data points due to fluctuations in the sedimentation rate and planktonic foraminiferal abundance (Pälike et al., 2010; Schulz, 2002). This method does not interpolate the data to an equal sample interval, which can bias results because data points become somewhat dependent after interpolation (Schulz and Stattegger, 1997).

Analysis was carried out using "PAST" software (Hammer et al., 2004). Spectral analysis (Lomb-Scargle Fourier transform method - REDFIT) was used to statistically test a null hypothesis of red (autocorrelated) noise in our data because red-noise backgrounds pose a particular problem in the analysis of palaeoclimate time series

(Schwarzacher, 1993). Statistical significance of spectral peaks was tested using a parametric approach (90%, 95%, and 99% false-alarm levels).

2.7.1 Wavelet analysis

In order to track the spectral characteristics and frequency behaviour in the time domain in more detail, wavelet analysis is also applied. Wavelet analysis provides a way to assess the presence and relative strength of orbital rhythms in stable isotope records, and to identify pivotal transitions in the global climate (Lau and Weng, 1995).

A wavelet is a function that represents a waveform where the oscillations die away to zero rather than going on indefinitely as in Fourier analysis (Graps, 1995). A finite domain allows wavelets to more accurately approximate sudden shifts in data, like that typical of $\delta^{18}O$ during warming and cooling events, and retains the spatial context of the data (Torrence and Compo, 1998).

The stable isotope data were interpolated to an equal interval (1 kyr) for wavelet analyses to detect non-stationary periodicities. Continuous wavelet analysis using a Morlet wavelet was applied to $\delta^{18}O$ and $\delta^{13}C$ to test time series in the frequency domain (Grossmann and Morlet, 1984; Morlet, 1983; Morlet et al., 1982; Torrence and Compo, 1998).

2.7.2 Cross Wavelet Transform

In palaeoclimate data, common features in wavelet power of two time series can occur, but at times can be mere coincidence (Maraun and Kurths, 2004). Cross Wavelet Transform (XWT) permits the detection of cross-magnitude, phase differences (= lag time), and coherency between signals from different palaeoclimate records that may exhibit large stratigraphic uncertainties and noise (Prokoph and El Bilali, 2008).

A cross wavelet transform of the planktonic data and benthic data (Holbourn et al., 2014) from Site U1338 was performed to identify and test the significance of common power, using the Cross Wavelet package in MatLab (Grinsted et al., 2004; Hudgins et al., 1993; Maraun and Kurths, 2004; Torrence and Compo, 1998). The phase arrows show the relative phasing of two time series under investigation. This can also be interpreted as a lead/lag.

Phase arrows pointing:

- right: in-phase

- left: anti-phase
- down: X leading Y by 90°
- up: Y leading X by 90°

It should be noted that interpreting the phase as a lead (/lag) should always be done with care. A lead of 90° can also be interpreted as a lag of 270° or a lag of 90° relative to the anti-phase (opposite sign) (Torrence and Compo, 1998).

3. Taxonomy of early-middle Miocene planktonic foraminifera from the equatorial Pacific Ocean

3.1 Introduction

The taxonomy of planktonic foraminifera is the foundation for understanding palaeoclimate proxy measurements. To reconstruct Miocene palaeoclimate records with any certainty, planktonic foraminifera must be analysed at the species level. Foraminifera are classified primarily on the composition and morphology of the test, i.e. chamber arrangement and aperture style. However, the test of individual planktonic foraminifera can be extremely variable and large collections of specimens are needed to understand the variation within a species. High-resolution scanning electron microscope (SEM) analyses of well-preserved planktonic foraminifera can reveal primary wall fabrics that have not previously been observed. Detailed taxonomic studies are critical to understanding the phylogeny and evolution of planktonic foraminifera through the Miocene. In this chapter well preserved early-middle Miocene planktonic foraminifera from Integrated Ocean Drilling Program (IODP) Site U1338 are illustrated through detailed SEM analysis, to document taxonomic variability, wall textures and provide insights into the phylogeny of extinct species. Furthermore, comparison of the preservation state at Site U1338 is made with specimens of planktonic foraminifera from the Brasso and Cipero Fm. type sections of Trinidad, West Indies, were many of the species illustrated in this chapter were first described.

3.1.1 Summary evolutionary history of the Miocene planktonic foraminifera

Morphospecies diversity of planktonic foraminifera increased in two phases during in the Miocene (Aze et al., 2011). The first was a gradual increase in diversity between 17–14 Ma with the proliferation of spinose *Globigerinoides* and smooth-walled, nonspinose globorotaliform species (Aze et al., 2011; Wei and Kennett, 1986). The second, much larger expansion occurred at the Miocene/Pliocene transition (7–4 Ma). After the evolution of major lineages in the middle Miocene (*Globigerinoides, Orbulina*, and *Globorotalia*), planktonic foraminiferal populations are structured like the modern with all the extant species or their direct ancestors present.

3.2 Classification of the foraminifera

3.2.1 Criteria for the classification of the foraminifera

The foraminifera are numerous and varied in their shell morphology and biology, making the task of compiling a single informative classification extremely difficult. Traditional foraminiferal classification is based almost exclusively on the characteristics of the test, primarily its chemical composition, ultrastructure, mode of formation, and mode of growth (continuous or periodic) (Loeblich and Tappan, 1992). Supraordinal classification is usually based on numerous combinations of a diverse range of morphological features including wall pores, wall passages, principal apertural features (separating superfamilies), free or fixed nature of the test, mode of chamber addition, simple or divided nature of the chamber interior and apertural modifications (separating families) (Loeblich and Tappan, 1987). Other factors, such as geological history, and some biological characters may also be taken into account (Loeblich and Tappan, 1987).

3.2.2 Current classification of the foraminifera

The classification revised in this chapter is a modified version of Loeblich and Tappan (1992), with morphological criteria taken from Kennett and Srinivasan (1983). Figure 1 shows the amended classification of the genera illustrated in this thesis. The Phylum Globigerinida, which represents the planktonic foraminifera, includes 3 superfamilies (the Heteroheilicacea, Globorotaliacea, and Globigerinacea), and 5 families (Globorotaliidae, Pulleniatinidae, Candeinidae, Globigerinidae, and Hastigerinidae).

ORDER: FORAMINIFERA

- Phylum: Globigerinida [Planktonic foraminifera]
  - Superfamily: Hererohelicacea] Non-spiral test
  - Superfamily: Globigerinacea
    - Family: Globigerinidae
      - Genus: *Clavatorella*
      - Genus: *Dentoglobigerina*
      - Genus: *Globigerinoides*
      - Genus: *Globoquadrina*
      - Genus: *Globorotaloides*
      - Genus: *Globoturborotalita*
      - Genus: *Paraglobotalia*
      - Genus: *Praeorbulina*
      - Genus: *Sphaeroidinellopsis*
    - Family: Pulleniatinidae
    - Family: Globorotaliidae
      - Genus: *Fohsella*
      - Genus: *Globorotalia*
    - Family: Hastigerinidae

    Macroperforate trochospiral or planispiral test
  - Superfamily: Candeinacea
    - Family: Globigerinitidae
      - Genus: *Globigerinatella*
      - Genus: *Globigerinita*
      - Genus: *Tenuitella*

    Microperforate trochospiral or planispiral or streptospiral test.

Figure 3. 1. Modified and abridged classification of Miocene planktonic foraminifera, based on the morphological characteristics of the test. Adapted from Loeblich & Tappan (1992). The families; Globigerinidae, Globorotaliidae, and Globigerinitidae, are expanded to show genera illustrated in this chapter.

3.3 Results

3.3.1 Foraminifera

All samples yielded abundant planktonic foraminifera; dominant genera included *Paragloborotalia* and *Globigerinoides*, with common *Dentoglobigerina.* Specimens of *Clavatorella bermudezi* were also unusually abundant. Using insights gained through SEM studies, the range charts for extinct taxa have been revised. *Globorotaloides hexagonus* and *Globorotaloides* sp. are commonly found in many of the middle Miocene samples. However, further work is required to constrain their biostratigraphic range. Light microscope and SEM investigation also allowed the identification of *Dentoglobigerina juxtabinaiensis* (Plates 4–5), a new species named in Fox and Wade (2013). Test preservation is excellent throughout the sampled interval, with open pore spaces, little calcitic overgrowth, and in many cases spines, though fragmentation occurs in some samples. Specimens show little evidence of diagenetic alteration in transmitted light, and their test walls are optically translucent (Plates 16–19).

3.3.2 *Dentoglobigerina juxtabinaiensis* (Fox & Wade, 2013)

Dentoglobigerina binaiensis is used as a secondary biostratigraphic marker within Zone M2 (Wade et al., 2011). However, four-chambered forms referred to as *Globoquadrina* cf. *binaiensis* were found at Sites U1337 and U1338 (Pälike et al., 2010). To retain the utility of *D. binaiensis* as a bioevent a strict species concept was applied and *D. binaiensis* was confined to the three chambered forms, consistent with the original description (Plate 2, Fig. 3a). This, therefore, necessitates describing the common four-chambered forms that are found in the early Miocene and earliest middle Miocene as a new species (Fox and Wade, 2013).

D. juxtabinaiensis is distinguished from its ancestor *D. binaiensis* by its greater number of chambers (4 rather than 3) in the final whorl, which are also more wedge shaped. It differs from *Globoquadrina dehiscens* by its more circular periphery and lack of umbilical shoulders. Specimens commonly show evidence of a broken ultimate chamber as seen in Plate 6, Figures 2 and 5. The lip is highly variable and can appear tooth-like in some specimens.

Spezzaferri (1994) recognised these forms as the more evolved *D. binaiensis* in the early Miocene from the eastern tropical Atlantic Ocean (Site 667) and equatorial Indian Ocean (Site 709). Chaisson and Leckie (1993) also distinguished between the three- and four-chambered specimens of *D. binaiensis* in their study from the western equatorial Pacific Ocean (Site 806). Significantly many of our specimens show evidence of spine holes, indicative of a spinose wall texture. Previously, *Dentoglobigerina* and *Globoquadrina* have been considered non-spinose (e.g., Pearson et al., 2006).

3.4 Discussion

3.4.1 Foraminiferal Assemblages

Fifty-five planktonic foraminiferal species were identified in this study and a range of specimens are illustrated in Plates 1–19. These Miocene planktonic foraminiferal assemblages are characterised by high occurrences of mixed-layer, warm-water taxa such as *Globigerinoides* and eutrophic, thermocline-dwelling taxa such as *Paragloborotalia* (Wade et al., 2007).

The range chart in Pälike et al. (2010) identifies several taxa which were absent in this study, including *Catapsydrax unicavus* (Bolli, 1957) and *Mutabella miriablis* (Pearson et al., 2001). Post-cruise SEM examination of wall textures revealed that specimens previously identified shipboard as *M. miriablis* are not microperforate, and many specimens of *Catpsydrax* may in fact be bullate *Dentoglobigerina tripartita*. The absence of primary marker species *Catapsydrax dissimilis* and *Globigerinatella* sp. prevented the differentiation between Zones M3 and M4. Zones M6 and M7 appear reduced due to the proximity of the lowest occurrence of marker species *Orbulina suturalis* (Bronnimann, 1954) and *Fohsella peripheroacuta*.

3.4.2 Preservation

After burial, the preservation of foraminiferal tests can be affected by a variety of diagenetic processes; these can be loosely categorised as dissolution, overgrowth, and recrystallisation, although the processes are interrelated. Foraminiferal tests are prone to diagenetic alteration by overgrowth, changes in the shell crystal structure at the micron scale, and/or infilling of the original shell, all of which can significantly affect their geochemical composition (Pearson and Burgess, 2008). Therefore, it is important to identify fossil material that is well-preserved.

Dissolution results from the action of migrating pore waters. The process begins by stripping the outer layers of calcite from the test, thus weakening and destroying the relatively thin, latest chambers first (Collen and Burgess, 1979). Partial dissolution or "etching" of test surfaces has been observed on a number of specimens of thin-walled *Clavatorella*, causing test surfaces that were originally smooth to appear roughened and pores to be enlarged. Species-specific fragmentation was also observed, resulting in chamber holes (e.g., Plates 13 and 16) and missing ultimate chambers (e.g., Plates 3–6, 9, and 10), which may explain the wide variation in test size of *Dentoglobigerina altispira*.

Overgrowth occurs when inorganic calcite crystals are precipitated from solution onto the outer or internal surface of the test, where they then progressively increase in size and merge (Pearson and Burgess, 2008). Overgrowths can obscure ornamentation and prevent identification; however, almost no overgrowth has been observed in the U1338 samples during this study, with the exception of some rare individual specimens exhibiting minor to moderate overgrowth.

Recrystallisation develops when the internal microgranular structure of the test is replaced by larger crystals (Pearson and Burgess, 2008). In contrast to glassy preservation in clay-rich facies, recrystallized specimens appear opaque in reflected light (Bown et al., 2008; Pearson et al., 2001; 2007). Tests also crumble much more easily under moderate compressive stress and they are less able to withstand ultrasonic cleaning (Pearson and Burgess, 2008).

Pearson and Burgess (2008) presented four criteria for distinguishing foraminiferal shells that are not significantly recrystallised: 1) shells should be glassy or translucent in reflected light; 2) ultrafine features such as spines should survive (e.g., Plate 10, Fig. 3c); 3) smooth parts of the shell such as the apertural lips, sutures, outer surface (in some species), and inner surface (in most species) should appear smooth at the submicron scale in high resolution SEM images (e.g., Plates 18, 20, 21); and 4) in cross-section, the original submicron microgranular wall texture should be clear when the shell is broken (Pl. 18, 19). The U1338 specimens from Hole A (Pl. 3–21) were recorded as having poor to moderate preservation during the expedition (Table 5.3); however, post-cruise studies found that preservation of foraminiferal tests (see Plates 18–21) satisfied criteria 2–4 of Pearson and Burgess (2008). The lithological transition at ~378 mcd from ooze to chalk has no obvious effect on preservation.

In Plates 20–23, Miocene aged specimens collected from the Cipero and Brasso Formations of Trinidad are illustrated for comparison. The preservation is extremely variable and although spines are preserved on some specimens (Pl 20, Fig. 5b), many exhibit overgrowth of pyrite crystals (Pl 20, Fig. 5, Pl 21, Fig. 6–7). In addition to SEM examination of whole specimens (Pl. 3-17), the wall structures of 4 crushed specimens (Pl. 16–19) were analysed, which indicate that foraminifera from Site U1338 have not undergone substantial recrystallisation. Previous studies of well-preserved calcareous microfossils have attributed excellent preservation to shallow burial depth and impermeable clay-rich facies that restricted pore water movement and post-depositional recrystallisation (Bown et al., 2008; Pearson et al., 2001). In contrast, these well-preserved specimens come from >400 m burial depth in low clay sediment, averaging ~90% combined $CaCO_3$ and SiO_2. Good preservation is rare in these conditions, and the preservation at Site U1338 is distinctly superior to nearby Site U1337. The enhanced preservation at Site U1338 is attributed to the relatively high sedimentation rates (30 m/Myr (Lyle et al., 2009) in comparison to a linear sedimentation rate of 17–21 m/Myr. during the middle Miocene at Site U1337 (Pälike et al., 2010).

These observations suggest that Site U1338 is ideal for the establishment of tropical sea-surface temperatures in the Miocene. Stable isotope studies presented in Chapter 4 provide a new eastern equatorial Pacific Ocean climate record for the middle Miocene that is of higher resolution than those currently in existence.

3.4.3 Diversity

The diversity of foraminiferal assemblages at Site U1338 is relatively high compared to Miocene sections drilled at other sites. Site 806 on the northeastern margin of the Ontong Java Plateau identified <45 species for the same interval (Chaisson and Leckie, 1993). In middle Miocene sediments at Site 1126 (western Great Australian Bight), <30 species were found, and planktonic foraminifera were rare and poorly preserved in sediments from shallower locations, especially Sites 1127, 1129, and 1131 (Li et al., 2003b). At Site U1337, a slightly higher diversity was recorded (58 species) over the same interval. However, assemblages are dominated by large dissolution-resistant forms such as *Dentoglobigerina venezuelana* (Pälike et al., 2010).

3.4.4 Biogeography and palaeoecology

In the modern ocean, upwelling of nutrient rich subsurface water in the equatorial Pacific Ocean sustains a band of high primary productivity, where distinctive planktonic foraminifera such as *Globigerinita glutinata* thrive (Cayre et al., 1999). The planktonic foraminiferal assemblages found in the Miocene sediments of Site U1338 can be compared with those that characterise present-day upwelling waters, due to the high abundance of *Globigerinoides ruber* and presence of *G. glutinata* and *G. menardii* (d' Orbigny, 1826) (Watkins et al., 1996, 1998).

3.5 Systematic palaeontology

The systematic descriptions in this study follow the existing understanding of early-middle Miocene planktonic foraminiferal taxonomy (Chaisson and Pearson, 1997; Chaisson and Leckie, 1993; Kennett and Srinivasan, 1983; Spezzaferri, 1994; Spezzaferri and Premoli Silva, 1991). The primary classification is based on the wall structure, and principally spinose or non-spinose ornamentation (Fleisher, 1974; Olsson et al., 1992).

In this study, all species are documented to provide a database of planktonic foraminiferal taxon ranges for the early–middle Miocene at Site U1338. The original reference for each species is given, as are subsequent references relevant to the progression toward the currently used species concept. Synonymies are limited to the original descriptions; additional references are included when needed to support the species concept. Taxa are listed alphabetically by genus and species name within individual families. Full systematic details are given for our new species.

The SEM images (Plates 1–19) illustrate the morphologic criteria that were used to distinguish between ancestral and descendant forms in some important lineages. In many instances, the individual images have been arranged “stratigraphically” on the figures to help illustrate size and morphologic changes between phylogenetically related species. Short comments are included in order to clarify the taxonomic concepts followed in this study and to note significant morphological features. IODP material is held at the University of Kiel, Germany, except for the type specimens of *D. juxtabinaiensis* held at the Natural History Museum, London.

Order FORAMINIFERIDA d'Orbigny, 1826

Superfamily GLOBIGERINACEAE Carpenter, Parker and Jones, 1862

Family GLOBIGERINIDAE Carpenter, Parker and Jones, 1862

Genus *Clavatorella* Blow, 1965

Type species: *Hastigerinella bermudezi* Bolli, 1957

Clavatorella bermudezi (Bolli, 1957)

Plate 1, Figures 1–6.

Hastigerinella bermudezi Bolli, 1957, p. 112, pl. 25, Figs. 1a–c.

Clavatorella bermudezi (Bolli). Kennett and Srinivasan, 1983, p. 218, pl. 54, Figs. 2, 6–8.

Stratigraphic range: U1338A-37X-CC → U1338C-39H-6, 140–142 cm.

Remarks: This species was found in only one core-catcher sample during shipboard studies (Pälike and others, 2010); however, during the examination of Holes B and C for this study, it was found present in most samples between U1338B-37H-4–U1338C-39H-4 (370–387 mcd). Specimens exhibit a broad spectrum of morphologic variation as demonstrated in Figure 3.

Genus *Dentoglobigerina* Blow, 1979

Type species: *Globigerina galavisi*, Bermudez, 1961

Dentoglobigerina altispira (Cushman and Jarvis, 1936)

Plate 2, Figures 1–6.

Globigerina altispira Cushman and Jarvis, 1936, p. 5, pl. 1, figs. 13a–c.

Dentoglobigerina altispira altispira (Cushman and Jarvis). Kennett and Srinivasan, 1983, p. 188, pl. 46, Figs. 4–6.

Dentoglobigerina altispira (Cushman and Jarvis). Chaisson and Leckie, 1993, p.177, pl. 9, Fig. 8.

Stratigraphic range: U1338A-5X-CC → U1338A-43X-2, 18–20 cm.

Remarks: This species is abundant in samples above U1338A-38X-CC. *Dentoglobigerina altispira* varies widely in test size, trochospire height, and chamber embracement. Spine holes were not evident on any specimens, suggesting this species is non-spinose or that a gametogenic crust prevents the identification of the spinose wall. All examined specimens exhibited fragmentation of the final chamber.

Dentoglobigerina baroemoenensis (LeRoy, 1939)
Plate 3, Figures 1–2.

Globigerina baroemoenensis LeRoy, 1939, p. 263, pl. 6, Figs. 1, 2.
Dentoglobigerina baroemoenensis (LeRoy). Kennett and Srinivasan, *1983,* p. 186, pl. 46, Figs. 1–3.

Stratigraphic range: U1338A-8H-5, 106–108 cm → U1338A-44X-3, 102–104 cm.
Remarks: Typical specimens exhibit a wide umbilicus and slightly flattened chambers, which increase rapidly in size in the final whorl. These features distinguish it from "*D.*" *venezuelana*, which has a more closed umbilicus and more embracing chambers.

Dentoglobigerina binaiensis (Koch, 1935)
Plate 3, Figures 3–4.

Globigerina binaiensis Koch, 1935, p. 558; Kennett and Srinivasan, 1983, p. 183, pl. 45, Figs. 1–3.
Globoquadrina binaiensis (Koch). Chaisson and Leckie, 1993, p. 159, pl. 9, Fig. 13; Spezzaferri, 1994, p. 42, pl. 42, Figs. 3a–c.

Stratigraphic range: U1338A-38X-2, 35–37 cm → U1338A-44X-CC.
Remarks: *Dentoglobigerina binaiensis* evolved from *D. sellii* in the latest Oligocene (Spezzaferri and Premoli Silva, 1990). It is distinguished by 3 chambers in the final whorl with a flattened, commonly pustulose apertural face. The final chamber is large and occupies about half of the test. It gave rise to *D. juxtabinaiensis* in the early Miocene.

Dentoglobigerina globosa (Bolli, 1957)
Plate 3, Figures 5–6.

Globoquadrina altispira subsp. *globosa* Bolli, 1957, p. 111, pl. 24, Figs. 9a–c, 10a–c.
Dentoglobigerina altispira globosa (Bolli). Kennett and Srinivasan, 1983 p. 189, pl. 46, Figs. 7–9.

Stratigraphic range: U1338A-7H-CC → U1338A-44X-CC.
Remarks: This species was present in most samples; *D. altispira* was distinguished from *D. globosa* by the higher number of chambers in the final whorl, with *D. altispira* possessing 4 and *D. globosa*, 5–6. The latter also differs in having more rounded chambers and a more circular outline compared to *D. altispira*, which is slightly lobate.

Dentoglobigerina juxtabinaiensis
Plate 4, Figures 1-5; Plate 6, Figures 1–6.

Globoquadrina dehiscens Chapman, Parr, and Collins. Chaisson and Leckie, 1993, pl. 9, Fig. 14. Not *Globoquadrina dehiscens* Chapman, Parr, and Collins, 1934, p. 569, pl. 11, Figs. 36a–c.
Globoquadrina binaiensis (Koch). Spezzaferri, 1994, p. 42, pl. 38, Figs. 1a–d, pl. 42, Figs. 4a–c.
Not *Globoquadrina binaiensis* (Koch). Chaisson and Leckie, 1993, p. 159, pl. 9, Fig. 13; Spezzaferri, 1994, p. 42, pl. 42, Figs. 3a–c.

Stratigraphic range: U1338A-38X-2, 35–37 cm → U1338A-44X-3, 102–104 cm. The highest occurrence is not currently well constrained. It is abundant up to Zone M5a at Site U1338, with intermittent occurrences to the top of Zone M5b (recorded as *Globoquadrina* cf. *binaiensis in* Pälike et al., 2010). The lowest occurrence is in Zone M2 at Site U1337.

Type specimens: Deposited in the Natural History Museum, London (NHMUK). Holotype: PM PF 70870 (Site U1337-42X-CC). Paratypes: PM PF 70871, 70872 (Site U1338B-41H-3, 30–32cm), 70873, 70875–70877 (Site U1338A-42X-CC), 70879, (Site

U1337A-38CX-CC), 70880 (Site U1337-42X-CC), 70874 (Site 871-15H-1, 124–126cm), and 70878, 70881 (Site 871-12H-2, 59–61cm).

Etymology: Derived from juxta referring to its close relationship to its ancestor *D. binaiensis*.

Description: "Test wall macroperforate, spinose; chambers arranged in a moderate trochospiral; test tightly coiled with 3 whorls, 4 chambers in the final whorl, increasing slowly then rapidly in size with the arched final chamber accounting for half of the test; peripheral outline rounded in umbilical and spiral view, semi-circular to major circular sectoral in edge view; chambers on umbilical side, wedge shaped, with final chamber semi-circular and flattened; dense and fused pustules concentrated around the periphery; sutures distinct, incised, straight to slightly curved; deep umbilical aperture bordered by a thin to broad lip, sometimes pustulose, with an imperforate area on the umbilical face; on spiral side chambers ovoid; sutures weakly depressed, curved." (Fox and Wade, 2013).

Remarks: D. juxtabinaiensis is distinguished from its ancestor *D. binaiensis* by its greater number of chambers (4 rather than 3) in the final whorl, which are also more wedge shaped. It differs from *G. dehiscens* by its more circular periphery and lack of umbilical shoulders. Specimens commonly show evidence of a broken ultimate chamber as seen in Plate 6, Figures 2 and 6. The lip is highly variable and can appear tooth-like in some specimens.

Significantly many of the specimens under investigation show evidence of spine holes, indicative of a spinose wall texture. Previously, *Dentoglobigerina* and *Globoquadrina* have been considered non-spinose (e.g., Pearson et al., 2006).

Phylogeny: Dentoglobigerina juxtabinaiensis evolved from *D. binaiensis* in the early Miocene by developing four chambers in the final whorl and a more open aperture.

Distribution: Probably restricted to low latitudes; known from the equatorial regions of the Indian Ocean, Atlantic Ocean (Spezzaferri, 1994), and Pacific Ocean (Chaisson and Leckie, 1993; this study).

Dentoglobigerina tripartita (Koch, 1926)
Plates 6, Figures 1–3.

Globigerina bulloides d'Orbigny var. *tripartita* Koch, 1926, p. 742, text-figs. 21a, b.
Globigerina tripartita Koch. Blow and Banner, 1962, p. 96, pl. 10, Figs. A–C (reillustrated holotype).
Dentoglobigerina tripartita (Koch). Pearson et al., 2006, p.409, pl. 13.3, Figs. 1–3 (reillustrated holotype), 4–8, 12, 13, 15, 16.

Stratigraphic range: U1338A-29X-2, 136–138 cm → U1338A-44X-CC.
Remarks: Dentoglobigerina tripartita is characterised by its large size, with three chambers in the final whorl. Specimens of *D. tripartita* commonly have pustules around the umbilicus and appear to intergrade with *Globoquadrina dehiscens*. Many specimens have a bulla of variable size. In Plate 6 three specimens are illustrated which appear very different morphologically but fit the taxonomic description of *D. tripartita* in Kennett and Srinivasan, (1983). The extensive morphological variability has also been noted by Leckie et al. (1993). *Catapsydrax unicavus* was recorded as abundant during shipboard studies at Site U1338 (Pälike et al., 2010), but post-cruise investigation suggests many of the forms are bullate *D. tripartita.*

***Dentoglobigerina* sp**.
Plate 7, Figure 4.

Stratigraphic range: U1338B-41H-3, 30–32 cm.
Remarks: Although referred to here as *Dentoglobigerina* sp., the specimen resembles *Dentoglobigerina* aff. *D. larmeui in* Spezzaferri and Premoli Silva (1991, pl. 17, Fig. 3).

"Dentoglobigerina" venezuelana (Hedberg, 1937)
Plate 6, Figures 4–6; Plate 11, Figure 4.

Globigerina venezuelana Hedberg, 1937, p. 681, pl. 92, Fig. 72b; Kennett and Srinivasan, 1983, p. 180, pl. 44, Figs. 5–7.

Stratigraphic range: U1338A-7H-CC → U1338A-44X-CC.

Remarks: This species is abundant in most samples. The shape of the chambers in the final whorl can vary noticeably from specimen to specimen. Stewart et al. (2012) separate "*D.*" *venezuelana* into three distinct morphotypes: 1) specimens with a kummerform, flattened, final chamber, and rectangular aperture; 2) individuals possessing kummerform, flattened, final chambers, and low arched (often asymmetrical) apertures; and 3) specimens with a large, embracing final chamber and rectangular aperture. The specimens illustrated here fall into the first and second categories. The specimen illustrated in Plate 11, Fig.4 is referred to as "*D.*" *venezuelana* but has been illustrated separately with other unusual specimens found in the U1338 samples on Plate 11.

Genus *Globigerinella* Cushman, 1927
Type species: *Globogerinella aequilateralis* Brady 1879

Globigerinella praesiphonifera (Blow, 1969)
Plate 9, Figure 1.

Hastigerina siphonifera praesiphonifera Blow, 1969, p. 408, pl. 54, Figs. 7–9.
Globigerinella praesiphonifera (Blow). Kennett and Srinivasan, 1983, p. 239, pl. 60, Figs. 4–6.

Stratigraphic range: U1338A-25H-CC → U1338A-40X-CC.
Remarks: This species is very rare. Only single specimens were found, appearing intermittently in samples throughout its range, many of which have spines preserved around the aperture (Plate 9, Fig. 1c).

Genus *Globigerinoides* Cushman, 1927
Type species: *Globigerina ruber* (d'Orbigny) 1839

Globigerinoides bisphericus Todd, 1954
Plate 10, Figure 1.

Globigerinoides bisphericus Todd, 1954, p. 681, pl. 1, Figs. 1a–c, 4; Jenkins and others, 1981, p. 265, pl. 1, Fig. 1a–c.

Stratigraphic range: U1338B-35H-5, 50–52 cm → U1338C-41H-4, 30–32 cm.

Remarks: Specimens of *Globigerinoides bisphericus* in many samples tend to grade toward *G. trilobus.* The former is distinguished by its more enveloping final chamber and more reduced umbilicus. Further work is required to constrain its stratigraphic range.

Globigerinoides diminutus Bolli, 1957

Plate 10, Figure 6.

Globigerinoides diminutus Bolli, 1957, p. 114, pl. 25, Figs. 11a–c; Kennett and Srinivasan, 1983, p. 74, pl. 16, Figs. 4–6.

Stratigraphic range: Presently unconstrained.

Remarks: Globigerinoides diminutus is smaller than *G. subquadratus* and has a distinctly more compact test. This small and easily recognisable species is abundant in the <150 µm fraction of the Site U1338 samples.

Globigerinoides* aff. *G. grilli Schmid, 1967

Plate 11, Figure 1.

Stratigraphic range: U1338B-42H-2, 40–42 cm.

Remarks. This specimen has a cancellate and spinose wall texture and possesses sutural apertures on the spiral side comparable to the type examples of *Globigerinoides grilli* illustrated by Schmid (1967). However, the illustrated specimen differs in having a high arched aperture and much lower trochospire.

Globigerinoides quadrilobatus (d'Orbigny, 1846)

Plate 9, Figure 4.

Globigerina quadrilobatus d'Orbigny, 1846, p.164, pl. 9, Figs. 7–10.

Globigerinoides quadrilobatus (d'Orbigny). Kennett and Srinivasan, 1983, p. 66, pl. 14, Figs. 1–3.

Stratigraphic range: U1338A-8H-2, 43–45 cm → U1338A-44X-3, 102–104 cm.

Remarks: Globigerinoides quadrilobatus is very common throughout its range at Site U1338, and many specimens were found with spines preserved around the primary aperture. This species is closely related to *G. sacculifer* (Brady, 1879), which differs from *G. quadrilobatus* in its stronger cancellate wall texture and possession of an elongate sack like terminal chamber. It is distinguished from *G. trilobus* by its greater number of chambers (4 rather than 3) in the final whorl.

***Globigerinoides* sp.**

Plate 9, Figure 2.

Stratigraphic range: U1338C-41H-4, 30–32 cm.

Remarks: *Globigerinoides* sp. appears intermittently in our samples, and further work is required to constrain its stratigraphic range. The test is small and compact in size with 3 high trochospiral whorls.

Globigerinoides subquadratus Brönnimann, 1954

Plate 9, Figure 3; Plate 20, Figure 6.

Globigerinoides subquadrata Brönnimann, 1954, p. 680, pl. 1, Figs. 8a–c.

Globigerinoides subquadratus Brönnimann. Kennett and Srinivasan, 1983, p. 74, pl. 16, Figs. 1–3.

Stratigraphic range: U1338C-39H-7, 40–42 cm → U1338A-42X-CC.

Remarks: Globigerinoides subquadratus is the most common species in the early Miocene samples. Specimens display a distinct rim around the primary aperture, and possess two or more supplementary apertures. Many specimens also have spines. Wall cross-sections are illustrated in Plate 18.

The extinction of *G. subquadratus* has previously been located within the *Globorotalia mayeri* Zone (M11). However, at Site U1338 this event is recorded in the far older planktonic foraminferal Zone M5b. A thickness of 23 m (~750 kyr) was measured between the last occurrence of *G. subquadratus* and the first occurrence of its homeomorph *G. ruber* (d'Orbigny, 1839). This non-overlapping interval has been mentioned by various authors (Blow, 1969; Bolli, 1957; Liska, 1985; Martinotti, 1990;

Stainforth et al., 1975), with the length of the interval varying between sites. Therefore, further high resolution biostratigraphic research is needed to determine the diachronism of this event.

***Globigerinoides trilobus* (Reuss, 1850)**
Plate 10, Figures 2–3, 5.

Globigerina triloba Reuss, 1850, p. 374, pl. 447, Figs. 11a–c.
Globigerinoides triloba triloba (Reuss). Bolli, 1957, p. 112, pl. 25, Figs. 2a-c; Blow, 1959, p. 187, pl. 11, Figs. 60a, b.
Globigerinoides trilobus (Reuss). Bermudez, 1961, p. 1244, pl. 12, Fig. 6; Kennett and Srinivasan, 1983, p. 62, pl. 13, Figs. 1–3.
Globigerinoides trilobus trilobus (Reuss). Gibson, 1983, p. 371, pl. 4, Fig. 12.

Stratigraphic range: U1338A-4H-5, 56–58 cm → U1338A-44X-3, 102–104 cm.
Remarks: Globigerinoides trilobus is common in most samples and abundant in samples U1338A-36X-1, 36–38 cm and U1338A-41X-4, 9–11 cm. The species is distinguished from all other *Globigerinoides* by its low arched slit-like primary and supplementary apertures. Typical specimens are coarsely cancellate and have a more compact test compared to *G. subquadratus* and *G. primordius*.

Genus *Globoquadrina* Finlay, 1947
Type species: *Globorotalia dehiscens* Chapman, Parr, and Collins, 1934

Globoquadrina dehiscens (Chapman, Parr, and Collins, 1934)
Plate 7, Figures 1–3.

Globorotalia dehiscens Chapman, Parr, and Collins, 1934, p. 569, pl. 11, Figs. 36a–c.
Globoquadrina dehiscens (Chapman, Parr, and Collins). Kennett and Srinivasan, 1983, p. 184, pl. 44, fig. 2, pl. 45, Figs. 7–9.

Stratigraphic range: U1338A-4H-5, 56–58 cm → U1338A-44X-CC.

Remarks: Globoquadrina dehiscens is characterised by its flattened umbilical face, pronounced umbilical shoulders, and “v”-shaped tooth. In spiral view, the early sutures are poorly incised. This species was common in most samples.

Genus *Globorotaloides* Bolli 1957
Type species: *Globorotaloides variabilis* Bolli, 1957

Globorotaloides* cf. *G. hexagonus (Natland, 1938)
Plate 11, Figure 2.

Globigerina hexagona Natland, 1938, p.149, pl. 7, Figs. 1a–c.
Globorotaloides hexagonus (Natland). Kennett and Srinivasan, 1983, p. 216, Figs. 1, 3, 5.

Stratigraphic range: U1338B-37H-6, 30–32 cm → U1338B-41H-3, 30-32 cm.
Remarks: This specimen possesses inflated globular chambers, slightly curved to radial sutures, and cancellate wall texture typical of *G. hexagonus*; however, it exhibits an unusually high trochospire and apertural tooth.

***Globorotaloides* sp**.
Plate 12, Figures 3–6.

Stratigraphic range: U1338B-37H-6, 30–32 cm → U1338C-39H-4, 140–142 cm.
Remarks: The genus *Globorotaloides* includes forms with a low trochospiral test, ovate to spherical chambers and cancellate wall texture. The spiral side of the specimen illustrated in Figure 14.3b is flattened, with radial sutures and rapidly increasing chamber size in the final whorl. Similar to Figure 14.5, its final chamber is much larger than the penultimate chamber and the aperture is bordered by an unusually large lip. The specimen illustrated in Plate 11, Fig. 4 also exhibits a pronounced lip, but has slightly curved sutures. It is more compact than the other illustrated specimens. The specimen illustrated in Plate 11, Fig. 6 has a low trochospire and a more open aperture bordered by a thin lip.

Genus *Globoturborotalita* Hofker, 1976

Type species: *Globigerina rubescens* Hofker, 1956

***Globoturborotalita* sp.**

Plate 11, Figure 3.

Stratigraphic range: U1338A-40X-1, 115–117cm → U1338A-40X-3, 27–29cm.

Remarks: This small form has a compact test, moderate trochospire, and subglobular chambers. In shape and size it is comparable to *Globoturborotalita rubescens* illustrated by (Li et al., 2003a), but is distinguished by its lower arched aperture which does not possess a lip.

Genus *Paragloborotalia* Cifelli, 1982

Type species: *Globorotalia opima opima*, Bolli, 1957

Paragloborotalia continuosa (Blow, 1959)

Plate 12, Figure 1.

Globorotalia opima continuosa Blow, 1959, p. 218, pl.19, Figs. 125a–c.

Globorotalia continuosa Blow. Bolli and Saunders, 1985, p. 204, Figs. 26.8–26.14.

Paragloborotalia continuosa Blow. Spezzaferri, 1994, p. 54, pl. 20, Figs. 7a–c.

Stratigraphic range: U1338A-26H-CC → U1338A-44X-CC.

Remarks: Paragloborotalia continuosa differs from *P. siakensis* in having a more subquadrangular profile with fewer chambers in the final whorl. Wall texture is cancellate and no spines were found on the studied specimens. The species is very rare throughout its range.

Paragloborotalia siakensis (LeRoy, 1939)

Plate 13, Figures 1–5: Plate 21.

Globorotalia siakensis LeRoy, 1939, p. 262, pl. 4, Figs. 20–22.

Globorotalia (Jenkinsella) siakensis LeRoy. Kennett and Srinivasan, 1983, p. 172, pl. 42, Figs. 1, 6–8.

Paragloborotalia siakensis (LeRoy). Zachariasse, 2012, Figs. 5.1–5.3, 6.1–6.13.

Stratigraphic range: U1338A-25H-6, 5–7 cm → U1338A-44X-CC.
Remarks: In many samples, *P. siakensis* was the dominant species and represented a large proportion of the assemblage. The Site U1338 specimens are consistent with new SEMs of the holotype in Zachariasse (2012). Plate 9 illustrates a well preserved specimen which has been broken to reveal the wall structure.

Genus *Praeorbulina* Olsson, 1964
Type species: *Globigerinoides glomerosa* subsp. g*lomerosa*, Blow, 1956

Praeorbulina circularis (Blow, 1956)
Plate 15, Figures 1–5.

Globigerinoides glomerosa circularis Blow, 1956, p. 64, Figs. 2.3, 2.4; Kennett and Srinivasan, 1983, p.85, pl. 19, Figs. 1–5.

Stratigraphic range: U1338A-37X-CC → U1338A-39X-2, 72–74 cm.
Remarks: Praeorbulina circularis is distinguished from its ancestor *P. glomorosa* by having numerous apertures along the basal sutures and a more circular outline. It differs from the closely related *Orbulina universa* (d'Orbigny, 1839) in having the earlier chambers of the test breaking the outline of the sphere. Maximum numbers of this species were found in Sample U1338C-36H-2, 110–112 cm, and it was very common in Sample U1338B-36H-2, 40–42 cm.

Genus *Sphaeroidinellopsis* Banner and Blow, 1959
Type species: *Globigerina seminulina* Schwager, 1866

Sphaeroidinellopsis disjuncta (Finlay, 1940)
Plate 15, Figures 6–8; Plate 19.

Sphaeroidinella disjuncta Finlay, 1940, p. 467, pl. 67, Figs. 224–228.
Sphaeroidinellopsis disjuncta (Finlay). Kennett and Srinivasan, 1983, p. 206, pl. 51, Figs. 3–5.

Stratigraphic range: U1338A-25H-6, 5–7 cm → U1338A-42X-4, 114–116 cm.

Remarks: *Sphaeroidinellopsis disjuncta* is a fairly persistent taxon throughout the middle Miocene sediments of Holes 1338B and C, and has intermittent bursts of high abundance in the middle Miocene. This species has a coarsely cancellate and thickened test wall, which can be observed in detail in Plate 17.

Family GLOBOROTALIIDAE Cushman, 1927

Genus *Fohsella* Bandy, 1972

Type species: *Globorotalia* (*Fohsella*) *praefohsi* Blow and Banner, 1966

Fohsella peripheroacuta (Blow and Banner, 1966)

Plate 14, Figure 3.

Globorotalia (*Turborotalia*) *peripheroacuta* Blow and Banner, 1966, p. 294, pl. 1, Figs. 2a–c.

Globorotalia (*Fohsella*) *peripheroacuta* Blow and Banner. Kennett and Srinivasan, 1983, p. 96, pl. 22, Figs. 4–6.

Globorotalia fohsi peripheroacuta Blow and Banner. Bolli and Saunders, 1985, p. 213, Figs. 29.5a–c, 29.13a–c.

Fohsella peripheroacuta (Blow and Banner). Pearson and Chaisson, 1997, p. 58.

Stratigraphic range: U1338C-35H-5, 90–92 cm → U1338B-36H-2, 40–42 cm.

Remarks: This species differs from *F. "praefohsi"* in being noncarinate, and from its ancestor *F. peripheroronda* by having a more angular peripheral margin.

Fohsella peripheroronda (Blow and Banner, 1966)

Plate 13, Figure 6.

Globorotalia (*Turborotalia*) *peripheroronda* Blow and Banner, 1966, p. 294, pl. 1, Figs. 1a–c.

Globorotalia (*Fohsella*) *peripheroronda* Blow and Banner. Kennett and Srinivasan, 1983, p. 96, pl. 22, Figs. 1–3.

Fohsella peripheroronda (Blow and Banner). Pearson and Chaisson, 1997, p. 58.

Stratigraphic range: U1338A-36X-1, 36–38 cm → U1338A-43X-CC.
Remarks: This species is found intermittently throughout its range and has low abundance in the few samples where it is observed. Specimens tend to have poorly incised sutures and 5–6 chambers in the final whorl. *Fohsella peripheroronda* has a round to subround peripheral margin compared with the keeled edge of *F. peripheroacuta.*

Genus *Globorotalia* Cushman and Stainforth, 1945
Type species *Pulvinulina menardii* var. *tumida* Brady, 1877

Globorotalia praemenardii Cushman and Stainforth, 1945
Plate 15, Figures 1–2, 4–6; Plate 16.

Globorotalia praemenardii Cushman and Stainforth, 1945, p. 70, pl. 13, Figs. 14a–c; Bolli and Saunders, 1985, p. 220, Figs. 32.7a–c; Chaisson and Leckie, 1993, p. 162, pl. 5, Figs. 12–14.
Globorotalia (Menardella) praemenardii Cushman and Stainforth. Kennett and Srinivasan, 1983, p. 122, pl. 28, Figs. 6–8.

Stratigraphc range: U1338A-11H-5, 65–67 cm → U1338C-35X-2, 9–11 cm.
Remarks: Globorotalia praemenardii was common in the uppermost samples from this section. The species is distinguished from its ancestor, *G. archeomenardii*, by being larger and possessing a peripheral keel, and from its descendent, *G. menardii*, by being smaller, more lobate, having a thinner keel, and having only five chambers in the final whorl. The wall structure is illustrated in detail on Plate 16.

Superfamily CANDEINACEA Cushman, 1927
Family GLOBIGERINITIDAE Bermudez, 1961
Genus *Globigerinatella* Cushman and Stainforth, 1945
Type species: *Globigerinatella insueta* Cushman and Stainforth, 1945

Globigerinatella insueta Cushman and Stainforth, 1945
Plate 8, Figures 1–2.

Globigerinatella insueta Cushman and Stainforth, 1945, p. 69, pl. 13, Figs. 7–9; Kennett and Srinivasan, 1983, p. 228, pl. 56, fig. 2, pl. 57, Figs. 4, 5.

Stratigraphic range: U1338A-38X-CC → U1338A-43X-CC.
Remarks: Globigerinatella insueta is found intermittently in samples from Site U1338. It differs from its ancestor *Globigerinatella* sp. in possessing numerous areal apertures bordered by a thick lip on one side of the large embracing final chamber (Pearson, 1995). This species is very similar in shape to *Praeorbulina* but is distinguished by its microperferorate wall texture, largely covered by small crystallites.

Genus *Globigerinita* Brönnimann, 1951
Type species: *Globigerinita naparimaensis,* Brönniman, 1951

Globigerinita glutinata (Egger, 1893)
Plate 8, Figures 5–7.

Globigerina glutinata Egger, 1893, p. 371, pl. 13, Figs. 19–21.
Globigerinita glutinata (Egger). Kennett and Srinivasan, 1983, p. 224, pl. 56, Figs. 1, 3–5.

Stratigraphic range: U1338A-1H-CC → U1338A-42X-2, 31–33 cm.
Remarks: This species was rare in most samples and many specimens lack bullae.

Globigerinita uvula (Ehrenberg, 1861)
Plate 8, Figs 3–4

Pylodexia uvula Ehrenberg, 1861, p. 276, pl. 2, figs. 24, 25.
Globigerinita uvula (Ehrenberg). Kennett and Srinivasan, 1983, p. 224, pl. 56, figs. 6–8.

Stratigraphic range: U1338A-24H-2, 50–52 cm → U1338A-44X-3, 102–104 cm.
Remarks: Globigerinita uvula is rarely seen in Holes U1338B and C; only two specimens were found in samples from Hole U1338A. This species is characterized by

its microperforate wall texture and high trochospire; the primary aperture is bordered by a thin lip.

Genus *Tenuitella* Fleisher, 1974

Type species: *Globorotalia gemma* (Jenkins, 1966)

Tenuitella munda (Jenkins, 1966)

Plate 12, Figure 2.

Globorotalia munda Jenkins, 1966, p. 1121, Fig. 14, nos. 126–133, pl. 13, nos. 152–156.

Globorotalia (*Tenuitella*) *munda* Jenkins. Kennett and Srinivasan, 1983, p. 162, pl. 39, Figs. 5–7.

Tenuitella munda (Jenkins). Li, 1987, p. 310, pl. 2, Fig. 13.

Stratigraphic range: U1338A-42X-4, 114–116cm → U1338A-44X-CC.

Remarks: *Tenuitella munda* was very rare and present in only two samples. This microperforate species is described in Kennett and Srinivasan (1983) as having subspherical chambers, but the specimens observed in the Site U1338 samples have moderately lobate ones. The wall texture is typically smooth, although pustules (Pl. 12, Fig. 2) surround the umbilical-extraumbilical aperture, which is bordered by a very thin lip.

PLATE 1

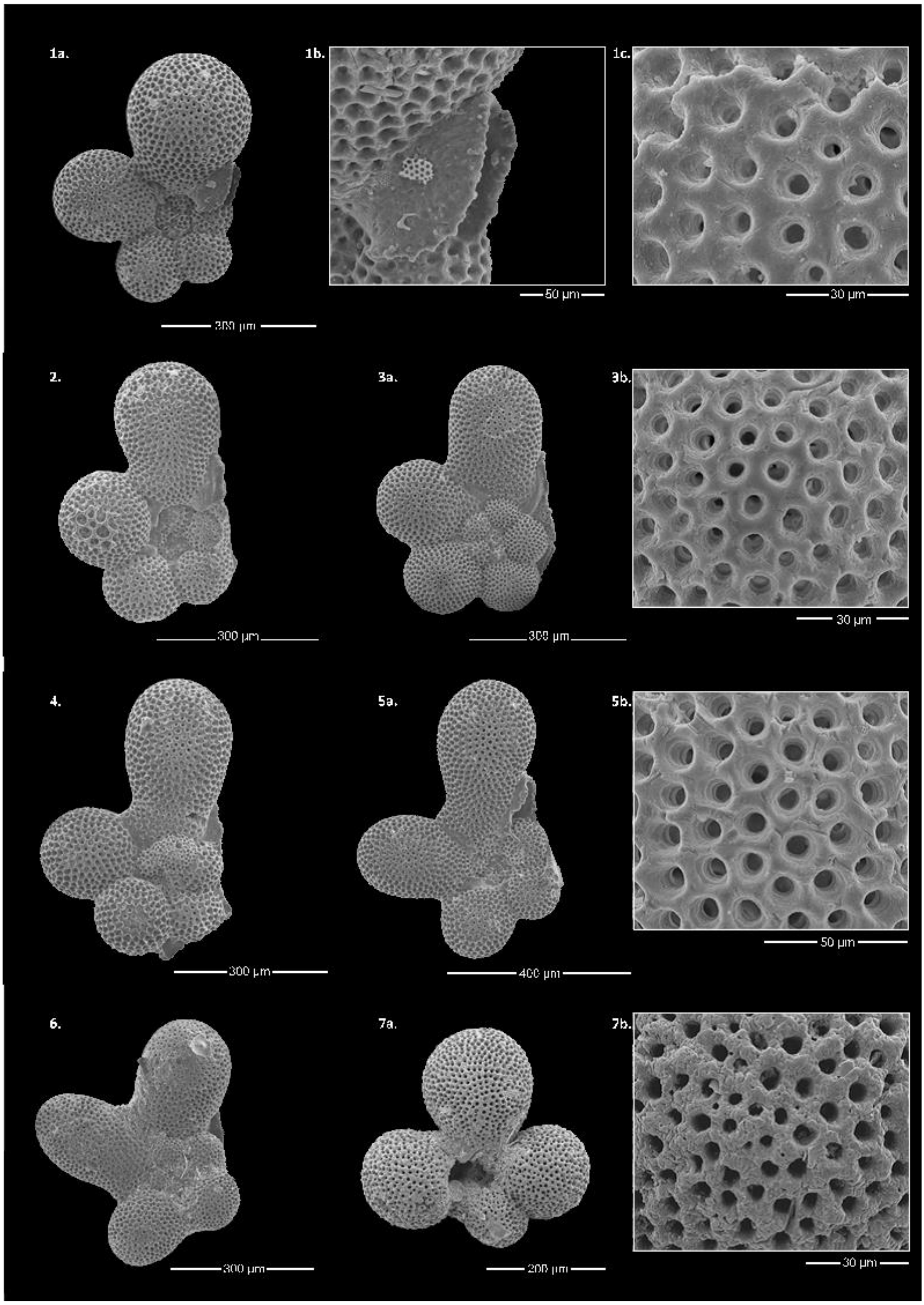

Plate 1, Figures 1–6. *Clavatorella bermudezi*, U1338C-39H-6, 140–142cm. 7 *Clavatorella* sp., U1338B-42H-2, 40–42cm.

PLATE 2

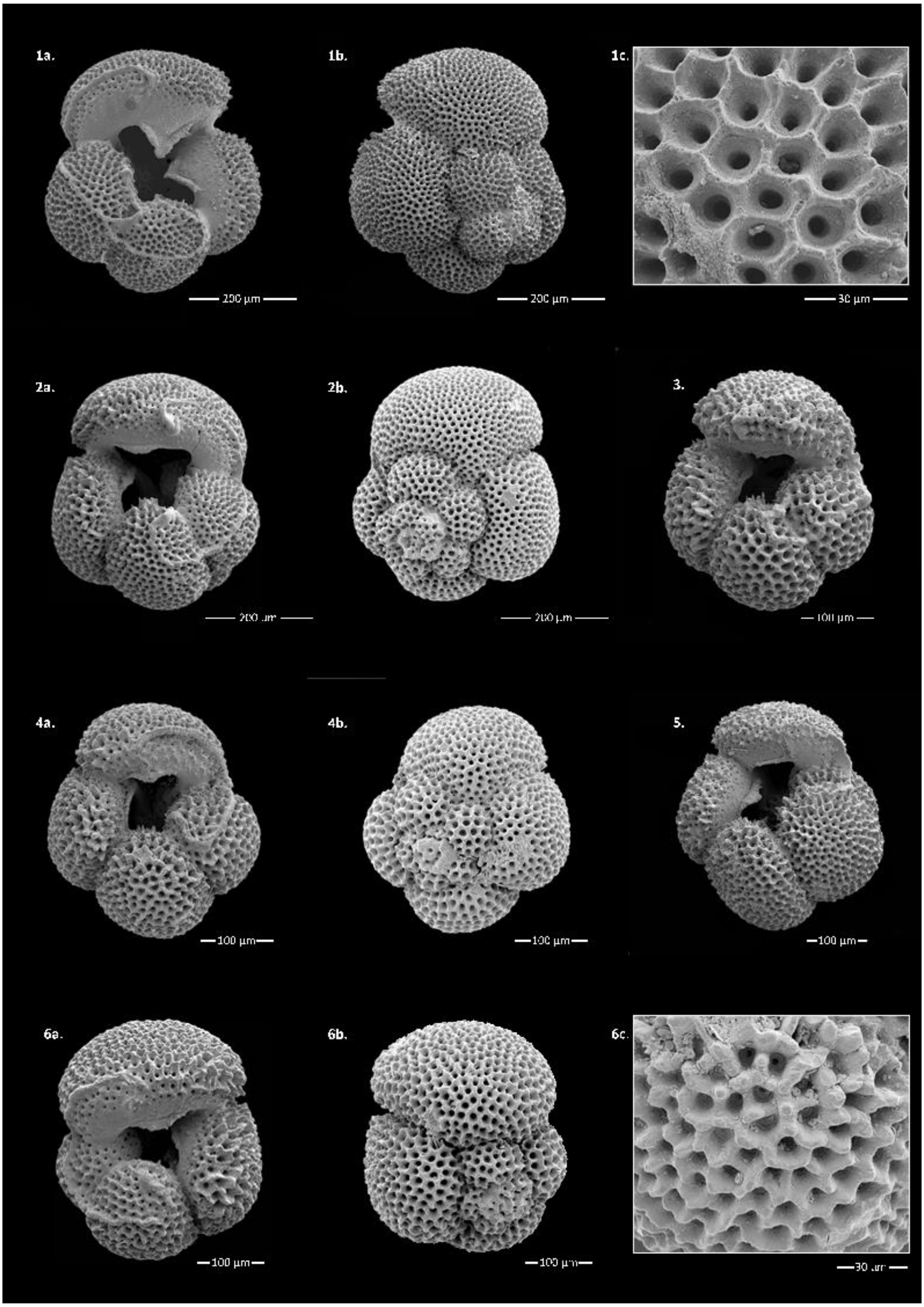

Plate 2, Figures 1–6. *Dentoglobigerina altispira*, U1338C-37H-1, 130–132cm.

PLATE 3

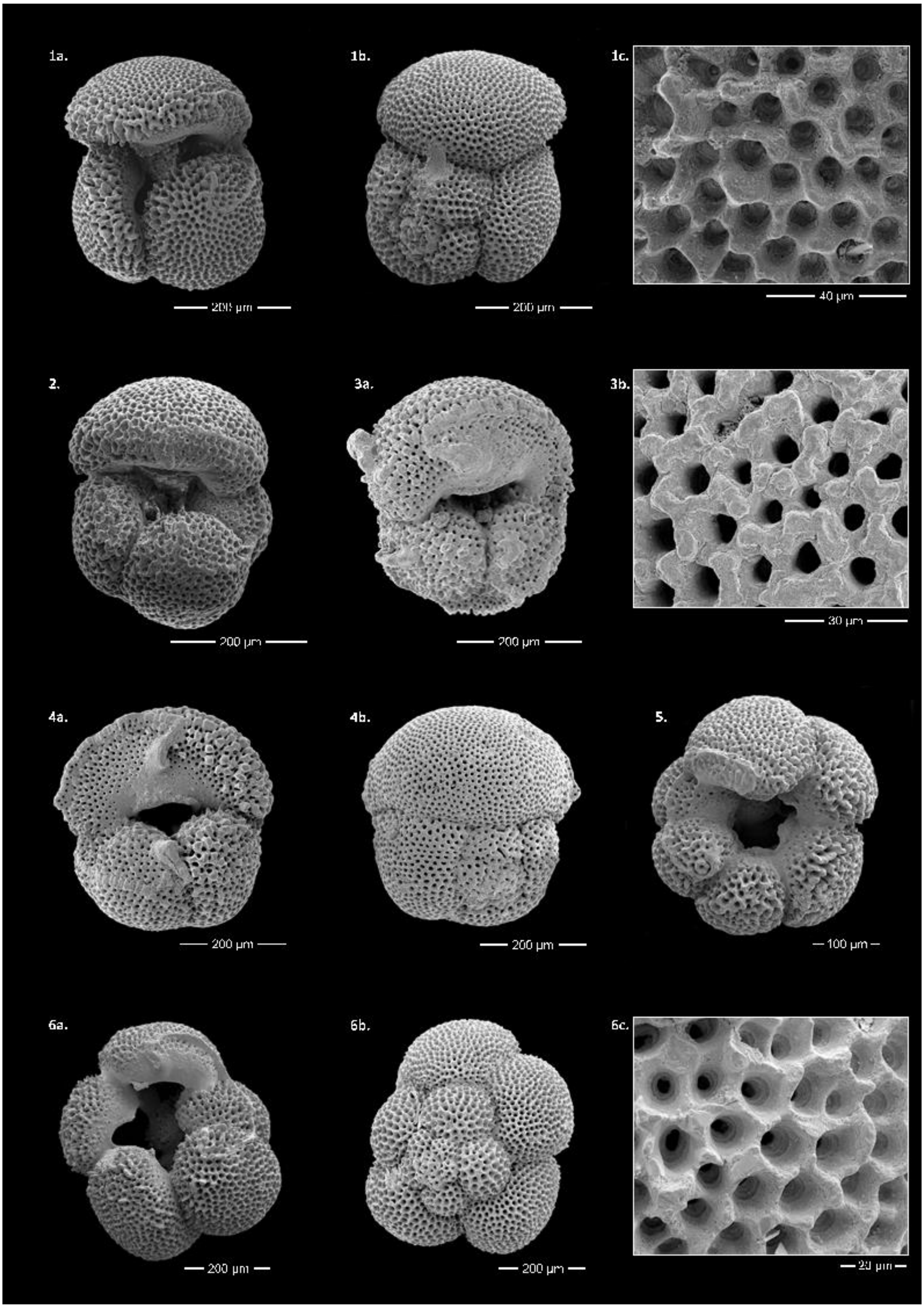

Plate 3, Figures 1, 2. *Dentoglobigerina baroemoenensis*, U1338B-41H-3, 30–32cm. **3**, **4** *Dentoglobigerina binaiensis*, U1338B-41H-3, 30–32cm. **5, 6** *Dentoglobigerina globosa*, U1338B-36H-2, 40–42cm.

PLATE 4

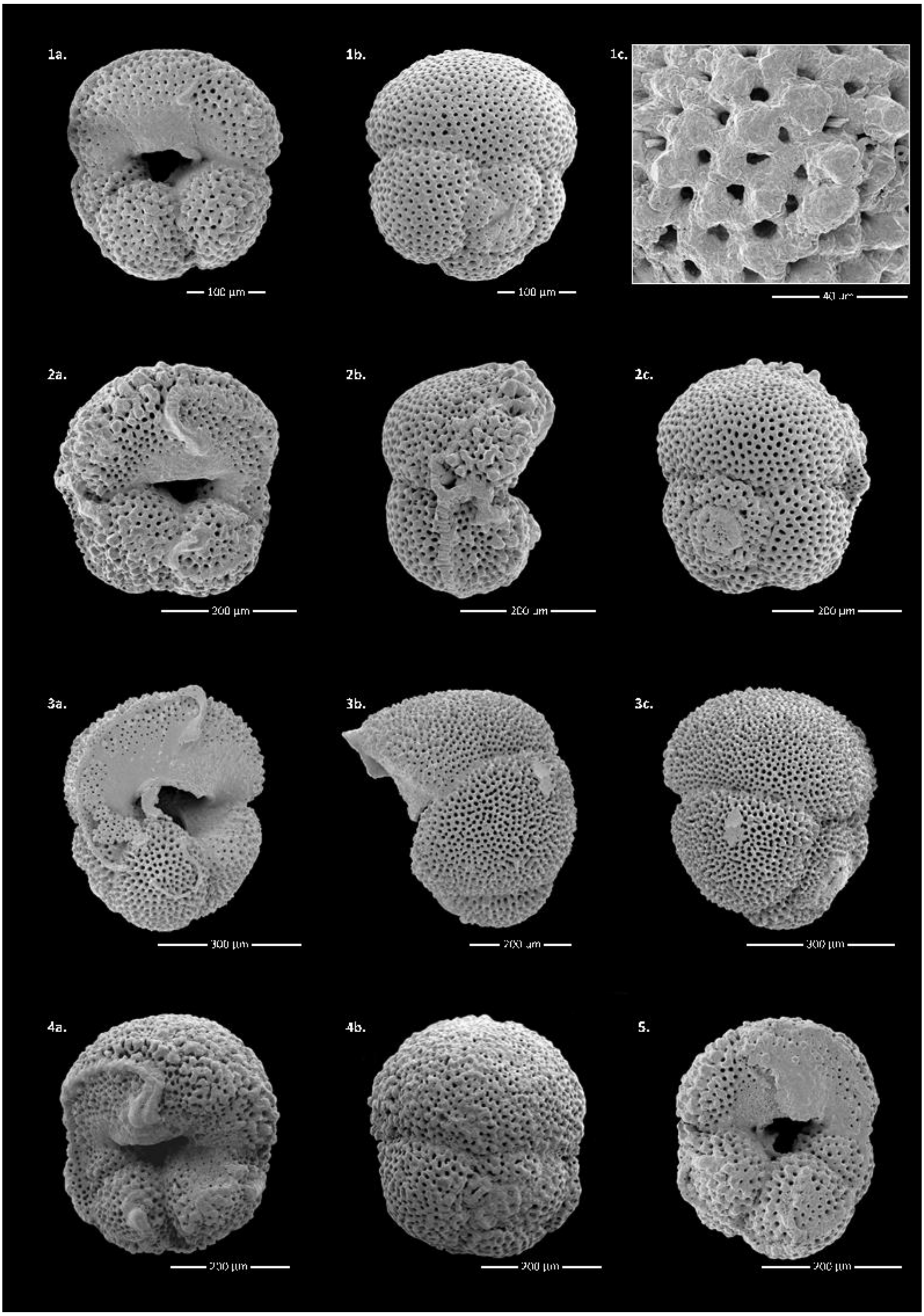

Plate 4, Figures 1–5. *Dentoglobigerina juxtabinaiensis* n. sp.: **1–3**, **5**, paratypes (NHMUK PM PF 70875–70877,70873), U1338A-42X-CC; **4**, paratype (70871), U1338B-41H-3, 30–32cm.

PLATE 5

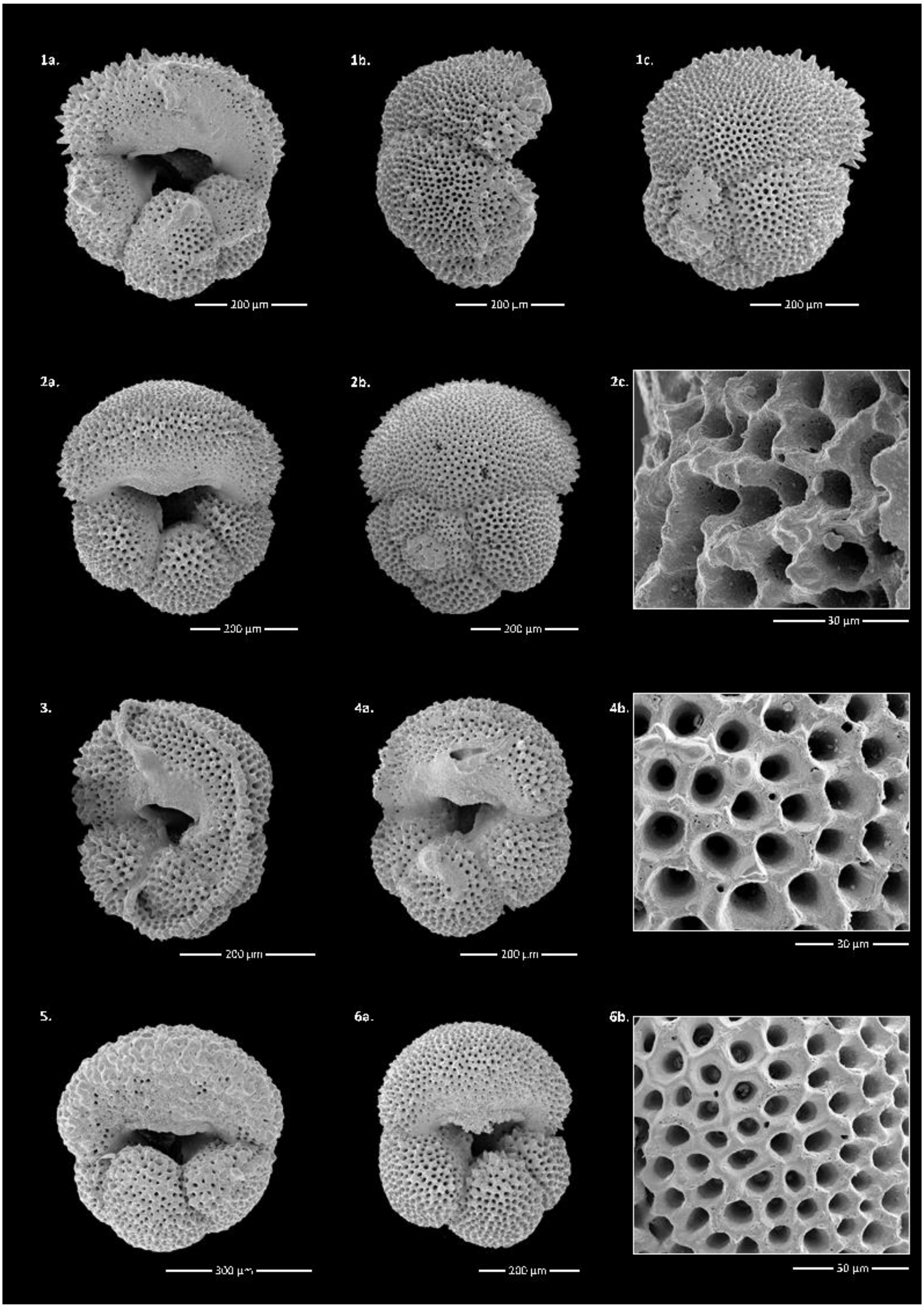

Plate 5, Figures 1–6. *Dentoglobigerina juxtabinaiensis* n. sp.: **1**, holotype (NHMUK PM PF 70870), U1337A-42X-CC; **2**, **6**, paratypes (70878, 70881), 871-12H-2, 59–61 cm; **3**, paratype (70879), U1337A-38X-CC; **4**, paratype (70874), 871-15H-1, 124–126 cm; **5**, paratype (70880),U1337A-42X-CC.

PLATE 6

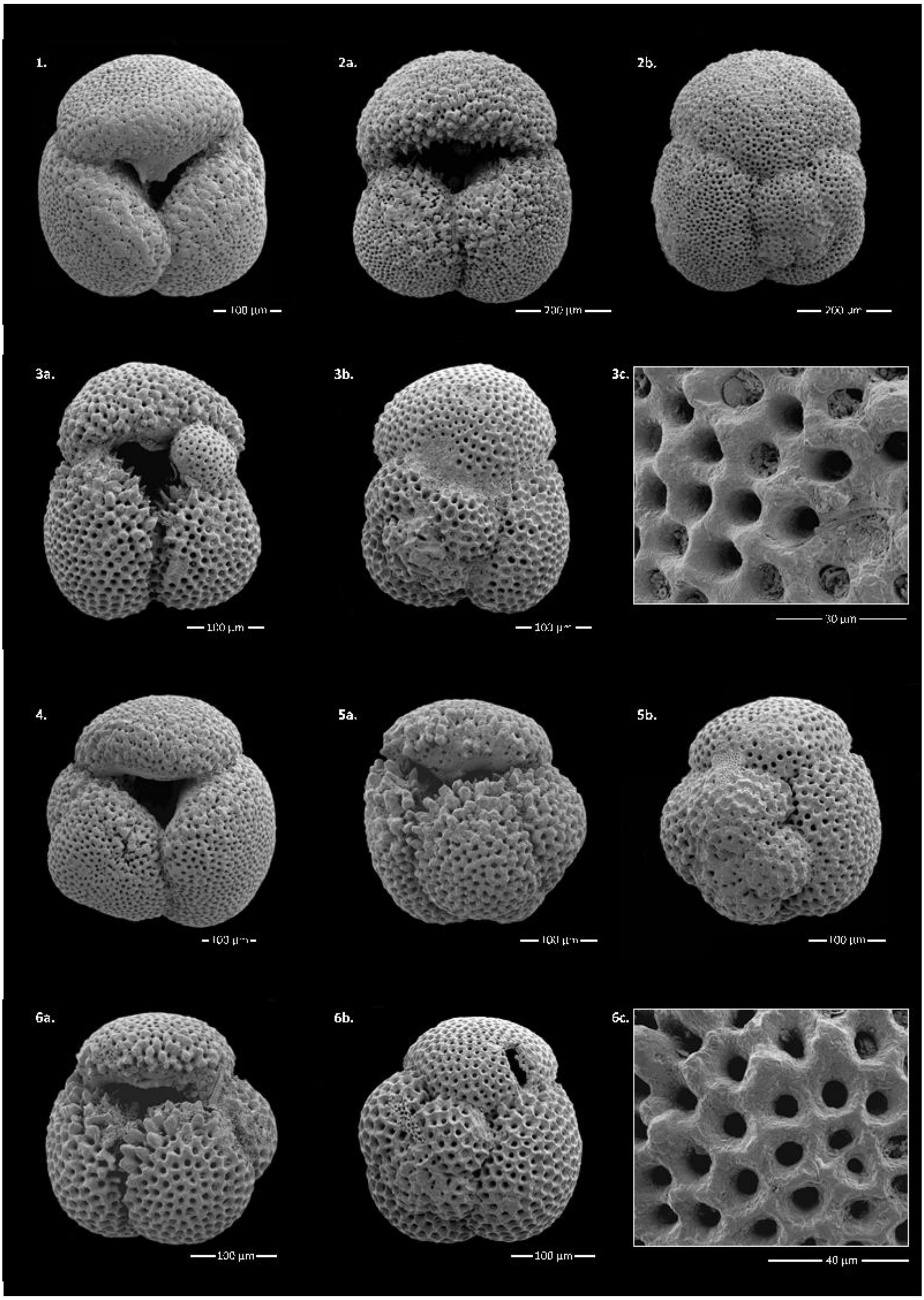

Plate 6, Figures 1–3. *Dentoglobigerina tripartita*, U1338B-36H-2, 40–42cm. **4–6** *''Dentoglobigerina'' venezuelana*, U1338B-41H-3, 30–32cm.

PLATE 7

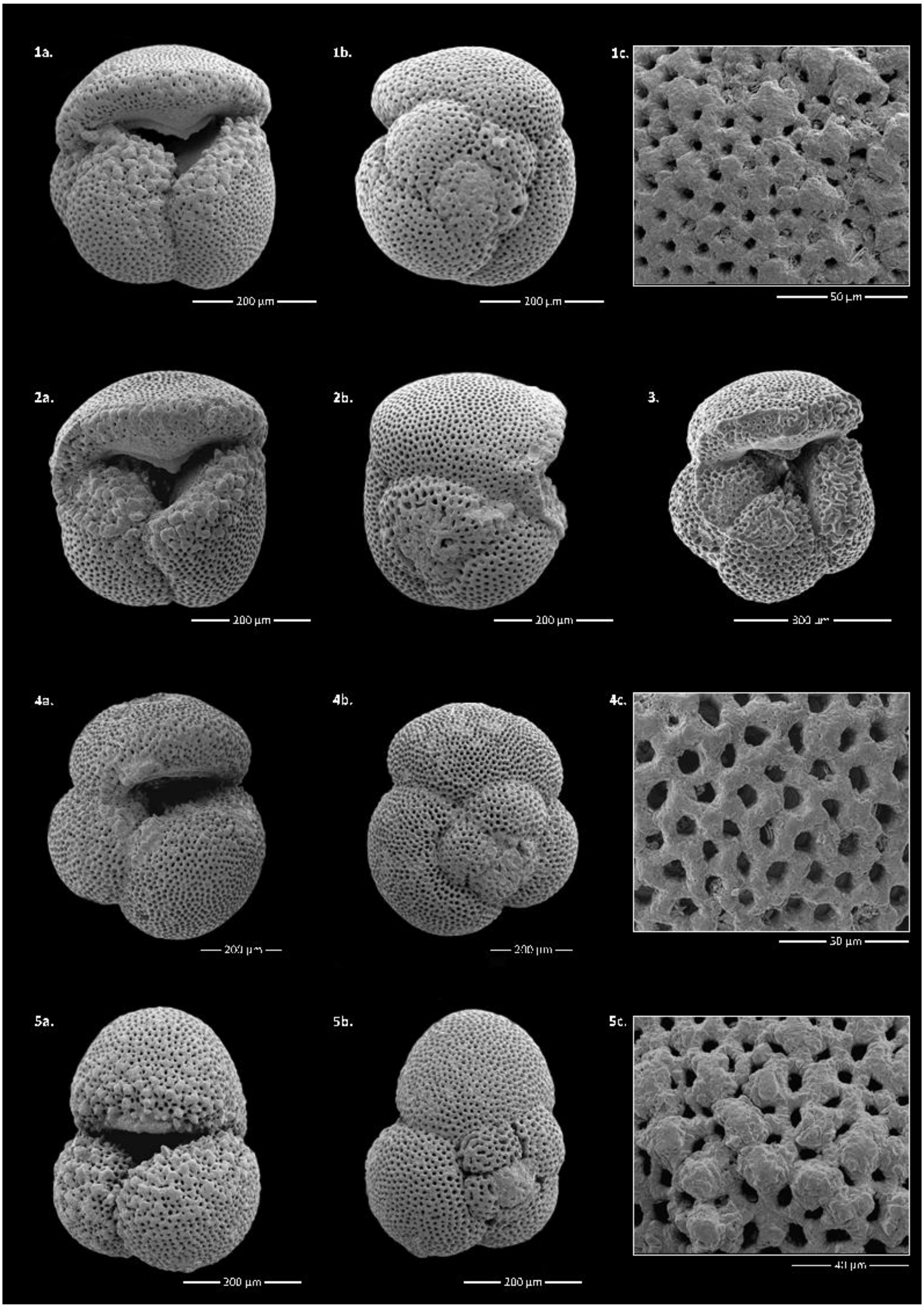

Plate 7, Figures 1–3. *Globoquadrina dehiscens*, U1338B-41H-4, 30–32cm. **4** *Dentoglobigerina* sp., U1338B-36H-2, 40–42cm. **5** *Sphaeroidinellopsis* sp., U1338B-41H-4, 30–32cm.

PLATE 8

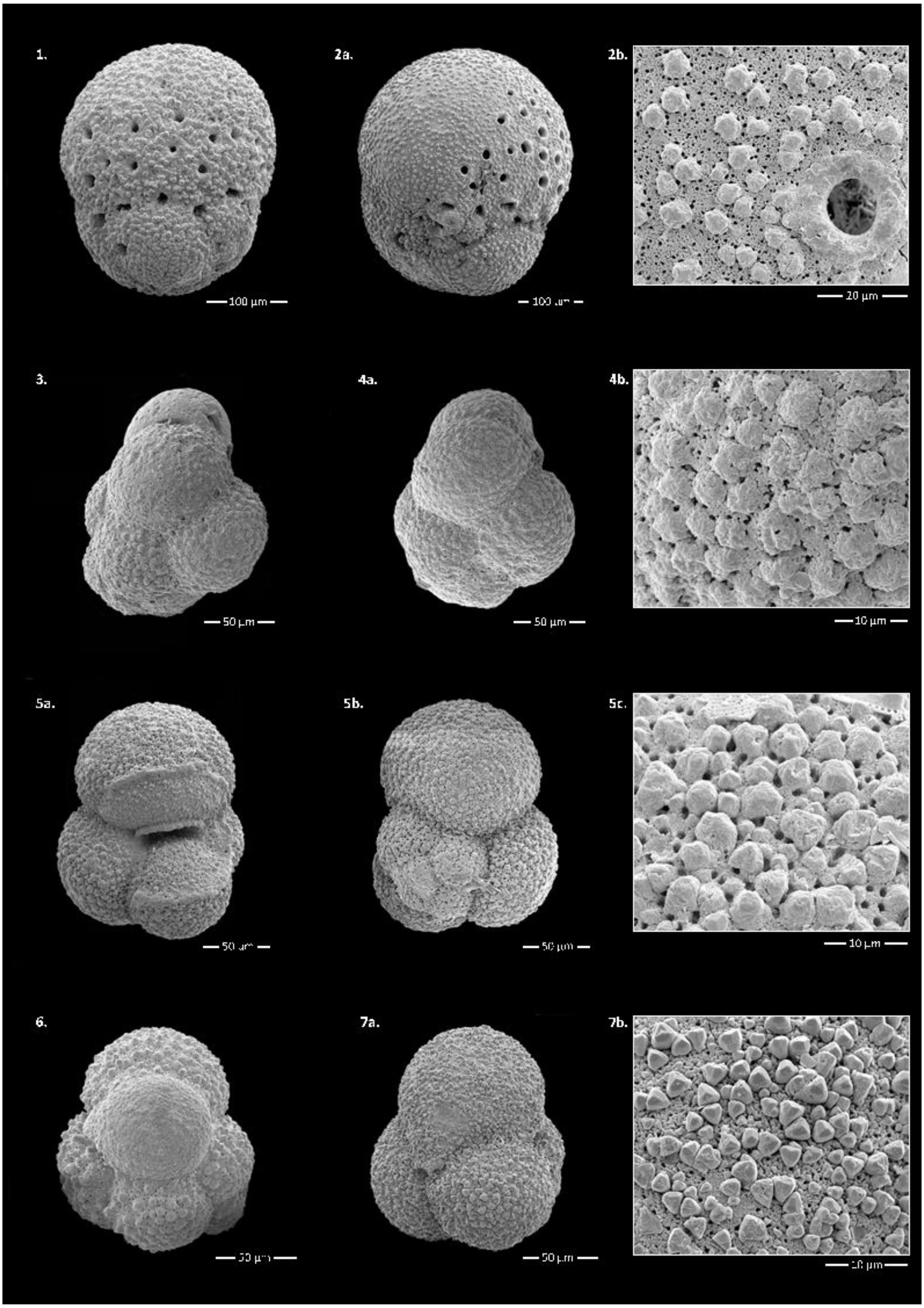

Plate 8, Figures 1, 2. *Globigerinatella insueta*, U1338B-41H-3, 30–32 cm. **3, 4** *Globigerinita uvula*, U1338A-44X-3. **5–7** *Globigerinita glutinata* U1338B-36H-2, 40–42 cm.

PLATE 9

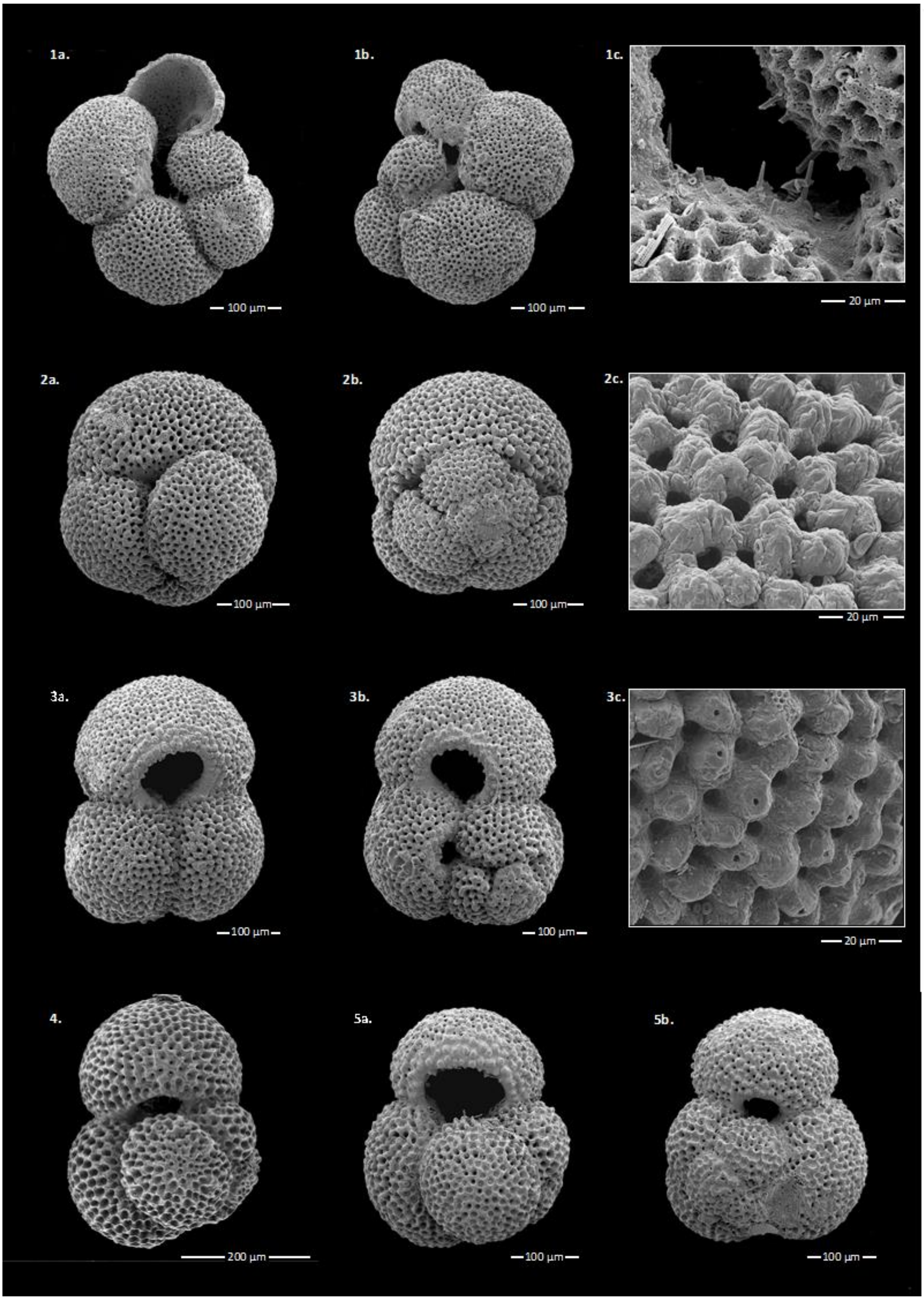

Plate 9, Figure 1. *Globigerinella praesiphonifera*, U1338B-42H-2, 40–42 cm. **2** *Globigerinoides* sp., U1338C-41H-4, 30–32 cm. **3** *Globigerinoides subquadratus*, U1338B-42H-2, 40–42 cm. **4** *Globigerinoides quadrilobatus*, U1338A-38X-CC. **5** *Globigerinoides* cf. *G. obliquus*, U1338-41H-4, 30–32 cm.

PLATE 10

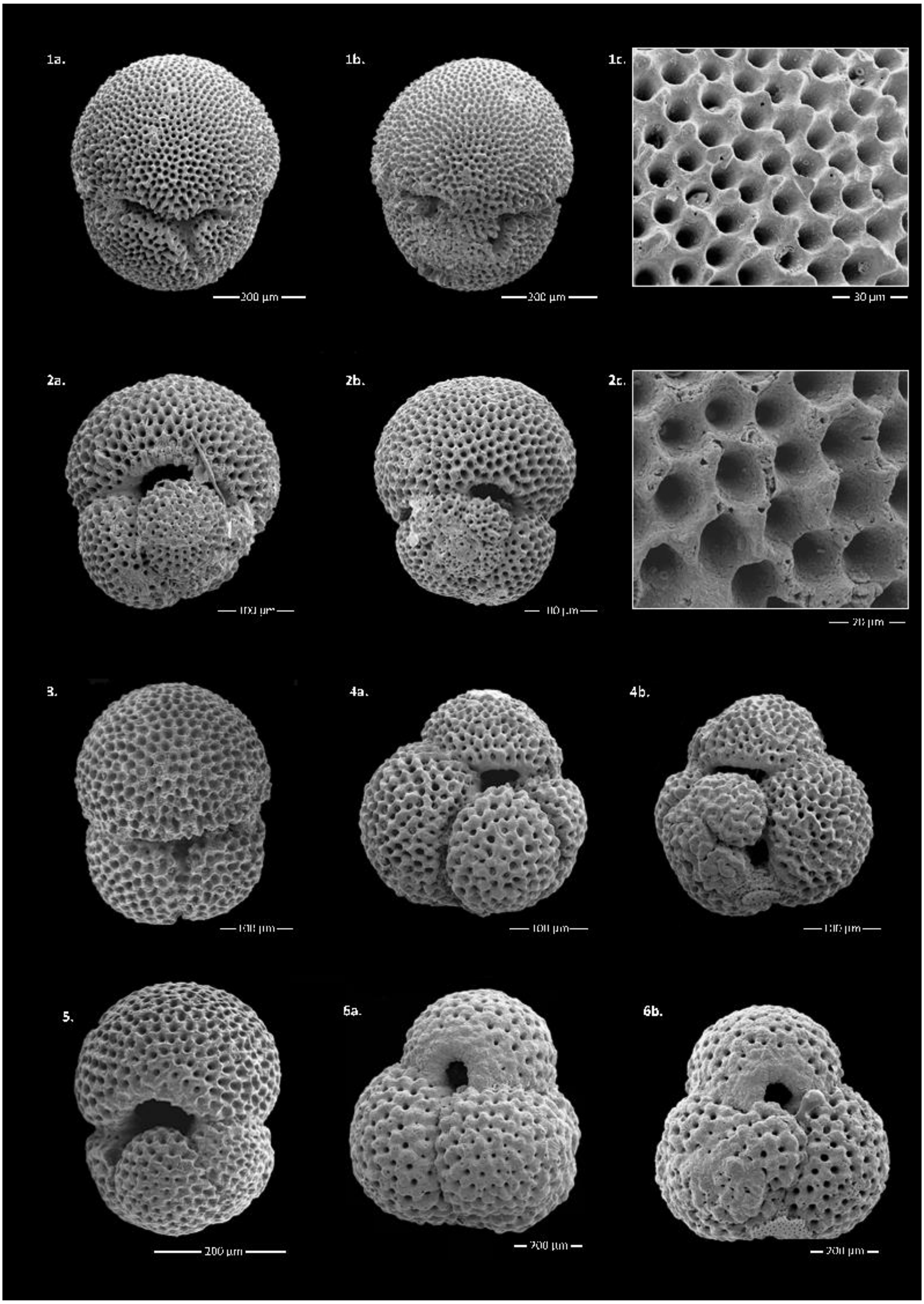

Plate 10, Figure 1 *Globigerinoides bisphericus*, U1338C-41H-4, 30–32cm. **2, 3** *Globigerinoides trilobus,* U1338C-41H-4, 30–32cm. **4** *Globigerinoide*s sp., U1338A-34X-2, 78–80cm, **5** *Globigerinoides trilobus*, U1338A-42X-CC. ***6*** *Globigerinoides diminitus*, U1338B-41H-4, 30–32cm.

PLATE 11

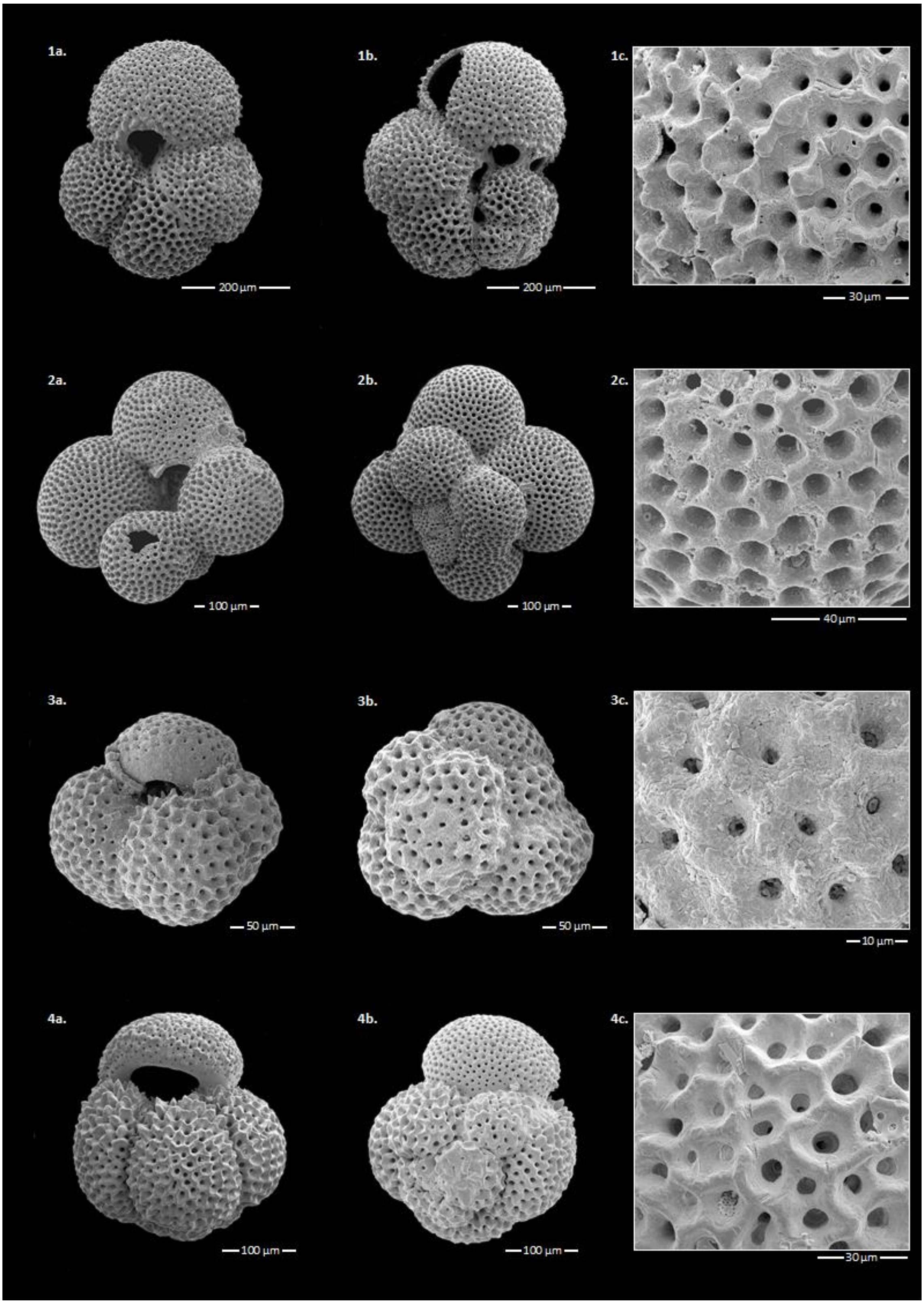

Plate 11, Figure 1 *Globigerinoides* aff. *G. grilli*, U1338B-42H-2, 40–42cm. **2** *Globorotaloides* cf. *G. hexagonus*, U1338B-41H-3, 30–32cm. **3** *Globoturborotalita* sp., U1338A-40X-2, 78–80cm. **4** *''Dentoglobigerina'' venezuelana*, U1338B-41H-4, 30–32cm.

PLATE 12

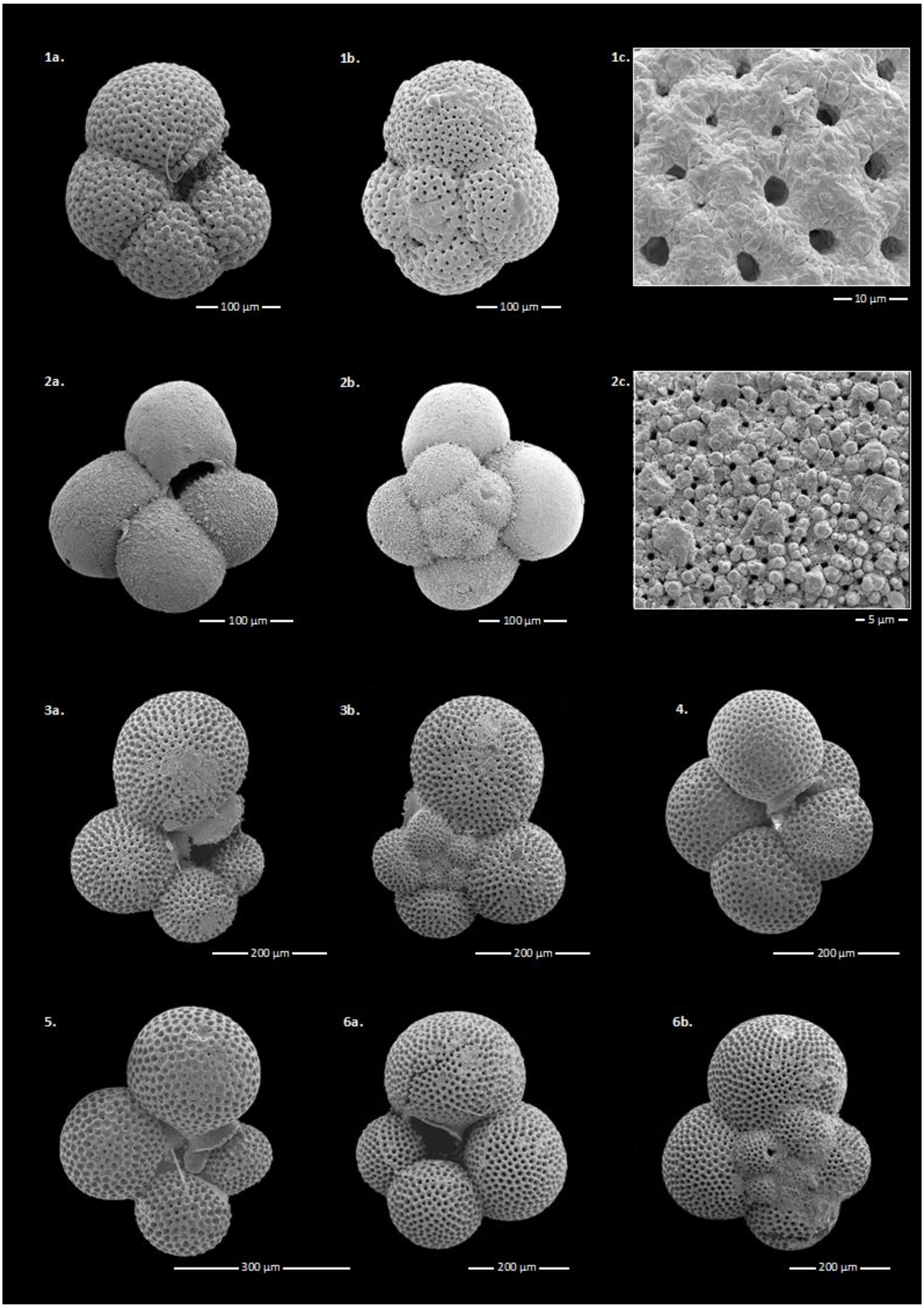

Plate 12, Figure 1. *Paragoborotalia continuosa*, U1338B-41H-4, 30–32cm. **2** *Tenuitella munda* U1338B-38H-5, 20–22cm. **3–6** *Globorotaloides* sp., U1338B-38H-4, 0–2 cm.

PLATE 13

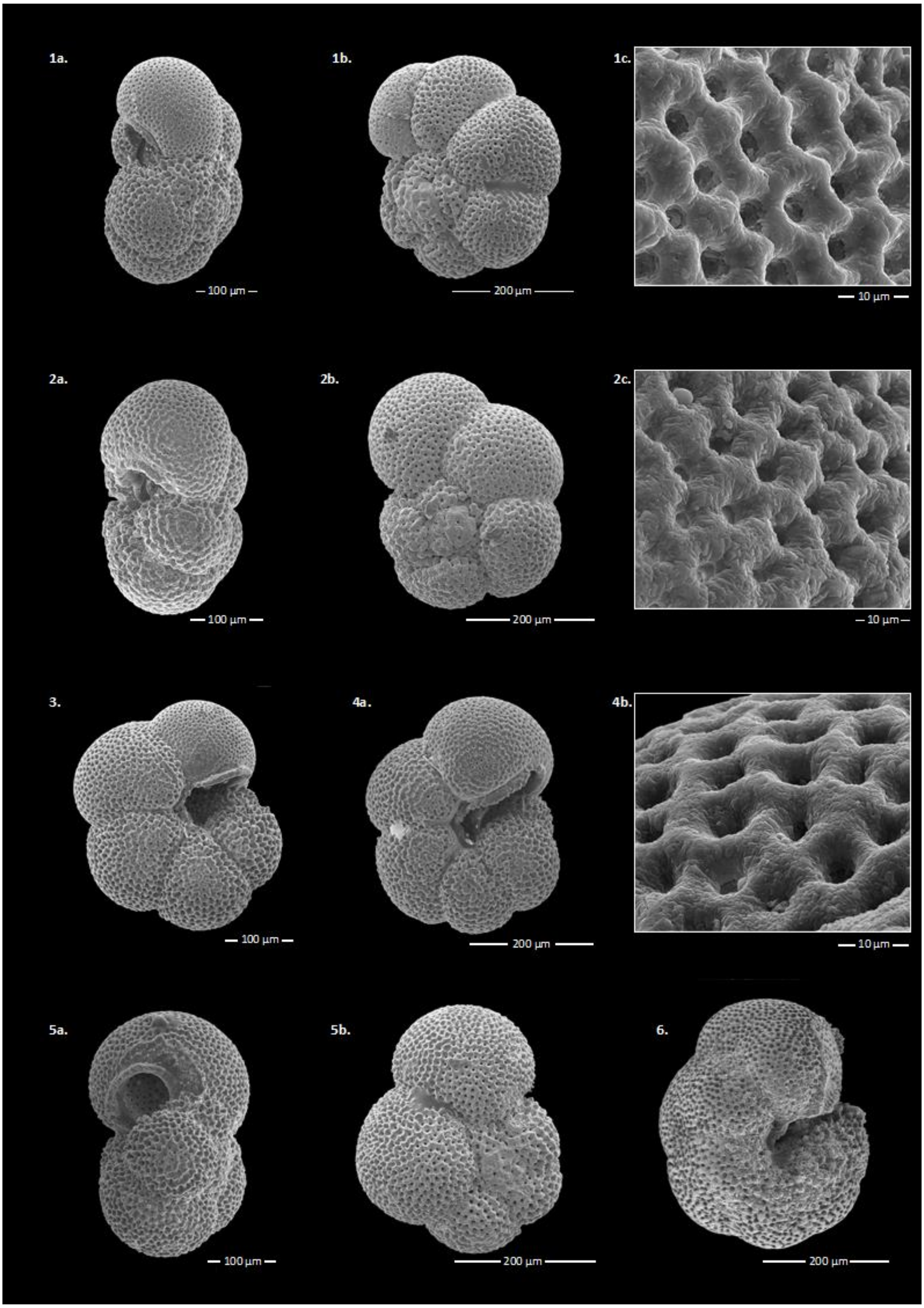

Plate 13, Figures 1–5. *Paragloborotalia siakensis*, U1338C-37H-4, 130–132cm. **6** *Fohsella peripheroronda*, U1338A-38X-CC.

PLATE 14

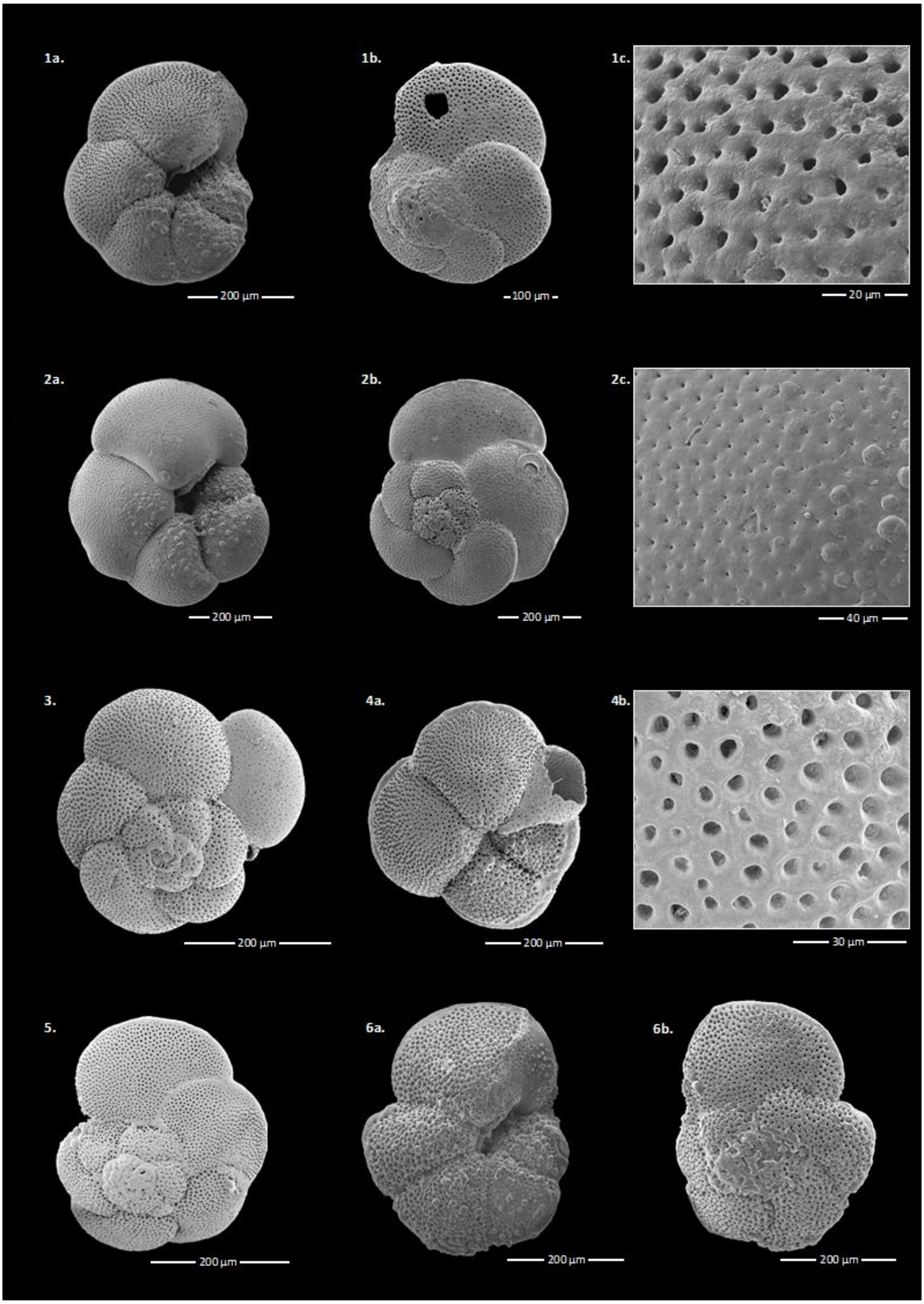

Plate 14, Figures 1, 2, 4–6 *Globorotalia praemenardii*, U1338C-35H-5, 90–92cm. **3** *Fohsella peripheroacuta* U1338B-36H-2, 30–32cm.

PLATE 15

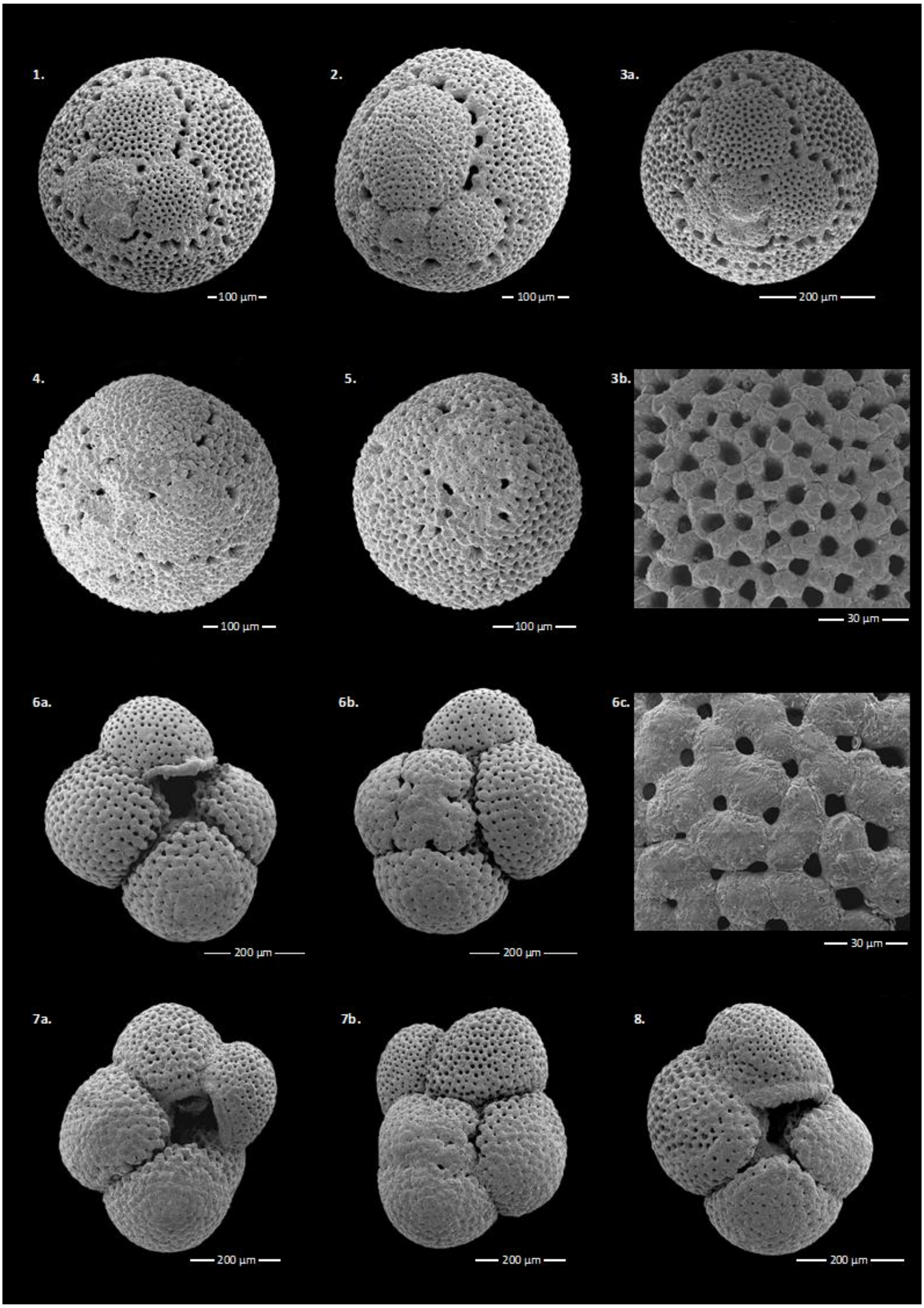

Plate 15, Figures. 1–5 *Praeorbulina circularis*, U1338B-42H-2, 40–42 cm. **6–8** *Sphaeroidinellopsis disjuncta*, U1338C-35H-5, 90–92 cm.

PLATE 16

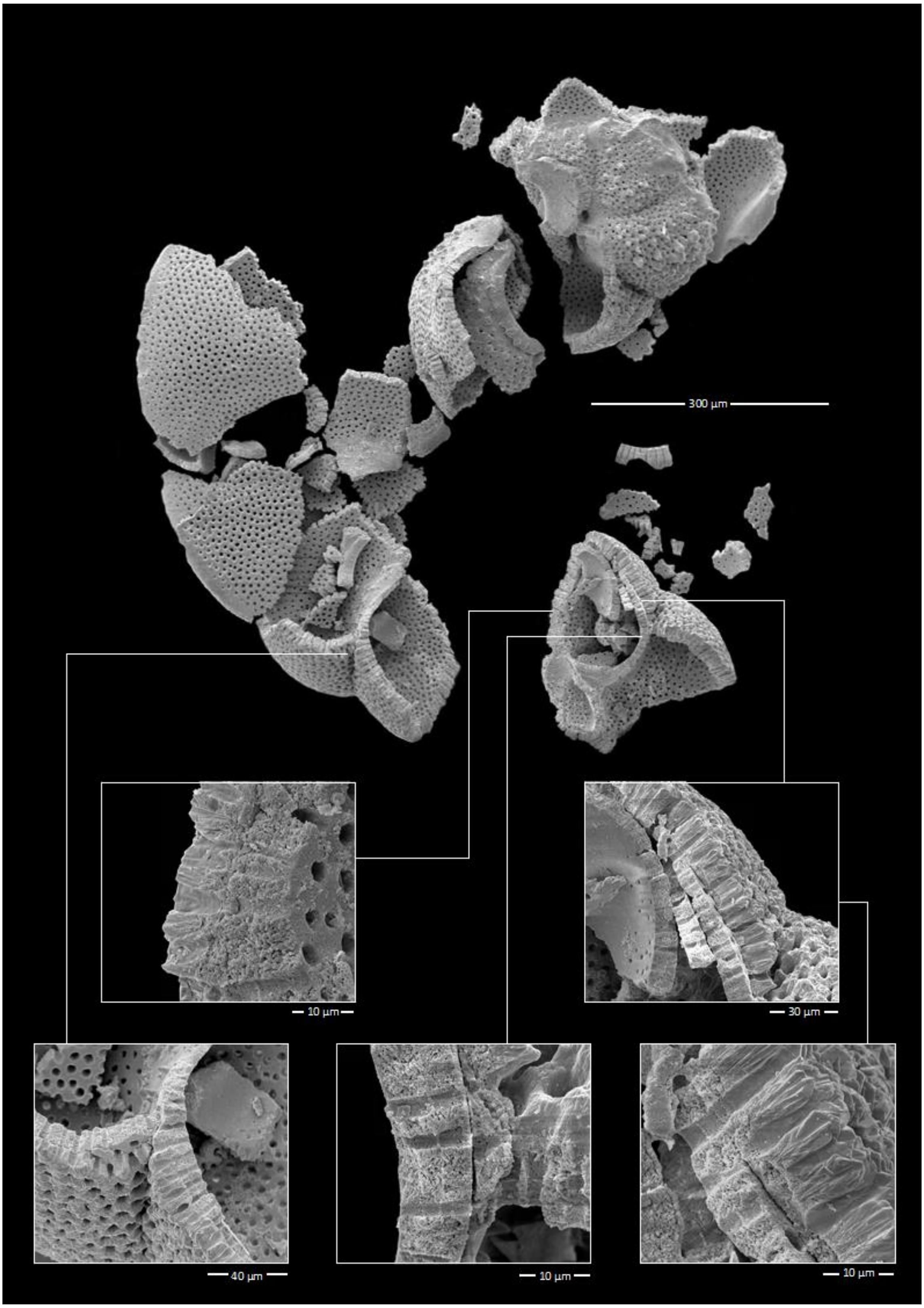

Plate 16. *Globorotalia praemenardii*, U1338B-36H-2, 30–32 cm; test broken to reveal wall structure.

PLATE 17

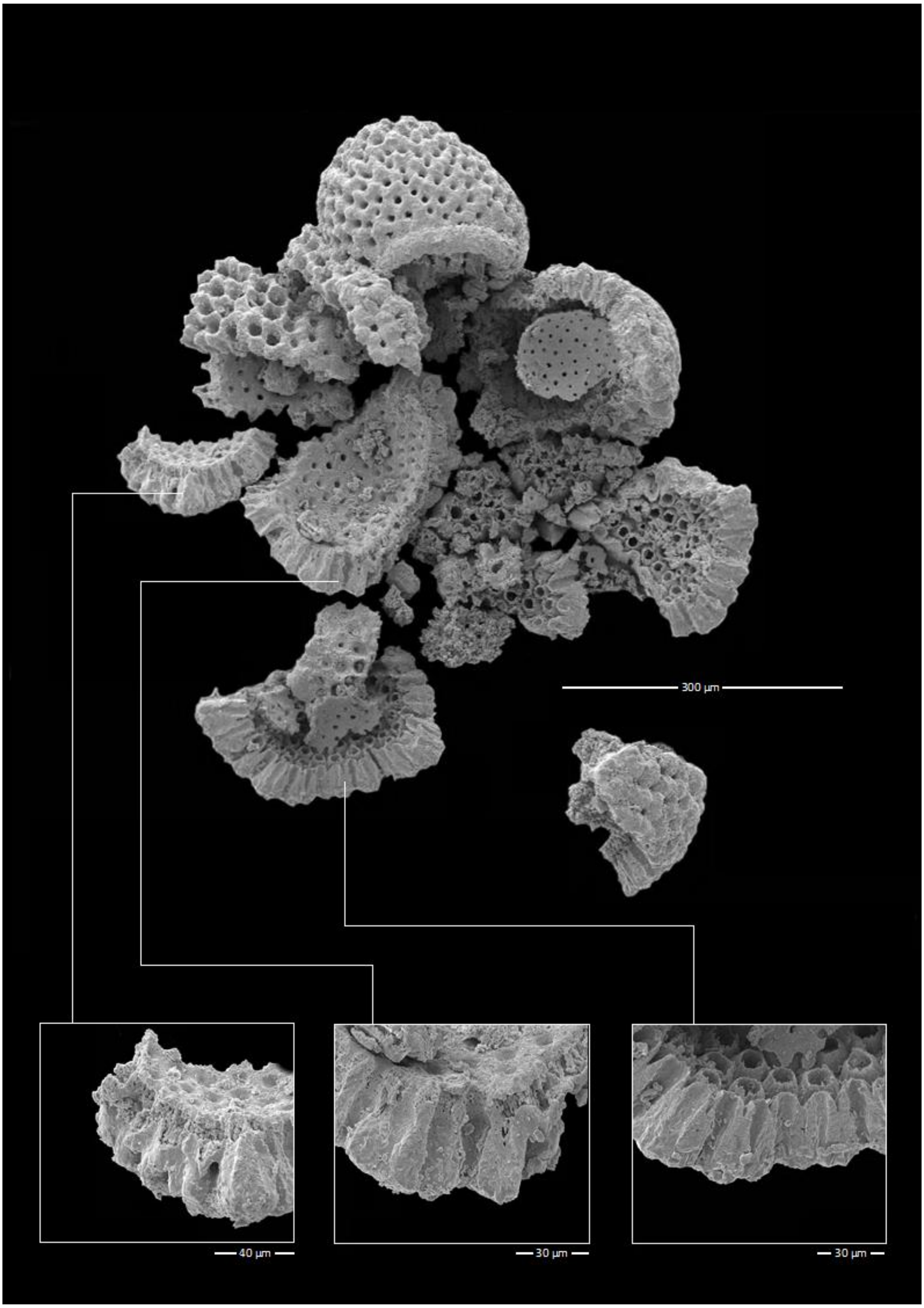

Plate 17. *Sphaeroidinellopsis disjuncta*, U1338C-35H-5, 90–92 cm; test broken to reveal internal wall structure.

PLATE 18

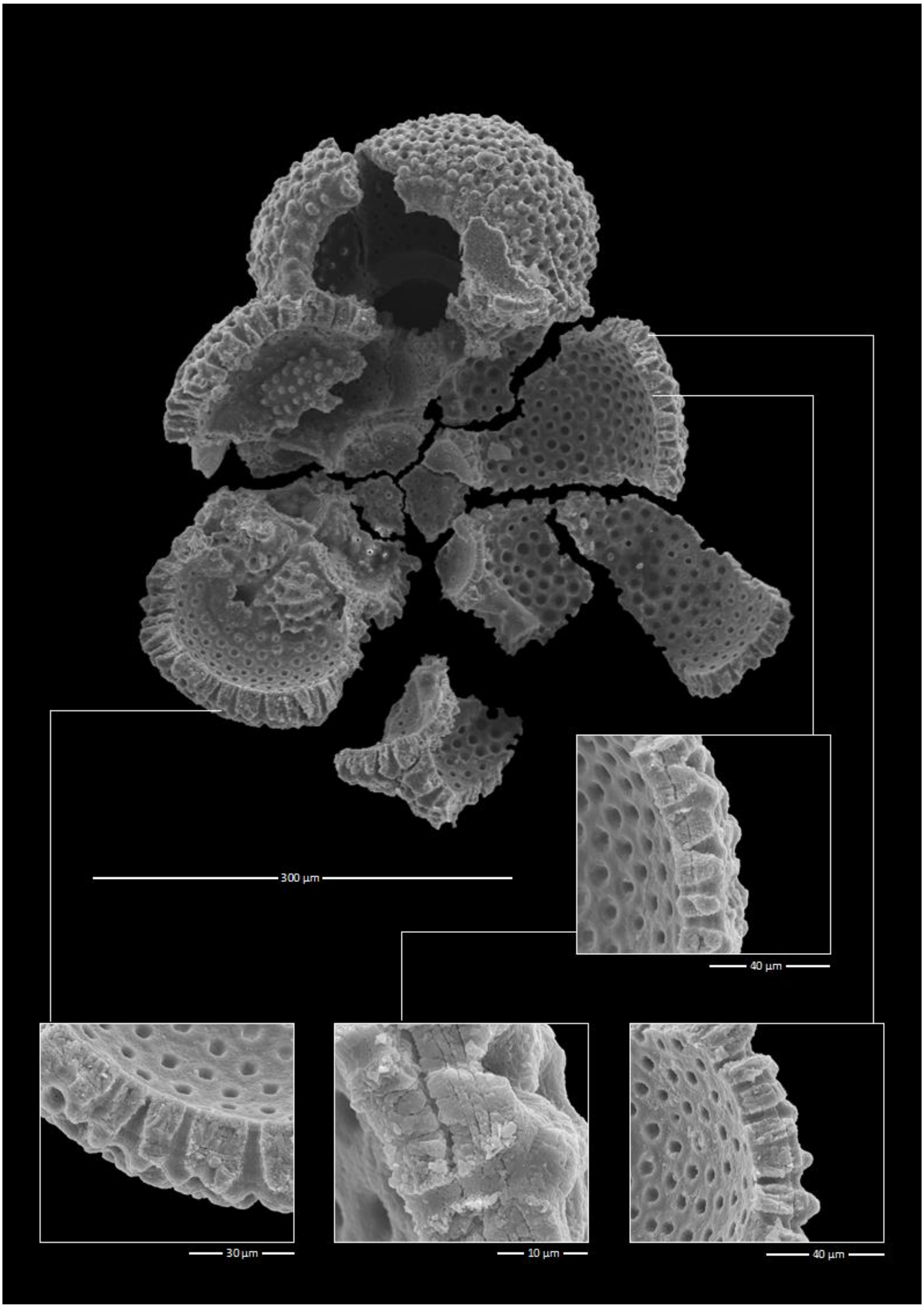

Plate 18. *Globigerinoides subquadratus*, U1338B-42H-2, 40–42 cm; test broken to reveal wall structure.

PLATE 19

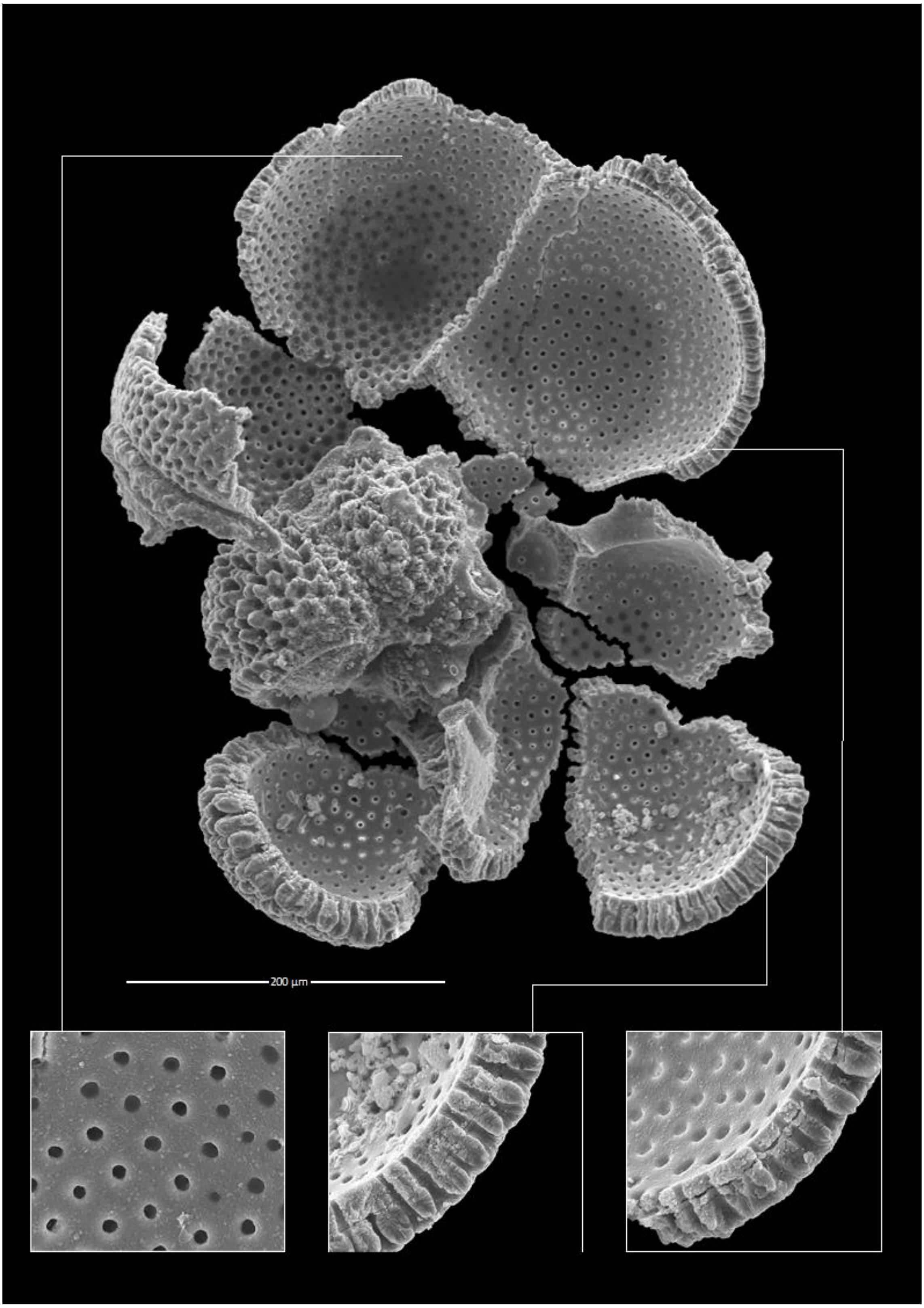

Plate 19. *Paragloborotalia siakensis*, U1338C-37H-4, 130–132 cm; test broken to reveal internal wall structure.

PLATE 20

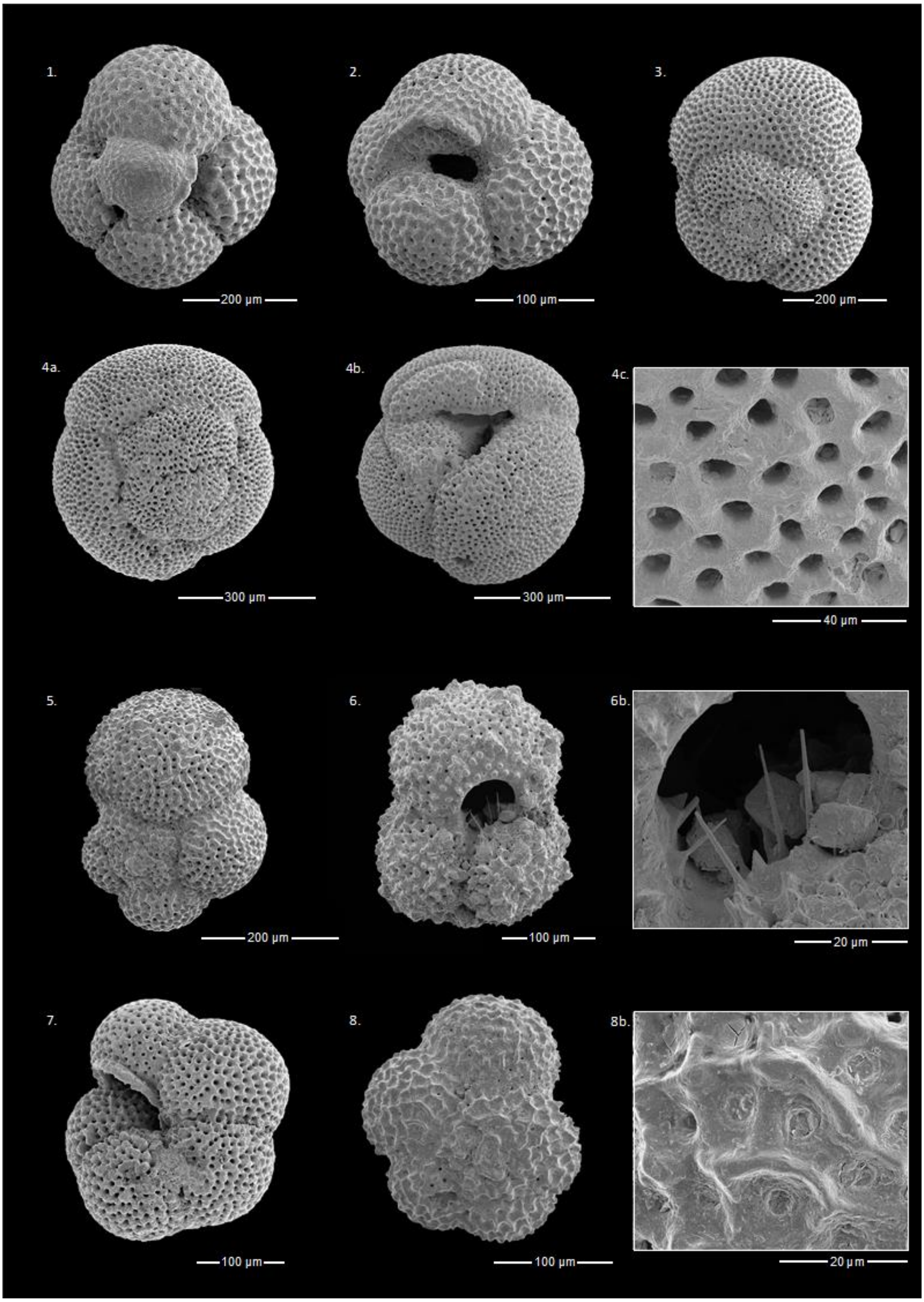

Plate 20, Planktonic foraminifera from the Cipero Formation, Trinidad. **1** *Catapsydrax dissimilis,* **2** Catapsydrax sp., **3** *Dentoglobigerina tripartita*, **4** *Dentoglobigerina* sp., **5** *Paragloborotalia* sp., **6** *Globigerinoides subquadratus*, **7** *Paragloborotalia siakensis***, 8** *Paragloborotalia* sp.

PLATE 21

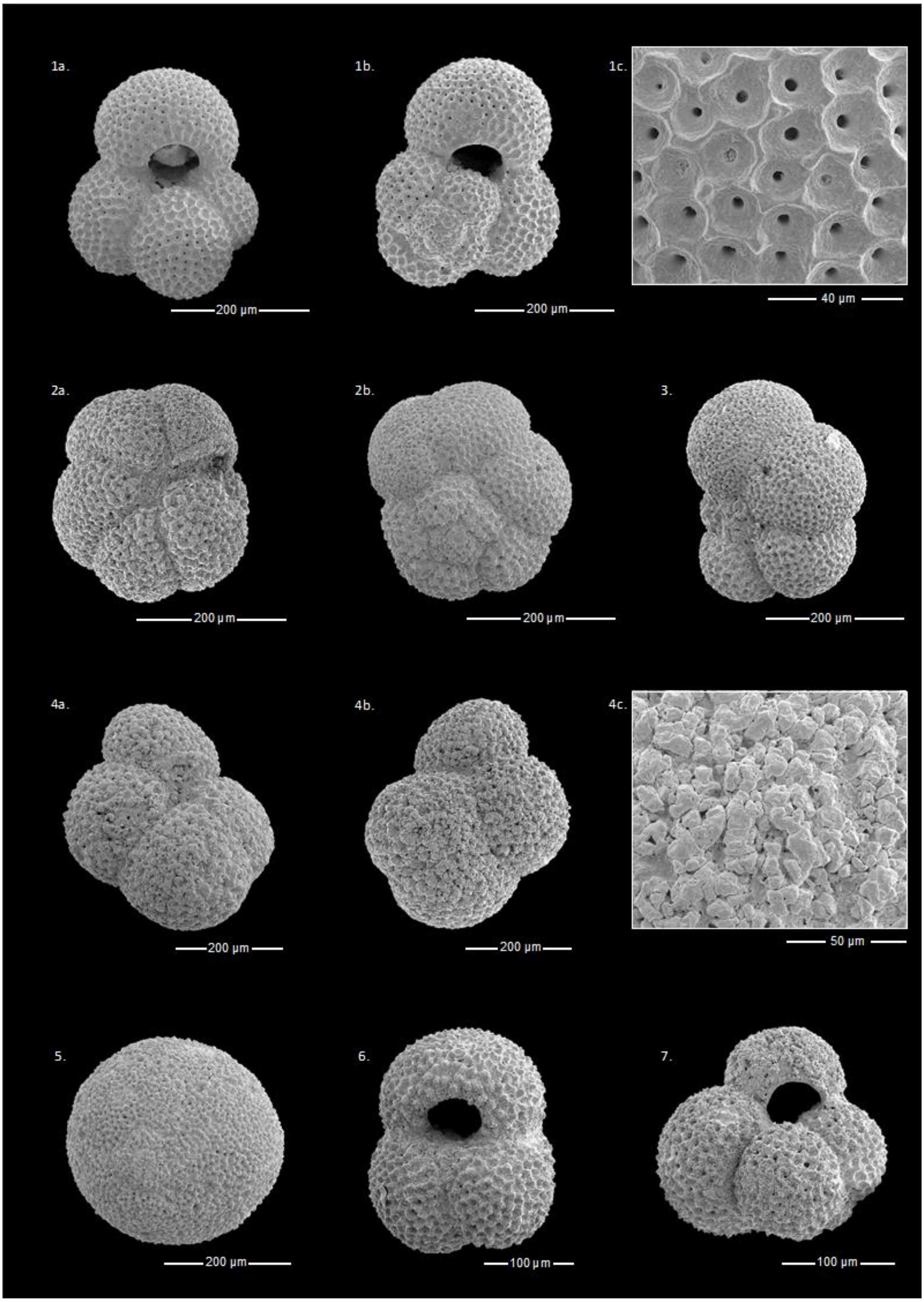

Plate 21. Planktonic foraminifera from the Brasso Formation, Trinidad. **1** *Globigerinoides* sp., **2** *Paragloborotalia* sp., **3** *Paragloborotalia* sp., **4** *Sphearoidinellopsis disjuncta*, **5** *Praeorbulina* sp., **6** *Globigerinoides subquadratus*, **7** *Turborotalita* sp.

PLATE 22

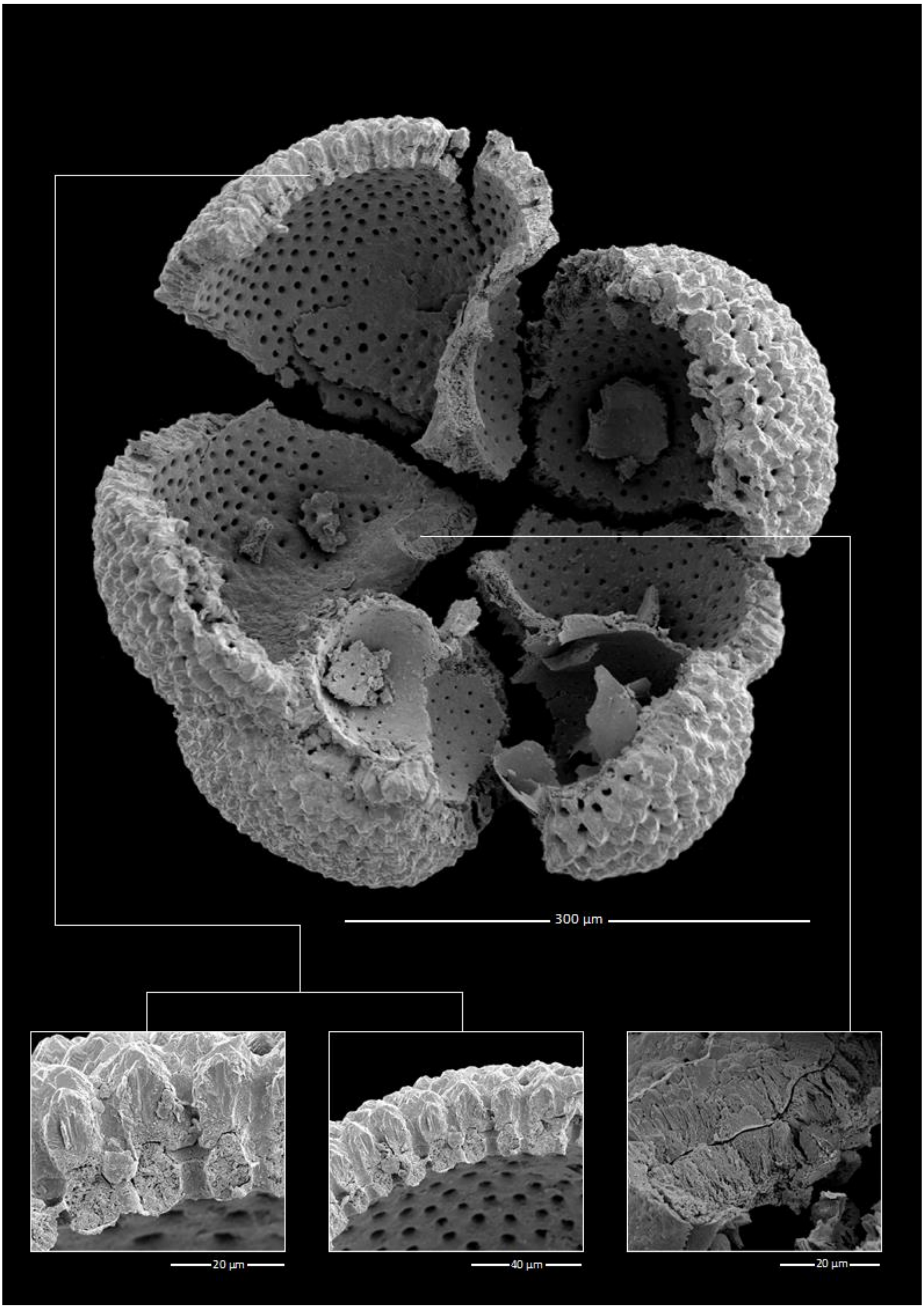

Plate 22. *Dentoglobigerina* sp. from the Cipero Fm; test broken to reveal internal wall structure.

PLATE 23

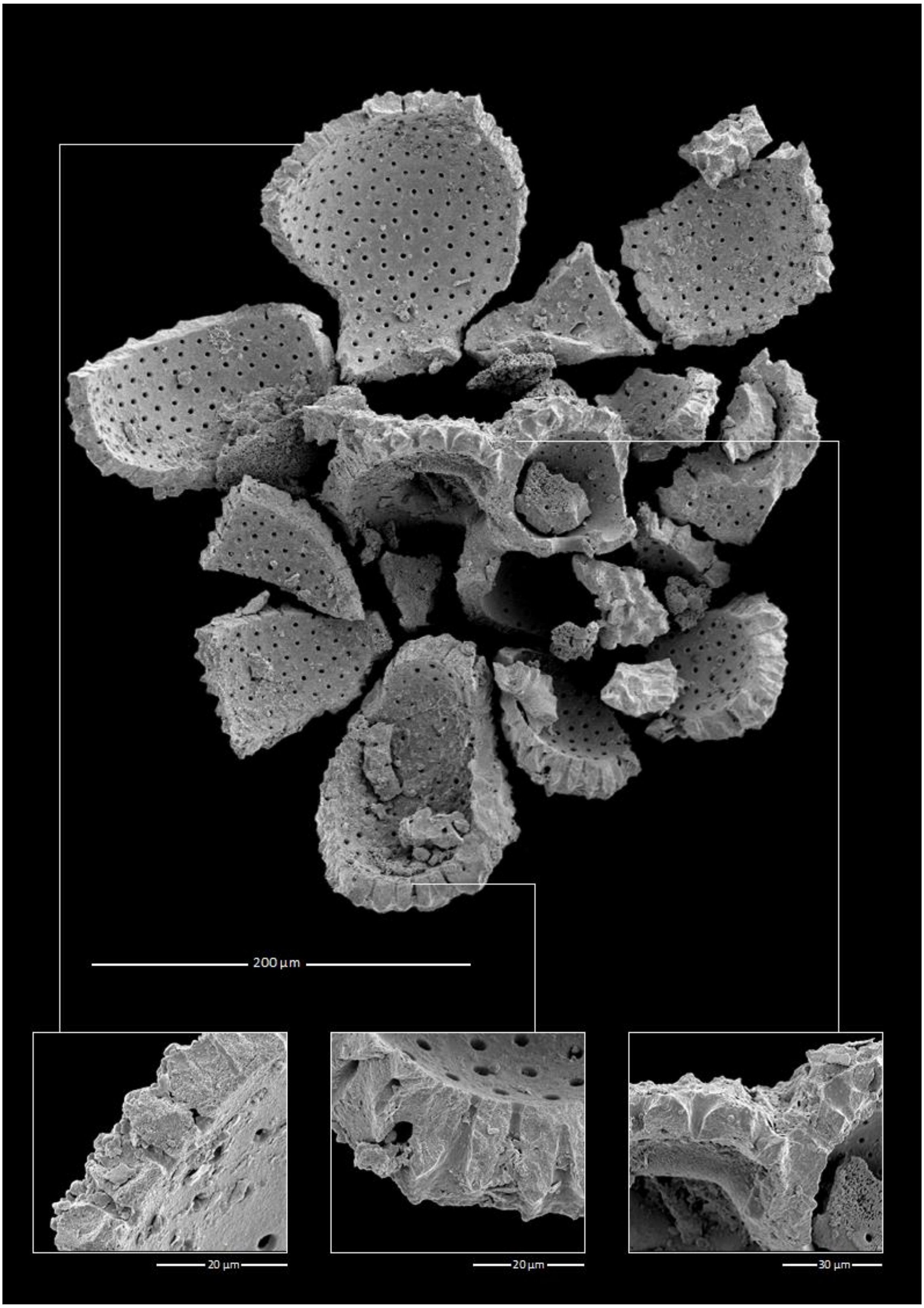

Plate 23. *Dentoglobigerina* sp. from the Brasso Fm; test broken to reveal internal wall structure.

3.7 Summary

This Chapter presents detailed taxonomic analysis of the U1338 planktonic foraminifera and focusses discussions upon the state of preservation. Fifty-five species are recorded, including *Dentoglobigerina juxtabinaiensis*. Dominant genera include *Paragloborotalia* and G*lobigerinoide*s with common *Dentoglobigerina*. Specimens from the classic Cipero Fm. of Trinidad are illustrated for comparison. The biostratigraphy f Site U1338 is discussed in detail in Chapter 5.

Key findings:

(1) The middle Miocene planktonic foraminiferal assemblages from Site U1338 exhibit exceptional preservation and diversity, which suggests they are ideal for the stable isotope analyses presented in Chapter 4.

4. Middle Miocene Climatic changes on orbital time scale recorded by planktonic foraminifera

4.1 Introduction

This Chapter examines the timing and magnitude of stable isotope events in the planktonic foraminiferal record with comparison to the deep ocean. A high resolution (3 kyr) planktonic foraminiferal $\delta^{18}O$ and $\delta^{13}C$ record spanning the period of 15.6–13.3 Ma from IODP Site U1338 in the eastern equatorial Pacific Ocean is presented here, in addition to the first planktonic foraminiferal record of trace metal ratios for this interval. Separation of the components of the $\delta^{18}O$ signal is required to improve understanding of the processes and feedbacks involved in this dynamic climate reorganization. Therefore, in this chapter Mg/Ca ratios are used as a palaeotemperature proxy to provide an independent temperature record necessary to reveal the ice volume component of the middle Miocene $\delta^{18}O$ signal. This Chapter further investigates the Middle Miocene astronomical imprints in the planktonic foraminiferal isotopic records through spectral and wavelet analysis and develops the discussions on the impact of orbital forcing on Miocene ice sheet expansion.

4.1.1 Miocene climate

The middle Miocene (~16–13 Ma), was a time of major changes in the ocean–atmosphere system, during which the global climate shifted from an interval of climatic warmth to a period of rapid cooling and major expansion of the East Antarctic Ice Sheet (EAIS) (Flower and Kennett, 1994; Holbourn et al., 2007; Shackleton and Kennett, 1975; Shevenell et al., 2004; Westerhold et al., 2005). This cooling event termed the "mid Miocene Climate Transition" (MMCT) is recorded world-wide as a ∼1‰ increase in the oxygen isotopic composition ($\delta^{18}O$) of carbonates and forms a major step in the evolution of Cenozoic climate (Miller et al., 1987; Zachos et al., 2001).

There are several significant climatic and palaeoceanographic events related to the MMCT, most notably the long-lasting positive carbon-isotope excursion between ~17 and 13.5 Ma (the "Monterey Excursion" of Vincent and Berger, 1985; described in Section 1.5.3). Within this broad $\delta^{13}C$ excursion, low-frequency fluctuations have been recognised with seven defined carbon isotope maxima (CM) (Woodruff and Savin, 1991). These positive carbon isotope excursions, together with the deposition of large amounts of organic rich sediments along the circum-Pacific margins (Compton et al., 1990; Vincent and Berger, 1985) are typically interpreted as reflecting increased burial of organic matter leading to a drawdown of atmospheric carbon dioxide and subsequent global cooling and ice build-up (Flower and Kennett, 1993). However, this hypothesis is not supported by recent Miocene $p$$CO_2$ reconstructions which indicate relatively low levels during both periods of inferred global warming and high latitude cooling (Badger et al., 2013; Pagani et al., 1999; 2005).

An alternative mechanism to explain the MMCT is a favourable orbital configuration. The amount of insolation received at the upper atmosphere is affected by changes to the Earth's orbital eccentricity, obliquity and precession (see also Section 1.6.3). These three components have played an important role in regulating global climate changes. Studies of benthic foraminiferal isotopic records across the MMCT reveal the astronomical imprints from the obliquity (40 kyr) and eccentricity (100 kyr and 400 kyr) cycles (Holbourn et al., 2005; Shevenell et al., 2004), and suggest orbital configurations across the MMCT resulted in relatively low summer insolation over Antarctica (Holbourn et al., 2005).

Detailed planktonic foraminiferal geochemical records are crucial to any reconstruction and modelling of past ocean salinity and density, water column stratification, thermohaline circulation, and ice volume. Despite extensive studies of benthic foraminiferal isotopes (Holbourn et al., 2005; 2007; Shevenell et al., 2004; Tian et al., 2013) existing planktonic foraminiferal isotopic records of this interval are scarce and of low resolution (Badger et al., 2013; Gasperi and Kennett, 1993b), due to sedimentary successions spanning this interval having been strongly affected by carbonate dissolution or burial diagenesis (Holbourn et al., 2005), or proved incomplete due to hiatuses (ODP Leg 144, Pearson (1995)). Consequently, the impact of global warming and cooling on tropical surface waters and the propagation of orbital cycles in the Earth System are unknown. Thus, the data presented in this Chapter provides exciting new information on sea surface temperatures and primary productivity changes at the tropics during the middle Miocene at a resolution not achieved in any previous study, which sheds new light on the middle Miocene climatic transition (MMCT) and associated carbon-isotope excursion.

4.1.2 Modern oceanography

4.1.2.1 Deep Pacific Ocean Basin

The deep Pacific basin is supplied by Circumpolar Deep Water (CPDW), a mixture of Antarctic Bottom Water (AABW) generated by evaporative cooling off the coast of Antarctica, and North Atlantic Deep Water (NADW) produced where the surface ocean is cooled in the Norwegian Sea. This dense water body accumulates nutrients and loses oxygen as it flows northwards into the North Pacific before returning as a nutrient enriched, oxygen depleted southward flow (Pacific Central Water, PCW) at 1–3 km depth (Holbourn et al., 2013).

4.1.2.2 Surface and subsurface currents

In the modern Equatorial Pacific Ocean the trade winds drive surface waters from east to west generating the North and South Equatorial Currents (NEC and SEC) (Fig. 4.1). This causes warm water to "pile up" in the western Pacific where the sea surface is 0.5 meters higher than in the east (Talley et al., 2011). This creates a pressure gradient that produces a strong eastward flow just beneath the surface layer (150–200 metres depth), known as the Equatorial Undercurrent (EUC) (Cromwell et al., 1954; 1963; Knauss, 1960) (Fig. 4.1). The EUC is a major sub-surface ocean current that is present in all three equatorial oceans but is strongest in the Pacific.

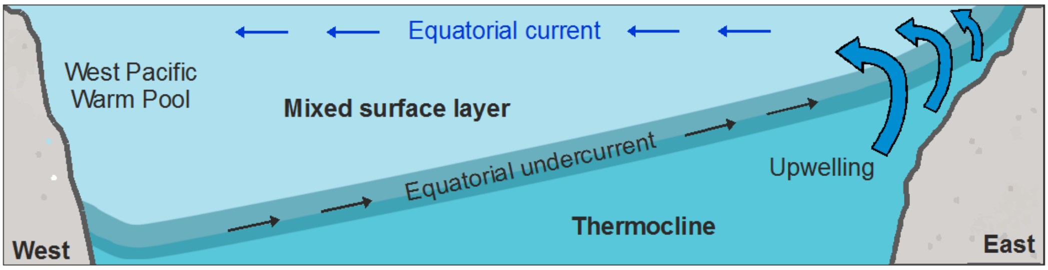

Figure 4.1. Schematic cross section of equatorial Pacific Ocean showing the depth and direction of the Equatorial undercurrent, and shoaling of the thermocline.

Just north of the equator (5°N to 10°N), the intense North Equatorial Counter-current (NECC) is driven eastward by cyclonic wind stress curl associated with the Inter-tropical Convergence Zone (ITCZ), and separates the broader westward flowing NEC and SEC (Kessler, 2006) (Fig. 4.2). The main flow of the counter current is concentrated in the shallow surface layer and velocities decrease rapidly with depth (Wyrtki, 1967). When the NEC reaches the western boundary it bifurcates into the Kuroshio and Mindanao Currents (Nitani, 1972) and the SEC is broken up into many branches and filaments whose structure and timescales remain poorly understood (Kessler and Gourdeau, 2006; Morris et al., 1996).

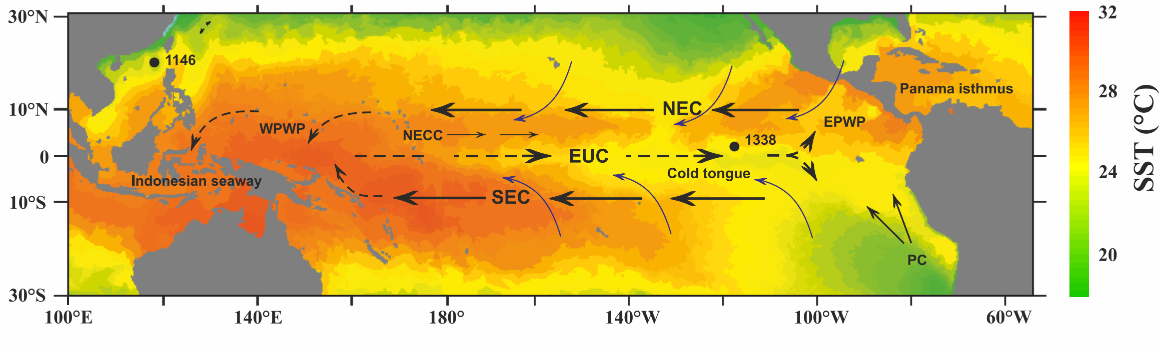

Figure 4.2. Equatorial Pacific Map showing the position of IODP Site U1338 and ODP Site 1146, the general surface and subsurface currents and the mean annual sea surface temperatures across the Equator (data from NOAA). PC: Peru Current, NEC: North Equatorial Current, SEC: South Equatorial Current, EUC: Equatorial Under Current, NECC: North Equatorial Counter Current, WPWP: West Pacific Warm Pool, EPWP: East Pacific Warm Pool.

4.1.2.3 Upwelling

Surface waters in the equatorial Pacific Ocean are warmest in the west in the “Western Pacific-Warm Pool” (WPWP), where the mixed layer is deeper (Fig. 4.1). This is due to easterly Trade Winds driving a divergent Ekman transport near the equator. This upwelling of cool water in the central/eastern Pacific causes shoaling of the EUC and thermocline layer (Fig. 4.1), and gives rise to a “cold tongue” where normally there is much more rainfall than in the central and eastern Equatorial Pacific equator from the continental margins, and is surrounded by warmer surface water in both hemispheres. The cold tongue of the Pacific Ocean is considerably stronger than that of the Atlantic Ocean, and has major influence on global climate patterns (Wyrtki, 1967).

4.1.2.4 Pacific Ocean sea surface salinity

Under normal conditions, present day surface water salinities are low in the western tropical Pacific Ocean and increase towards the eastern part of the basin (Fig. 4.3) (Levitus et al., 2013). This is controlled by a combination of atmospheric convection, precipitation, evaporation and ocean dynamics (Cronin and McPhaden, 1998). Low salinities occur near the equator due to rain from rising atmospheric circulation. High salinities are typical of the hot dry gyres flanking the equator (20-30 degrees latitude) where atmospheric circulation cells descend.

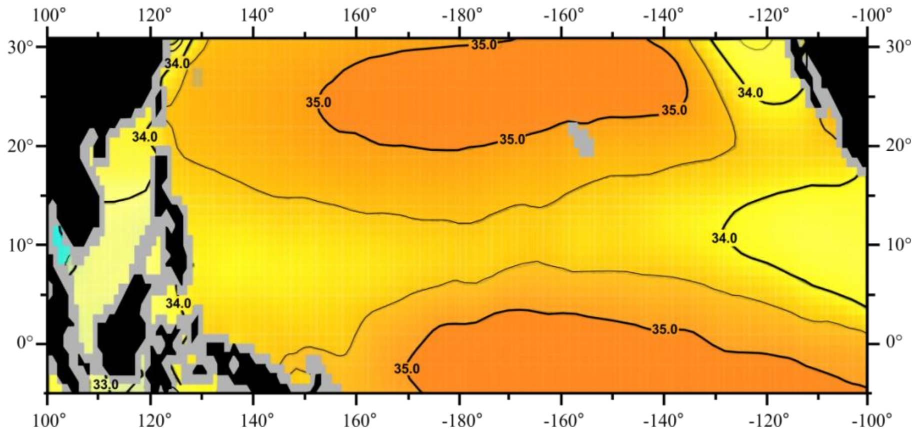

Figure 4.3. Equatorial Pacific Map illustrating modern average annual mean sea surface salinities. Adapted from Levitus world ocean atlas (Levitus et al., 2013). P.S.U = Practical Salinity Unit.

4.1.2.5 El Niño-Southern Oscillation

The El Niño-Southern Oscillation (ENSO) is a complex interaction between the ocean and atmosphere in the tropical Pacific. The key feature of ENSO is a positive feedback between trade winds and zonal sea surface temperature (SST) gradients known as Bjerknes feedback (Bjerknes, 1969). Under normal conditions warm moist air rises over the Western Pacific Warm Pool, which leads to low surface pressure. The rising air reaches the tropopause and returns eastward where it subsides. High pressure in the eastern Pacific reinforces the trade winds and completes the Walker circulation. El Niño occurs when anomalously high SSTs in the eastern equatorial Pacific reduces the east-west SST gradient and hence the strength of the Walker circulation (Gill, 1980; Lindzen and Nigam, 1987), resulting in weaker Trade Winds around the equator. This in turn, drives ocean circulation changes that further reinforce the SST anomaly, as the Western Pacific Warm Pool moves eastward. This positive ocean-atmosphere feedback leads to a warm state in the equatorial Pacific, i.e., the warm phase of ENSO –El Niño (Fig. 4.4) (Wang et al., 2012), which results in drought in the western Pacific and increased precipitation and reduced upwelling in the eastern Pacific (Cane, 2005; Wang and Fiedler, 2006). When the ocean-atmosphere system returns to its normal state, it sometimes "overshoots", resulting in a 'La Niña', a state of extreme east–west contrast (Batenburg et al., 2011). The El Niño/Southern Oscillation (ENSO) also causes large changes in salinity over the equatorial Pacific as the warm, low-salinity waters from the western tropical Pacific (WTP) are advected east into the central Pacific (Stott et al., 2004).

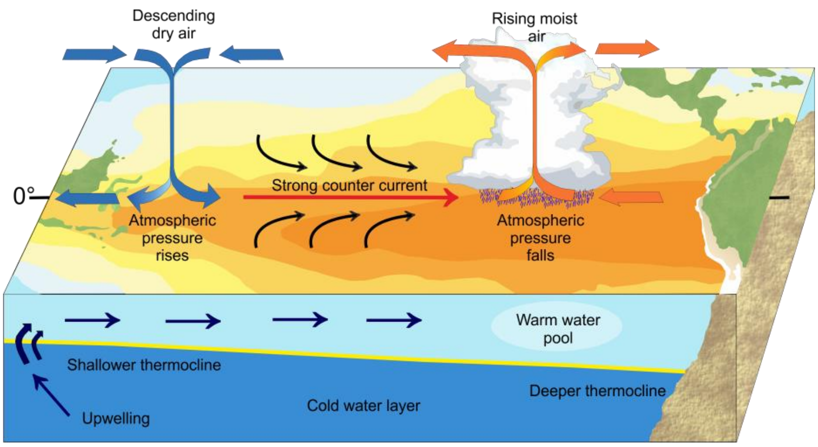

Figure 4.4. Schematic diagram of Pacific Ocean sea surface temperatures during El Nino conditions. Adapted from Thompson (2007).

Studies of ENSO dynamics and impacts in the modern demonstrate that the equatorial Pacific ocean-atmosphere system influences global climate on interannual to decadal time scales (Koutavas et al., 2002; Trenberth, 1997). Typically, one El Niño "cycle" occurs every 3-7 years, although the term ENSO includes the word oscillation, analysis of real climate ENSO showed that it behaves more like a series of single events rather than a cycle between positive and negative phases (Kessler, 2002).

Modelling studies indicate that this system is sensitive to orbital forcing which regulates the annual insolation cycle and affects the seasonal strength of the trade winds and the intensity of upwelling (Clement et al., 1999). Orbital perturbations of the seasonal cycle are believed to be crucial factors determining the long-term behaviour of ENSO (Clement et al., 1999). Studies of primary production in nannoplankton, and Mg/Ca data from Quaternary planktonic foraminifera from the tropical Pacific region reveal significant spectral power at precessional periods (19 to 23 kyr) (Beaufort et al., 2001; Lea et al., 2000), but the specific mechanisms by which precession affects basin-scale ocean atmosphere dynamics and their interaction with global climate remains poorly understood (Koutavas et al., 2002).

There is also evidence for persisting ENSO variability during past warmer climates. The $\delta^{18}O$ record obtained from 3–5 million year old coral skeletons in the tropical Pacific reveals interannual variability on ENSO time scales (Watanabe et al., 2011). In the late Miocene (~5.6 Ma), evaporite deposits from the Mediterranean have also recently been found to resemble the modern spectrum of ENSO (Galeotti et al., 2010). The authors hypothesise ENSO teleconnections may have been stronger during the late Miocene due to a reduced meridional temperature gradient (Galeotti et al., 2010). A middle to late Miocene (10–13 Ma) stable isotope record from giant clams found in Indonesia, also shows ENSO-like interannual variability (Batenburg et al., 2011). Palaeoclimatic evidence for middle Miocene (17–13 Ma) ENSO conditions is scarce because of a lack of detailed, well-dated climate records from this region.

4.2 Results

Down core high resolution planktonic foraminiferal $\delta^{18}O$ and $\delta^{13}C$ profiles versus age are shown in figure 4.5. Paired measurements in 113 samples indicate no significant offset in $\delta^{18}O$ and $\delta^{13}C$ between *G. subquadratus* and *Globigerinoides* spp.

From 15.57 to 13.36 Ma mean planktonic foraminiferal $\delta^{13}C$ values generally fluctuate between 3.2 and 2.2‰, except for two abrupt positive shifts reaching ~ 3.4‰ at 14.65 and 13.9 Ma (Fig. 4.5). Amplitude variability is generally between 0.2‰ and 0.8‰, except during the positive shifts where it reaches >1.2‰. The planktonic foraminiferal $\delta^{13}C$ record of Site U1338 displays a series of globally recognised carbon maxima (CM events, Vincent and Berger, 1985; Woodruff and Savin, 1991) the period of the Monterrey Carbon Isotope Excursion (16.5–13.5 Ma). Four CM events from CM5a to CM6b are identified in the $\delta^{13}C$ record (Fig. 4.5), which recur every 400 kyr (Woodruff and Savin, 1991).

Mean $\delta^{18}O$ values generally fluctuate between approximately -0.2 and -1.8‰ (Fig. 4.5) and maximum and minimum values are recorded between 13.36–14.0 Ma and 15.56–14.75 Ma respectively. There is a prominent short-term increase where oxygen isotope values shift by ~0.8‰ over a ~200 kyr interval beginning at ~14 Ma, which signifies the expansion of the East Antarctic Ice Sheet (EAIS). This is further discussed in Section 4.5.1. Based on the $\delta^{18}O$ signal, three distinct phases of climate evolution are identified through the interval 15.57 to 13.36 Ma (Figs. 4.6–4.8).

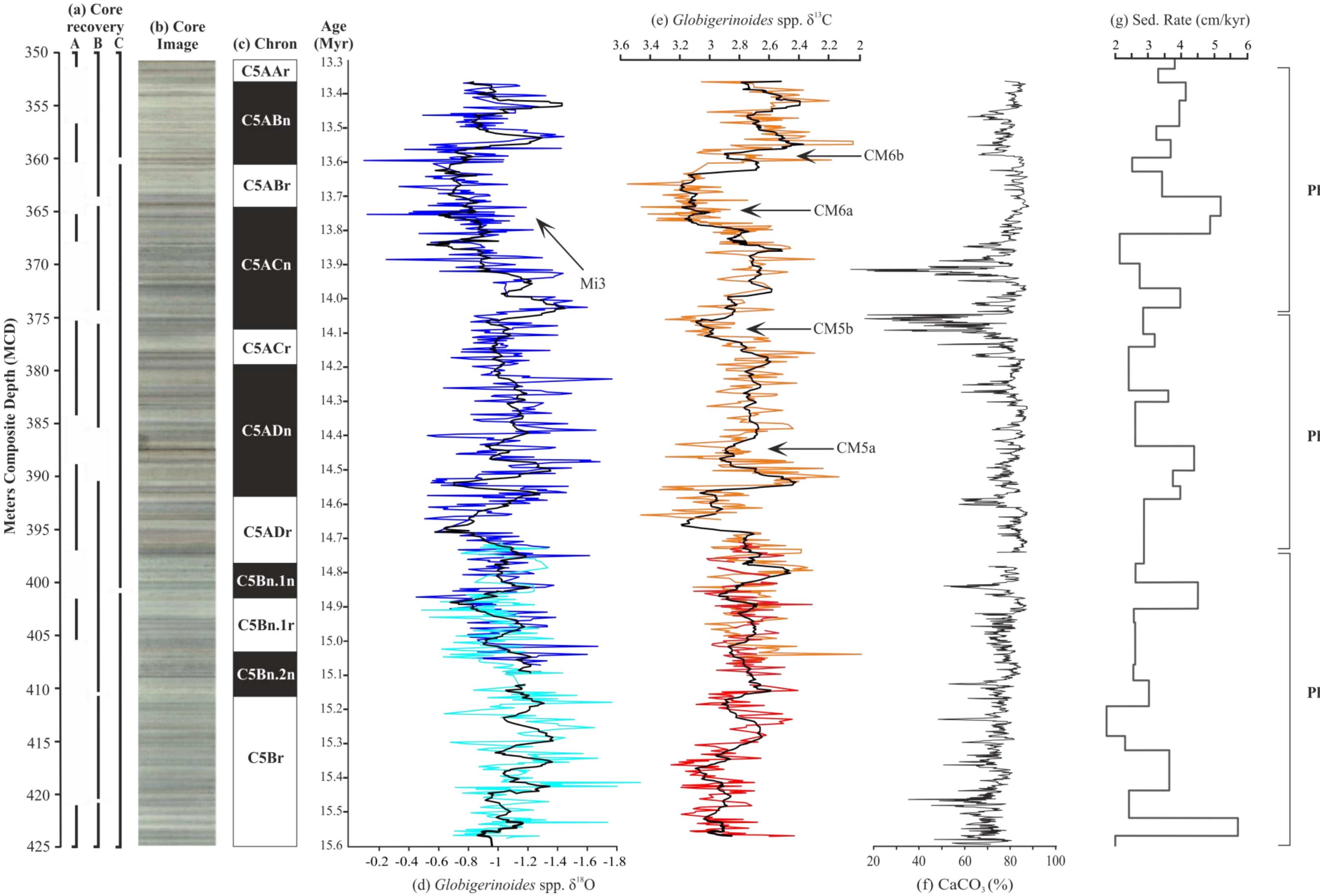

Figure 4.5. High-resolution (~3 kyr) planktonic isotopic records for IODP Site U1338 from 15.57 to 13.36 Ma. (a) Core recovery; (b) digitized core photograph; (c) Chron data as per Gradstein et al. (2004); (d) *Globigerinoides* spp. (dark blue) and *G. subquadratus* (light blue) $\delta^{18}O$, the black lines denote 10-point moving average through the record; (e) *Globigerinoides* spp. (orange) and *G. subquadratus* (red) $\delta^{13}C$; (f) % $CaCO_3$ curve comes from (Lyle et al., 2010); (g) Sedimentation Rates.

4.2.1 Phase 1: 15.57 to 14.70 Ma

From ~15.57 to 14.70 Ma (phase 1) $\delta^{18}O$ values oscillate between approximately -1.8 and -0.6‰ and reveal a succession of well-defined 100 kyr cycles between 15.2 and 15.6 Ma with high amplitude variability (Fig. 4. 6). The $\delta^{13}C$ values over this interval vary between 2.4 and 3.2‰, with lower amplitude variation compared to the $\delta^{18}O$.

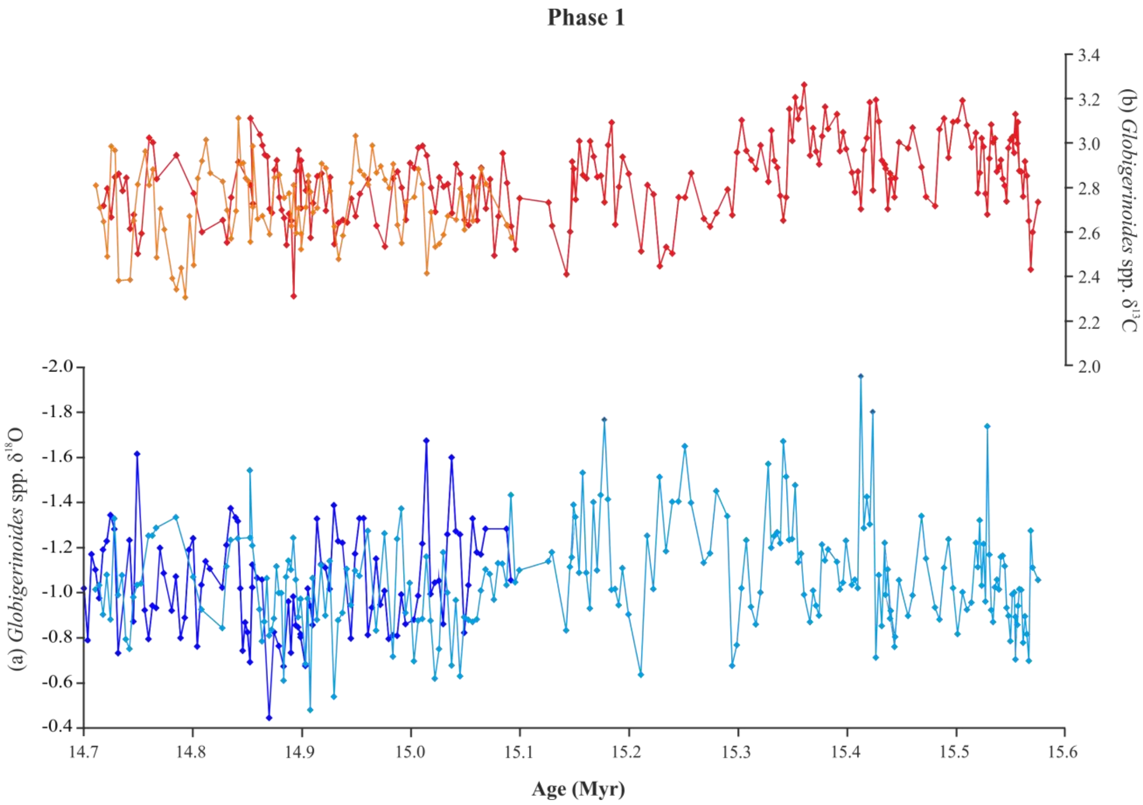

Figure 4.6. High-resolution (~3 kyr) planktonic foraminiferal isotopic records for IODP Site U1338 from 15.57 to 14.7 Ma. (a) *Globigerinoides* spp. (dark blue) and *G. subquadratus* (light blue) $\delta^{18}O$; (b) *Globigerinoides* spp. (orange) and *G. subquadratus* (red) $\delta^{13}C$.

4.2.2 Phase 2: 14.7 to 14.0 Ma

From 14.7 to 14.0 Ma (phase 2) the $\delta^{18}O$ values fluctuate between approximately -1.8 and -0.5 ‰ (Fig. 4. 7) and the 100 kyr cyclicity that was apparent in phase 1 is supressed. The $\delta^{13}C$ record for this interval is characterised by two positive shifts at ~14.43 and ~14.15 Ma, which correspond to carbon maxima events CM5a and CM5b of the globally recognised Monterey excursion.

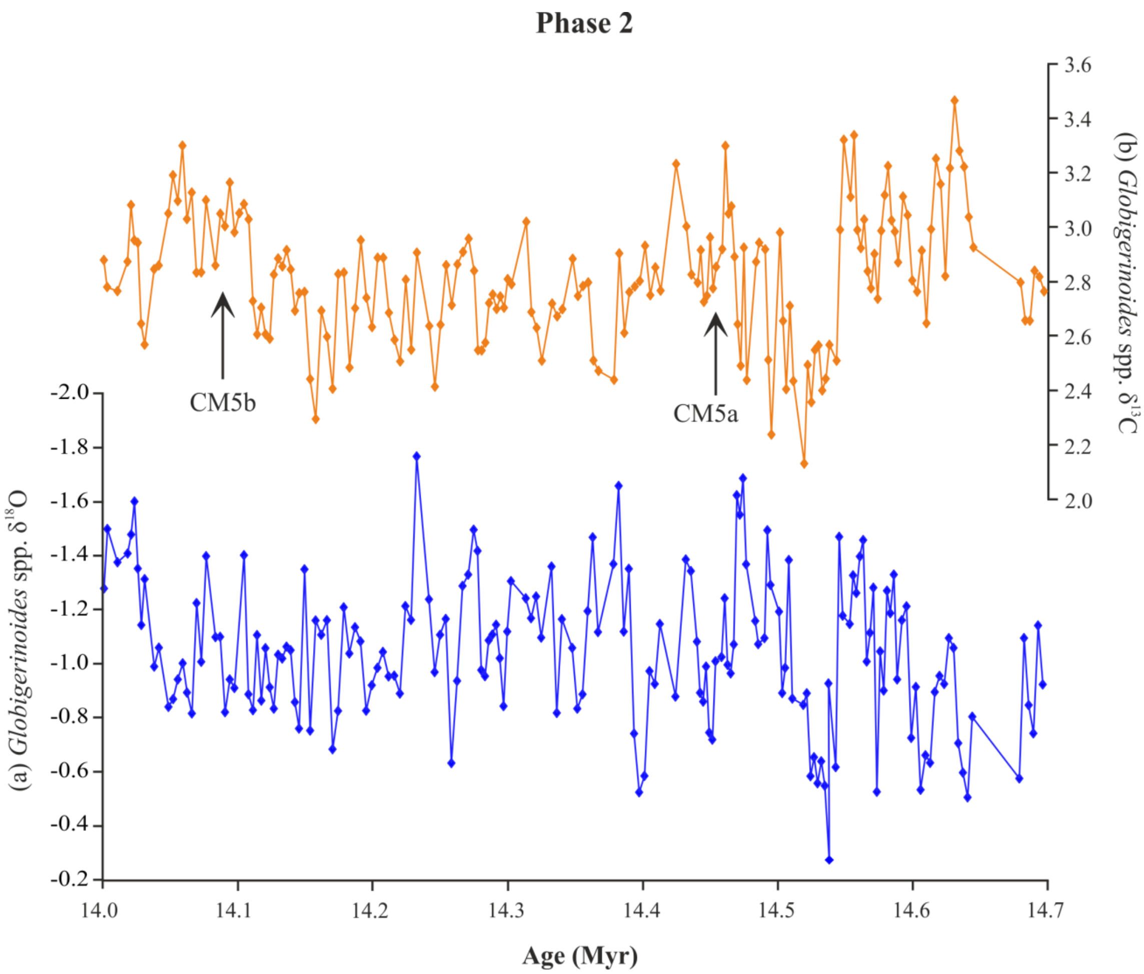

Figure 4.7. High-resolution (~3 kyr) planktonic foraminiferal isotopic records for IODP Site U1338 from 14.7 to 14.0 Ma. (a) *Globigerinoides* spp. $\delta^{18}O$; (b) *Globigerinoides* spp. $\delta^{13}C$.

4.2.3 Phase 3: 14.0 to 13.36 Ma

From 14.0 to 13.36 Ma the $\delta^{18}O$ curve is marked by a positive trend of ~1‰ occurring over 200 kyr, beginning at ~13.9 Ma. This increase in $\delta^{18}O$ is followed by a rapid increase in $\delta^{13}C$ values that leads to the most pronounced of the CM events; the double peaked CM6 event (Fig. 4.8).

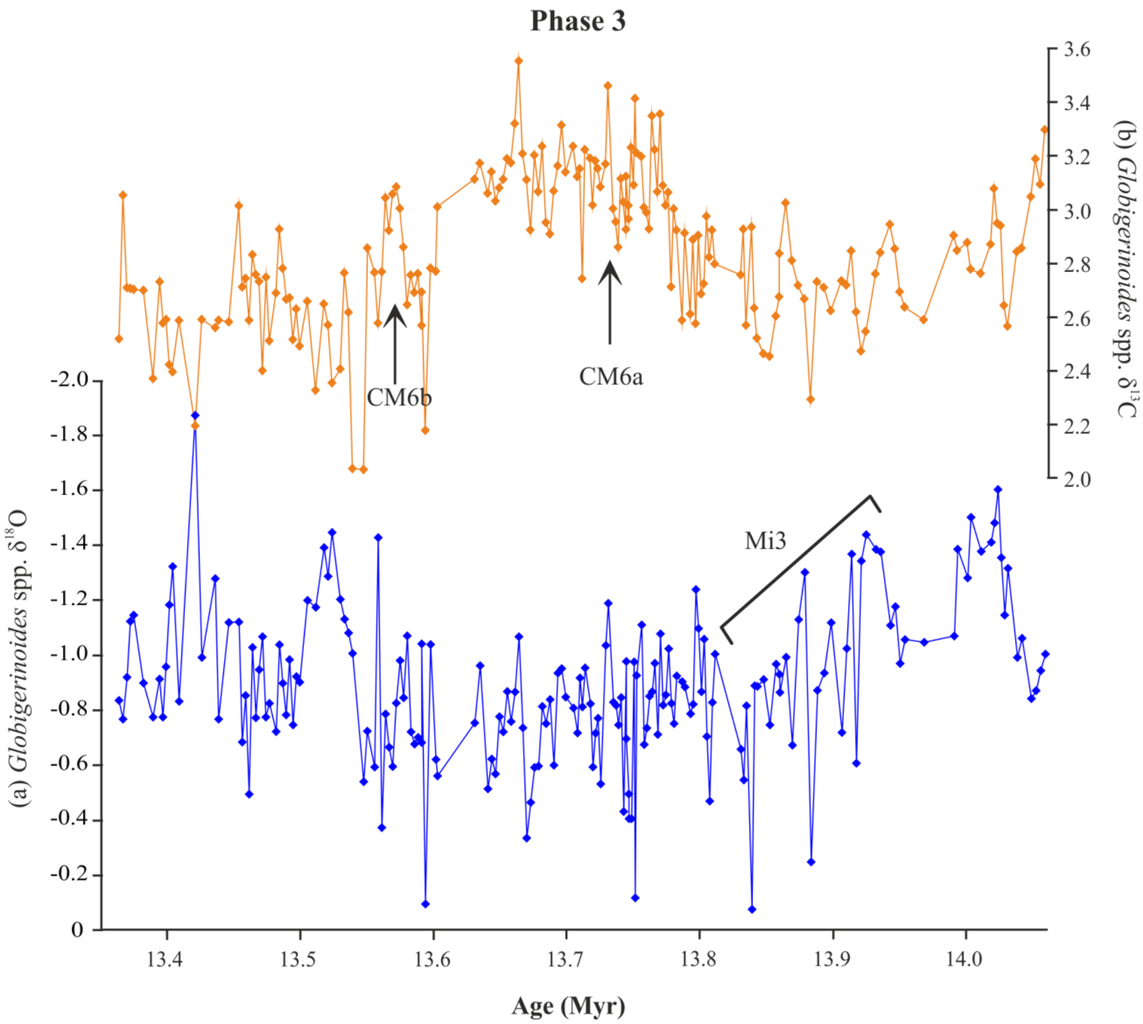

Figure 4.8. Planktonic foraminiferal isotope records of Site U1338, 13.36 to 14.0 Ma. (a) *Globigerinoides* spp. $\delta^{18}O$; (b) *Globigerinoides* spp. $\delta^{13}C$. CM events denote the "Monterey Carbon excursion".

4.2.4 Comparison of benthic and planktonic foraminiferal $\delta^{18}O$ at Site U1338

The benthic foraminiferal isotope record provided by Holbourn et al. (2014) based on stable isotope measurements performed on specimens of *Cibicidoides* spp. uses the same samples from Site U1338 as those used for the planktonic foraminiferal analyses in this study. This allows direct comparisons to be made between the two data sets. By comparing the planktonic and benthic foraminiferal $\delta^{18}O$ records, the timing and magnitude of $\delta^{18}O$ changes through the water column can be examined.

The amplitude variation of the benthic foraminiferal $\delta^{18}O$ record is slightly less than the planktonic foraminiferal record, with values fluctuating between 2.3‰ and 0.7‰ (Fig. 4.9), and oscillations in $\delta^{18}O$ (~0.8‰) with a period of ∼100 kyr are evident from 15.6 Ma to 15.0 Ma. Between 13.3 and 14.8 Ma, the benthic foraminiferal record is sampled at a higher resolution (~1.5 kyr) than the planktonic record (~3 kyr) and oscillations with a period of ~40 kyr become apparent from 14.6 Ma onwards. An abrupt positive shift of approximately 1‰ is observed at 13.9 Ma, where benthic foraminiferal values shift from ~1.2‰ to 2.2‰ over a 200 kyr interval. This feature is also seen in the planktonic isotope data set, but as a much more gradual trend.

The vertical oxygen isotope difference between planktonic and benthic foraminifera ($\Delta\delta^{18}O$) was calculated and is also shown in figure 4.9c. The benthic-planktonic foraminiferal $\delta^{18}O$ difference removes the global ice volume effects and mainly reserves the temperature and salinity effects of bottom and surface waters. An increase in the difference between planktonic and benthic foraminiferal $\delta^{18}O$ indicates cooling of the deep oceans. Calculated $\Delta\delta^{18}O$ values oscillate between 1.8 and 3.8‰ in the early part of the record (15.6–15.0 Ma). This is followed by an abrupt shift of ~1.6 at 13.9 Ma caused by the more rapid positive shift in the benthic foraminiferal $\delta^{18}O$ relative to the planktonic foraminiferal $\delta^{18}O$, after which values remain lower, fluctuating between 1.9 and 2.8‰. The two oxygen isotope records appear 180 degrees out of phase in the earliest part of the record (between 15.6–15.1 Ma), where the lightest values in the benthic foraminiferal records occur at intervals of most positive planktonic foraminiferal isotope values.

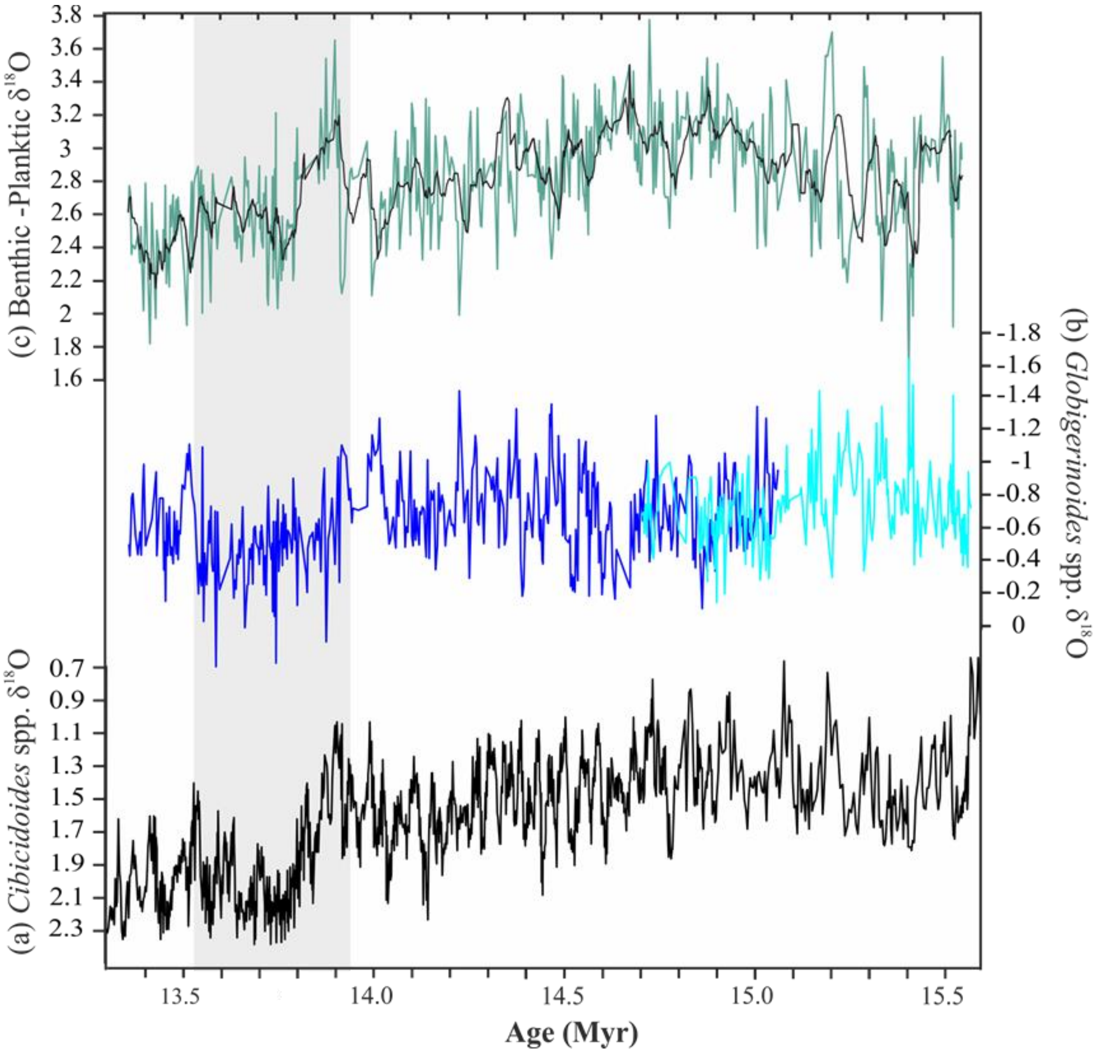

Figure. 4.9. Comparison of planktonic and benthic foraminiferal $\delta^{18}O$ records from IODP Site U1338; (a) *Cibicidoides* spp. $\delta^{18}O$ (Holbourn et al., 2014); (b) *Globigerinoides* spp. $\delta^{18}O$; (c) $\Delta\delta^{18}O$ Site U1338.

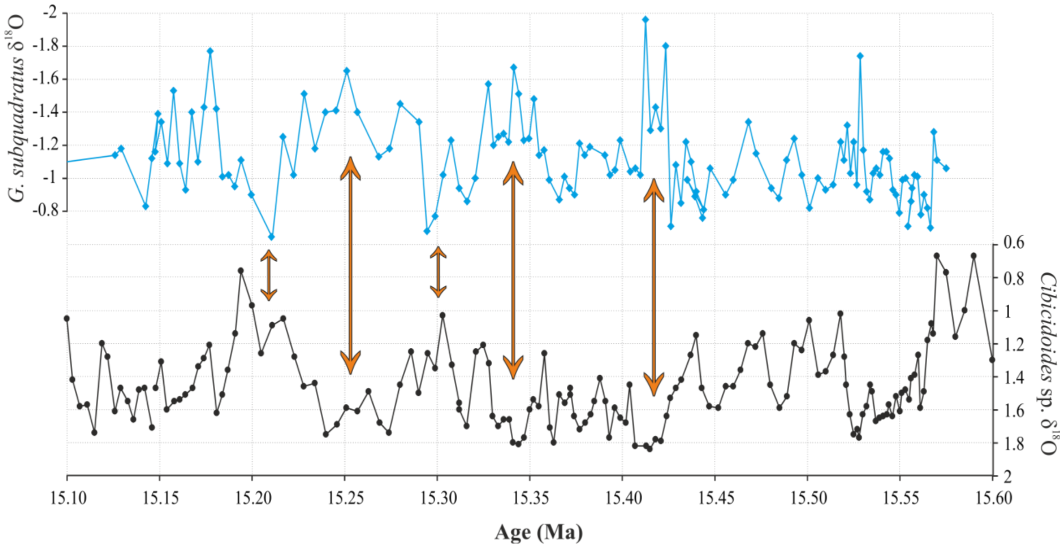

Figure 4.10. Close up of planktonic and benthic foraminiferal $\delta^{18}O$ records from IODP Site U1338 between 15.1 and 15.6 Ma; (a) *Cibicidoides* spp. $\delta^{18}O$ (Holbourn et al., 2014); (b) *Globigerinoides* spp. $\delta^{18}O$.

4.2.5 Comparison of benthic and planktonic foraminiferal $\delta^{13}C$ at Site U1338

Comparison of the planktonic and benthic foraminiferal $\delta^{13}C$ records (Fig. 4.11) reveals a strong correlation between the two data sets, both the long and short term trends, including amplitude and phase. Benthic foraminiferal $\delta^{13}C$ values fluctuate between 2.0‰ and 0.7‰ (Fig. 4.11a), and positive shifts of 0.8‰ and 1.0‰ are seen at 14.7 and 13.9 Ma respectively. In both the planktonic and benthic foraminiferal records, intervals of lighter $\delta^{13}C$ occur every 400 kyr. Higher frequency variability is also evident on 40 kyr cycles. Maxima in planktonic (~3.6‰) and benthic foraminiferal $\delta^{13}C$ (~2.0‰) occur at 13.7 Ma and coincide with an increase in $\delta^{18}O$. The vertical carbon isotope difference between planktonic and benthic foraminifera ($\Delta\delta^{13}C$) is relatively stable throughout the studied interval, with values fluctuating between -0.8 and -2.2‰. In general, trends in the planktonic foraminiferal $\delta^{13}C$ record match those from the benthic foraminiferal $\delta^{13}C$ record, but with higher degree of variability.

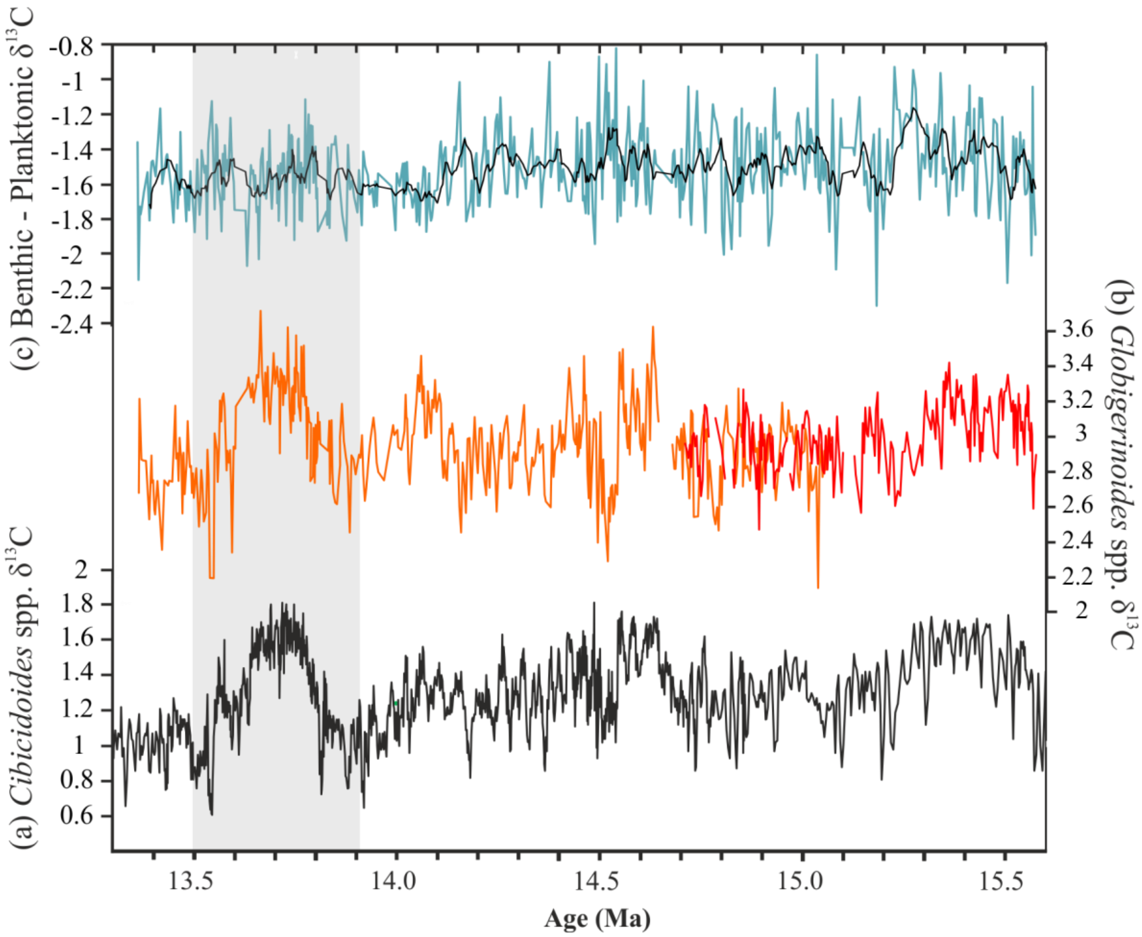

Figure 4.11. Comparison of planktonic and benthic foraminiferal $\delta^{13}C$ records from IODP Site U1338; (a) *Cibicidoides* spp. $\delta^{13}C$ (Holbourn et al., 2014); (b) *Globigerinoides* spp. $\delta^{13}C$; (c) $\Delta\delta^{13}C$ Site U1338

4.2.6 *Paragloborotalia siakensis* stable isotope record

High resolution $\delta^{13}C$ and $\delta^{18}O$ isotope records from shallow thermocline dwelling planktonic foraminifera *Paragloborotalia. siakensis* are shown in figure 4.12. A number of large gaps exist in the record due to insufficient numbers of specimens (>10) in the samples prior to 13.9 Ma. Mean *P. siakensis* $\delta^{13}C$ values fluctuate between 2.2 and 0.8‰. Amplitude variability is approximately 0.5‰ except during positive shifts where it reaches 1.0‰. The onset of the CM6 event is displayed in the record at 13.8 Ma where $\delta^{13}C$ values reach a peak of 2.4‰. The *P. siakensis* $\delta^{13}C$ record is consistently offset from the *Globigerinoides* spp. record by 1.0‰. Mean $\delta^{18}O$ values fluctuate between -1.4 and 0.2‰. The amplitude variation in the *P. siakensis* $\delta^{18}O$ record is slightly higher than that of mixed layer taxa *Globigerinoides* spp. and the two $\delta^{18}O$ records are generally offset by ~0.4‰. However between 13.7 and 13.6 Ma, the two records appear congruent, i.e., during the peak of CM6.

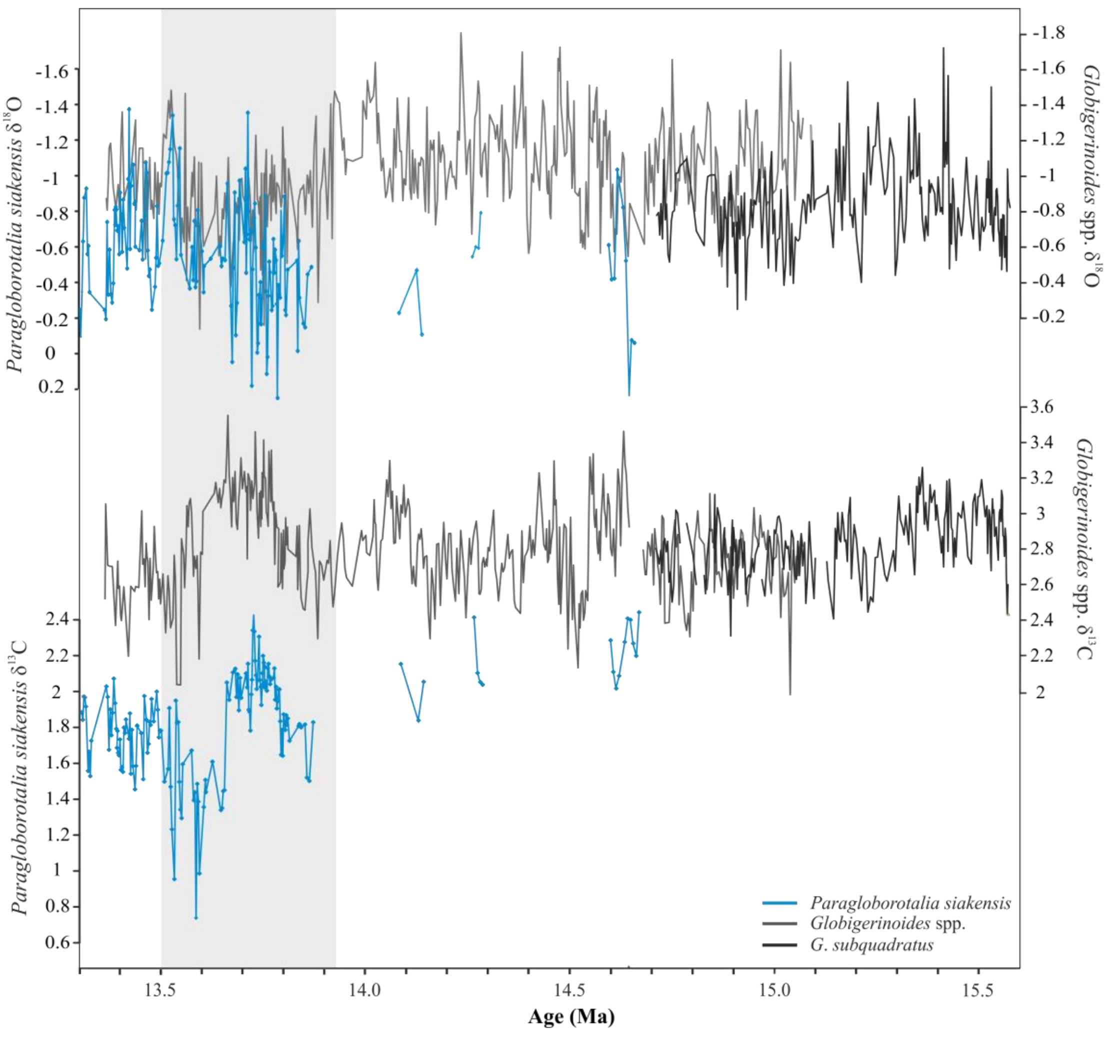

Figure 4.12 *P. siakensis* $\delta^{18}O$ and $\delta^{13}C$ records from IODP Site U1338 plotted against *Globigerinoides* spp. data.

4.3 Orbital Forcing

Redfit spectral analysis, using the REDFIT program by Hammer et al. (2004), has been performed to reveal cyclicity in the planktonic foraminiferal $\delta^{13}C$ and $\delta^{18}O$ isotope records in the time domain which can potentially be linked to the astronomical parameters (See Section 2.7 for detailed methodology). Significant peaks in the $\delta^{18}O$ spectrum are present (Fig. 4.13), which correspond to 100 kyr (eccentricity), and 22 kyr (precession) cycles, with confidence levels greater than 99%. Peaks corresponding to the 40 kyr obliquity and 26 kyr precession cycles are also present, with confidence levels between 90 and 95% (Fig. 4.13). The redfit power spectrum of $\delta^{13}C$ shows a significant peak at 40 kyr with confidence levels greater than 99%, but eccentricity and precessional cycles appear dampened.

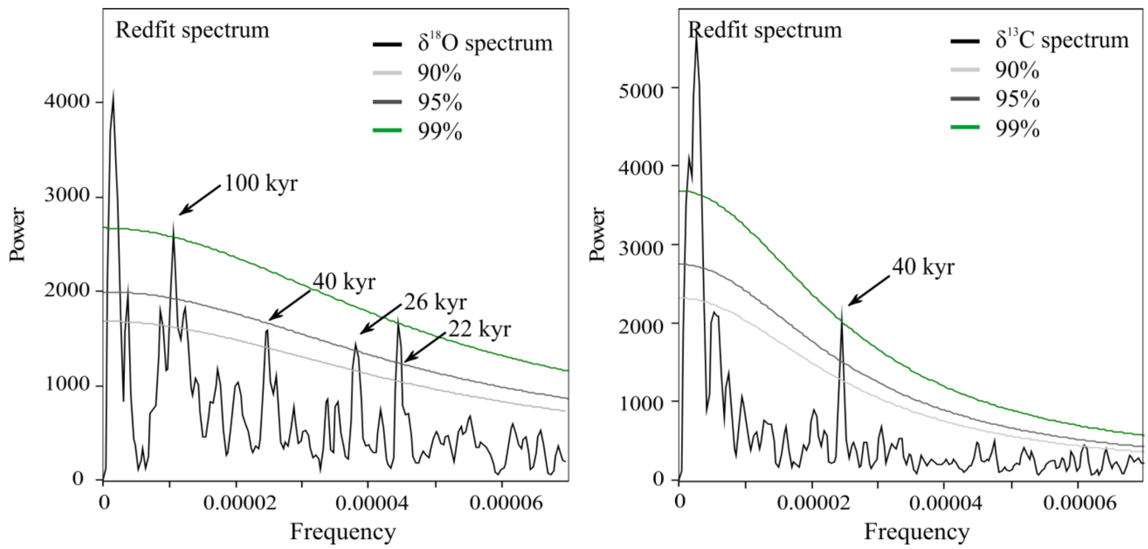

Figure 4.13. Redfit spectral plots of entire unedited planktonic foraminiferal $\delta^{18}O$ and $\delta^{13}C$ data against age.

Redfit spectral analysis of the benthic foraminiferal data set reveals a significant peak present in the $\delta^{18}O$ spectrum (Fig. 4.14), which corresponds to 40 kyr (obliquity) cycles, with confidence levels greater than 99%. Peaks corresponding to the 100 kyr eccentricity and 22 kyr precession cycles are also present, with confidence levels between 90 and 95%. The redfit power spectrum of the benthic foraminiferal $\delta^{13}C$ record does not show any significant peaks corresponding to orbital cycles.

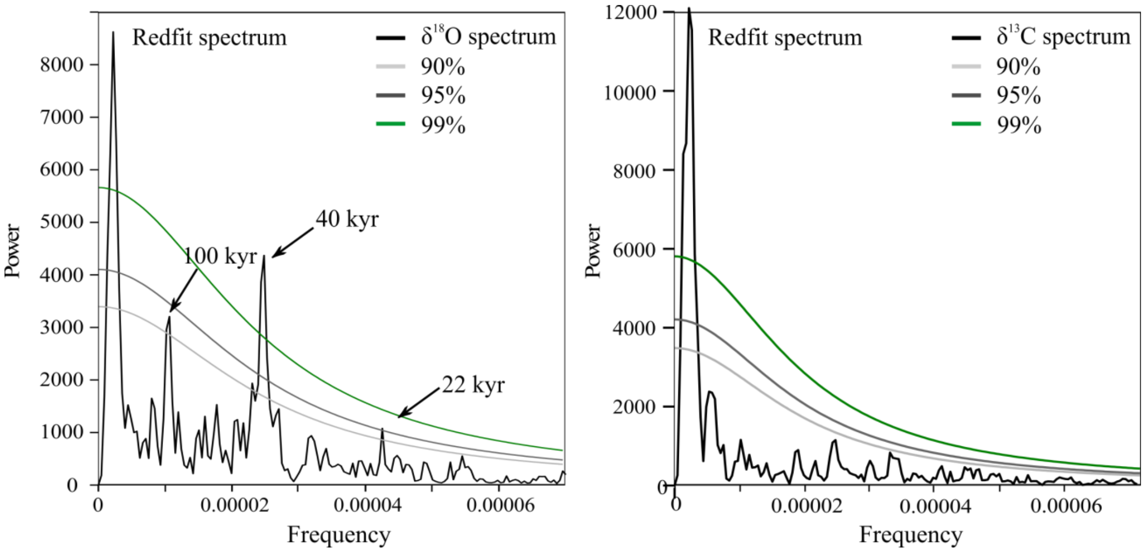

Figure 4.14 Redfit spectral plots of entire benthic foraminiferal $\delta^{18}O$ and $\delta^{13}C$ data against age.

4.3.1 Wavelet and Cross Wavelet analysis

The high resolution stable isotope records of Site U1338 reveal the long-term relationship between astronomical forcing and the response of the ocean/climate, which is embedded in the planktonic foraminiferal isotope data set. Wavelet and cross-wavelet analyses were performed between the benthic and planktonic foraminiferal $\delta^{18}O$ and $\delta^{13}C$ measurements that were presented in figures 4.15–4.16.

The wavelet plots revealed significant precession signal in both the $\delta^{13}C$ and $\delta^{18}O$ records (Fig. 4.5), and both long (400 kyr) and short eccentricity (100 kyr) are clearly imprinted on the $\delta^{18}O$ record, however enhanced 40 kyr variability stands out between 14.6 and 14.1 Ma. The long eccentricity is a prominent feature in the $\delta^{13}C$ record through most of the middle Miocene (13.3–15.5 Ma), and the obliquity cycle is especially prominent between 14.6 and 13.9 Ma.

Cross-wavelet analysis reveals significant coherency between the stable isotope records and orbital forcing and indicates that middle Miocene climate was sensitive to orbital changes in solar insolation (Fig. 4.18–4.17). The phase relationships of the planktonic and benthic foraminiferal isotope series show significant coherence in both long and short eccentricity from 13.4 to 15.0 Ma, and in the 40 kyr band between 14.6 and 14.1 Ma, however from 15.0 to 15.6 the response of planktonic foraminiferal $\delta^{18}O$ is 180 degrees out of phase.

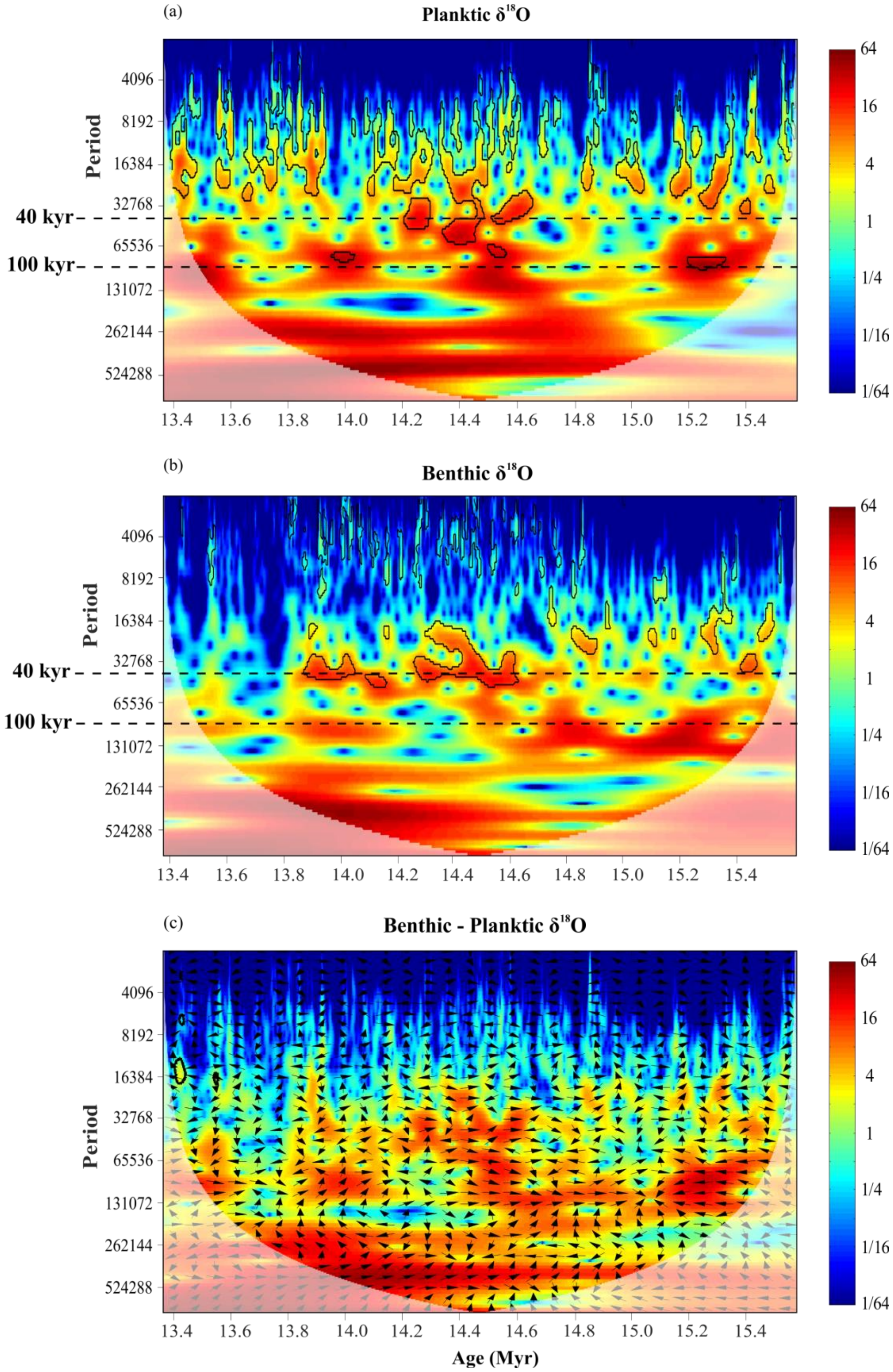

Figure 4.15. (a) Wavelet spectra of Site U1338 planktonic foraminiferal $\delta^{18}O$ time series; (b) Wavelet spectra of benthic foraminiferal $\delta^{18}O$ time series; (c) Cross wavelet transform between planktonic and benthic foraminiferal $\delta^{18}O$. Warm colours indicate regions of high common spectral power between the two time series. Regions within bold black contours are significant at the 95% confidence level against red noise. Phase arrows pointing: right: in-phase, left: anti-phase, down: benthic leading planktonic by 90°, up: planktonic leading benthic by 90.

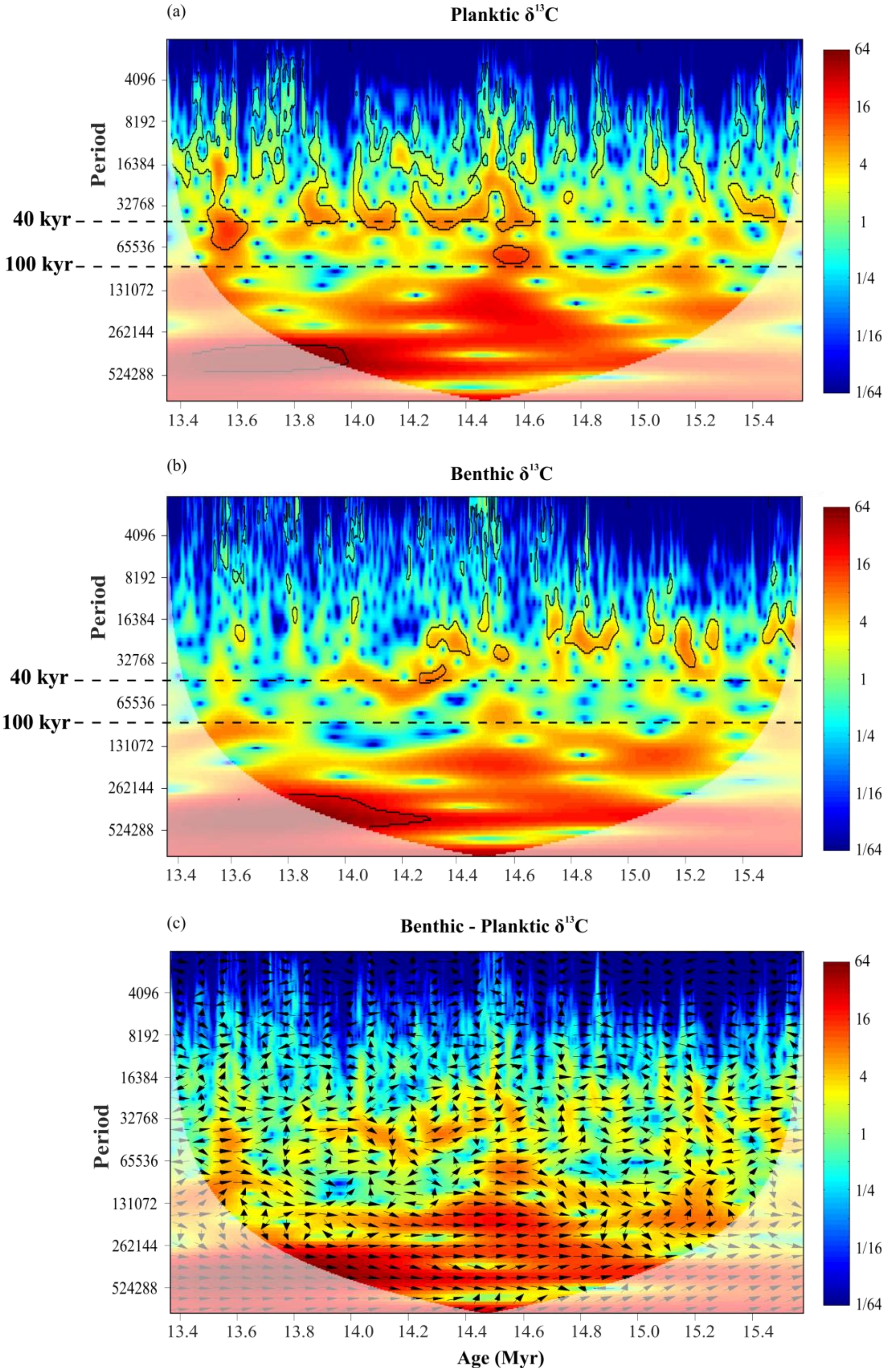

Figure 4.16. (a) Wavelet spectra of Site U1338 planktonic foraminiferal $\delta^{13}C$ time series; (b) Wavelet spectra of benthic foraminiferal $\delta^{13}C$ time series; (c) Cross wavelet transform between planktonic and benthic foraminiferal $\delta^{13}C$. Warm colours indicate regions of high common spectral power between the two time series. Regions within bold black contours are significant at the 95% confidence level against red noise Phase arrows pointing: right: in-phase, left: anti-phase, down: benthic leading planktonic by 90°, up: planktonic leading benthic by 90.

4.4 Trace metal analysis and sea surface temperatures

Low resolution planktonic foraminiferal Mg/Ca ratios, Sr/Ca, and sea surface temperature estimates are presented in table 2 (Appendix A) and plotted against $\delta^{18}O$ in figure 4.17.

4.4.1 Mg/Ca ratios

Measured Mg/Ca ratios for mixed layer dwelling species *G. quadrilobatus* range from approximately 2.80 to 3.80 mmol/mol, giving a mean value of ~3.20 mmol/mol (Fig. 4.17). Peak values of 3.83 mmol/mol supported by multiple data points are seen at 13.83 and 13.75 Ma. Average Mg/Ca values for *G. subquadratus* range between 3.5 and 4.55 mmol/mol. Between 15.4 and 15.2 Ma values increase from 3.6 to peak values of 4.55 mmol/mol, then gradually decrease to values of 3.5 mmol/mol at 14.6 Ma. Mg/Ca ratios are within the range of values observed in modern low-latitude planktonic foraminifera (Anand et al., 2003; Elderfield and Ganssen, 2000). Paired measurements in 10 samples reveal an offset of approximately 0.5 mmol/mol between specimens of *G. subquadratus* and *G. quadrilobatus* (Fig. 4.14) although no substantial offset exists in the Sr/Ca data set.

4.4.2 Sr/Ca

Sr/Ca values fluctuate between values of 1.17 and 1.35 mmol/mol (Fig. 4.17c). Between 14.4 and 15.6 Ma values remain relatively constant; ranging between 1.20 and 1.25 mmol/mol. Peak values of 1.39 and 1.35 mmol/mol are seen at 14.15 and 13.80 Ma respectively. Sr/Ca ratios are within the range of values (1.25–1.45) mmol/mol reported for low-latitude planktonic foraminifera by (Elderfield and Ganssen, 2000), and are consistent with excellent preservation and minimal recrystallization (e.g., Thomas et al., 1999). No trend is observed between Mg/Ca and Sr/Ca ratios.

4.4.3 Sea Surface Temperature estimates

SST estimates (Fig. 4.17d) calculated following Anand et al. (2003) (see Chapter 2, Eq. 2.5) based on Mg/Ca ratios from specimens of *G. quadrilobatus* (Fig. 4.17b), reveal SSTs of between 22 and 25°C for the middle Miocene eastern equatorial Pacific Ocean. Peak warmth is seen within the Mi3 excursion at 13.83 and 13.75 Ma with temperatures of 25.7 and 25.2°C respectively. Temperatures of 26°C are also seen at 13.47 Ma but are only supported by a single data point. SST estimates calculated from Mg/Ca values from specimens of *G. subquadratus* reveal a warming trend from 25 to 27.6°C over a 200 kyr interval at 15.4 Ma, after which sea surface waters cool to 25°C. The 2°C temperature offset between the two mixed layer dwelling species is discussed in section 4.5.

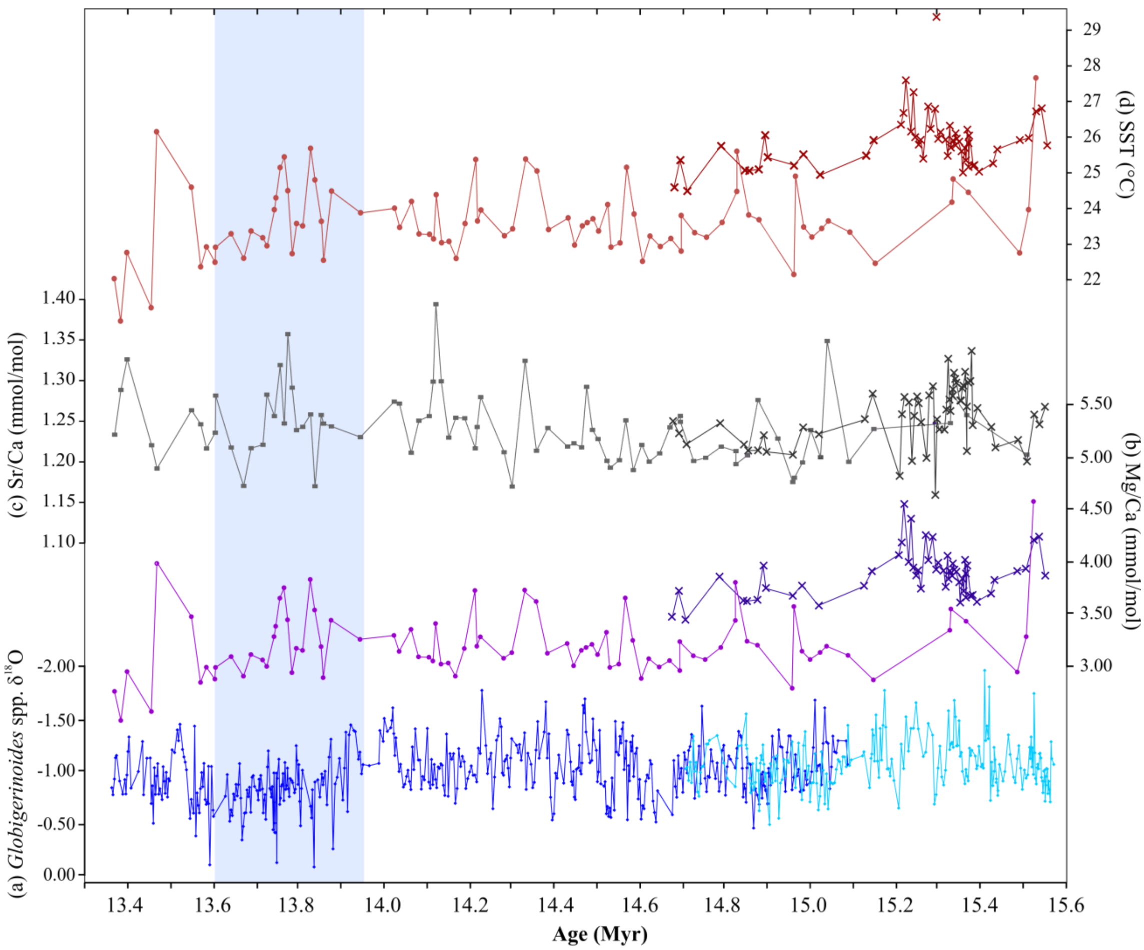

Figure 4.17. Records of $\delta^{18}O$, Mg/Ca, Sr/Ca, and reconstructed palaeotemperatures for the middle Miocene using planktonic foraminifera from Site U1338; (a) *Globigerinoides* spp. (dark blue) and *G. subquadratus* (light blue) $\delta^{18}O$; (b) Mg/Ca ratio of *G. quadrilobatus* (light purple) and *G. subquadratus* (dark purple); (c) Sr/Ca ratio of *G. quadrilobatus* (light grey) and *G. subquadratus* (dark grey); (d) Sea Surface Temperature estimates following the equation of Anand et al., (2003), from Mg/Ca ratio of *G. quadrilobatus* (light red) and *G. subquadratus* (dark red). Blue box highlights the interval of the Mi3 glaciation event and East Antarctic Ice sheet Expansion.

4.5 Discussion

The U1338 stable isotope stratigraphy is the highest resolution planktonic foraminiferal record for the middle Miocene currently available. The excellent preservation of the specimens and coherence with the benthic foraminiferal data set suggests these results are reliable and a good record of changing ocean conditions. The use of wavelet and cross-wavelet analysis is an innovative aspect of this study as it has not previously been attempted on a planktonic foraminiferal record from this interval, most likely due to the requirement for a high resolution and continuous data set. The oscillations apparent in the planktonic foraminiferal stable isotope record are interpreted to be related to Milankovitch cycles. These data are used to examine orbital variations in solar insolation through the middle Miocene and their effect on Antarctic ice volume, tropical productivity, and sea surface waters.

4.5.1 Ice volume/temperature

The U1338 planktonic foraminiferal stable isotope record, coupled with the benthic foraminiferal data and the astronomical time scale, allows documentation of the timing and magnitude of changes in past ocean conditions. The positive shift of ~ 1.2‰ in the benthic foraminiferal $\delta^{18}O$ at 13.9 Ma (Fig. 4.9) is interpreted as the expression of the major middle Miocene ice sheet expansion, referred to as the Mi3 event (Miller et al., 1991). Any change in the global ice volume should have an equal positive impact on the planktonic and benthic foraminiferal $\delta^{18}O$. However, between 13.9 and 13.7 Ma, the amplitude change in the benthic and planktonic $\delta^{18}O$ are ~1.2‰ and ~0.8‰ respectively. As ice volume fluctuations cannot exceed the variation recorded in the planktonic foraminifera, the remaining 0.4‰ $\delta^{18}O$ change has to be attributed to deep sea temperature changes and/or salinity variations.

The timing of this glaciation event is consistent with the astronomical theory of climatic change, which predicts that ice sheet growth requires low polar summertime insolation and temperatures. Specifically, high amplitude in the obliquity cycle which leads to cool high latitude summers and an insolation minimum, which in turn hinders seasonal ice melt and promotes ice build-up (Berger, 1977; Hays et al., 1976). The planktonic foraminiferal isotope records clearly show the amplitude of obliquity cycles increased suddenly during the middle Miocene (between 14.6 and 14.0 Ma) (Figs. 4.15, 4.16 and 4.18), which is suggested as a trigger for East Antarctic ice sheet expansion (Holbourn et al., 2005; 2007).

Between 15.6 and 15.0 Ma the benthic and planktonic foraminiferal $\delta^{18}O$ records show a strong anti-phase relationship in the eccentricity cycles (Figs. 4.9, 4.10 and 4.15) implying high amplitude SST and bottom water temperature changes. This is discussed in detail in the context of the global ocean in Chapter 7.

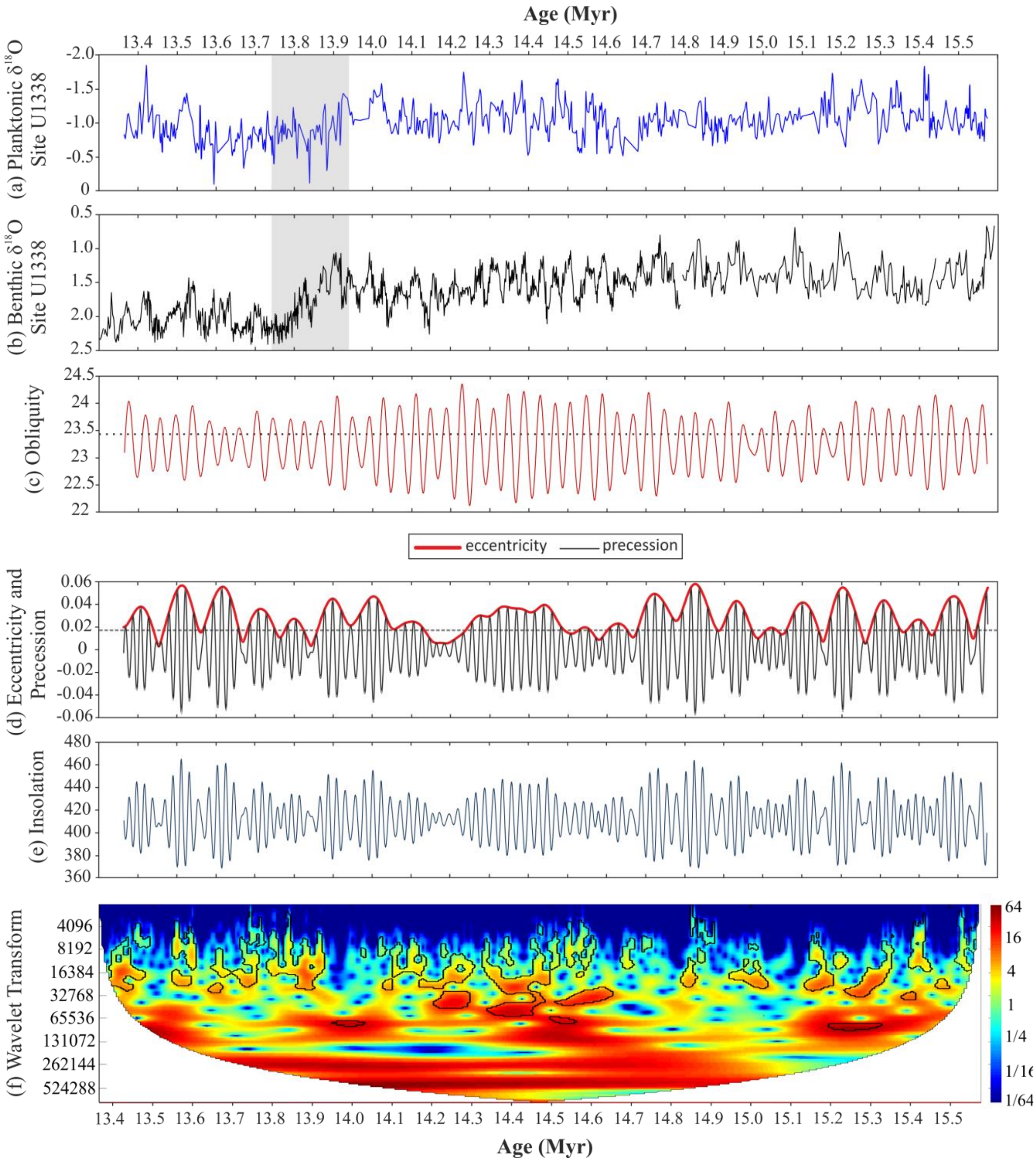

Figure 4.18. (a) Planktonic foraminiferal $\delta^{18}O$ interpolated to 1 kyr spacing ; (b) benthic foraminiferal $\delta^{18}O$ (Holbourn et al., 2014); (c) obliquity, with dashed horizontal line showing the present-day value; (d) precession and eccentricity as derived from the astronomical solution of Laskar et al. (2004), with horizontal dotted black line showing present-day values for eccentricity; (e) the variation in global mean insolation according to Laskar et al. (2004); (f) Continuous Wavelet Transform (CWT) analysis of planktonic foraminiferal $\delta^{18}O$ from Site U1338. CWT analyses program is from (Torrence and Compo, 1998).

4.5.2 Mg/Ca-based palaeotemperatures

Previous to this study, no planktonic foraminifera based SST estimates existed for the mid-Miocene eastern Equatorial Pacific Ocean. Diagenesis and the preservation of foraminiferal tests are known to have a major impact on shell geochemistry (Brown and Elderfield, 1996; Rosenthal et al., 2000), however as discussed in detail in Chapter 3, preservation is generally excellent at Site U1338. Therefore, precipitation of secondary calcite is not considered to be significantly altering the Mg/Ca record. There is an interspecies offset between *G. subquadratus* and *G. quadrilobatus* in their Mg/Ca ratios of 0.5 mmol/mol, and hence the temperature estimates, which may be due to seasonality (i.e., summer and winter temperatures) or differences in habitat depth within the water column. Studies of interspecies offsets in test Mg/Ca in modern species of *G. ruber* and *G. sacculifer* reveal the average Mg/Ca values of *G. ruber* reflect seawater temperature of the surface water mixed layer (0–25 m), whereas those of *G. sacculifer* correlate best with temperatures at 50–75 m (Sadekov et al., 2009). Measurements of Sr/Ca and other trace metals (e.g., Fe, Al, Mn, Appendix B, Fig. 2) reveal no such trend or offset. Palaeoecology of selected species of Miocene planktonic foraminifera is investigated further in Chapter 5.

Calculated palaeotemperatures based on Site U1338 foraminiferal Mg/Ca data range between 23 and 27°C (Fig. 4.17). Based on Mg/Ca values from specimens of *G. subquadratus*, temperatures rapidly warmed during the early middle Miocene from 15.4 to 15.2 Ma, to 27°C, but remained relatively stable through the middle Miocene based on temperature reconstructions from *G. quadrilobatus* (23–25°C). For comparison, modern SST's at similar equatorial Pacific sites are 26–28°C (Levitus et al., 2013), therefore, Site U1338 reveals average middle Miocene SSTs to be ~2°C cooler relative to modern mean annual conditions.

Paired analyses of Mg/Ca and stable isotope measurements highlight discrepancies between the foraminiferal Mg/Ca and $\delta^{18}O$ records (Fig. 4.17). The positive trend seen in $\delta^{18}O$ between 13.9 and 13.7 Ma linked to East Antarctic Ice Sheet expansion corresponds to marked maximum in the Mg/Ca record. The increase in Mg/Ca ratios at 13.8 Ma accommodates a ~3°C increase in water temperature. Higher resolution (< 6kyr) Mg/Ca analysis was conducted over two 100 kyr cycles to test whether SST variations were coherent with orbital variations (Fig. 4.19), however, no trend is observed between the two data sets. The apparent lack of agreement between the planktonic foraminiferal Mg/Ca and $\delta^{18}O$ records despite the excellent preservation of the specimens, suggests that ice volume and salinity must be a key components of the planktonic foraminiferal $\delta^{18}O$ record as the Mg/Ca record reveals relatively consistent tropical SSTs.

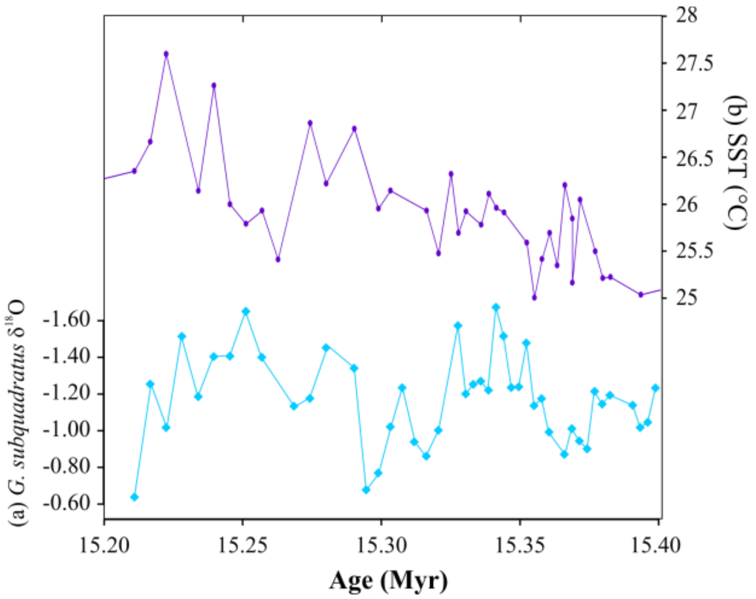

Figure 4.19. (a) *Globigerinoides subquadratus* $\delta^{18}O$; (b) Sea Surface Temperatures calculated from Mg/Ca ratios from specimens of *G. subquadratus*.

4.5.3 Carbon cycling/productivity

The planktonic foraminiferal $\delta^{13}C$ record from Site U1338 is characterised by high frequency variations (41 kyr), superimposed on lower frequency (400 kyr period) oscillations that exhibit a high degree of coherence with the benthic foraminiferal $\delta^{13}C$ (Fig. 4.16). The synchronous positive $\delta^{13}C$ (Fig. 4.11) excursions in the surface and deep ocean waters reflect major changes in the global carbon reservoir.

These carbon maxima are traditionally interpreted as primary productivity phases, which promoted the sequestration of carbon in organic rich sediments (Flower and Kennett, 1993a; Vincent and Berger, 1985), leading to a drawdown of atmospheric CO_2, and subsequent global cooling (Badger et al., 2013; Holbourn et al., 2005; Shevenell et al., 2008). At Site U1338, the argument for a more active biological pump is tentatively supported by recently published Si/Ti records for the eastern equatorial Pacific (Holbourn et al., 2014) which reveal large spikes in opal accumulation during the CM6, thus suggesting a substantial increase in EEP primary production. In addition, increased sedimentation rates during intervals of carbon maxima, in particular the CM6 (Fig. 4.5), and low $\Delta\delta^{13}C$ values are recorded at the onset of Mi3 (Fig. 4.11). The record of $\delta^{13}C$ gradient between near surface and deep waters ($\Delta\delta^{13}C$) provides a proxy of atmospheric CO_2 levels with stronger gradients signifying increased productivity at the surface and hence lower CO_2. However, pCO_2 reconstructions for the Miocene still present major challenges and require further investigation as the time scales on which CO_2 drawdown occurred remain unclear. Furthermore, modelling studies and palaeoproductivity reconstructions from Atlantic sites (DSDP 608; ODP 925, 1265) do not show any relationship between marine palaeoproductivity and benthic foraminiferal $\delta^{13}C$ excursions (Diester-Haass et al., 2009).

Additionally, if increased productivity and consequently organic carbon burial in the tropical Pacific Ocean were driving CO_2 drawdown and global cooling during the MMCT, we would expect to see $\delta^{13}C$ leading $\delta^{18}O$ in the foraminiferal stable isotope records. Yet at Site U1338 the reverse is true. Figures 4.5 and 4.8 reveal the onset of the positive trend in planktonic foraminiferal $\delta^{18}O$ at 13.9 Ma predates that of the Carbon Maxima (CM6) at 13.8 Ma suggesting that increased productivity, and hence carbon burial, followed Antarctic ice volume changes and deep water cooling but contributed as a positive feedback. Based on these results it is hypothesised that increased Antarctic ice volume, due to favourable orbital configuration, resulted in increased meridional temperature gradients which strengthened global wind patterns and thus intensified upwelling and productivity in the eastern equatorial Pacific. The highly variable $CaCO_3$ content in the period immediately before 13.9 Ma, and the relatively stable $CaCO_3$ burial afterward (Fig. 4.5), are evidence for the switch in upwelling and carbon storage (Tian et. al., 2014). In addition, the negative $\delta^{18}O$ values recorded by specimens of *Paragloborotalia siakensis* suggest a shallow thermocline in the east equatorial Pacific after the expansion if the EAIS (Fig. 4.12)

It should also be noted that ocean circulation, which plays a key role in regulating the global climate through latitudinal heat transport and CO_2 storage, is incredibly complex in the modern Pacific. For the Miocene, ocean currents and water mass distribution, though critical for understanding long term climate development, are poorly understood. In Chapter 7 modelled reconstructions of Miocene Pacific circulation are discussed with reference to Site U1338 and Site 1146 in the west Pacific Ocean.

4.6 Summary & conclusions

This chapter presents the highest resolution (3 kyr) planktonic foraminiferal $\delta^{18}O$ and $\delta^{13}C$ record currently available for the interval of 15.6–13.3 Ma in the eastern equatorial Pacific Ocean. Wavelet analysis of this data reveals clear orbital frequencies, which are illustrated for the first time in a planktonic foraminiferal data set. This chapter additionally presents the first planktonic foraminiferal record of trace metal ratios for this interval.

Key findings:

(1) The planktonic foraminiferal $\delta^{18}O$ record produced in this study reveals a positive excursion of ~0.8‰ at approximately ~14 Ma, which coincides with a ~1.2‰ excursion in the benthic foraminiferal $\delta^{18}O$ record, this is interpreted to reflect the Mi3 glaciation (Figs. 4.11 and 4.18).

(2) The planktonic foraminiferal $\delta^{13}C$ record is dominated by obliquity and displays a series of globally recognized carbon maxima (CM-events) associated with the Monterrey Carbon Isotope Excursion. Four CM events from CM5a to CM6b are identified in the $\delta^{13}C$ record. There is a strong correlation between the planktonic and benthic $\delta^{13}C$ data sets, which suggests they are recording changes in the global carbon reservoir (Figs. 4.5 and 4.11).

(3) The onset of the Mi3 glaciation predates the onset of the CM6 event, the most significant among all the CM-events (Fig. 4.8) suggesting that increased productivity, and hence carbon burial, followed Antarctic ice volume changes and deep water cooling and contributed as a positive feedback.

(4) Wavelet analysis of the foraminiferal stable isotope records reveal deep-water cooling and Antarctic ice-sheet expansion coincided with a transition from high amplitude in the 41 kyr band to high amplitude in the 100 kyr band (Fig. 4.18).

(5) The negative $\delta^{18}O$ values recorded by specimens of *Paragloborotalia siakensis* suggests a shallow thermocline in the east equatorial Pacific after the expansion if the EAIS (Fig. 4.12), which lends support to a hypothesis of increased upwelling during the Mi3 event.

(6) Sea surface temperature estimates for the eastern equatorial Pacific Ocean during the interval of 13.3 and 15.6 Ma based on Mg/Ca estimates range between 22 and 25°C (Fig. 4.17). The SST record does not reflect major increases in benthic $\delta^{18}O$ ca. 14.6 and 13.9 Ma, interpreted as ice volume growth.

5. Calibration of planktonic foraminiferal bioevents and palaeoecology

5.1 Introduction

This chapter examines the key bioevents over the middle Miocene climate transition, paying particular attention to changes in coiling direction in *Paragloborotalia siakensis*, its use as a biostratigraphic tool and the timing of this event in relation to changing surface water conditions in the Miocene equatorial Pacific Ocean. This chapter also presents multispecies stable isotope and Mg/Ca results, and investigates the palaeoecology of several species of planktonic foraminifera as identifying the depth habitat of extinct species is critical in reconstructing past sea surface temperatures (SST) and thermal gradients through the water column.

5.1.1 Biostratigraphy

Biostratigraphy – or the use of fossils for correlation and relative age assignments of sediment sequences – is the backbone of geology. In marine biostratigraphic studies, microfossils are commonly used to constrain or construct age models as well as to reconstruct palaeoceanographic conditions. One of the major marine calcareous microfossil groups in palaeoceanographic studies is foraminifera.

Planktonic foraminifera are highly important indicators of major global events, such as sea-level changes and ocean anoxic events, and their long term biological evolution is known to have been affected by many different kinds of environmental perturbation (Benton, 2009; Peters et al., 2013; Schulte et al., 2010). After the evolution of key lineages in the middle Miocene the planktonic foraminiferal population is basically structured like the modern. This means all the extant species or their direct ancestors are present and bio-provinces similar to the modern ones were established, including the low diversity or even single species dominating assemblages at high latitudes. Consequently, the climate signal can be directly derived from species distribution and abundance.

In terms of biostratigraphy the evolution and extinction of distinctive "marker species" during the Cenozoic has allowed the development of a well-established biozonation (Wade et al., 2011). The sedimentary record at Site U1338 is ideal to document the timing of planktonic foraminiferal bioevents, due to high sedimentation rates (~30 m/myr), complete recovery for the Miocene and a well-defined astronomical time scale (Holbourn et al., 2014). Additionally, the high resolution planktonic foraminiferal isotope stratigraphy generated for Site U1338 in this study creates the opportunity to identify links between biotic evolution and climate. The main focus of this project covers foraminiferal zones M5–M9 but extends to Zone M2. Several key lineages were identified: *Praeorbulina, Clavatorella, Globigerinatella and Fohsella.* However, the shipboard sampling was of low resolution with one sample taken every 3 m (roughly equivalent to 90 kyr). Therefore further high resolution biostratigraphical sampling is needed to constrain the timing of events and calibrate the foraminiferal bioevents with the magneto- and astro-chronology. This permits the timing of biotic and oceanographic events to be determined and thus has the potential to significantly enhance our understanding of both evolutionary and palaeoceanographic processes.

5.1.2 Coiling ratios

Many species of planktonic foraminifera build their tests by adding individual chambers in a trochospire which may be left-coiled (sinistral) or right-coiled (dextral). Often, a given population will exhibit "random" coiling, with 50% dextral and sinistral individuals, occasionally with a slight bias for either direction (Norris and Nishi, 2001). Other species display a strong preference toward one coiling direction or have different coiling directions in different hydrographic or biogeographic settings (Winter and Pearson, 2001). Over geological time, some taxa switch coiling direction from random or dominantly dextral to sinistral (Fig. 5.1) (Bolli, 1971). These "coiling flips" have been widely used for stratigraphic correlation as well as to infer changes in water mass conditions and sea surface temperatures (Bandy, 1960; Ruddiman, 1977; Saito, 1976; Winter and Pearson, 2001; Xu et al., 1995).

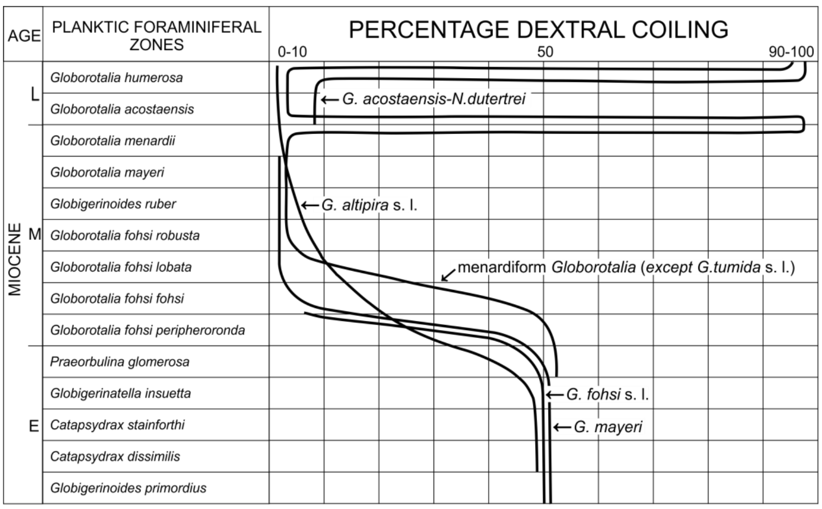

Figure 5.1. Coiling trends in selected Cenozoic taxa, adapted from Bolli (1971).

The coiling directions of foraminifera are one of the most studied morphological features for both palaeoclimate studies and local stratigraphic correlation (Darling et al., 2006; Naidu and Malmgren, 1996; Ujiié and Asami, 2014; Winter and Pearson, 2001), however, many contradictory results exist. It was Bolli who first suggested in 1950 that some lineages of foraminifera are typically characterised by an initial phase of random coiling, which is often followed by the development of a preference for either direction. Unfortunately, the trends indicated by Bolli in his synoptic text-figures are not supported by published data counts or sample locations, hence, it is difficult to assess their significance and reliability. Winter and Pearson (2001) conducted a study of the coiling direction of *Paragloborotalia mayeri* using samples from the western Atlantic and western Pacific (ODP Sites 925 and 871) to assess whether the transitions in Bolli's papers are as smooth and continuous as depicted. They found that the main transition to populations <20% dextral occurs within Zone M5. However, the study was of very low resolution and the results based upon 37 samples within a ~13.5 Myr interval (25.1–11.6 Ma). Therefore, further high resolution biostratigraphic analysis is required to test the potential of coiling direction in specimens of *Paragloborotalia* as a biostratigraphic tool.

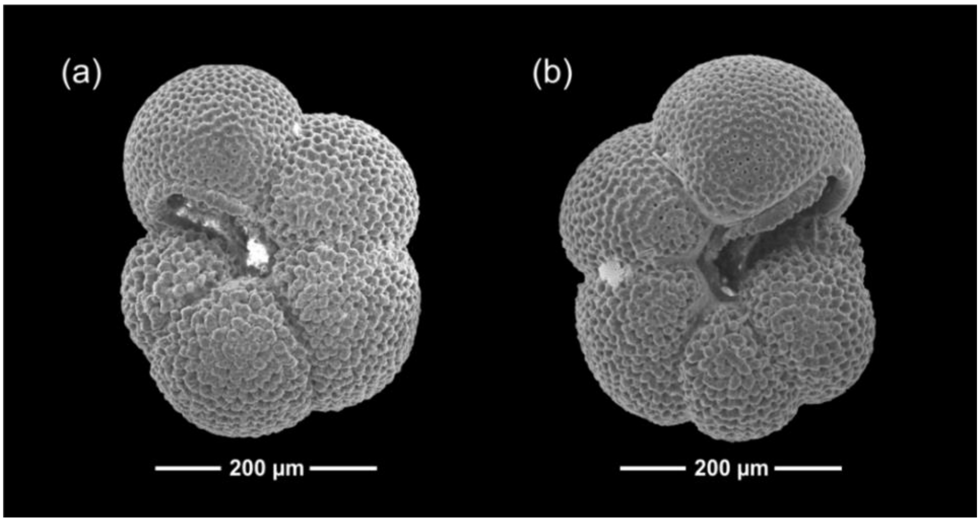

Figure 5.2. Specimens of dextral and sinistral coiling *Paragloborotalia siakensis* from IODP Site U1338; (a) Hole U1338C 39H-6, 130–132 cm; (b) Hole U1338C 39H-6,140–142 cm.

5.1.3 Planktonic foraminiferal palaeoecology and depth habitats

Planktonic foraminifera, although concentrated toward the surface, live over a range of depths in the upper part (~ top 500 m) of the oceanic water column with individual species showing depth preferences that are defined by their ecology, season of growth, local hydrographic conditions (Hemleben, 1989) as well as their life stage, as some planktonic foraminifera are known to migrate vertically during ontogeny (Deuser, 1986). The surface waters of the Ocean are typically depleted in $\delta^{18}O$ and enriched in $\delta^{13}C$ but in the deep Ocean the reverse is true (Spero et al., 1997). Consequently, the depth habitat of extinct forms of planktonic foraminifera can be inferred by performing stable isotope analysis (Norris, 1996; Wade et al., 2007). "Vital effects" (effects related to biological processes) also need to be taken into consideration when reconstructing sea surface conditions as these can cause foraminifera to calcify out of equilibrium with seawater (e.g. Katz et al., 2003). The focus of this PhD project has primarily been to reconstruct sea surface conditions in the eastern equatorial Pacific Ocean during the middle Miocene, but in order to assess the geochemical signal limited multispecies pilot data was generated. This project was challenged by finding sufficient numbers of different species and unfortunately a number of samples did not run due to small sample sizes. However, the data produced from this pilot study reveals the relative palaeo-depth habitats of a number of Miocene planktonic foraminifera.

5.2 Results

Almost all of the samples analysed contained abundant planktonic foraminifera. The fauna at Site U1338 is typical of tropical environments of the early and middle Miocene. The samples are commonly characterised by the presence of *Dentoglobigerina binaeinsis* and *Globigerinatella insueta*, *Fohsella* "*praefohsi"* and *F. fohsi*, indicating planktonic foraminiferal Zones M2 to M9 (early and middle Miocene) with *Globigerinoides* typically dominating the assemblages. Low-resolution shipboard biostratigraphic analysis was conducted during the Expedition (Pälike et al., 2010) at Hole U1338A using core catchers and supplemented by additional samples (usually two per core). The orbital chronology of Holbourn et al. (2013) and biostratigraphic analysis of assemblages from the B and C Holes, allowed a number of new and existing data to be constrained to within 3 kyr resolution (based on average sedimentation rates). The range chart in Pälike et al. (2010) identifies several taxa which were absent in this study, including *Catapsydrax unicavus* (Bolli, 1957) and *Mutabella miriablis* (Pearson et al., 2001). SEM examination of wall textures during this study revealed that specimens previously identified shipboard as *M. miriablis* are not microperforate and many specimens of *Catapsydrax* may in fact be bullate *Dentoglobigerina tripartita* (Fox and Wade, 2013).

Using insights gained through SEM studies, the shipboard range charts have been revised for extinct taxa and follows the planktonic foraminiferal zonal scheme presented in Wade et al. (2011). The biostratigraphic events have been calibrated to the orbital-chronology of Holbourn et al. (2013). The existing and revised biostratigraphic data and ranges of key planktonic foraminiferal species are shown in figure 5.3 and listed in table 5.2. Key planktonic foraminiferal species are illustrated in Chapter 3. The abbreviations LO and HO indicate the lowest and highest stratigraphic occurrence of taxa, respectively. A highest common occurrence (HCO) marks the highest sample in which a particular species is noticeably abundant, although it may occur above this level in much lower numbers.

5.2.1 Biostratigraphy of Site U1338

The absence of primary marker species *Catapsydrax dissimilis* and *Globigerinatella* sp. prevented the differentiation between Zones M3 and M4 at Site U1338. The HO of *Globigerinoides subquadratus* occurs at 390.40 mcd between samples U1338C-39H-7, 40-42 cm and C-39H-7, 30-32 cm, constraining the extinction of this species to within a 10 cm interval.

Globigerinatella insueta occurs commonly throughout Zones M3–M5 at Site U1338. The HO of this taxon is found at 385.33 mcd within Chron C5ADn (samples U1338A-38X-1, 109-111 cm–U1338A-38X-CC). However, (Pearson and Chaisson, 1997) reported the first occurrence of *G. insueta* at ODP Site 871 close to the base of C5ADr.

The boundary between Zones M5 and M6 is marked by the base of *Orbulina* spp. (*Orbulina suturalis* and *Orbulina universa*) within sample U1338A-37X-CC (368.78 mcd). This depth is based upon shipboard analysis of core-catcher samples as neither species was found during analysis of Holes U1338B and U1338C. The HO of *Clavatorella bermudezi* is located between samples U1338A-37X-CC and U1338B-38H-4, 40-42cm (368.78 mcd) within Chron C5ACn. This species was reported in only one core-catcher sample during shipboard studies (Pälike et al., 2010); however, in the post-cruise examination of Holes B and C it was present in most samples between U1338B-37H-4 and U1338C-39H-4 (369–387 mcd).

The boundary between zones M6 and M7, marked by the base of *Fohsella peripheroacuta*, was found between samples U133A-36X-CC and U1338A-35X-CC (363.86 mcd) within Chron C5ABr. Zones M6 and M7 appear reduced due to the proximity of the lowest occurrence of marker species *Orbulina suturalis* (368.78 mcd) and *F. peripheroacuta* (363.86 mcd). The LO of *Globigerinoides ruber* is found at 365.48 mcd between samples U1338B-36H-5, 140-142 cm and B-36H-5,150-152 cm. *Fohsella praefohsi* is rare in samples at Site U1338; the LO of this species, which marks the base of Zone M8, is recognised at 360.66 mcd between samples U1338A-36H-1, 38-40 cm and U1338A-36X-CC within Chron C5ABr (Fig. 5.3). This differs from previous studies which place the boundary within Chron C5ACn (Wade et al., 2011).

The LO of *Globorotalia praemenardii* was found between samples U1338A-35X-CC and U1338B-36H-2, 40-42cm (358.63 mcd) within Chron C5ABn. Above 358 mcd keeled *Globorotalia* become a frequent component of assemblages and *Paragloborotalia siakensis* increase their number of chambers in the final whorl from six to seven. The LO of *Fohsella fohsi*, which marks the base of Subzone M9a, was found between samples U1338A-35X-2, 9-11 cm and U1338A-34X-4, 91-93 cm (353.49 mcd) within Chron C5AAr.

The *Tenuitella* range into Subzone M5b, with a single specimen also recorded from Zone M8–M9/N12 in sample U1338-38H-5, 20-22 cm, (381.98 mcd), indicating a younger stratigraphic position than previously suggested by Huber et al. (2006) but consistent with Site U1337 and the southern Indian Ocean (ODP Site 744; Majewski, 2003).

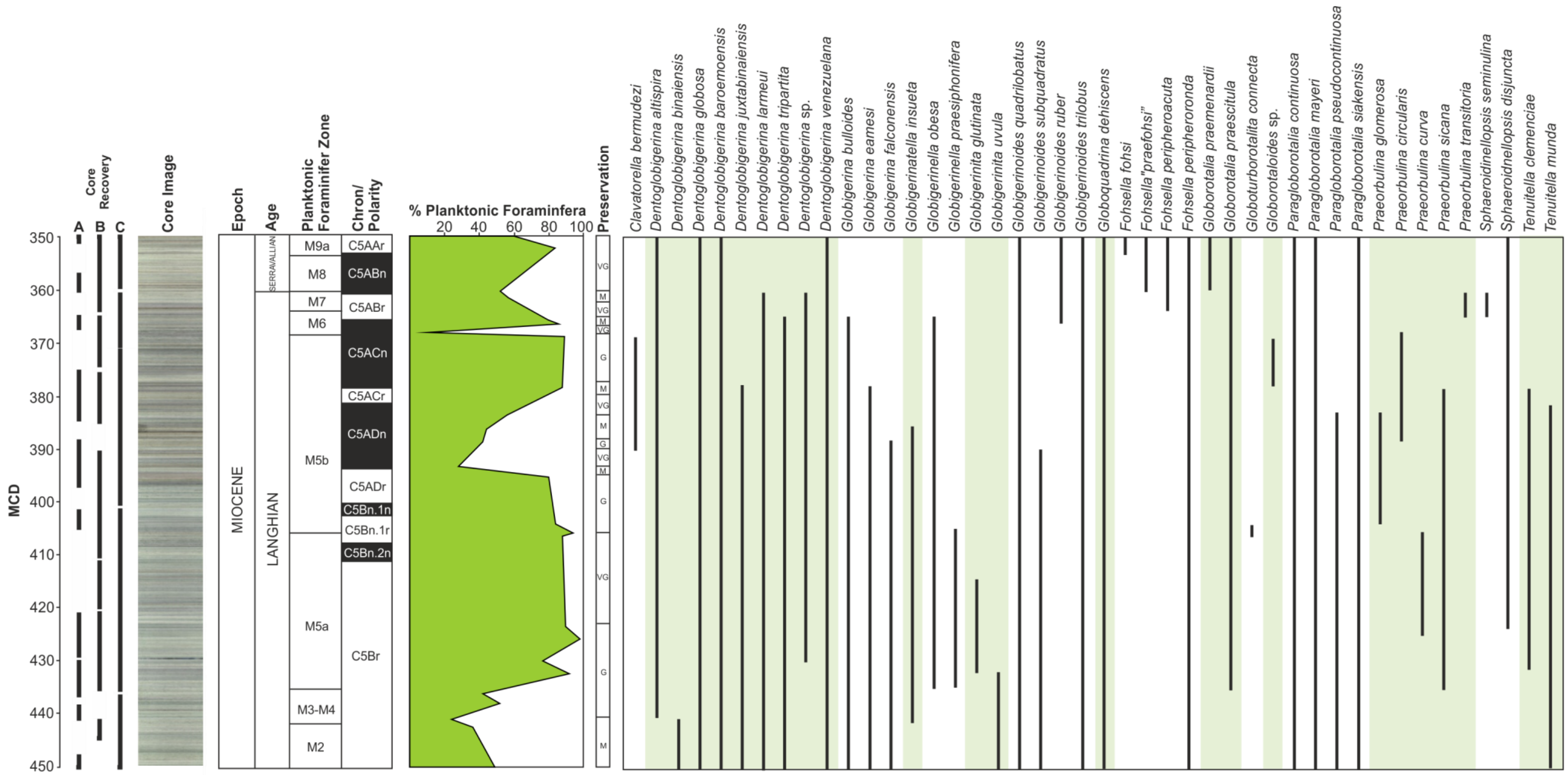

Figure 5.3. Composited foraminiferal ranges from U1338 cores A, B, and C, with taxonomic and zonal revisions (Wade et al., 2011). This study covers foraminiferal Zones M2–M9. MCD= meter composite depth. Preservation: VG 5 very good (no evidence of overgrowth, dissolution, or abrasion); G5 good (little evidence of overgrowth, dissolution, or abrasion); M 5 moderate (calcite overgrowth, dissolution, or abrasion are common but minor); P 5 poor (substantial overgrowth, dissolution, or fragmentation). (Adapted from Fox and Wade (2013)).

5.2.2 Coiling trends in Paragloborotalia siakensis

Using samples from IODP Site U1338 in the equatorial Pacific Ocean, the coiling directions of Miocene planktonic foraminifera *Paragloborotalia siakensis* have been measured at 3 kyr resolution, on 300 samples between 355–424 mcd (13.3 and 15.6 Ma). Figure 5.4 illustrates the percentage of dextral specimens of *Paragloborotalia siakensis* in samples with 10 or more specimens. The unedited data can be seen in Appendix A.

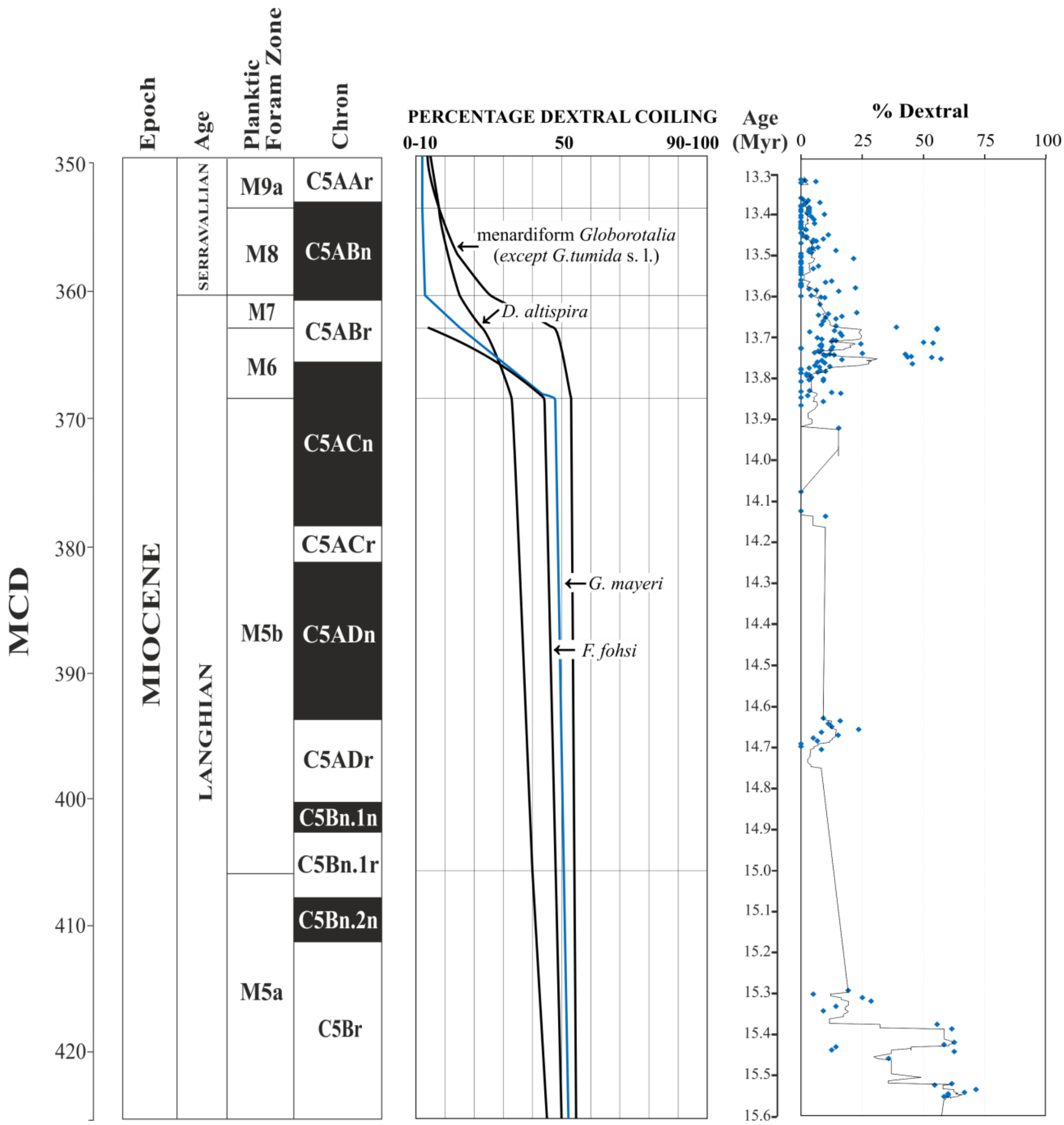

Figure 5.4. Percentage dextral coiling direction in *Paragloborotalia siakensis*, plotted next to Bolli's (1950) coiling data. Black line denotes 10 point moving average.

The initial coiling direction of *P. siakensis* appears random or slightly biased toward a dextral preference. The main transition to predominantly sinistral populations (<20% dextral) occurs over a 30 kyr interval between 15.37 and 15.34 Ma within planktonic foraminifera Zone M5a, Chron C5Br. With the exception of a brief resurgence of dextral specimens at 13.7 Ma populations remain predominantly dextral throughout the rest of the studied interval, although there are significant gaps in data coverage due to absence or low abundance of specimens.

5.3 Multispecies planktonic foraminiferal geochemistry

Multispecies geochemical data are shown in figures 5.5–5.7 and Appendix A and B.

5.3.1 Multispecies planktonic foraminiferal stable isotope results

On three samples representing 14.63 Ma, 13.60 Ma, and 13.58 Ma, measurements of $\delta^{18}O$ and $\delta^{13}C$ were made on 6 species of planktonic foraminifera from 3 different size fractions (>315μm, 250–315μm, and 150–250μm). This study was challenged by insufficient numbers of each species within the various size fractions from the same samples, and unfortunately some samples did not run. However, the multispecies stable isotope data does show a $\delta^{18}O$ gradient through the water column.

Globigerinoides quadrilobatus consistently records the most negative $\delta^{18}O$ values between -0.6 and -1.1‰, and the most positive $\delta^{13}C$ values which increase from approximately 2.5 to 3.2‰ as test size increases (Fig. 5. 6). *Dentoglobigerina venezuelana* reveals $\delta^{18}O$ values between 0.57 and −0.33‰ and carbon isotope values between 1.5 and 2.4‰. *Fohsella* sp. consistently records the heaviest $\delta^{18}O$ values and the lightest $\delta^{13}C$ values. *Dentoglobigerina altispira* and *Sphaeroidinellopsis disjuncta* appear to cluster together in the largest size fraction with $\delta^{18}O$ values between -0.4 and 0.0‰ and $\delta^{13}C$ values between 2.3 and 2.8‰. Both species show a slight trend towards decreasing $\delta^{18}O$ and increasing $\delta^{13}C$ values with increasing test size.

The size-controlled isotopic data plots reveal variable relationships between test size and $\delta^{18}O$ in the 6 species investigated (Fig. 5.6). For $\delta^{13}C$, there is evidence for positive correlations between test size and $\delta^{13}C$ for all species except *D. venezuelana,* where no clear relationship can be seen, however this may be a function of the small sample size.

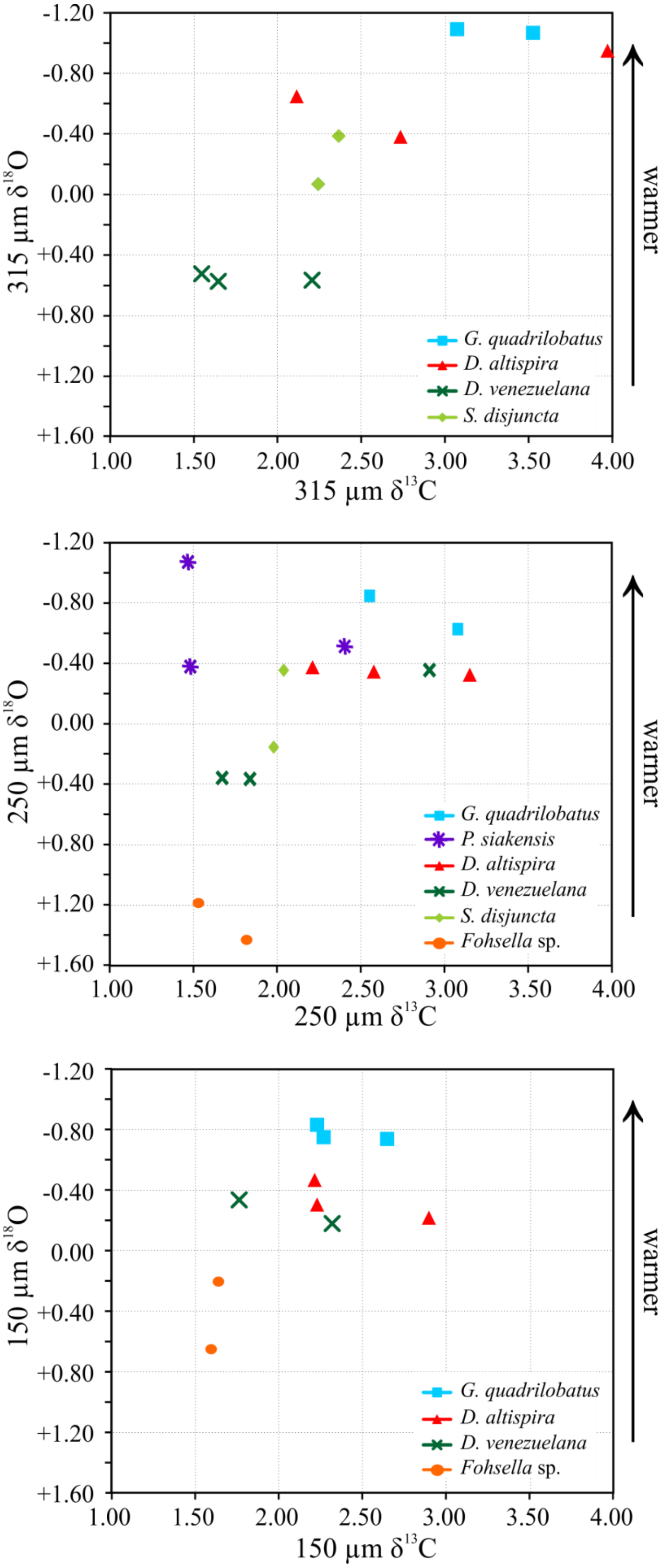

Figure 5.5. Multispecies stable isotope measurements from 3 size fractions (>315µm, 250–315µm, and 150–250µm) of planktonic foraminifera from samples: U1338B-36H-4, 40-42 cm (358.84 mcd), U1338B-36H-5, 130-132 cm (361.24 mcd), U1338C-40H-4, 40-42 cm (395.78). See Appendix A for data table.

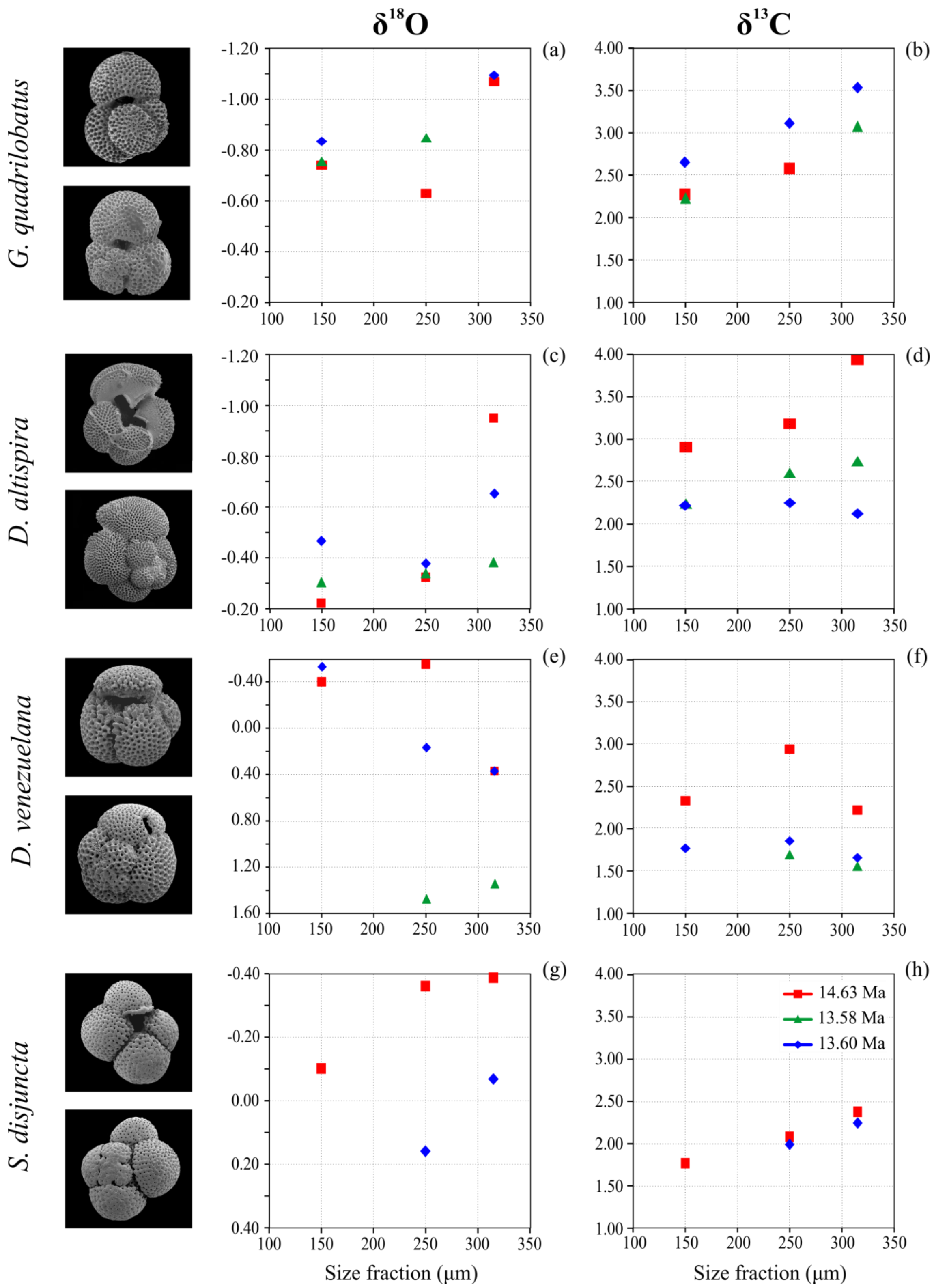

Figure 5.6. Variation in $\delta^{18}O$ and $\delta^{13}C$ compared with test size from samples: U1338B-36H-4, 40-42 cm (358.84 mcd), U1338B-36H-5, 130-132 cm (361.24 mcd), U1338C-40H-4, 40-42 cm (395.78). See Appendix A for data table.

5.3.1.1 *Clavatorella bermudezi*

Clavatorella bermudezi was found to be unusually abundant throughout its range in the Site U1338 samples which allowed multiple stable isotope analyses to be performed. The data generated sheds light on the palaeoecology of this distinct taxa and provides additional information on water column conditions over the interval of the MMCT.

The stable isotope results from *Clavatorella bermudezi* are so disparate from the multispecies data in the previous section that they are described here separately. The $\delta^{13}C$ values fall between ~1.37 and 2.20‰ (Fig. 5.7) which is consistent with the values recorded by the other sub-thermocline dwelling species such as *Catapsydrax* sp. (Wade et al., 2007) and *D. venezuelana* (Keller, 1985; Pearson et al., 1997). However, the $\delta^{18}O$ data shows extreme variability (Table 6.1) with values recorded between ~0.8 and 9.7‰.

Core, Interval, Section (cm)	MCD	Age (Ma)	$\delta^{13}C$	$\delta^{18}O$
B-37H-4, 110-112	369.98	13805096	+1.68	+2.09
B-37H-4, 120-122	370.08	13807146	+2.03	+4.06
B-37H-4, 130-132	370.18	13809196	+1.81	+3.65
B-37H-5, 100-102	371.38	13833796	+2.43	+9.73
B-37H-5, 110-112	371.48	13835846	+1.70	+3.19
B-37H-5, 120-122	371.58	13837896	+1.71	+2.07
B-37H-5, 130-132	371.68	13839946	+1.67	+2.27
B-37H-6, 0-2	371.88	13845391	+2.00	+5.24
B-37H-6, 10-12	371.98	13850078	+1.78	+2.30
C-38H-1, 120-122	372.19	13859828	+1.66	+3.53
C-38H-1, 140-142	372.39	13869203	+1.62	+2.15
C-38H-2, 0-2	372.49	13873891	+2.05	+6.01
C-38H-3, 30-32	374.29	13946464	+1.95	+2.92
C-38H-4, 140-142	376.89	14025943	+1.94	+2.65
C-38H-5, 10-12	377.09	14031000	+1.54	+2.02
C-38H-5, 50-52	377.49	14045029	+2.10	+5.14
C-38H-5, 70-72	377.69	14052061	+1.88	+2.73
B-38H-3, 60-62	379.38	14111208	+2.20	+2.84
B-38H-3, 90-92	379.68	14120552	+1.64	+1.44
B-38H-3, 110-112	379.88	14126782	+1.65	+1.93
C-39H-3, 30-32	384.30	14294389	+1.68	+2.10
C-39H-4, 20-22	385.70	14344210	+1.97	+1.88
C-39H-4, 40-42	385.90	14351854	+1.93	+1.66
C-39H-4, 60-62	386.10	14359499	+1.38	+0.81
C-39H-4, 70-72	386.40	14370965	+1.70	+1.56

Table 5.1. IODP Site U1338 *Clavatorella bermudezi* stable isotope data

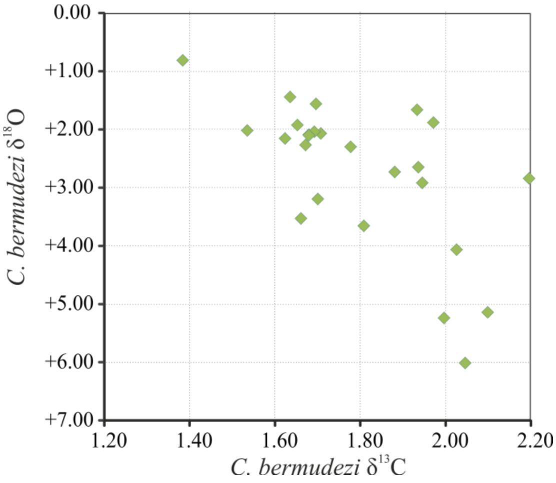

Figure 5.7. Stable isotope measurements from specimens of *Clavatorella bermudezi*.

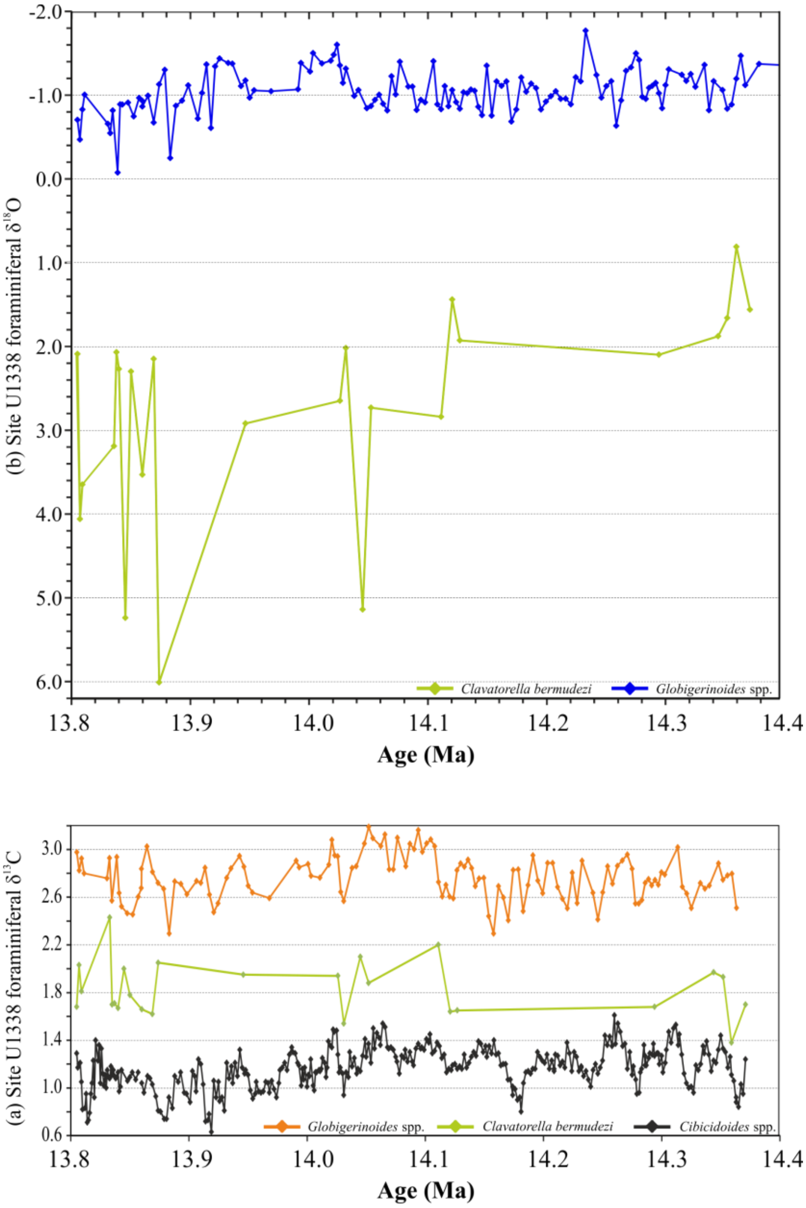

Figure 5. 8. Stable isotope measurements from specimens of *Clavatorella bermudezi* (green line) plotted against *Globigerinoides* spp (Blue line $\delta^{18}O$, Orange line $\delta^{13}C$).

5.3.2 Multispecies Mg/Ca results

Following the offset in Mg/Ca ratios between specimens of *G. quadrilobatus* and *G. subquadratus* highlighted in Chapter 4, Mg/Ca analyses were run on additional specimens of *D. altispira* and *D.venezuelana* to identify any further potential offsets in the fossil record. However, the Mg/Ca ratios for the 3 specimens shown in figure 5.9 reveal Mg/Ca ratios for all 3 species range between 2.5 and 3.5 mmol/mol with no discernable trend.

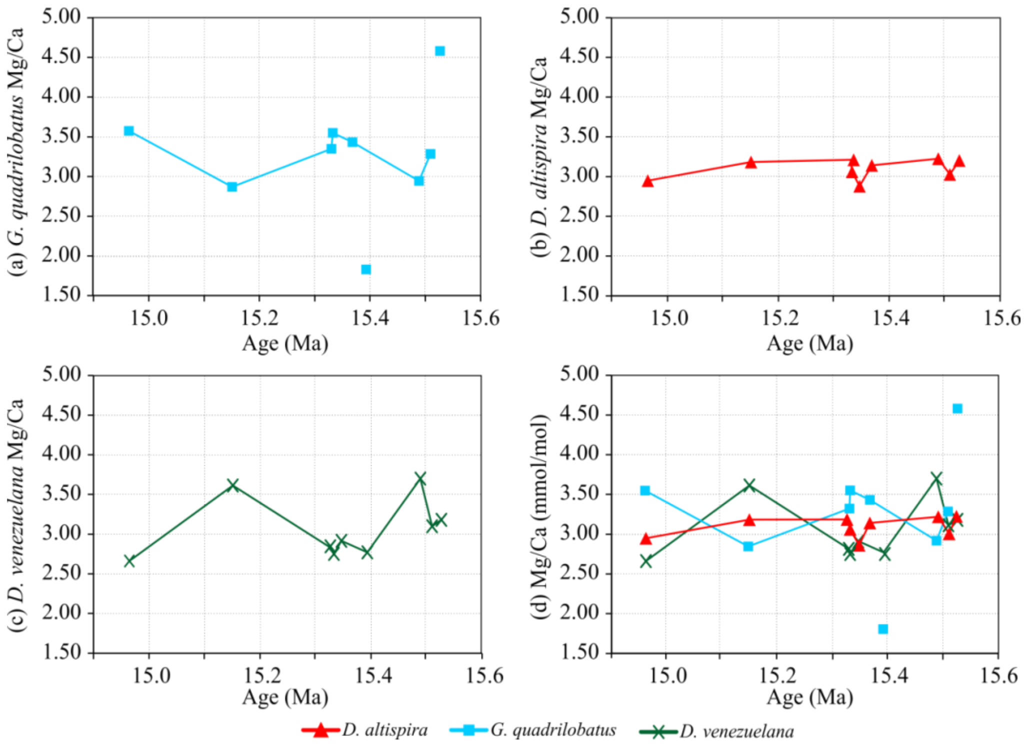

Figure 5.9. Mg/Ca ratios of selected planktonic foraminifera. Full table of results can be seen in Appendix A

5.4 Discussion

5.4.1 Recalibration of planktonic foraminiferal bioevents to the astrochronology

Neogene planktonic foraminifera have been widely studied in the subtropical and tropical Pacific (Bronnimann and Resig, 1971; Chaisson and Pearson, 1997; Jenkins and Orr, 1972; Keller, 1981; Srinivasan and Kennett, 1981). However, Miocene biostratigraphic studies suffer from a lack of open ocean sections with continuous recovery, clearly defined magnetostratigraphy and abundant well preserved planktonic foraminifera (Berggren, 1995). Previous work by Miller et al. (1985) to produce a magneto-biostratigraphy for DSDP Sites 563 and 558 in the North Atlantic was hindered by unconformities in the record. Site 925 at Ceara Rise in the western tropical Atlantic achieved continuous recovery but foraminiferal preservation at this Site is extremely variable (Chaisson and Pearson, 1997). Therefore, Site U1338 offers a unique opportunity to produce an astro-magneto tuned biostratigraphic record for the middle Miocene (Fig. 5.11). The resulting ages for many of the bioevents (Fig. 5.6) are significantly younger than those recorded in Berggren (1995) and Wade et al. (2011).

Diachrony is frequently reported for biostratigraphic datums in the geological record, however temporal discrepancies can reflect a number of factors. It is therefore important to distinguish between genuine and “apparent” diachrony. “Apparent” diachrony can arise in a number of ways; for example, through sampling artefacts. Biostratigraphic analysis is typically conducted on samples which are stratigraphically widely spaced, resulting in poor temporal and stratigraphic resolution of bioevents, thus creating potential offsets to bioevents when correlated between sites (Raffi, 1999). Furthermore, unreliable (or lack of) magnetostratigraphy at a number of sites limits the accuracy of the calibration of biostratigraphic datums to the GPTS (Edgar et al., 2010), and unrecognised unconformities in sample sections can distort species apparent ranges and give a false impression of diachrony (Aubry and van Couvering, 2005). A number of temporal offsets were found between the estimated first and last appearance datums at Site U1338 and the published datums for the Cenozoic time scale. These are discussed further in the following sections.

5.4.1.1 LO *Clavatorella bermudezi* (14.51 Ma)

At site U1338 the base of *Clavatorella bermudezi* is found at 387 mcd which places its lowest occurrence at ~14.51 Ma, revealing a much shorter range than previously recorded in the literature (Table 6.2) (Wade et al., 2011). This datum was found higher than expected in comparison with the Atlantic records of Sites 925 and 926 which places the first appearance datum (FAD) at ~15.73 Ma (Pearson and Chaisson, 1997; Wade et al., 2011). The consistent presence of this taxon in samples between 369–387 mcd (13.78–14.51 Ma) suggests that the level of this datum is accurate for Site U1338, and is not being misrepresented due to other factors such as poor preservation. Thus implying diachronism of this event between the eastern Pacific and the western Atlantic at Ceara Rise (Chaisson and Pearson, 1997), or strong environmental controls on distribution.

For some lineages the LO of a species can be difficult to identify accurately, however, *C. bermudezi* evolved from *Globorotaloides hexagonus* apparently by rapid transition (Pearson and Chaisson, 1997) and the latter species was not found in the Site U1338 sediments. The 1.2 Myr offset in the LO of *C. bermudezi* between Site U1338 and Ceara Rise (Chaisson and Pearson, 1997) exceeds the variability expected from methodological or age model inconsistencies. It is therefore interpreted to represent a case of geological diachrony, which suggests that *C. bermudezi* may have had its evolutionary first appearance in the western Atlantic and later expanded its biogeographic range.

5.4.1.2 HO *Clavatorella bermudezi* (13.79 Ma)

At Site U1338 *C. bermudezi* is found in almost every sample within its limited stratigraphic range. Its extinction at 369.28 mcd proved to be one of the most successful datums for correlation between the eastern Pacific Ocean and western Atlantic. In the most recent revision of the Cenozoic time scale (Wade et al., 2011) the datum was placed at 13.82 Ma based upon biostratigraphic analysis of samples from Ceara Rise, at a resolution of ~1.5 m (Site 925 (Pearson and Chaisson, 1997)). The high resolution study (10 cm intervals/3 kyr) presented here further refines this date to 13.79 Ma. The difference between the recalibrated age of 13.79 Ma at Site U1338 and 13.82 Ma at Site 925 is minimal (only 30 kyr) and can be accounted for by the lower resolution biostratigraphic analysis at Site 925. This indicates that the extinction of this taxon is near synchronous in the tropics, and provides a robust bioevent for the middle Miocene.

5.4.1.3 HO *Globigerinoides subquadratus*

G. subquadratus is the most common species in the early Miocene samples. The extinction of *G. subquadratus* has previously been located within the *Globorotalia mayeri* Zone (M11) (Martinotti, 1990). However, at Site U1338 this event is recorded at 14.41 Ma (387.35 mcd) in the far older planktonic foraminifera Zone M5b. A thickness of 23 m (750 kyr) was also measured between the last occurrence of *G. subquadratus* and the first occurrence of its homeomorph *Globigerinoides ruber* (d' Orbigny, 1839). This non-overlapping interval has been mentioned by various authors (Blow, 1969; Bolli, 1957; Chaisson and Leckie, 1993; Liska, 1985; Martinotti, 1990; Stainforth et al., 1975) with the length of the interval varying between sites. Therefore, further high resolution biostratigraphic research is needed to determine the diachronism of this event.

5.4.1.4 HO *Tenuitella munda*

The range of *Tenuitella* is poorly constrained for Site U1338 as the smallest size fraction (63–150 µm) was only scanned for distinctive taxa at low resolution. The highest occurrence however is recorded at 14.17 Ma (381 mcd, sample U1338B-38H-5, 20–22 cm); significantly younger (6 Ma) than recorded at other oceanic settings (Berggren, 1995; Pearson and Chaisson, 1997). There is no evidence for bioturbidation or otherwise at Site U1338, therefore this occurrence level can be assumed to be *in situ*. Based on this study a preliminary new range for this species is suggested, but further work on the smallest taxa are required in order to accurately constrain the age.

5.4.1.5 *Praeorbulina* lineage

Praeorbulina acts as the diagnostic index genus for the lower middle Miocene interval. However, specimens were found to be rare in Site U1338 samples. Therefore the shipboard biostratigraphy of the core-catcher samples is retained for biomarkers *Praeorbulina curva* and *P. glomerosa* and remains poorly constrained for the eastern Pacific. *Praeorbulina circularis* was the most consistently present species of its genus and is well constrained for this site.

5.4.1.6 *Fohsella* Lineage

The *Fohsella fohsi* group represents one of the best documented evolutionary sequences in Neogene planktonic foraminifera (Turco et al., 2002) and forms the basis of the middle Miocene planktonic foraminiferal zonation. In the evolutionary model described by Blow and Banner (1966) the *F. fohsi* lineage is characterised by the acquisition and the development of imperforate keel. The earliest gradual morphological changes are recorded in the Site U1338 samples above 369 mcd (Fig. 5.3). *Fohsella peripheroronda* represents the earliest member of the *F. fohsi* lineage and is characterised by a rounded axial periphery; its highest occurrence is recorded in samples at 350 mcd which are dated at 13.31 Ma. This places it as ~500 kyr younger than previously recorded in Wade et al. (2011). *F. "praefohsi"* is the intermediate form between *F. peripheroacuta* and *F. fohsi* and becomes progressively more compressed in the final chambers with the development of a distinctive imperforate keel in the final two chambers. At Site U1338 the keel is not well developed. However, a clear morphological change within *F. peripheroacuta* population towards *F. praefohsi* occurs at 365.48 mcd (between samples U1338A–36X–1, 36-38 cm, and U1338A–36X-CC). The inhibited development of the peripheral keel suggests that at Site U1338 the environmental conditions were not optimal for the *F. fohsi* lineage (Chaisson and d'Hondt, 2000). The timing of *Fohsella* evolution is generally consistent with the literature but on average is 200–500 kyr younger than recorded at other sites. However, the datums are defined by a gradual transition between two morphospecies which will be placed in subtly different places by different biostratigraphers, imparting a degree of uncertainty to the calibration of this datum (Pearson and Chaisson, 1997). This highlights the importance that all biostratigraphers adopt a strict species taxonomic concept and illustrate SEM images of specimens to enable accurate inter-site comparisons.

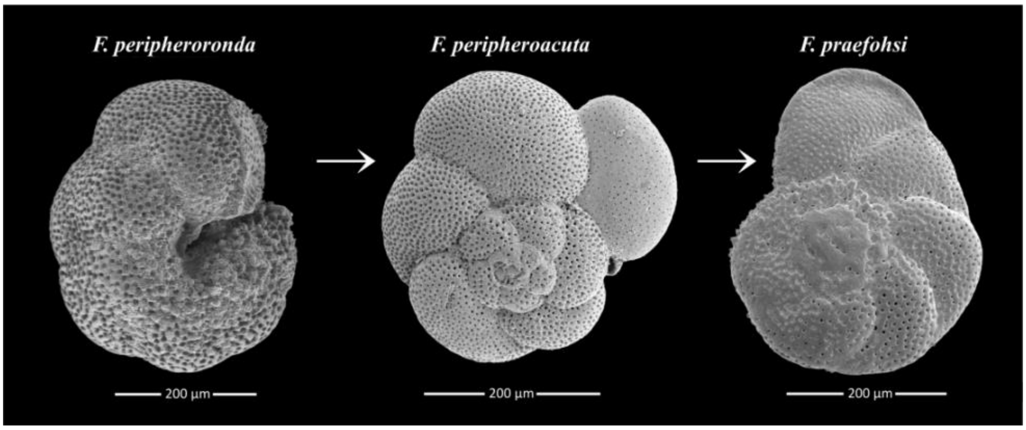

Figure 5.10. *Fohsella* lineage from Site U1338; *F. peripheroronda*, U1338A-38X-CC; *F. peripheroacuta*, U1338B-36H-2, 30-32cm; *F. praefohsi*, U1338B-36H-2, 40-42 cm.

5.4.1.7 *Globigerinatella* lineage

Although never common, *Globigerinatella insueta* is present in sufficient numbers at Site U1338 to provide a reliable datum. The LO of *G. insueta* is found at 446.70 mcd which places the first appearance datum at 16.42 Ma, ~1.17 Ma younger than previously recorded in Wade et al. (2011) from samples in the western Atlantic, and 2.2 Ma younger than reported at Sites 1146 and 1143 in the South China Sea (Nathan and Leckie, 2003), indicating marked diachrony in first appearance datum. This species was originally described as the only member of its genus by Cushman and Stainforth (1945), who used its first occurrence as the marker of the *G. insueta* Zone. The evolution of *G. insueta* is described in detail in Chaisson and Pearson (1997) with the earliest forms lacking any supplementary apertures which then became known as *Globigerinatella* sp. *Globigerinatella* sp. was not present at Site U1338 which prevented planktonic foraminifera Zone M3 from being defined here. *G. insueta* becomes extinct at 385.22 mcd, which places its last appearance datum at 14.33 Ma; ~300 kyr younger than the most recent calibration for this species at Ceara Rise (Wade et al., 2011).

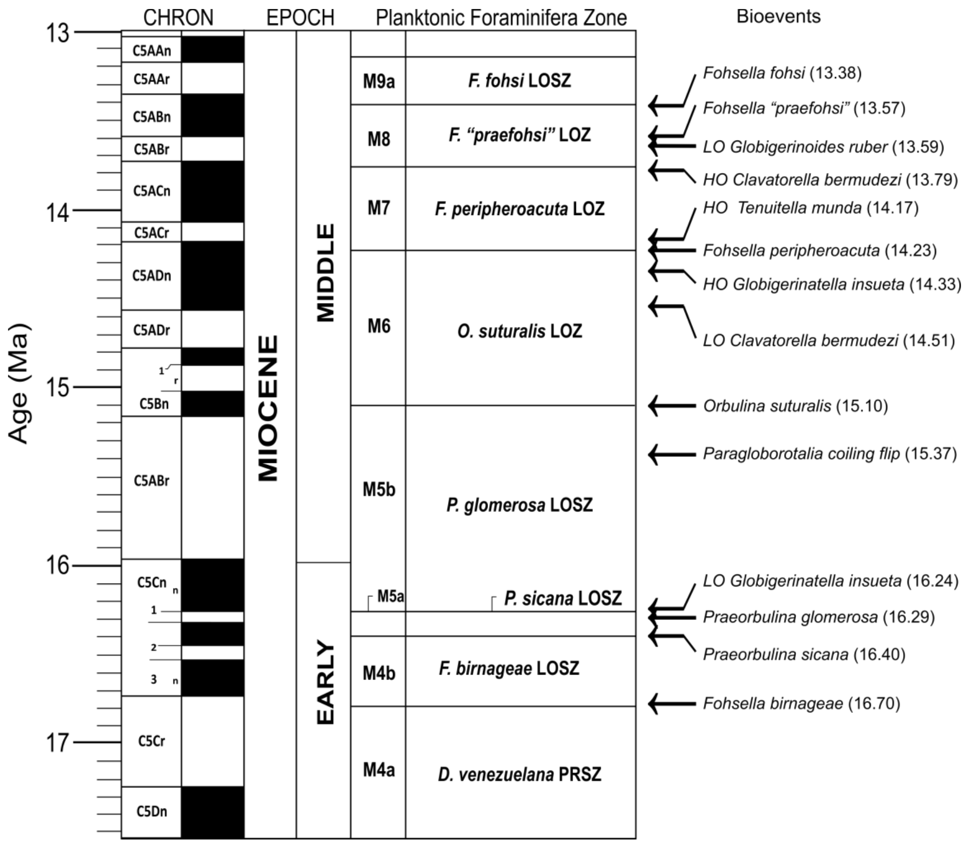

Figure 5. 11. Primary and secondary planktonic foraminiferal bioevents for the early-middle Miocene.

	Bioevent	Core, Interval, Section (cm)		Depth (mcd)			Age (Ma)			Age (Ma) This Study	Published age (Ma)
		Top	Bottom	Top	Bottom	Midpoint	Top	Bottom	Midpoint		
HO	*Clavatorella bermudezi*	U1338A-37X-CC	U1338B-38H-4, 40-42	368.78	369.78	369.28	13.780	13.805	13.792	13.79 ±12.3 kyr	13.82
HO	*Globigerinatella insueta*	U1338A-38X-1, 109-111	U1338A-38X-CC	383.62	386.81	385.22	14.275	14.386	14.330	14.33 ±55.6 kyr	14.66
LO	*Clavatorella bermudezi*	U1338C-39H-6, 140-142	U1338A-39X-5, 89-91	389.9	393.30	391.60	14.475	14.561	14.518	14.51 ±43.3 kyr	15.73
LO	*Globigerinatella insueta*	U1338A-43X-CC	U1338A-44X-2, 55-57	442.68	450.71	446.70	16.275	16.576	16.426	16. 42 ±150.6 kyr	17.59
HO	*Tenuitella munda*	U1338B-38H-4, 0-2	U1338B-38H-5, 20-22	380.28	381.98	381.13	14.139	14.207	14.173	14.17 ±34.2 kyr	20.78
HO	*Globigerinoides subquadratus*	U1338C-39H-7, 30-32	U1338C-39H-7, 40-42	387.30	387.40	387.35	14.405	14.409	14.407	14.41 ±1.9 kyr	-
LO	*Globigerinoides ruber*	U1338B-36H-5,140-142	U1338B-36H-5, 150-152	365.48	366.78	366.13	13.716	13.721	13.719	13.72 ±2.3 kyr	-
X	*P. siakensis Coiling flip*	U1338B-41H-4,20-22	U1338B-41H-4,140-142	415.57	416.77	416.17	15.344	15.376	15.360	15.36 ±32.8 kyr	-

Table 5.2.Key planktonic foraminiferal bioevents (lowest and highest occurrences of selected taxa) for the middle Miocene. Note: Biochronology is from Wade et al. (2011) and calibrated to the astronomical timescale of Lourens et al. (2004).

5.4.2 Biological meaning of coiling ratios

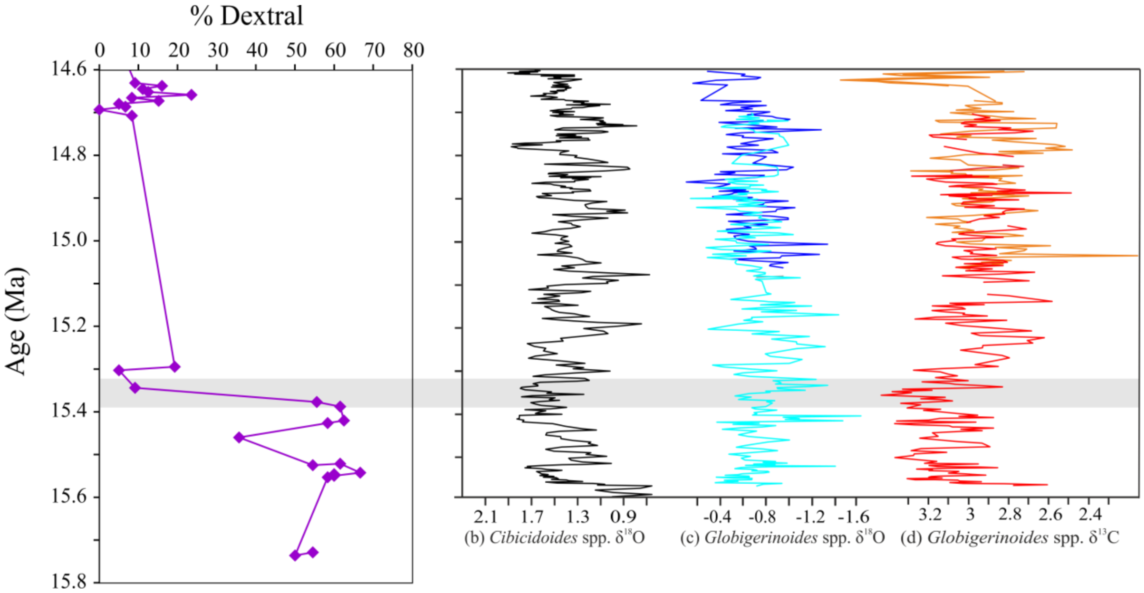

Figure 5.12. Close up of coiling change in specimens of *P. siakensis*, samples with greater than 10 specimens; (b) Site U1338 *Cibicidoides* spp. $\delta^{18}O$; (c) Site U1338 *Globigerinoides* spp. $\delta^{18}O$; (d) Site U1338 *Globigerinoides* spp. $\delta^{13}C$. Grey band highlights interval of coiling change.

Many previous investigations of planktonic foraminifera have linked coiling directions and environmental conditions (Hemleben, 1989; Kennett, 1968; Naidu and Malmgren, 1996). In figure 5.12 the coiling direction data from *Paragloborotalia siakensis* is plotted next to the planktonic and benthic foraminiferal stable isotope records of Site U1338 in order to identify any relationship between the coiling ratio of *P. siakensis* and changing sea surface conditions. During this interval a major transition from random to predominantly sinistral populations occurs at 15.4 Ma. However, the foraminiferal $\delta^{18}O$ and $\delta^{13}C$ records do not reveal any significant excursions over this event.

Figure 5.13 compares the *P. siakensis* coiling ratio data with the planktonic foraminiferal stable isotope records over the interval of the CM6 event and the EAIS expansion. Interestingly, there is close correspondence between carbon isotope variations in *Globigerinoides* spp. and the percentage of dextral specimens between 13.9 and 13.6 Ma, suggesting that this species responded directly to productivity fluctuations. Unfortunately there were insufficient numbers to see if this pattern was repeated over the other Carbon Maxima in the record.

Comparison of coiling signatures with $\delta^{18}O$ data does not reveal any simple environmental relationship and stable isotope analysis of left and right coiling specimens of *Paragloborotalia siakensis* picked from the same samples (Appendix A, Fig. 5.14) reveals no statistically significant difference in values. This suggests that the transition to predominantly sinistral populations at 15.4 Ma is not triggered by changes in sea water temperature or productivity changes. It would therefore appear that the coiling direction of *P. siakensis* is controlled by genetic mechanisms. Past research into DNA sequencing of modern planktonic foraminifera has suggested that morphospecies often comprise of multiple cryptic "species" (Darling et al., 2000; de Vargas et al., 1999; Huber et al., 2010) that may have different characteristic coiling directions. It may be the case that changes in the coiling ratio through time could reflect changes in the relative abundance of cryptic species, through competitive exclusion or otherwise. This hypothesis could not be tested within the time constraints of this project beyond observing that there are no obvious morphological differences between right and left coiling specimens.

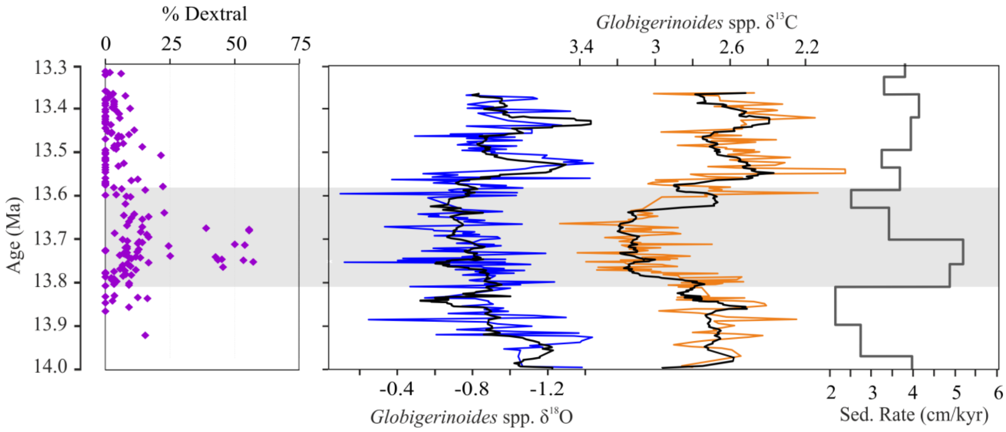

Figure 5.13. Close up of coiling change over CM6, samples with greater than 10 specimens.

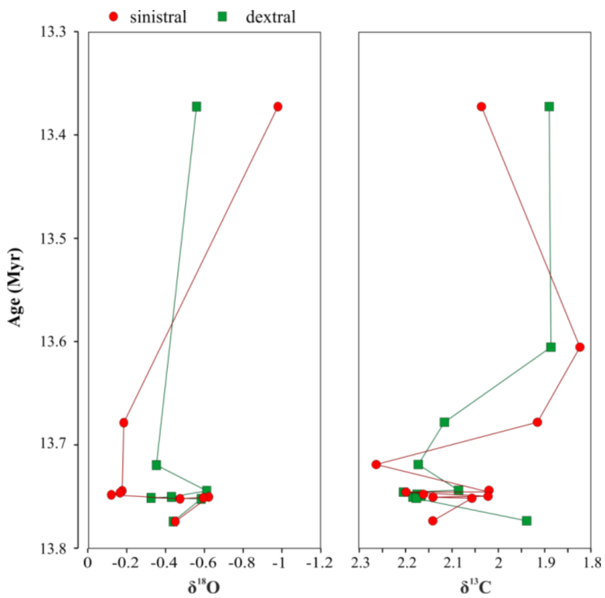

Figure 5.14. Stable isotope values for left and right coiling *Paragloborotalia siakensis*. Red circles denote sinistral specimens. Green squares denote dextral specimens.

5.4.3 Palaeoecology and depth habitat of some planktonic foraminifera

Living planktonic foraminifera are most abundant in the upper 150 metres of the water column (Hemleben, 1989). Below this depth they show an approximately exponential decline in abundance (Bé, 1977) as a result of controlling factors such as temperature, salinity, oxygen concentration and food availability, which vary greatly with depth within the water column (Hemleben, 1989; Lombard et al., 2011; Spero et al., 2003). Although not originally the focus of this project, understanding the palaeoecology of planktonic foraminifera is crucial to determining SSTs and the structure of the water column.

In the modern, the thermal gradient of the water column in tropical regions means that $\delta^{18}O$ of foraminiferal calcite can change by as much as 4‰ between species that inhabit in the mixed layer and those which reside deeper in the water column (Biolzi, 1983). Many species of planktonic foraminifera migrate through the water column during their life cycle, but the bulk of test calcite tends to be secreted within a restricted depth range (Hemleben, 1989) with the preferred depth of calcification varying from species to species. Generally speaking, open ocean taxa can be divided into mixed layer, thermocline and sub-thermocline calcifiers (Pearson et al., 1997). Species that calcify in the mixed layer tend to have the most negative $\delta^{18}O$ because they are in the warmest water (Emiliani, 1954), but often exhibit a range of $\delta^{13}C$ values caused by either depth stratification or by the presence in some species of photosymbionts. Important information on the palaeobiology of Miocene planktonic foraminifera can be gained by comparing the stable isotope results of multiple species. The multispecies stable isotope data at Site U1338 (Figs. 5.5–5.7) reveal small but marked offsets in $\delta^{18}O$ and $\delta^{13}C$ between species.

5.4.3.1 *Globigerinoides quadrilobatus*

The stable isotope measurements of specimens of *G. quadrilobatus* presented in figures 5.5 and 5.6 display a number of patterns generally consistent with those of extant species of planktonic foraminifera known or believed to harbour photosymbionts (Norris, 1996) (Figs. 5.5, 5.6, and 5.15).

Firstly it records the most negative $\delta^{18}O$ values of any coexisting species in a sample (Fig. 5.5), which does not change with increasing test size (Fig. 5.6). Photosymbiotic planktonic foraminifera must inhabit the photic zone of the ocean in order to maintain their symbionts (Norris, 1996). The warm surface water temperatures cause the shell calcite to be depleted in $\delta^{18}O$ compared to deeper-dwelling, asymbiotic taxa. *G. quadrilobatus* also generally records the most positive $\delta^{13}C$ of any species (with the exception of a single data point from *D. altispira*). This is because phytoplankton and foraminiferal photosymbionts preferentially take up ^{12}C (Spero et al. 1991) and leave the surrounding water enriched in ^{13}C which is used in foraminiferal calcification resulting in the shell calcite having enriched $\delta^{13}C$ relative to non-photosymbiotic species or thermocline dwelling species (see section 2.5.3). Figure 5.6 also demonstrates the $\delta^{13}C$ values rise with increasing shell size (typically >0.5-1.0 ‰), compared to other species analysed. This partly reflects an increase in symbiont activity and density of photosymbionts with increasing volume of the host shell (Spero, 1992; Spero and Lea, 1993; Spero et al., 1991). Miocene planktonic foraminifera are considerably smaller (>200 μm) than their modern descendants; therefore such offsets in stable isotope values between the size fractions are also likely to be smaller.

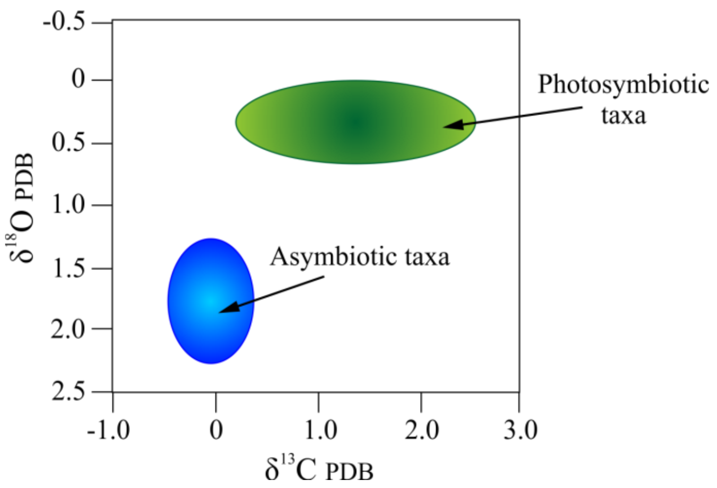

Figure 5.15. Model for oxygen/carbon isotopic variation in symbiotic and asymbiotic species adapted from Norris (1996).

5.4.3.3 *Dentoglobigerina altispira*

D. altispira evolved in the early Miocene, within Zone M1 and became extinct in the Pliocene. It is commonly used as an indicator of Miocene shallow water conditions (e.g., Hodell and Vayavananda, 1994; Nathan and Leckie, 1993; Norris et al., 1993). However, as it has no modern representative, isotopic data provides the only evidence for its depth ecology. *D. altispira* consistently records negative $\delta^{18}O$ and positive $\delta^{13}C$ relative to the other planktonic species in this study (Fig. 5.5), in line with findings reported by other authors (Pearson et al., 1993; Vincent et al., 1991) and supports a shallow-water habitat for *D. altispira*.

5.4.3.2 *Paragloborotalia siakensis*

Paragloborotaliids have previously been documented in the literature as shallow-water dwellers (Gasperi and Kennett, 1993a; Keller, 1985) and as sub-thermocline dwellers by Douglas and Savin (1978). The results from this study find that specimens of *P. siakensis* are, in general, enriched in $\delta^{18}O$ and depleted in $\delta^{13}C$ relative to mixed layer species *G. quadrilobatus* and *D. altispira* (Fig. 5.5), which is indicative of the upper thermocline (Pearson et al., 1997) and consistent with interpretations of *P. mayeri* in Pearson et al. (1997) and *P. opima* in Wade et al. (2007).

5.4.3.4 *Dentoglobigerina venezuelana*

Temperature changes most rapidly with depth through the thermocline, therefore, planktonic foraminifera calcifying within the thermocline should record a greater change in $\delta^{18}O$ than in $\delta^{13}C$ with increasing depth (Pearson et al., 1993). *D. venezuelana* consistently records the highest $\delta^{18}O$ values of planktonic foraminifera throughout the Miocene within the analysed samples, suggesting it inhabits the deep thermocline. These findings are supported by a recent in-depth study into the palaeoecology of *D. venezuelana* (Stewart et al., 2012).

5.4.3.5 *Sphaeroidinellopsis disjuncta*

No isotopic data has previously been gathered for *S. disjuncta*, however, this species yields slightly more positive $\delta^{18}O$ values (~0.4 ‰) than *D. altispira*, but in the 250 µm size fraction it yields very similar $\delta^{13}C$ values to *P. siakensis*, and *D. venezuelana*. Based on this it is tentatively classed as a thermocline dwelling species, however, further data is required to confirm this. The increase in $\delta^{13}C$ with sieved size fraction seen in figure 5.6 is well documented in other species of both living and fossil foraminifera (Elderfield et al., 2002; Franco-Fraguas et al., 2011; Spero et al., 1997). This increase is typically explained citing different rates of calcification, respiration and photosynthesis (in symbiotic species) along foraminiferal ontogeny. These factors influence the chemistry of the surrounding sea water of the foraminifera and hence the $\delta^{13}C$ recorded in the tests (Franco-Fraguas et al., 2011; Zeebe et al., 1999). These results highlight the importance of evaluating size-related stable isotope variability in areas of paleoceanographic interest.

5.4.3.6 *Fohsella* sp.

Previous work by Norris et al. (1993) proposed that the *Fohsella* lineage was initially a shallow-water dweller but shifted its habitat preference into deeper water between 13.0 and 12.7 Ma. At Site U1338, in samples dated at ~13.6 Ma, it was found that *Fohsella* sp. oxygen isotope values fall between 1.2‰ and 1.47‰ in the 250 μm size fraction and are consistently heavier than *D. venezuelana* by 1.0 ‰ ±0.2‰. The enriched $\delta^{18}O$ results in comparison to *D. venezuelana* suggest that these taxa occupy a deep-dwelling (sub-thermocline) habitat and do not support the conclusions of Norris et al. (1993) and perhaps shifted its habitat preference to deeper water earlier than previously thought. Unfortunately, there were insufficient numbers of specimens in the Site U1338 samples to investigate this further.

5.4.3.7 *Clavatorella bermudezi*

Clavatorella bermudezi was found to be unusually abundant throughout its range in the Site U1338 samples, which allowed the creation of a robust biostratigraphic calibration for this distinct clavate form and afforded the opportunity to perform multiple stable isotope analyses. The $\delta^{18}O$ and $\delta^{13}C$ of multiple species of planktonic foraminifera can be used to reconstruct the temperature structure of the upper water column (e.g., thermocline) and the productivity by establishing the isotopic gradients between species that live in the surface mixed layer and species that within or below the thermocline. It is well known that oceanic upwelling is accompanied by thermocline shallowing, thinning of the mixed layer, sea surface temperature decrease, and surface water nutrient enhancement (Calvo et al., 2011). These changes are recorded in the $\delta^{18}O$ and $\delta^{13}C$ of planktonic foraminiferal calcite (e.g., Prell and Curry, 1981; Sautter and Thunell, 1991; Ravelo and Fairbanks, 1992; Kroon and Darling, 1995; Thunell et al., 1999). Because upwelling may have a significant impact on surface productivity, and thus on the global carbon cycle, the identification of upwelling in fossil records is an important factor in understanding past climate change and the forcing mechanisms behind those changes (Pak and Kennett, 2002).

However, the interpretation of down core planktonic foraminiferal isotopic records is dependent on understanding the calcification depths of the different planktonic foraminiferal species and how these depths may vary seasonally and inter-annually in response to hydrographic changes (Pak and Kennett, 2002). The $\delta^{l3}C$ values recorded by *C. bermudezi* are consistent with a deep-water habitat, however, the $\delta^{18}O$ values fluctuate wildly between values typical of benthic foraminifera to seemingly unrealistic values of between 3.0 and 6.0‰ (Table 5.1, Fig. 5.7). Based upon its $\delta^{13}C$ values, *C. bermudezi* is interpreted as a sub-thermocline dweller, but unrelated to this there appears to be some unknown vital effect, which is radically altering the oxygen isotope signal. On close inspection maximum values in *C. bermudezi* $\delta^{18}O$ do not correspond to enriched data points in the *Globigerinoides* spp. $\delta^{18}O$ record and the magnitude of change seen in the *C. bermudezi* data set suggests caution is required when interpretating from this highly variable data set. The planktonic foraminiferal $\delta^{13}C$ record from *C. bermudezi* at Site U133, despite being of low resolution, reveal (sub)thermocline $\delta^{13}C$ values fall to approximately 1.6‰ at 13.86 Ma as the $\delta^{13}C$ of *Globigerinoides* spp. increase to ~3.0‰ (Fig. 5.8). This results in increased vertical carbon isotope gradients ($\delta^{13}C$) between surface and deeper dwelling planktonic foraminifera, which signify intervals of increased productivity as ^{12}C is preferentially removed from sea water during photosynthesis

Intriguingly, the sharply defined extinction of *C. bermudezi* is near synchronous in the Pacific and Atlantic Oceans (Pearson and Chaisson, 1997) and broadly coincides with the end of the MMCT at 13.79 Ma, leading to the possibility that deep water cooling may have played a role in the extinction of *C. bermudezi*. Although currently there is no detailed benthic foraminiferal assemblage data for Site U1338 over the MMCT, a period of major faunal change is recorded in the Indian Ocean between ~14 and 13 Ma (Smart et al., 2007), which tentatively supports the hypothesis that deep water cooling affected species living at depth in the water column. DSDP Site 289 also records the extinction of many Oligocene-early Miocene species between 16 and 13 Ma but the timing of these events are poorly constrained (Woodruff and Douglas, 1981).

5.4.3.8 Trace metal results

An unexpected result of this study was finding that there is no offset between species in Mg/Ca ratios (Fig. 5.7) which conflicts with the $\delta^{18}O$ values and interpretation of depth habitat. An interspecies offset in the Sr/Ca ratios would reveal if the values were being altered by vital effects as the Sr/Ca ratio should be consistent throughout the water column. However, no significant offset in Sr/Ca ratio is recorded between any of the species analysed (Appendix B). Unfortunately, there is no published multispecies planktonic foraminiferal trace element data available to compare.

5.5 Summary

This chapter examines the planktonic foraminiferal bioevents and the palaeoecology of selected species at Site U1338 over the middle Miocene climate transition. High-resolution biostratigraphic analysis of assemblages from the B and C Holes applied here allowed a number of new and existing data to be constrained to within 12 kyr resolution.

Key findings:

(1) New and more precise constraints are placed on the ranges of *C. bermudezi*, *G insueta, T. munda, G. subquadratus,* and *G. ruber* through high resolution biostratigraphy combined with the Holbourn et al. (2013) astronomically tuned time scale. The results of this study highlight the need for high resolution biostratigraphic work and integrated bio-chronologies in order to reduce the uncertainty of a number of events and study potential diachrony between the Atlantic and Pacific oceans.

(2) The high-resolution biostratigraphic and multispecies stable isotopic analyses at Site U1338 reveal the rapid coiling change of *Paragloborotalia siakensis* identified at 15.37 Ma is potentially of use as a new biostratigraphic correlation, the trend appears to be genetically controlled rather than by temperature of productivity changes.

(3) The life environment of a variety of planktonic foraminifera species have been inferred according to interspecies differences in their carbon and oxygen isotopic ratios:

Mixed-layer dwellers:	*Globigerinoides quadrilobatus* *Dentoglobigerina altispira*
Shallow thermocline dwellers:	*Paragloborotalia siakensis*
Thermocline dwellers:	*Dentoglobigerina venezuelana* *Sphaeroidinellopsis disjucta*
Sub-thermocline dwellers:	*Fohsella* sp. *Clavatorella bermudezi*

Sample Core, Interval, Section (cm)	**MCD**	**Preservation**	**% Planktic foraminifera**	**Planktic Foraminiferal Zone**	*Clavatorella bermudezi*	*Dentoglobigerina altispira*	*Dentoglobigerina binaiensis*	*Dentoglobigerina globosa*	*Dentoglobigerina baroemoensis*	*Dentoglobigerina juxtabinaiensis*	*Dentoglobigerina larmeui*	*Dentoglobigerina tripartita*	*Dentoglobigerina* sp.	*Dentoglobigerina venezuelana*	*Globigerina bulloides*	*Globigerina eamesi*	*Globigerina falconensis*	*Globigerinatella insueta*	*Globigerinella obesa*	*Globigerinella praesiphonifera*	*Globigerinita glutinata*	*Globigerinita uvula*
U1338C-35H-5, 90-92	345.81	VG	~	M9		●								●								
U1338C-36H-2, 110-112	352.44	VG	~	M9										●								
U1338B-36H-2, 40-42	355.84	VG	~	M9				●	●					●								
U1338A-35X-2, 9-11	360.12	M	52	M9		●					●		●	●								
U1338A-35X-CC	361.42	M	57	M8		●		●	●		●			●								
U1338C-37H-1, 130-132	362.17	VG	~	M8		●								●								
U1338A-36X-1, 36-38	365.48	M	80	M8		●		●			●	●		●	●				●			
U1338A-36X-CC	366.30	M	86	M7		●		●	●		●	●		●								
U1338C-37H-4, 130-132	366.78	VG	~	M6		●		●						●								
U1338A-37X-1, 43-45	368.01	M	10	M6				●							●							
U1338A-37X-CC	368.78	G	89	M6	●	●		●	●		●	●		●	●							
U1338B-38H-2, 40-42	377.68	VG	~	M5b	●	●		●				●		●								
U1338A-38X-2, 35-37	378.38	P-M	88	M5b				●	●	●	●			●		●						
U1338B-38H-4, 0-2	380.28	VG	~	M5b	●	●				●	●			●								
U1338B-38H-5, 20-22	381.98	VG	~	M5b	●	●				●	●	●		●								
U1338A-38X-5, 109-111	383.62	M-G	56	M5b	●	●		●			●			●	●							
U1338A-38X-CC	386.31	M	44	M5b		●					●	●		●				●				
U1338A-39X-2, 72-74	388.63	G	42	M5b	●				●			●	●	●	●		●	●	●			
U1338C-39H-6, 140-142	389.90	VG	~	M5b	●	●				●				●				●				
U1338A-39X-5, 89-91	393.30	M	28	M5b				●			●	●	●	●								
U1338A-39X-CC	395.37	G	80	M5b				●	●		●	●		●	●	●		●	●			
U1338A-40X-1, 115-117	404.26	G	84	M5b		●		●	●	●	●	●	●	●	●	●		●				
U1338A-40X-3, 27-29	405.87	G	94	M5b				●	●		●	●	●	●	●	●	●	●				
U1338A-40X-CC	406.45	G	88	M5b		●		●	●		●	●		●	●				●	●		
U1338C-41H-4, 30-32	406.69	VG	~	M5a		●				●				●				●		●		
U1338B-41H-3, 30-32	414.17	VG	~	M5a		●				●		●		●				●		●	●	
U1338B-42H-2, 40-42	423.04	VG	~	M5a		●			●	●				●				●		●		
U1338A-41X-2, 60-68	423.68	G	90	M5a				●			●	●		●	●		●				●	
U1338A-41X-4, 9-11	426.11	G	98	M5a		●		●	●	●	●	●		●	●	●	●		●		●	
U1338A-41X-CC	430.24	M-G	76	M5a				●	●	●	●	●	●	●					●			
U1338A-42X-2, 31-33	432.53	G	92	M5a				●		●	●	●		●		●	●	●	●		●	●
U1338A-42X-4, 114-116	436.36	G	42	M5a				●		●	●	●		●		●		●	●	●		
U1338A-42X-CC	438.19	G	52	M3-4				●	●	●	●	●		●	●			●				
U1338A-43X-2, 18-20	441.15	M	24	M3-4		●	●	●	●	●	●	●		●				●				
U1338A-43X-CC	442.68	M	36	M3-4				●		●	●	●		●				●				
U1338A-44X-2, 55-57	450.71	M-P	50	M2			●	●	●	●	●	●		●	●	●	●					
U1338A-44X-3, 102-104	452.68	M-P	40	M2			●	●	●	●	●	●		●	●				●			●
U1338A-44X-CC	454.20	M-P	48	M2			●	●		●	●	●		●	●							

Table 5. 3. Subset of the samples used for biostrat studies. Refined species datums are highlighted.

Sample Core, Interval, Section (cm)	**MCD**	**Preservation**	**% Planktic foraminifera**	**Planktic Foraminiferal Zone**	*Globigerinoides bisphericus*	*Globigerinoides diminitus*	*Globigerinoides mitra*	*Globigerinoides quadrilobatus*	*Globigerinoides subquadratus*	*Globigerinoides ruber*	*Globigerinoides trilobus*	*Globoquadrina dehiscens*	*Fohsella fohsi*	*Fohsella"praefohsi"*	*Fohsella peripheroacuta*	*Fohsella peripheroronda*	*Globorotalia praemenardii*	*Globorotalia birnageae*	*Globorotalia praescitula*	*Globoturborotalita connecta*	*Globorotaloides* sp.	*Orbulina suturalis*
U1338C-35H-5, 90-92	345.81	VG	~	M9				●		●		●		●	●	●	●					
U1338C-36H-2, 110-112	352.44	VG	~	M9				●		●		●										
U1338B-36H-2, 40-42	355.84	VG	~	M9				●		●		●		●	●	●	●					
U1338A-35X-2, 9-11	360.12	M	52	M9				●			●	●	●				●					
U1338A-35X-CC	361.42	M	57	M8							●	●			●							
U1338C-37H-1, 130-132	362.17	VG	~	M8				●		●	●	●										
U1338A-36X-1, 36-38	365.48	M	80	M8				●		●		●		●		●			●			
U1338A-36X-CC	366.30	M	86	M7				●				●			●							
U1338C-37H-4, 130-132	366.78	VG	~	M6				●		●	●	●				●						
U1338A-37X-1, 43-45	368.01	M	10	M6																		
U1338A-37X-CC	368.78	G	89	M6				●			●	●				●					●	●
U1338B-38H-2, 40-42	377.68	VG	~	M5b				●			●	●				●						
U1338A-38X-2, 35-37	378.38	P-M	88	M5b							●	●				●			●		●	
U1338B-38H-4, 0-2	380.28	VG	~	M5b				●			●	●				●						
U1338B-38H-5, 20-22	381.98	VG	~	M5b				●			●	●				●						
U1338A-38X-5, 109-111	383.62	M-G	56	M5b				●			●	●				●			●			
U1338A-38X-CC	386.31	M	44	M5b				●				●				●			●			
U1338A-39X-2, 72-74	388.63	G	42	M5b				●			●					●			●			
U1338C-39H-6, 140-142	389.90	VG	~	M5b				●	●		●	●				●						
U1338A-39X-5, 89-91	393.30	M	28	M5b					●										●			
U1338A-39X-CC	395.37	G	80	M5b				●			●	●				●		●	●			
U1338A-40X-1, 115-117	404.26	G	84	M5b				●	●		●	●				●			●	●		
U1338A-40X-3, 27-29	405.87	G	94	M5b							●	●								●		
U1338A-40X-CC	406.45	G	88	M5b			●	●	●		●	●				●			●			
U1338C-41H-4, 30-32	406.69	VG	~	M5a	●			●	●		●											
U1338B-41H-3, 30-32	414.17	VG	~	M5a		●		●	●		●	●										
U1338B-42H-2, 40-42	423.04	VG	~	M5a				●	●		●											
U1338A-41X-2, 60-68	423.68	G	90	M5a				●	●		●	●										
U1338A-41X-4, 9-11	426.11	G	98	M5a				●	●		●	●				●			●			
U1338A-41X-CC	430.24	M-G	76	M5a				●	●			●				●						
U1338A-42X-2, 31-33	432.53	G	92	M5a				●	●		●	●										
U1338A-42X-4, 114-116	436.36	G	42	M5a				●	●		●	●							●			
U1338A-42X-CC	438.19	G	52	M3-4				●	●		●	●				●						
U1338A-43X-2, 18-20	441.15	M	24	M3-4					●		●	●				●						
U1338A-43X-CC	442.68	M	36	M3-4					●		●	●				●						
U1338A-44X-2, 55-57	450.71	M-P	50	M2					●		●											
U1338A-44X-3, 102-104	452.68	M-P	40	M2				●	●		●	●										
U1338A-44X-CC	454.20	M-P	48	M2					●			●										

Table 5. 3. Subset of the samples used for biostrat studies. Refined species datums are highlighted.

Sample Core, Interval, Section (cm)	**MCD**	**Preservation**	**% Planktic foraminifera**	**Planktic Foraminiferal Zone**	*Paragloborotalia continuosa*	*Paragloborotalia mayeri*	*Paragloborotalia pseudocontinuosa*	*Paragloborotalia siakensis*	*Praeorbulina glomerosa*	*Praeorbulina circularis*	*Praeorbulina curva*	*Praeorbulina sicana*	*Praeorbulina transitoria*	*Sphaeroidinellopsis seminulina*	*Sphaeroidnellopsis disjuncta*	*Tenuitella clemenciae*	*Tenuitella munda*					
U1338C-35H-5, 90-92	345.81	VG	~	M9				●							●							
U1338C-36H-2, 110-112	352.44	VG	~	M9				●							●							
U1338B-36H-2, 40-42	355.84	VG	~	M9				●							●							
U1338A-35X-2, 9-11	360.12	M	52	M9		●		●					●	●								
U1338A-35X-CCL	361.42	M	57	M8	●			●					●	●	●							
U1338C-37H-1, 130-132	362.17	VG	~	M8				●														
U1338A-36X-1, 36-38	365.48	M	80	M8		●							●	●	●							
U1338A-36X-CC	366.30	M	86	M7	●			●							●							
U1338C-37H-4, 130-132	366.78	VG	~	M6	●																	
U1338A-37X-1, 43-45	368.01	M	10	M6		●									●							
U1338A-37X-CC	368.78	G	89	M6	●			●		●					●							
U1338B-38H-2, 40-42	377.68	VG	~	M5b				●														
U1338A-38X-2, 35-37	378.38	P-M	88	M5b	●	●		●				●			●	●						
U1338B-38H-4, 0-2	380.28	VG	~	M5b																		
U1338B-38H-5, 20-22	381.98	VG	~	M5b													●					
U1338A-38X-5, 109-111	383.62	M-G	56	M5b			●		●			●										
U1338A-38X-CC	386.31	M	44	M5b	●				●			●										
U1338A-39X-2, 72-74	388.63	G	42	M5b		●		●	●	●		●	●									
U1338C-39H-6, 140-142	389.90	VG	~	M5b	●			●							●							
U1338A-39X-5, 89-91	393.30	M	28	M5b		●		●														
U1338A-39X-CC	395.37	G	80	M5b	●		●	●	●													
U1338A-40X-1, 115-117	404.26	G	84	M5b	●	●		●	●			●			●							
U1338A-40X-3, 27-29	405.87	G	94	M5b	●	●		●			●				●							
U1338A-40X-CC	406.45	G	88	M5b	●		●	●	●			●										
U1338C-41H-4, 30-32	406.69	VG	~	M5a							●											
U1338B-41H-3, 30-32	414.17	VG	~	M5a											●							
U1338B-42H-2, 40-42	423.04	VG	~	M5a																		
U1338A-41X-2, 66-68	423.68	G	90	M5a	●	●		●			●	●			●							
U1338A-41X-4, 9-11	426.11	G	98	M5a	●	●	●	●			●	●										
U1338A-41X-CC	430.24	M-G	76	M5a	●			●														
U1338A-42X-2, 31-33	432.53	G	92	M5a	●	●		●				●				●						
U1338A-42X-4, 114-116	436.36	G	42	M5a		●		●				●					●					
U1338A-42X-CC	438.19	G	52	M3-4	●		●	●														
U1338A-43X-2, 18-20	441.15	M	24	M3-4	●	●		●														
U1338A-43X-CC	442.68	M	36	M3-4	●		●	●														
U1338A-44X-2, 55-57	450.71	M-P	50	M2	●	●		●														
U1338A-44X-3, 102-104	452.68	M-P	40	M2	●	●		●									●					
U1338A-44X-CC	454.20	M-P	48	M2	●		●	●														

Table 5. 3. Subset of the samples used for biostrat studies. Refined species datums are highlighted.

6. Synthesis: Orbitally forced environmental and biotic changes across the Pacific Ocean during the middle Miocene

The Pacific Ocean is a key component of the global climate system, as it represents the world's largest oceanic source of water vapour and CO_2 to the atmosphere. Today, surface water conditions in the equatorial Pacific Ocean are characterised by strong E-W gradients in SST (~6 °C) and thermocline depth (~50 m in the EEP versus >150 m in the WEP), with the thermocline and nutricline usually tightly coupled in tropical systems (Bjerknes, 1969; Cane, 2005; Turk et al., 2001).

To date, there have been few Miocene studies addressing sea surface conditions in both the Equatorial Pacific 'warm pool' and 'cold tongue' systems, therefore our understanding of both the mean oceanographic state and dominant forcing mechanisms during an interval of climate transition is limited. The orbitally tuned timescale and detailed stable isotope data sets for both planktonic and benthic foraminifera from Sites U1338 and 1146 provide a comprehensive analysis of oceanographic development during the middle Miocene, particularly with regards to temperature, palaeoproductivity and the influence of orbital forcing on Miocene climate.

6.1 Comparison with previous studies across the MMCT

High resolution (<5 kyr) planktonic foraminiferal stable isotope records during the middle Miocene period are sparse. In this chapter, the foraminiferal $\delta^{18}O$ and $\delta^{13}C$ records from the eastern equatorial Pacific Ocean produced in this study are compared with those from ODP Site 1146 from the northern South China Sea (Figs. 6.1 and 6.2). The similarities and differences between middle Miocene isotope records from marginal and open ocean settings are discussed as well as their potential causes. The aim of this chapter is to place the Site U1338 planktonic foraminiferal isotope record within the context of the global ocean. Comparison of the data from Site U1338 in the eastern equatorial Pacific with data from the western equatorial Pacific Ocean provides a unique opportunity to examine changes across the entire Pacific basin. Discussions are focused on the impact of orbital forcing on the equatorial Pacific Ocean.

6.1.1 Benthic foraminiferal stable isotope records

Comparison of the $\delta^{18}O$ records between Site U1338 and Site 1146 (Fig. 6.1) in the West Pacific Ocean reveals strong correlation between the two benthic $\delta^{18}O$ data-sets, in terms of amplitude and timing of both the long-term trend and glacial-interglacial cycles. The timing of the "Mi-3 event", highlighted on figure 6.1, is synchronous at both sites, displaying the same ~1‰ increase in the benthic foraminiferal $\delta^{18}O$. The high resolution benthic foraminiferal $\delta^{13}C$ records of Site U1338 and Site 1146 also display similarities. The most significant CM6 event, which is synchronous with the Mi-3 event in the $\delta^{18}O$ record, shows nearly identical amplitude and duration at both Site U1338 and Site 1146.

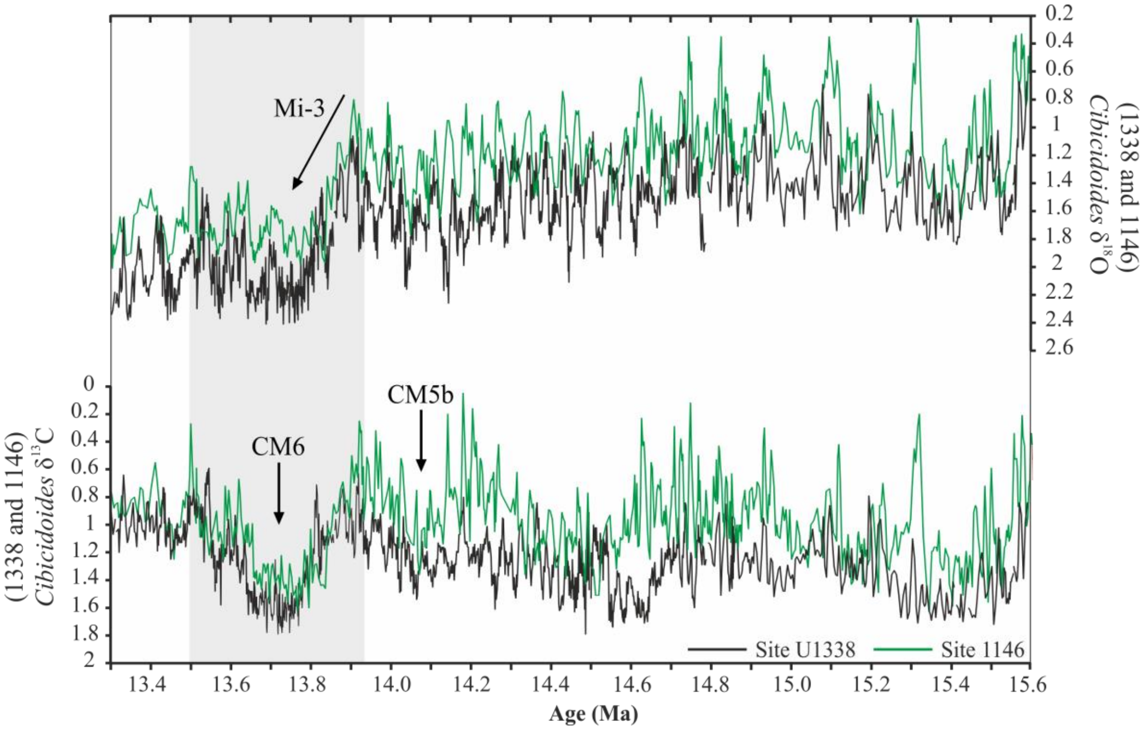

Figure 6.1. (a) Benthic foraminiferal $\delta^{18}O$ records of Site U1338 and 1146 (b) Benthic foraminiferal $\delta^{13}C$ records. Green curve denotes Site 1146 (Holbourn et al., 2013). Black curve denotes Site U1338 (Holbourn et al., 2014). The grey box highlights the intervals on the Mi-3 event and CM6 event.

6.1.2 Planktonic foraminiferal stable isotope records

Comparison of the planktonic foraminiferal $\delta^{18}O$ records between Site U1338 and Site 1146 reveals an offset of approximately 1.5‰ in $\delta^{18}O$ and 0.8‰ in $\delta^{13}C$ (Fig. 6.2a). The $\delta^{18}O$ record of Site 1146 shows considerably higher amplitude variability than the Site U1338 data, with values fluctuating between approximately -3.8‰ and -2.0‰. The timing of the Mi-3 glaciation event is synchronous between the two sites, displaying the same ~0.8‰ increase in the planktonic foraminiferal $\delta^{18}O$ records.

The high resolution $\delta^{13}C$ records of Site U1338 and Site 1146 (Fig. 6.2b) also display similarities at 13.9 Ma, with the CM6 event showing nearly identical amplitude and duration. However, discrepancies exist between the two records. At 14.10 Ma the CM5 event, which is evident in the U1338 $\delta^{13}C$ record as a ~0.8‰ positive trend, is not seen in the 1146 record due to the presence of extremely high amplitude variability (between ~0.8 and ~2.6‰) during this interval. Additionally a well-defined positive trend of 1.2‰ is seen over a 100 kyr interval at 14.5 Ma in the 1146 record, at which point a negative excursion of ~1.0‰ takes place in the U1338 planktonic foraminiferal $\delta^{13}C$ record.

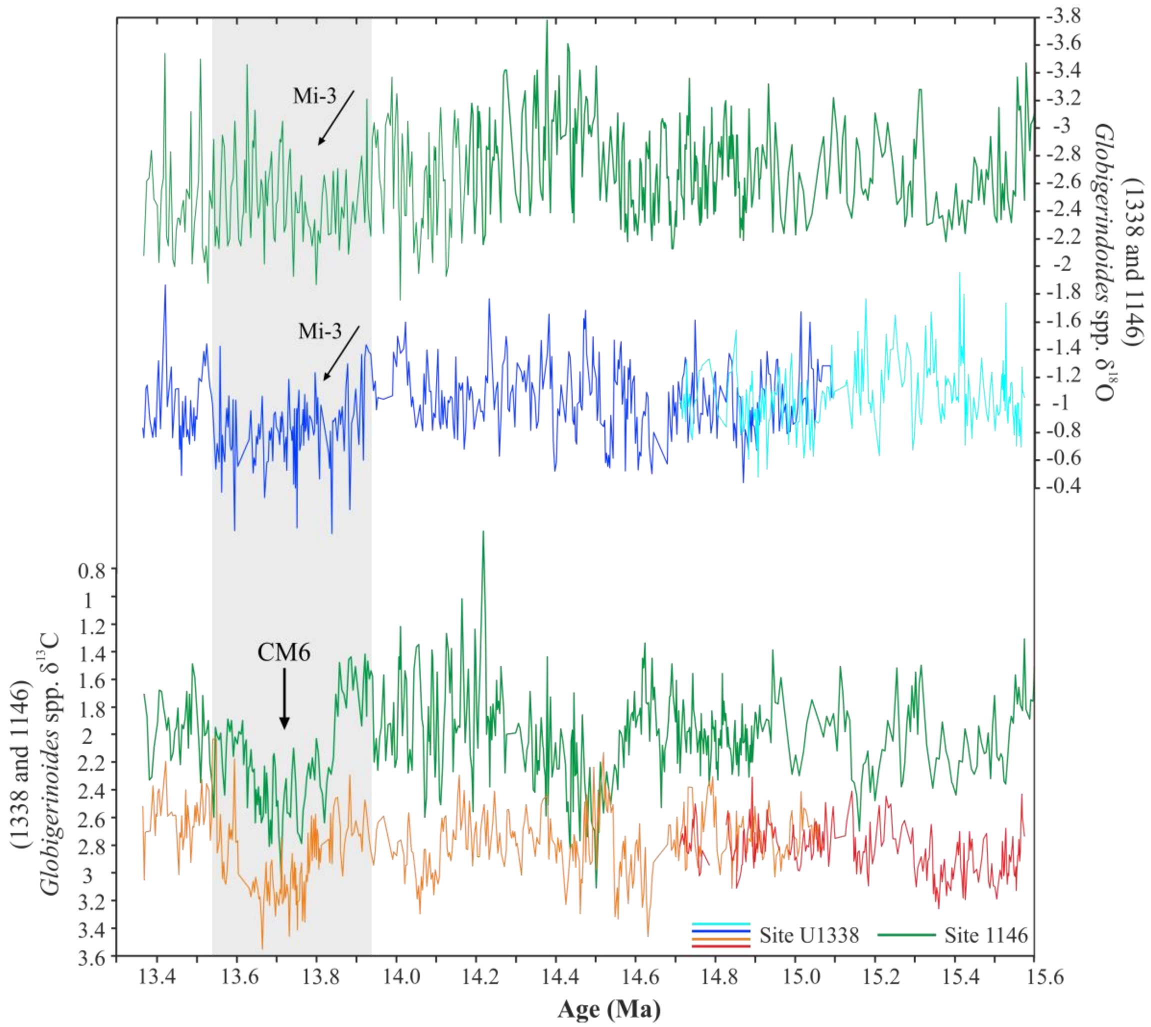

Figure 6.2. (a) Planktonic foraminiferal $\delta^{13}C$ records. Green line denotes Site 1146 (Holbourn et al, 2007). Red line denotes *Globigerinoides* spp. $\delta^{13}C$, orange line *G. subquadratus* $\delta^{13}C$ from Site U1338; (b) Planktonic foraminiferal $\delta^{18}O$ records. Dark blue line denotes *Globigerinoides* spp. $\delta^{18}O$, light blue line *G. subquadratus* $\delta^{18}O$ from Site U1338. The grey box highlights the intervals on the Mi-3 event and CM6 event.

6.1.3 East-West sea surface temperature gradients

Separation of the various components of the $\delta^{18}O$ signal is required to improve understanding of the processes and feedbacks at work during this interval of dynamic climate reorganisation. The upper ocean temperature estimates are based on Mg/Ca ratios in foraminiferal calcite, which vary exponentially with temperature. The average temperature offset between the two records (Fig. 6.3) is approximately 4°C. This closely follows the modern SST gradient between the "warm pool" and "cold tongue", which averages 4°C to 5°C (Karnauskas et al., 2009) and varies in response to ENSO.

Assuming a scale of 0.22‰ per °C (Kim and O'Neil, 1997), approximately 1‰ of the 1.5‰ offset in planktonic foraminiferal $\delta^{18}O$ between the two sites can be explained by temperature. The remaining 0.5‰ must therefore relate to differences in sea surface salinity. On the basis of the modern $\delta^{18}O$–salinity relationship (Fairbanks et al., 1997; Morimoto et al., 2002), a change of 0.5‰ in the $\delta^{18}O$ of sea water reflects a change in surface salinity of between 1 and 1.5 p.s.u (Stott et al., 2004). Present-day surface salinities at both sites are approximately 34 p.s.u, although generally surface water salinities are low in the western tropical Pacific Ocean and increase towards the eastern part of the basin. Hence, the salinity gradient across the tropical Pacific was likely significantly greater in the middle Miocene.

In addition, both planktonic foraminiferal oxygen isotope records reveal enrichment in $\delta^{18}O_p$ that coincides with the benthic enrichment. This interval (Mi-3) has previously been interpreted as a major expansion of the EAIS (Holbourn et al., 2005; Shevenell et al., 2008). This is further supported by the Mg/Ca SST estimates, illustrated in figure 6.3, which show minimal cooling between 13.9 and 13.6 Ma. Thus implying that the increase in $\delta^{18}O_p$ is primarily a reservoir change due to increased ice volume. The observed divergence between the degree of positive $\delta^{18}O$ enrichment observed at 13.9 Ma in the surface and deep water records suggests that deep sea temperature changes also had a significant impact on the benthic foraminiferal $\delta^{18}O$ record.

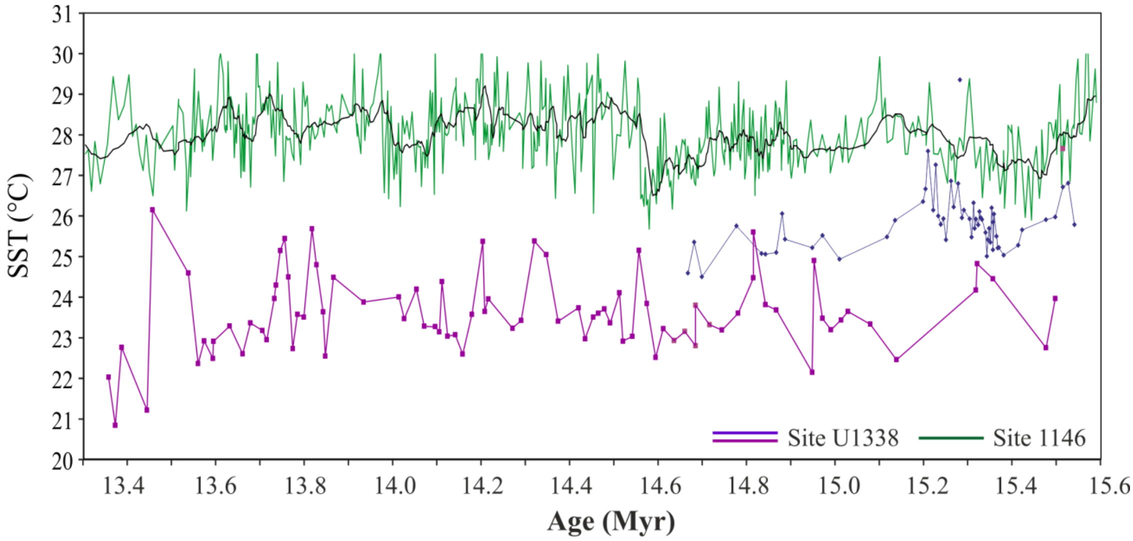

Figure 6.3. SST records for the eastern and western equatorial Pacific Ocean from Mg/Ca ratios measured on planktonic foraminifera. Green line denotes ODP Site 1146. Light purple line denotes SST estimated from specimens of *G. quadrilobatus*. Dark purple line denotes SST estimated from specimens of *G. subquadratus*.

6.1.4 Across the Pacific

The sea surface temperatures of the equatorial Pacific Ocean substantially influence regional and global climates. The present day eastern Equatorial Pacific "cold tongue" is characterised by cold nutrient–rich waters that result from a shallow thermocline and intense upwelling rates, whereas in the western Pacific, the "warm pool" is home to some of the warmest surface water temperatures on Earth. The modern SST gradient between these two water masses averages 4°C to 5°C (Karnauskas et al., 2009) and varies in response to ENSO (Zhang et al., 2014). The absence of an equatorial temperature gradient, caused by weak Trade Winds and the eastward propagation of warm western Pacific equatorial waters, is thought to reflect a "permanent El Niño" state, which results in deeper thermocline depths and attenuated upwelling rates across the eastern equatorial Pacific (Wara et al., 2005).

Such conditions are argued to have taken place during intervals of global warmth, for example during the early Pliocene when planktonic foraminiferal Mg/Ca data reveal that the east-west temperature gradient was nearly absent (Fedorov et al., 2006; Wara et al., 2005). More recently, this hypothesis has been challenged as new SST reconstructions from TEX_{86}^{H} and UK_{37} reveal a continued temperature gradient between the east and west Pacific extending back 12 million years (O'Brien et al., 2014; Zhang et al., 2014).

Until now, no sea surface temperature records for the east and west Pacific extended to the middle Miocene, but the SST records generated for Sites U1338 and 1146 (Fig. 6.3) reveal a clear and consistent temperature asymmetry across the Equatorial Pacific. From the MMCO (~15 Ma) to the end of the MMCT, the warmest interval of the Neogene, the east-west gradient never approached zero as implied for a permanent El Niño–like state. The findings of this study therefore suggest that the oceanographic processes that produce the modern "cold tongue", such as a shallow thermocline in the eastern Pacific and active upwelling, were also present and active in the middle Miocene, providing the necessary conditions for ENSO- type interannual climate variability (Fig. 6.4).

Several lines of evidence support an intensification of equatorial upwelling during the middle Miocene prior to and during the Mi-3 event at 13.9 Ma. In particular, massive spikes in biogenic opal accumulation at 14.04 and 13.84 Ma in the eastern equatorial Pacific Ocean (Holbourn et al., 2014). These coincide with transient decreases in benthic foraminiferal $\delta^{13}C$, suggesting a substantial increase in eastern equatorial Pacific primary production and hence a more active biological pump. In addition, high sedimentation rates during these intervals (Holbourn et al., 2014) further promote the argument of an intensified equatorial primary productivity. The aforementioned $\delta^{13}C$ decreases are poorly defined in the planktonic foraminiferal data set, most likely due to the record being of lower resolution (3 kyr) than the benthic foraminiferal record (1.5 kyr) over this interval.

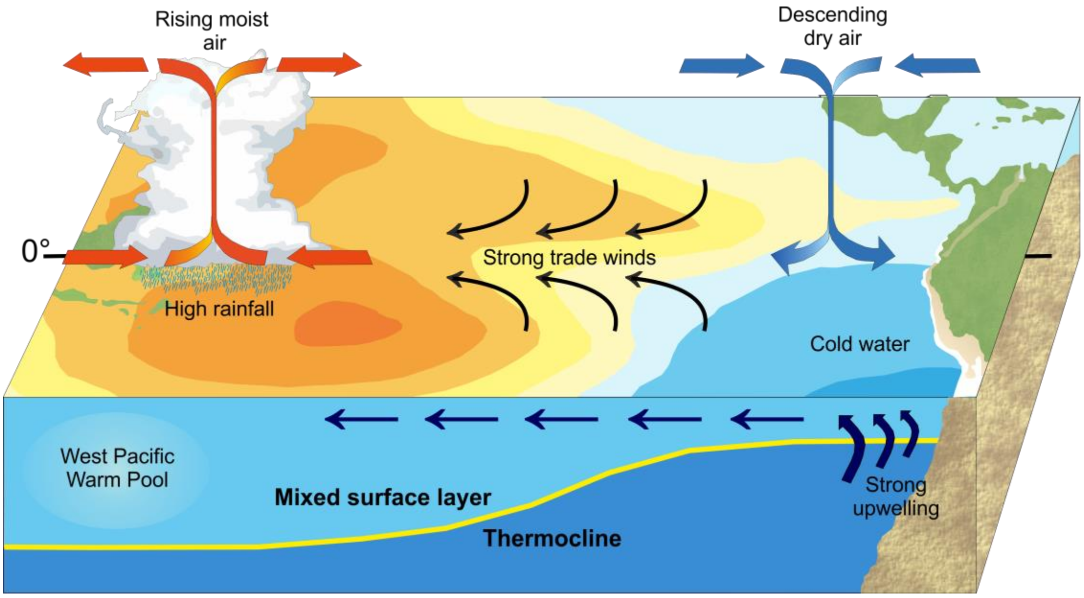

Figure 6.4. Schematic diagram of hypothesised equatorial Pacific ENSO conditions during the middle Miocene.

6.2 Middle Miocene climatic response to orbital forcing

The global and annual mean insolation changes only moderately in response to changes in Earth's orbit, but the associated geographic and seasonal redistribution of solar radiation on Earth may dramatically affect global climate (Laskar, 1993; Milankovitch, 1941; Paillard, 2001). Based on new geochemical records from Site U1338 three distinct phases of climatic evolution are identified for the interval of 15.56 Ma to 13.33 Ma, each with distinct imprints of different orbital variations affecting climate signal. These are discussed in the following sections.

6.2.1 Phase 1

During Phase 1 (15.56–14.7 Ma), continuous wavelet analysis of the planktonic foraminiferal $\delta^{18}O$ record reveals high variance in the precessional band (Fig. 6.7). Phase 1 is also characterised by high amplitude 100 kyr variability in both the planktonic and benthic foraminiferal $\delta^{18}O$ records, which are 180 degrees out of phase over this interval; the lightest values in the benthic foraminiferal $\delta^{18}O$ record occurring during intervals of heaviest planktonic foraminiferal isotope values (Fig. 6.5). Cyclic oscillations in the benthic foraminiferal $\delta^{18}O$ records are usually interpreted to reflect the rapid waxing and waning of an unstable Antarctic sheet. However, the planktonic foraminiferal data do not support this. The observed shifts cannot be related to changes in global ice volume as the surface and bottom water records would respond in the same way (see Chapter 4).

If the 100 kyr cycles were instead entirely related to temperature changes, then a 1‰ shift would be interpreted as a 4°C shift in SST. In order to test this hypothesis, higher resolution Mg/Ca ratio analysis was conducted over two 100 kyr cycles to see if the cyclicity was also recorded by this proxy. Figure 6.6 shows planktonic foraminiferal $\delta^{18}O$ plotted against Mg/Ca. Both data sets were obtained from specimens of *G. subquadratus* from the same samples. However, the analyses were performed independently. The Mg/Ca data does not appear to record any cyclicity, although a gradual positive trend of 1 mmol/mol can be identified over the 200 kyr interval.

An alternative explanation for the isotopic shifts is that the planktonic foraminiferal signature (Fig. 6.5) reflects decreases in the oxygen isotope composition of seawater ($\delta^{18}O_{sw}$), which would give rise to isotopically light $\delta^{18}O$ values. However, significant changes in local $\delta^{18}O_{sw}$ are required for the isotopic fluctuations recorded at Site U1338. If a constant temperature is invoked, $\delta^{18}O_{sw}$ must have changed by 1‰, equivalent to a 4 ppt shift in salinity (Broecker and Denton, 1989; Fairbanks et al., 1992).

In the modern, Site U1338 is located within the eastern equatorial Pacific (EEP) “cold tongue” (Levitus et al., 2013). Here, the Peru Current merges with the Southern Equatorial Current (see Chapter 4 Fig. 4.2) and cold SSTs result from the shoaling of the Equatorial Undercurrent and advection of water from the eastern boundary current along the Peru–Chile margin. The eastern boundary currents and the Southern Equatorial Current are strongly influenced by the changes in the atmospheric circulation of the Southern Hemisphere trade winds on seasonal and interannual timescales (Liu and Herbert, 2004). The prominence of the 22 kyr period prior to 14.7 Ma suggests a strong response to precession and eccentricity forcing, implying combined high- and low-latitude control on tropical wind and precipitation patterns. Given that modern salinity variations across eastern equatorial Pacific vary by 1.0 p.s.u within a few degrees latitude north to south it is conceivable that precession modulated latitudinal migrations of the ITCZ, and hence precipitation and sea surface temperature, could alter the Site U1338 $\delta^{18}O$ values. During Phase 1 it is hypothesised that cyclic shifts in the boundaries between the equatorial currents and counter currents, caused by orbital modulation of wind patterns, caused the recorded changes in surface water $\delta^{18}O$. However the effect of an open Isthmus of Panama on the strength and position of Miocene equatorial ocean currents remains unclear and requires further investigation. These hypotheses could further be tested by a modelling study to see how the ITCZ and ocean currents respond to orbital forcing in the Miocene.

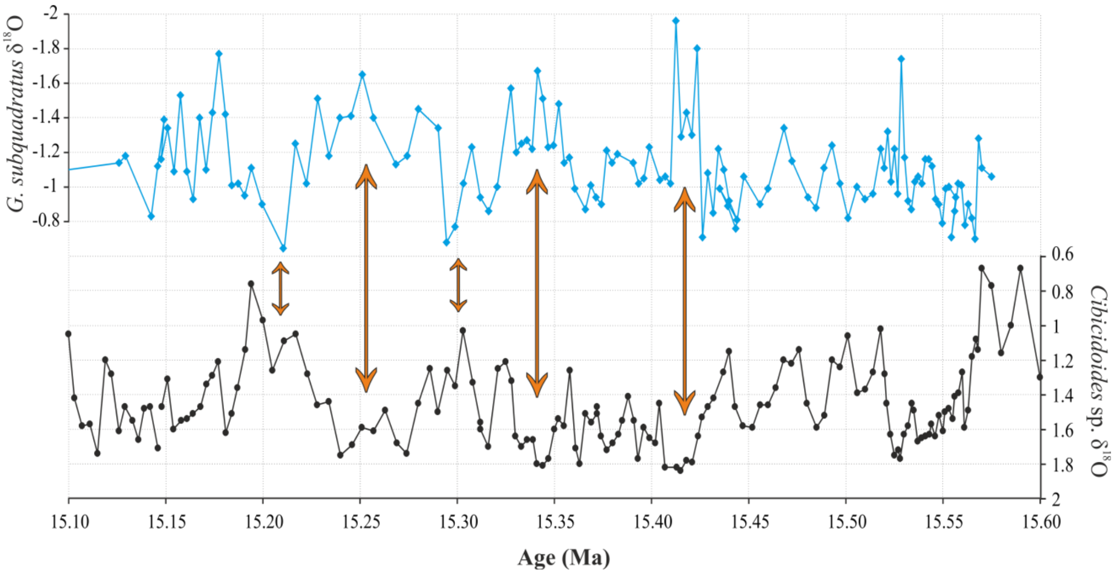

Figure 6.5. Close up of planktonic and benthic foraminiferal $\delta^{18}O$ records from IODP Site U1338 between 15.1 and 15.6 Ma; (a) *Cibicidoides* spp. $\delta^{18}O$ (Holbourn et al., 2014); (b) *Globigerinoides* spp. $\delta^{18}O$.

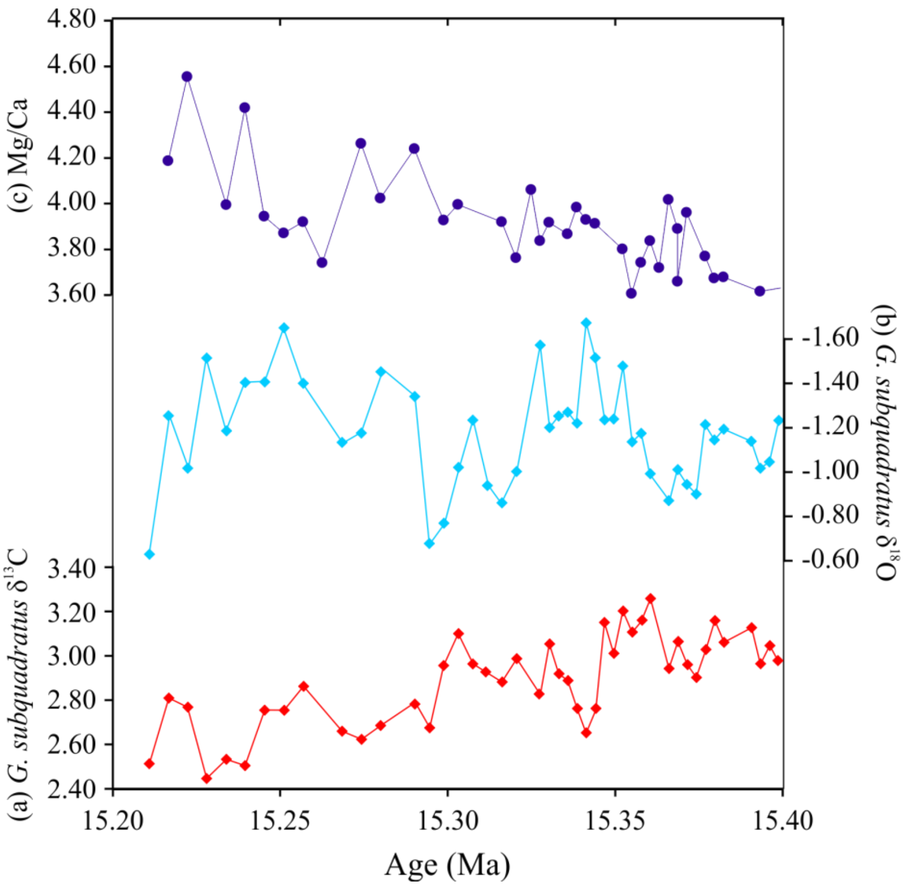

Figure 6.6. (a) *G. subquadratus* $\delta^{18}O$; (b) Mg/Ca ratios from specimens of *G. subquadratus* over two 100 kyr cycles.

6.2.2 Phase 2

During Phase 2 (14.7–13.9 Ma) continuous wavelet analysis of the U1338 benthic and planktonic foraminiferal $\delta^{18}O$ records reveals a shortening of the dominant period from 100 kyr to 41 kyr (Fig. 6.7). This 41 kyr obliquity cycle is especially prominent from ~14.6 to 14.1 Ma during configurations of the Earth's orbit occurring only every ~2.4 Ma, when high-amplitude variability in obliquity is congruent with extremely low amplitude variability in short eccentricity (Holbourn et al., 2013). This transition marked a major turning point in middle Miocene climate evolution.

Obliquity affects Earth's climate by controlling the insolation contrast between low and high latitudes, which drives the atmospheric general circulation and the associated meridional heat and moisture fluxes (Trenberth and Caron, 2001). The equatorial Pacific records from Site U1338 are remarkable because in theory, local insolation forcing due to obliquity cycles is relatively small in the tropics, unlike at high latitudes: Mean annual insolation forcing at the equator differs by -3 Wm^{-2} between times of high (i.e. axial tilt of 24.5°), and low (i.e. axial tilt of 22.2°) obliquity, representing an annual change of approximately -0.4%. In comparison, mean annual insolation differs by 15.4 Wm^{-2} at 90° latitude, representing an increase of 9.3% (Lee and Poulsen, 2005). In light of the small influence of obliquity on low latitude insolation, the 41 kyr periodicities in planktonic $\delta^{18}O$ and $\delta^{13}C$ records from Sites 1146 and U1338 are unlikely to have arisen as a direct climate response to obliquity forcing of local insolation.

During this interval (14.7-13.9 Ma), the planktonic and benthic 41 kyr oscillations in the $\delta^{18}O$ and $\delta^{13}C$ records are in-phase with one another. In terms of the $\delta^{18}O$ record this could be interpreted as a response to an already expanded Antarctic ice-sheet fluctuating in response to obliquity forcing. This implies that Southern Hemisphere ice growth during this interval was most likely modulated by atmospheric heat and moisture transport rather than by changing oceanic circulation patterns (Holbourn et al., 2007). A further important result of this study is the strength of the 41 kyr signal in the planktonic foraminiferal $\delta^{13}C$ record (Fig. 6.8), which suggests that tropical climate may have been forced by additional factors.

Climate model simulations for the last glacial period indicate that atmospheric CO_2 concentrations are the dominant source of radiative forcing in the tropics (Broccoli, 2000; 2006), and the strong coherence between the Miocene planktonic and benthic $\delta^{13}C$ records are indicative of changes in the global carbon reservoir. However, pCO_2 reconstructions for the middle Miocene are currently of insufficient resolution to reveal a CO_2 feedback in response to obliquity changes (Badger et al., 2013; Tripati et al., 2009).

A second hypothesis capable of explaining the 41 kyr signal in the $\delta^{13}C$ records at Site U1338 involves changes in the flux of nutrients from deep waters into the photic zone, resulting in obliquity paced productivity oscillations. A reduced vertical temperature gradient across the thermocline, associated with lower glacial SSTs, could result in an enhanced nutrient flux (Bolton et al., 2010; Fedorov and Philander, 2001). Weakened thermal stratification has been hypothesised to account for greater equatorial Pacific productivity during the late Pleistocene glacials (Beaufort et al., 2001). A similar mechanism may account for higher glacial biological productivity in the EEP during the middle Miocene. In order to better understand the effects of obliquity forcing on the tropics and global carbon cycle during the Middle Miocene, a systematic and detailed model study should be considered in the future.

6.2.3 Phase 3

During Phase 3 (13.9-13.36 Ma) both planktonic and benthic $\delta^{18}O$ and $\delta^{13}C$ records from Sites 1146 and U1338 show a marked transition of the dominant cycle from 41 kyr to 100 kyr around the time of the Mi-3 event (Figs. 6.7 and 6.8). Particularly in the benthic foraminiferal $\delta^{18}O$ records, the 41 kyr cycle becomes very weak and almost negligible after 14 Ma, whereas the 41 kyr cycle is still notable in the 1146 planktonic record (Fig 6.7-6.8). The $\delta^{13}C$ records display the highest values of the entire studied interval at 13.8–13.6 Ma (CM6), and the $\delta^{13}C$ gradient between Sites U1338 and 1146 remains relatively constant during this eccentricity-paced climate mode. It has been suggested that glaciations are enhanced during intervals of reduced amplitude variations in obliquity (Wade and Pälike, 2004), concurrent with low eccentricity (Holbourn et al., 2007; Pälike et al., 2006; Zachos et al., 2001). Such conditions foster high latitude cooling, and prevents ice from melting during the summer, which thought to be instrumental during time periods when ice sheets are still highly dynamic (DeConto et al., 2008). The high resolution planktonic foraminiferal datasets generated for the equatorial Pacific Ocean show that the major $\delta^{18}O$ excursion at ~13.9 Ma coincides with an obliquity node which would favour ice growth. However, as no positive $\delta^{18}O$ trend corresponds with the obliquity node prior to 15.0 Ma, additional factors must be required to force the climate across critical thresholds.

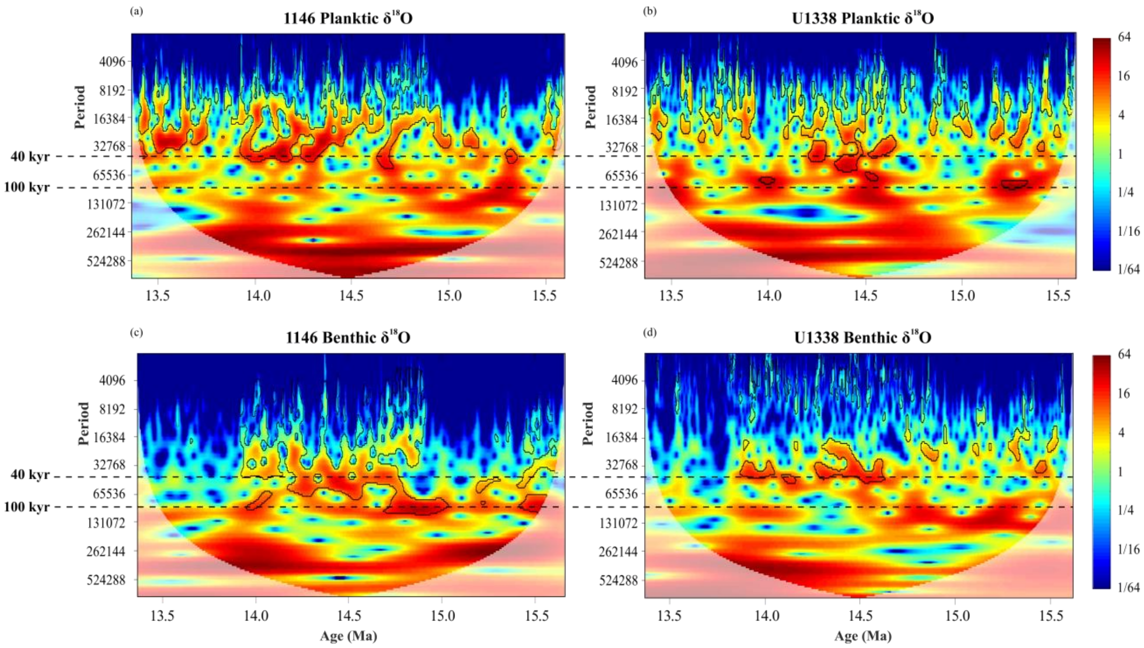

Figure 6.7. (a) Wavelet spectra of Site 1146 planktonic foraminiferal $\delta^{18}O$ time series; (b) Wavelet spectra of Site U1338 planktonic foraminiferal $\delta^{18}O$ time series; (c) Wavelet spectra of Site 1146 benthic foraminiferal $\delta^{18}O$ time series; (d) Wavelet spectra of Site U1338 benthic foraminiferal $\delta^{18}O$ time series. Warm colours indicate regions of high common spectral power between the two time series. Regions within bold black contours are significant at the 95% confidence level against red noise.

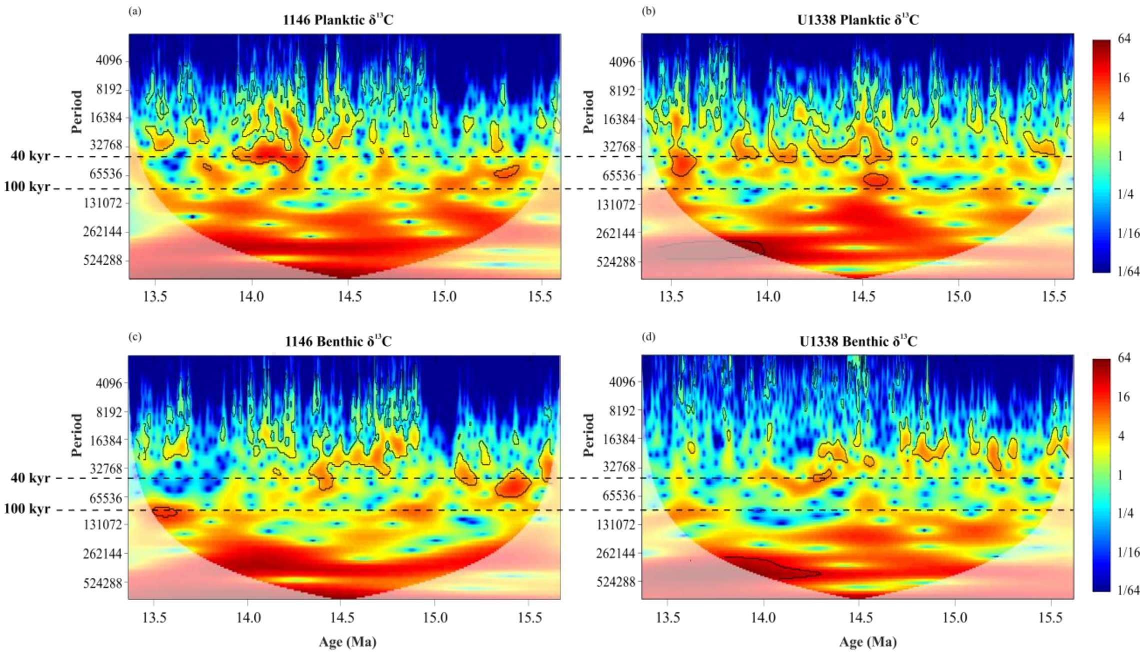

Figure 6.8. (a) Wavelet spectra of Site 1146 planktonic foraminiferal $\delta^{13}C$ time series; (b) Wavelet spectra of Site U1338 planktonic foraminiferal $\delta^{13}C$ time series; (c) Wavelet spectra of Site 1146 benthic foraminiferal $\delta^{13}C$ time series; (d) Wavelet spectra of Site U1338 benthic foraminiferal $\delta^{13}C$ time series. Warm colours indicate regions of high common spectral power between the two time series. Regions within bold black contours are significant at the 95% confidence level against red noise.

6.3 The Mi-3 event and ice volume estimates

While the timing and duration of the benthic foraminiferal $\delta^{18}O$ shift (Mi3 event) that characterizes the marine record of the middle Miocene is well constrained through astronomical tuning of ODP Site U1338 (Holbourn et al., 2013), its interpretation in terms of ice-volume and temperature effects is less clear. Any change in global ice volume should lead to a positive shift in both planktonic and benthic foraminiferal $\delta^{18}O$ values (Tian et al., 2004). However, between 13.9 and 13.7 Ma the amplitude change in benthic and planktonic $\delta^{18}O$ differ with ~1.2‰ and ~0.8‰ respectively. As ice volume fluctuations cannot exceed the variation recorded in the planktonic foraminifera, the remaining 0.4‰ benthic foraminiferal $\delta^{18}O$ change has to be attributed to deep sea temperature changes and/or salinity variations. Estimates from other studies of the magnitude of Antarctic ice growth and temperature change during the middle Miocene also suggest that ~70% of the ~1‰ shift in the benthic foraminiferal $\delta^{18}O$ is related to ice volume changes (Billups and Schrag, 2002; Holbourn et al., 2007). If this is the case then the residual ~0.4‰ shift in the benthic record would translate to a 2°C deep water temperature decrease.

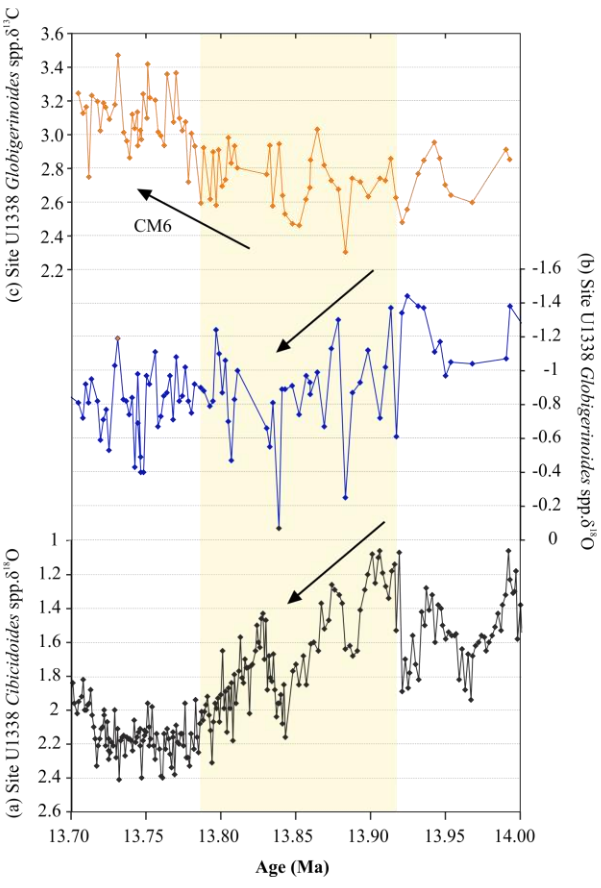

Figure 6.9. (a) IODP Site U1338 Benthic $\delta^{18}O$ record; (b) Site U1338 Planktonic $\delta^{18}O$ record; (c) Site U1338 Planktonic $\delta^{13}C$ record. Yellow shading highlights interval of Mi-3 event.

The case for major ice growth at 13.9 Ma is supported by a coincident fall in global sea level. The Haq et al. (1987) sea-level curve for this interval shows a lowering of >100 m at ~13.9 Ma. However, the record is assembled from many basins around the world with different subsidence histories and poor biostratigraphic age control. To date, the New Jersey margin transect (ODP Legs 150, 174 and IODP Expedition 313) has recovered the longest stratigraphic record to help constrain eustasy, however, the estimates of sea-level amplitude from this section are poorly constrained for the Miocene (Kominz et al., 2008). More recent studies from the Marion Plateau carbonate system, drilled offshore northeast Australia, provide a stratigraphic record for precise sea-level reconstructions (John et al., 2004). A study by John et al. (2011) investigating the amplitude of glacio-eustatic fluctuation in the Miocene, combines back stripping with $\delta^{18}O$ estimates and yields sea level fall amplitudes of 59 ± 6 m at 13.9 Ma. This is in close agreement with the Site U1338 data if the "$\delta^{18}O$ vs sea level" calibration (0.11‰ per 10 m of change in sea level) derived by Fairbanks and Matthews (1978) is applied to the ~0.8‰ shift in $\delta^{18}O$.

Previous palaeotemperature reconstructions over this interval have focused on the high-latitudes because regional climate there is thought to respond more sensitively to climate forcing than those at lower latitudes (Crowley and Zachos 2000). However, establishing the amount of temperature change at the tropics is vital for understanding the mechanisms behind the MMCT and other similar events. Sea surface temperature records from planktonic foraminiferal Mg/Ca from the Southern Ocean reveal sea surface cooling of 6-7°C (Shevenell et al., 2004; Verducci et al., 2007) between 14.2 and 13.8 Ma. If the ice sheet growth were being driven purely by changes in atmospheric CO_2 the entire globe would be expected to cool. However, the Mg/Ca ratio-based SST records for both the west and east equatorial Pacific Ocean exhibit no clear signals of cooling in tropical surface waters (Figs. 6.3 and 6.10). The apparent lack of agreement between the planktonic foraminiferal Mg/Ca and $\delta^{18}O$ records despite the excellent preservation of the specimens, suggests that ice volume and salinity must be a key components of the planktonic foraminiferal $\delta^{18}O$ record. These results suggest an increase in the thermal gradient between high and low latitudes at 13.9 Ma, and challenge the notion that pCO_2 drawdown was the primary control on middle Miocene climate variability. This suggests that other feedbacks such as orbital forcing and ocean circulation played a more significant role than pCO_2 in this climate transition.

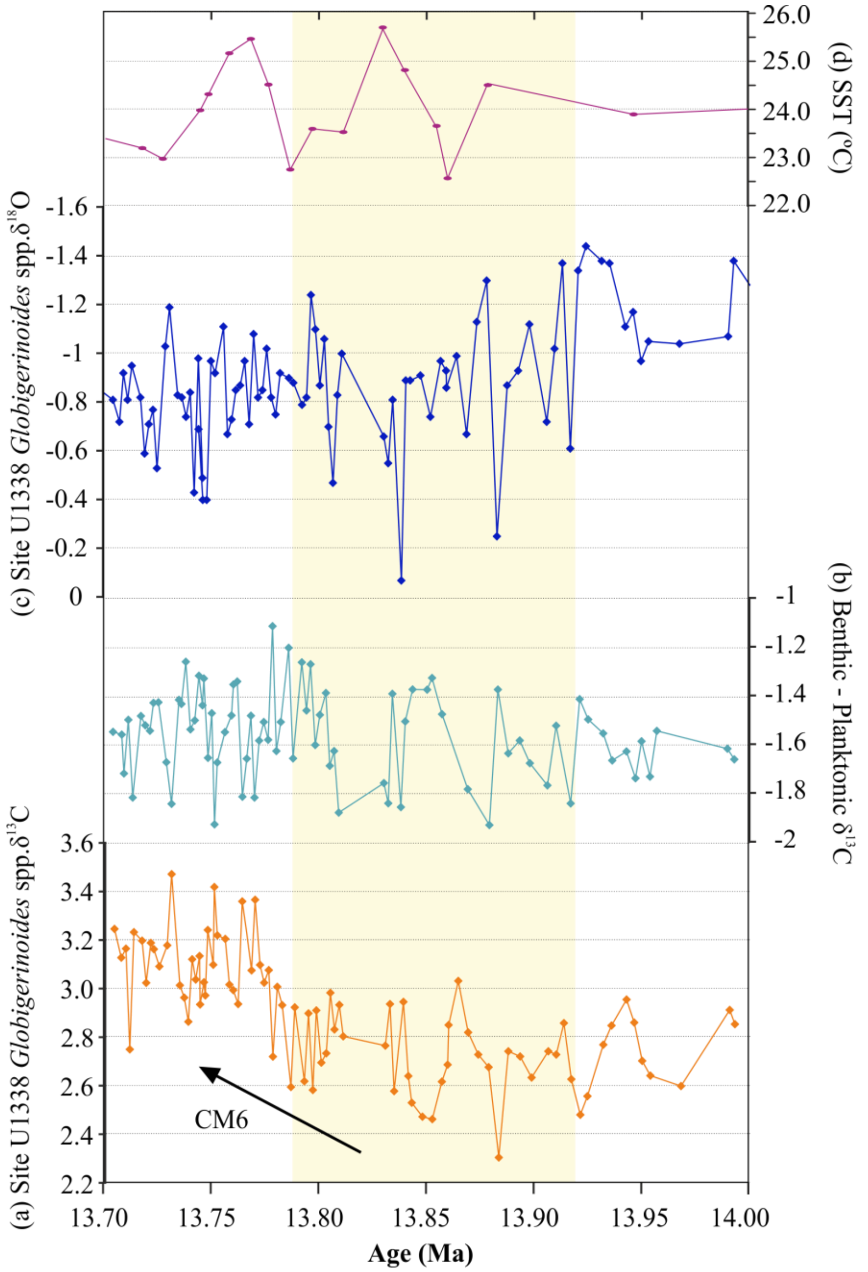

Figure 6.10. (a) Site U1338 Planktonic $\delta^{13}C$ record; (b) Site U1338 Benthic- Planktonic $\delta^{13}C$ record; (c) Site U1338 Planktonic $\delta^{18}O$ record; (d) SST estimates from Mg/Ca ratios. Yellow shading highlights interval of Mi-3 event.

6.4 Miocene $\delta^{13}C$ variations and ocean-atmosphere carbon transfer

Accompanying the middle Miocene growth of the East Antarctic Ice Sheet (EAIS) are major perturbations in the global carbon system, represented by large fluctuations in marine carbonate $\delta^{13}C$ values (Badger et al., 2013; Flower and Kennett, 1993; Zachos et al., 2008). The planktonic foraminiferal $\delta^{13}C$ record from Site U1338 is characterised by high frequency variations (41 kyr), superimposed on lower frequency (400 kyr) oscillations that exhibit a high degree of coherence with the benthic foraminiferal $\delta^{13}C$ (Fig. 4.12). The synchronous positive $\delta^{13}C$ excursions (Figs. 6.1 and 6.2) in the surface and deep ocean waters reflect major changes in the global carbon reservoir.

The 400 kyr cycle originates from the amplitude variation of the eccentricity of the Earth's orbit, which affects the global climate via amplitude modulation of the precession cycles (Tian et al., 2013). Figure 6.7 reveals the strong 400-kyr long eccentricity cycles have been found to be dominant throughout the middle Miocene records of planktonic and benthic foraminiferal $\delta^{13}C$. However, it should be noted that a short record length, such as the Site U1338 planktonic stable isotope record of 2.2 Myr, may introduce an aliasing effect which can ultimately yield biased periodicities.

A box model study by Ma et al. (2011) simulated 400 kyr cycles in the surface waters and deep Ocean for the Miocene Climatic Optimum period (17–14 Ma). The results reveal that carbon input by orbitally-forced changes in weathering change the burial ratio of carbonates to organic carbon and result in periodic changes in the oceanic $\delta^{13}C$. Though the data gathered from Site U1338 more closely supports the interpretation of these carbon maxima as primary productivity phases, which promoted the sequestration of carbon in organic-rich sediments (Flower and Kennett, 1993; Vincent and Berger, 1985). At Site U1338 the argument for a more active biological pump is tentatively supported by increased sedimentation rates during intervals of carbon maxima, in particular the CM6, in addition to recently published Si/Ti records for the eastern equatorial Pacific (Holbourn et al., 2014), which reveal large spikes in opal accumulation during the CM6, thus suggesting a substantial increase in EEP primary production. Furthermore, the low $\Delta\delta^{13}C$ values recorded during and after the Mi3 (Fig. 6.10) reveal stronger gradients between the surface and deep Ocean $\delta^{13}C$ signifying intervals of increased productivity as ^{12}C is preferentially removed from sea water during photosynthesis.

However, rather than support the traditional interpretation of increased primary productivity causing drawdown of atmospheric CO_2 and driving global cooling during the MMCT (Badger et al., 2013; Holbourn et al., 2005; Shevenell et al., 2008), the planktonic foraminiferal records reveal that the CM6 event actually follows the Mi3 glaciation event rather than leading it. Figures 6.9 and 6.10 reveal the onset of the positive trend in planktonic foraminiferal $\delta^{18}O$ at 13.9 Ma predates that of the Carbon Maxima (CM6) at 13.8 Ma suggesting that increased productivity, and hence carbon burial, followed Antarctic ice volume changes and deep water cooling. Based on these results it is hypothesised that increased Antarctic ice volume, due to favourable orbital configuration, resulted in increased meridional temperature gradients which intensified convective atmospheric circulation, thereby increasing the delivery of dust to the upper ocean and shoaling of the thermocline. This promoted upwelling of nutrient rich waters within the EEP which resulted in increased productivity in the eastern equatorial Pacific, further contributing as a positive feedback through the drawdown of atmospheric CO_2.

A new pCO_2 record was reconstructed from planktonic foraminiferal $\delta^{11}B$ found that the CM6 event was associated with a pCO_2 decrease of 82 ±72 ppm (from $\delta^{11}B$ *Globigerinoides trilobus*) or 59 ±63ppm (from $\delta^{13}C^{37}$) (Badger et al., 2013). Both the magnitude and direction of the observed pCO_2 change and isotopic shift and are consistent with an increase in organic carbon burial. However, the boron record consists of only 6 data points over a 100 kyr interval (13.7-13.8 Ma), and therefore lacks the resolution required to demonstrate changes in global pCO_2 on orbital cycles. The estimated atmospheric pCO_2 levels from this study of approximately 300 ppm are in agreement with other recently published long term records (Foster et al., 2012; Kürschner et al., 2008). However, accurate *p*CO2 reconstructions and the time scales on which CO_2 drawdown occurred still remain unclear.

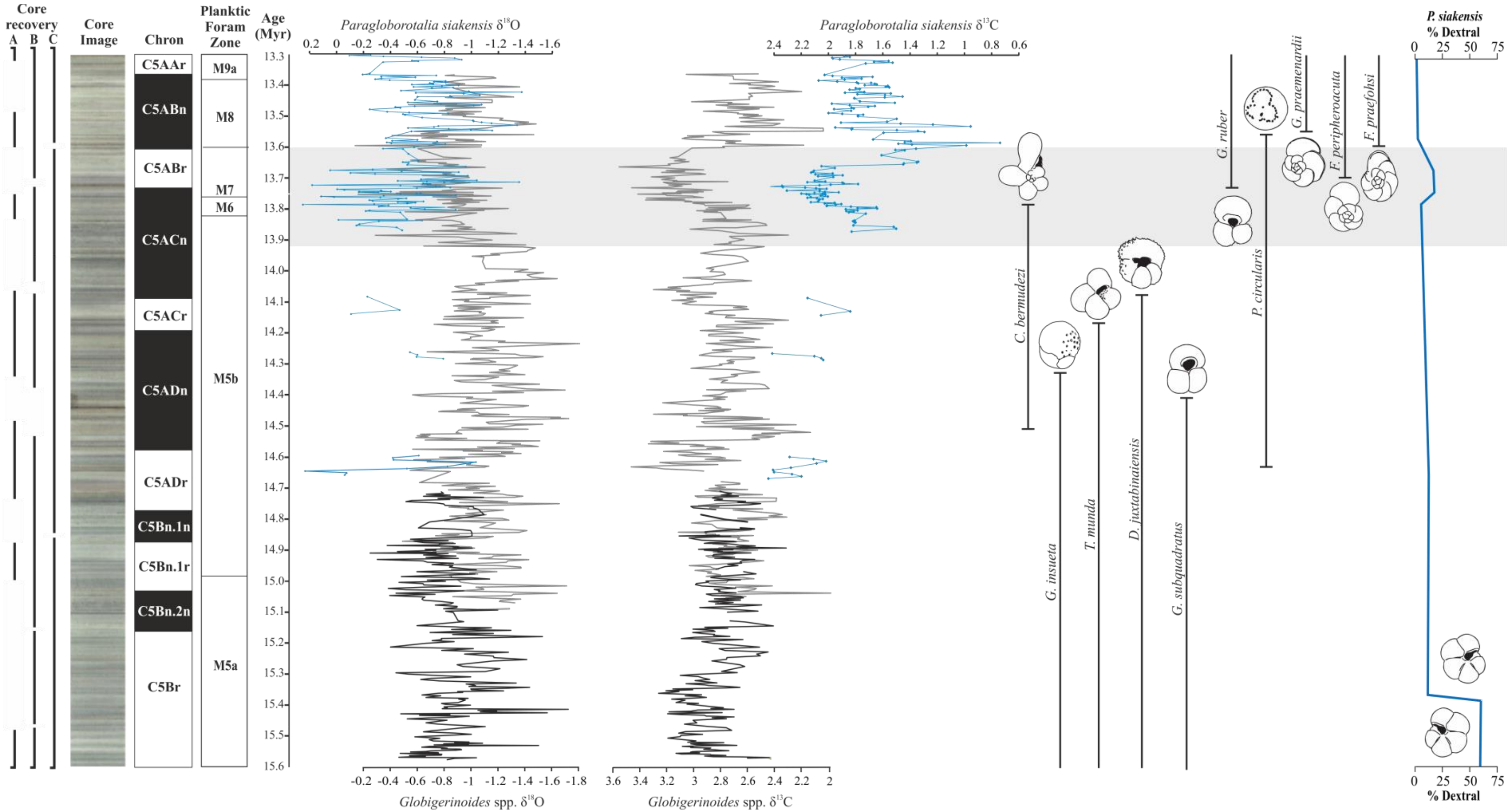

Figure 6.11. Summary figure of key data gathered from this study. Planktonic foraminiferal stable isotope records are plotted against the ranges of selected taxa. Shading = interval of the CM6 and Mi3 events.

6.5 Planktonic foraminiferal response to environmental changes during the MMCT

The mixed layer dwelling planktonic foraminifera from Site U1338 appear to be largely unaffected by palaeoceanographic changes during the studied interval, with no major extinctions or speciation events recorded (see Chapter 5). Despite this, planktonic foraminifera inhabiting the thermocline and below are likely to have been affected by the 2°C deep water cooling associated with the MMCT.

Clavatorella bermudezi was identified in Chapter 5 as a subthermocline species, owing to its remarkably positive oxygen isotope signatures. In this respect, *C. bermudezi* is comparable with the Eocene clavate form, *Clavigerinella eocanica*, which is also thought to be a deep-water form (Pearson et al., 1993). The $\delta^{18}O$ values recorded by *C. bermudezi* (between ~0.8 and 6.1‰) become more extreme (see table 5.1) after the positive benthic foraminiferal $\delta^{18}O$ excursion at 13.9 Ma, which indicates that changes in water column temperature gradients during the MMCT likely contributed to the abrupt extinction of this species at 13.8 Ma. Although currently there is no detailed benthic foraminifera assemblage data for Site U1338 over the MMCT, a period of major faunal change is recorded in the Indian Ocean between ~14 and 13 Ma (Smart et al., 2007), which tentatively supports the hypothesis that deep water cooling affected species living at depth. DSDP Site 289 also records the extinction of many Oligocene-early Miocene species between 16 and 13 Ma but the timing of these events are poorly constrained (Woodruff and Douglas, 1981).

Shortly after the MMCT planktonic foraminiferal assemblages record the emergence of the *Fohsella* lineage (which consists of the successive overlapping morphospecies *F. peripheroronda, F. peripheroacuta, F. praefohsi,* and *F. fohsi*). These species have previously been described from west Pacific Ocean cores (ODP Hole 806B, Ontong Java Plateau) as being mixed layer dwelling species during the middle Miocene until approximately 13 Ma, when they change their depth preference to deeper water (Norris et al., 1993). However, multispecies stable isotope data from specimens of *Fohsella* sp. at Site U1338 suggest these species were already living at depth within the thermocline prior to 13 Ma. Their first appearance in the fossil record shortly after the cooling event alludes to the possibility that the evolution of this species was influenced by changing palaeoceanographic conditions. However further species specific stable isotope data are required in order to confidently identify their preferred depth habitat.

The data presented in chapter five indicate that some Miocene planktonic foraminifer bioevents, namely the lowest occurrence (LO) of *Clavatorella bermudezi*, the LO of *Globigerinatella insueta* (top of Zone M6, Berggren and Pearson 2005), the LO of *Globogerinoides ruber,* and the highest occurrence (HO) of *Tenuitella Munda* and HO of *Globigerinoides subquadratus* occur 0.3-1.2 Myr later in the eastern equatorial Pacific than at other tropical sites such as the western Atlantic Ocean (Wade et al., 2011). Analysis of the Site U1338 Core sediments and SEM analyses of planktonic foraminifera from the U1338 samples indicates that these discrepancies do not arise from poor fossil preservation, reworking, or inadequate sampling resolution. Whilst diachronism and poor or lack of magnetostratigraphy at other Sites is invoked to explain many of the apparent offsets, environmental controls must also be considered as a possible explanation. It is well established that modern planktonic foraminiferal species are limited in their distribution to certain water masses and latitudinal ranges (Be1977; Ruddimanetal.1970; Parker 1971), as foraminifera, and other plankton, have specific temperature and salinity tolerance ranges. At any time the biogeographic distribution of plankton in the ocean is controlled by prevailing circulation patterns, physical-chemical characteristics of surface water masses and ocean basin configuration (Watkins et al., 1998).

Near the equator, strong winds and a shallow thermocline produce strong upwelling signatures in temperature and nutrients (Murray et al., 1994). The thermocline is a dynamic feature of the tropical Pacific Ocean that responds to, as well as influences, wind-driven circulation and tropical climatic conditions. As the most complex region of the tropical Pacific, with large seasonal and interannual variations and strong climatic asymmetries, the eastern equatorial Pacific (EEP) represents a sensitive diagnostic of coupled ocean-atmosphere dynamics across the entire Pacific basin. The middle Miocene was a time of rapidly changing palaeoceanographic conditions and the planktonic foraminiferal stable isotope record provides evidence for 100 kyr forcing of the position of the “cold tongue”, (Fig. 6.5) it may therefore be the case that changes in Miocene biogeographic pattern occurred as a result of major changes in the boundary conditions of the Pacific tropical oceans and of global climates. In order to better assess the effect of changes in the palaeoenvironmental and palaeoceanographical parameters on the spatial distribution of middle Miocene foraminiferal provinces detailed assemblage counts of the Site U1338 samples are required for comparison with sites north and south of the equator.

6.6 Summary & conclusions

Based on these new records from Site U1338 the initiations of new climatic phases appear to coincide with marked changes in the Earth's orbital rhythm, which have been recorded for the first time in the isotopic signature of Miocene planktonic foraminifera. The long-term evolution of the Site U1338 stable isotope signal demonstrates that astronomical forcing has a major impact on climate development. They also shed light upon additional forcing factors with intricate feedback processes including latitudinal temperature distribution, equatorial circulation, primary productivity, and ice sheet dynamics.

Key Findings:

- The SST records generated for Sites U1338 and 1146 reveal a clear temperature asymmetry across the equatorial Pacific. This implies the oceanographic processes that produce the modern "cold tongue", such as a shallow thermocline in the eastern Pacific and active upwelling, were present during the middle Miocene. There is no evidence for a "permanent El Nino" during the warmth of the early middle Miocene (Section 6.1.3, Figs 6.1–6.3).
- Cyclic shifts in the boundaries between the equatorial currents and counter currents, caused by orbital modulation of wind patterns is suggested as an alternative explanation of the anti-phase 100 kyr cycles seen in the planktonic and benthic $\delta^{18}O$ records (Section 6.2.1, Fig. 6.5).
- High-resolution stable isotope studies from the east and west Pacific Ocean reveal a close correspondence of the MMCT and Mi-3 event with the transition of the dominant cycle from 41 kyr to 100 kyr.
- The apparent lack of agreement between the planktonic foraminiferal Mg/Ca and $\delta^{18}O$ records despite the excellent preservation of the specimens, suggests that ice volume and salinity must be a key components of the planktonic foraminiferal $\delta^{18}O$ record as the Mg/Ca record reveals relatively consistent tropical SSTs.
- The 0.4‰ offset in magnitude change between the planktonic and benthic foraminiferal $\delta^{18}O$ records suggest that deep sea temperature changes also had a significant impact on the benthic foraminiferal $\delta^{18}O$ record.
- CO_2 drawdown related to increased primary productivity at the tropics likely contributed to cooling across the MMCT, but is unlikely be the primary control

on Miocene climate variability as revealed by the absence of significant cooling at the equator at 13.9 Ma.

- Orbital forcing and ocean circulation changes which altered meridional heat/vapour transport are tentatively suggested as the dominant drivers of ice growth and deep water cooling at the MMCT.
- Planktonic foraminiferal populations were largely unaffected by palaeoceanographic changes in the East Pacific over the MMCT with the exception of deep dwelling species, which further supports the argument that substantial cooling was limited to the deep ocean.

7. Conclusions and recommendations

In this thesis, I have presented new records of tropical planktonic foraminiferal distributions, stable isotopes, and trace metals, from the interval 15.56 to 13.33 million years ago that contribute to our understanding of middle Miocene climate variability and forcing. Specifically, I have focused in detail on palaeoceanographic conditions across the Middle Miocene Climate Transition in the eastern Equatorial Pacific Ocean, and constructed the highest resolution planktonic foraminiferal stable isotope record currently available for an eastern tropical Pacific Site.

7.1 Key conclusions: returning to original questions

(Q. 1) How does the timing and magnitude of stable isotope events in the planktonic foraminiferal record compare with the deep ocean?

The planktonic foraminiferal $\delta^{18}O$ data set differs noticeably from benthic $\delta^{18}O$, and even shows anti-phase behaviour prior to 15.0 Ma, although a similar ice volume component is embedded into the two records at 13.9 Ma. This divergence supports that changes in planktonic $\delta^{18}O$ prior to 15 Ma are compensated by variations in local salinity, and the global cooling hypothesised for the MMCT is restricted to the deep ocean. The high resolution $\delta^{13}C$ records of Site U1338 however, display great similarities. The most significant CM6 event, which follows the Mi3 event in the $\delta^{18}O$, shows nearly identical amplitude and duration in both records.

(Q. 2) Were fluctuations in tropical surface water conditions driven by Orbital forcing?

Initiation of new climatic phases appears to coincide with marked changes in the Earth's orbital rhythm, which have been recorded for the first time in the comparison of the isotopic signature of Miocene planktonic and benthic foraminifera. Based on wavelet analysis of the benthic and planktic stable isotope records, three successive intervals of climate variability are identified between 15.6 and 13.3 Ma. During Phase 1 (15.6 to 14.6 Ma), planktonic foraminiferal $\delta^{18}O$ display oscillations that follow the 100 kyr eccentricity period. Phase 2 denotes the onset of a new pattern of climate variability with the shortening of the dominant rhythm from ~100 to ~40 kyr periods at 14.6 Ma. Finally, between 13.9 and 13.33 Ma, Phase 3 records a marked transition of the dominant cycle from 41 kyr to 100 kyr around the time of the Mi-3 event, and ultimately signalled entry into a more stable icehouse pattern in the late middle Miocene. In sum, the high resolution planktonic foraminiferal datasets generated for the equatorial Pacific Ocean shows that the middle Miocene climate system was paced mainly by obliquity at times with some evidence for the influence of eccentricity and precession pacing at other times.

The onset of the positive trend in planktonic foraminiferal $\delta^{18}O$ at 13.9 Ma predates that of the Carbon Maxima (CM6) at 13.8 Ma suggesting that increased productivity, and hence carbon burial, followed Antarctic ice volume changes and deep water cooling but contributed as a positive feedback. Based on these results it is hypothesised that increased Antarctic ice volume, due to favourable orbital configurations, resulted in increased meridional temperature gradients which strengthened global wind patterns and thus intensified upwelling and productivity in the eastern equatorial Pacific

(Q. 3) To what extent was there an east-west sea surface temperature contrast in the Miocene equatorial Pacific Ocean?

Planktonic foraminiferal stable isotope and trace element records from Integrated Ocean Drilling Program (IODP) Site U1338 in the eastern equatorial Pacific (EEP) and ODP Site 1146 in the western equatorial Pacific (WEP) during the middle Miocene were used to resolve temperature variations across the equatorial Pacific Ocean. The continuous and consistent offset between the two $\delta^{18}O$ records and Mg/Ca records points towards a 4°C sea surface temperature difference across the pacific, thus providing the necessary conditions for ENSO- type interannual climate variability. This finding is not consistent with the “Permanent El Nino” hypothesis which suggests permanent El Nino state in a warmer world.

(Q. 4) What is the biotic response to inferred major shifts in ice volume and cooling during the middle Miocene?

Planktonic foraminiferal populations were largely unaffected by palaeoceanographic changes in the East Pacific over the MMCT with the exception of deep dwelling species, which further supports that significant cooling was limited to the deep Ocean.

(Q. 5) What are the key bioevents during the middle Miocene?

The rapid coiling transition of *Paragloborotalia siakensis* identified in this project at 15.3 Ma may prove to be of use in biostratigraphic correlation. The extinction of *Clavatorella bermudezi* at 13.8 Ma following the MMCT has been refined to 12 kyr resolution in this study. This event is ubiquitous across the Pacific and in the equatorial Atlantic. The evolution of the *Fohsella* group is also a key event of this interval but low abundance of this species at Site U1338 suggests further work is required to constrain the timings of first and last occurrences.

7.2 Future perspectives and recommendations

Our understanding of Miocene climate dynamics has increased dramatically since the early 2000's, in most part because of the increased recovery of more continuous and expanded deep sea sediments enabling the generation of palaeoceanographic records for the Miocene at temporal resolutions that in the past were rarely obtained beyond the Pliocene. Despite recent advances in our understanding of Miocene climatic behaviour some fairly significant gaps persist in our knowledge of short–term climate variability, the mechanisms responsible and the impacts of climate change on the environment.

7.2.1 The importance of low-latitude planktonic foraminiferal records

In Chapter 4, data from IODP Site U1338 in the EEP provide the first high-resolution study of past sea surface conditions in this important region for air-sea CO_2 exchange. As a consequence of the relative paucity of planktonic records in the eastern tropical Pacific, the down-core reconstructions presented in this thesis are, in many cases, the first that span the MMCT. It is, therefore, entirely unsurprising that the analysis of the U1338 records has led to at least as many, if not more, future research directions than those addressed in the initial aims of the thesis.

It is suggested that generating further planktonic records for the Pacific Ocean will help clarify the position of the various ocean currents and further shed light on the effect of ice growth, CO_2 exchange and orbital cyclicity on the tropics during the Miocene.

Key questions:

- *Did large amplitude orbital variability in planktonic foraminiferal $\delta^{18}O$ occur in the middle Miocene at sites further north and South than site U1338?*
- *Were foraminiferal populations more affected by global cooling at high latitude sites?*

7.2.2 The importance of productivity variations in forcing climate

The subject of the Monterey Carbon excursion and associated productivity changes is touched upon in Chapters 4 and 6, via the investigation of planktonic foraminiferal $\delta^{13}C$ variability across the studied interval. Additional work, for example determination of high-resolution nannofossil, organic carbon and opal mass accumulation rates (MARs), as well as detailed work on productivity and nutrient chemistry proxies at multiple sites in the Pacific Ocean over the middle Miocene would contribute to a global synthesis of productivity changes and nutrient distributions and changes at this time.

Key questions:

- *What role did productivity variations in the equatorial upwelling areas play in forcing middle Miocene climate change?*

7.2.3 Assessing the reliability of SST reconstructions

It is clear from this study that the planktonic foraminiferal $\delta^{18}O$ signal is strongly influenced by local changes in salinity and temperature. Therefore it is suggested that future work should concentrate on generating high resolution SST records from multiple Sites for the middle Miocene. Not only using Mg/Ca ratio analysis, but also TEX_{86}^{H} and UK_{37} as these have recently been used to great effect to reconstruct Pliocene Pacific Ocean temperatures (Dowsett and Robinson, 2009). More SST reconstructions from areas peripheral or outside the modern "cold tongue", in both hemispheres, are needed in order to better describe this pattern and constrain its impact on the wider ocean/atmosphere system.

Additionally, the Mg/Ca proxy system, especially the influence of salinity on the incorporation of Mg into foraminiferal calcite, is still not yet well enough understood. This situation, whilst improving rapidly, requires both more controlled condition culture studies and, crucially from a palaeoceanographic perspective, more single-core multi-proxy SST reconstructions, to allow better evaluation of the relative performances of the proxy systems.

7.2.3 The effect of orbital forcing on the tropics

More modelling studies are required to improve our understanding of the effects of obliquity forcing on the tropics, and global carbon cycle during the Middle Miocene. The high-resolution data from Site U1338 also reveal that the $\delta^{18}O$ record carries a strong precessional signal, supporting a contributing role for insolation in modulating variations in the position of the ITCZ, and hence precipitation and sea surface temperature. This hypothesis could further be tested by a modelling study to see how the ocean currents respond to orbital forcing.

REFERENCES

Abels, H.A., Hilgen, F.J., Krijgsman, W., Kruk, R.W., Raffi, I., Turco, E., Zachariasse, W.J., 2005. Long-period orbital control on middle Miocene global cooling: Integrated stratigraphy and astronomical tuning of the Blue Clay Formation on Malta. Paleoceanography 20, PA4012.

Aceñolaza, P., Sprechmann, P., 2002. The Miocene marine transgression in the meridional Atlantic of South America. Neues Jahrbuch Fur Geologie Und Palaontologie-Abhandlungen 225, 75-84.

Allen, M.B., Armstrong, H.A., 2008. Arabia–Eurasia collision and the forcing of mid-Cenozoic global cooling. Palaeogeography, Palaeoclimatology, Palaeoecology 265, 52-58.

Anand, P., Elderfield, H., Conte, M.H., 2003. Calibration of Mg/Ca thermometry in planktonic foraminifera from a sediment trap time series. Paleoceanography 18.

Anderson, T.F., Arthur, M.A., 1983. Atable Isotopes of oxygen and carbon and their application to sedimentologic and paleoenvironmental problems, in: Arthur, M.A., Anderson, T.F., Kaplan, I.R., Veizer, J., Land, L.S. (Eds.), Stable isotopes in sedimentary geology. SEPM Short Course, Columbia, pp. 1-151.

Aubry, M.-P., van Couvering, J.A., 2005. Buried time: chronostratigraphy as a research tool, Applied Stratigraphy. Springer, pp. 23-53.

Aze, T., Ezard, T.H.G., Purvis, A., Coxall, H.K., Stewart, D.R.M., Wade, B.S., Pearson, P.N., 2011. A phylogeny of Cenozoic macroperforate planktonic foraminifera from fossil data. Biological Reviews 86, 900-927.

Badger, M.P.S., Lear, C.H., Pancost, R.D., Foster, G.L., Bailey, T.R., Leng, M.J., Abels, H.A., 2013. CO2 drawdown following the middle Miocene expansion of the Antarctic Ice Sheet. Paleoceanography 28, 42-53.

Bandy, O.L., 1960. The geological significance of coiling ratios in the Foraminifer *Globigerina pachyderma* (Ehrenberg). Journal of Paleontology 34, 671–681.

Bandy, O.L., 1972. Origin and development of Globorotalia (Turborotalia) pachyderma (Ehrenberg). Micropaleontology 18, 294–318.

Banner, F.T., Blow, W.H., 1959. The classification and stratigraphical distribution of the Globigerinaceae. Paleontology 1.

Barker, S., Greaves, M., Elderfield, H., 2003. A study of cleaning procedures used for foraminiferal Mg/Ca paleothermometry. Geochemistry, Geophysics, Geosystems 4, 8407.

Batenburg, S.J., Reichart, G.-J., Jilbert, T., Janse, M., Wesselingh, F.P., Renema, W., 2011. Interannual climate variability in the Miocene: High resolution trace element and stable isotope ratios in giant clams. Palaeogeography, Palaeoclimatology, Palaeoecology 306, 75-81.

Bé, A.W.H., 1977. An ecological, zoogeographic and taxonomic review of recent planktonic foraminifera. Oceanic Micropaleontology 1, 1-100.

Beaufort, L., de Garidel-Thoron, T., Mix, A.C., Pisias, N.G., 2001. ENSO-like forcing on oceanic primary production during the late Pleistocene. Science 293, 2440-2444.

Beerling, D.J., Fox, A., Anderson, C.W., 2009. Quantitative uncertainty analyses of ancient atmospheric CO2 estimates from fossil leaves. American Journal of Science 309, 775-787.

Beerling, D.J., Royer, D. L.,, 2011. Convergent Cenozoic CO2 history. Nature Geoscience 4, 418-420.

Bemis, B.E., Spero, H.J., Bijma, J., Lea, D.W., 1998. Re-evaluation of the oxygen isotopic composition of planktonic foraminifera: Experimental results and revised paleotemperature equations. Paleoceanography 13, 150-160.

Benton, M.J., 2009. The Red Queen and the Court Jester: Species Diversity and the Role of Biotic and Abiotic Factors Through Time. Science 323, 728-732.

Berger, A., 1977. Support for the astronomical theory of climatic change. Nature 269, 44-45.

Berger, A., 1988. Milankovitch theory and climate. Reviews of geophysics 26, 624-657.

Berger, W., 1979. Preservation of foraminifera.

Berggren, W.A., 1995. A revised Cenozoic geochronology and chronostratigraphy.

Bermudez, P., 1961. Contribucion al estudio de las Globigerinidea de la region Caribe-Antillana (Paleocene-Reciente). Boletino Geologia (Venezuela), Special Publicacion 3, 1119-1393.

Billups, K., Schrag, D., 2002. Paleotemperatures and ice volume of the past 27 Myr revisited with paired Mg/Ca and 18O/16O measurements on benthic foraminifera. Paleoceanography 17, 3-1-3-11.

Biolzi, M., 1983. Stable isotopic study of Oligocene-Miocene sediments from DSDP Site 354, equatorial Atlantic. Marine Micropaleontology 8, 121-139.

Bishop, J.K., Edmond, J.M., Ketten, D.R., Bacon, M.P., Silker, W.B., 1977. The chemistry, biology, and vertical flux of particulate matter from the upper 400 m of the equatorial Atlantic Ocean. Deep Sea Research 24, 511-548.

Bjerknes, J., 1969. Atmospheric teleconections from the equatorial Pacific. Monthly Weather Review 97, 163-172.

Blow, W., 1965. Clavatorella, a new genus of the Globorotaliidae. Micropaleontology, 365-368.

Blow, W.H., 1969. Late middle Eocene to Recent Planktonic foraminiferal biostratigraphy, in: Bronnimann, P., H, R.H. (Eds.), the First International Conference on Planktonic Microfossils. E. J. Brill, Leiden, pp. 199–422.

Blow, W.H., 1979. The Cainozoic Globigerinida: A study of the morphology, taxonomy, evolutionary relationships and the stratigraphical distribution of some Globigerinida (mainly Globigerinacea). Brill.

Blow, W.H., Banner, F., 1966. The morphology, taxonomy and biostratigraphy of Globorotalia barisanensis LeRoy, Globorotalia fohsi Cushman and Ellisor, and related taxa. Micropaleontology 12, 286-302.

Boersma, A., Silva, I.P., Shackleton, N., 1987. Atlantic Eocene planktonic foraminiferal paleohydrographic indicators and stable isotope paleoceanography. Paleoceanography 2, 287-331.

Bolli, H., 1957. Planktonic foraminifera from the Oligocene-Miocene Cipero and Lengua formations of Trinidad, B.W.I, in: Loeblich, A.R.J., et al (Ed.), Studies in

Foraminifera. U.S. National Museum Bulletin, U.S. Government Printing Office,, Washington, D.C.

Bolli, H.M., 1971. The direction of coiling in planktonic foraminifera, in: Funnel, B.M., Riedel, W.R. (Eds.), The Micropaleontology of the Oceans. Cambridge University Press, Cambridge, pp. 639–648.

Bolton, C.T., Gibbs, S.J., Wilson, P.A., 2010. Evolution of nutricline dynamics in the equatorial Pacific during the late Pliocene. Paleoceanography 25, PA1207.

Bown, P.R., Jones, T.D., Lees, J., Randell, R., Mizzi, J., Pearson, P., Coxall, H., Young, J., Nicholas, C., Karega, A., 2008. A Paleogene calcareous microfossil Konservat-Lagerstätte from the Kilwa Group of coastal Tanzania. Geological Society of America Bulletin 120, 3-12.

Brady, H.B., 1879. Supplementary note on the foraminifers of the Chalk of the New Britain Group. Geological Magazine London 4, 534-536.

Broccoli, A.J., 2000. Tropical cooling at the Last Glacial Maximum: an atmosphere-mixed layer ocean model simulation. Journal of Climate 13, 951-976.

Broccoli, A.J., Dahl, K.A., Stouffer, R.J., 2006. Response of the ITCZ to Northern Hemisphere cooling. Geophysical Research Letters 33.

Broecker, W.S., Denton, G.H., 1989. The role of ocean-atmosphere reorganizations in glacial cycles. Geochimica et Cosmochimica Acta 53, 2465-2501.

Broecker, W.S., Peng, T.-H., Beng, Z., 1982. Tracers in the Sea. Lamont-Doherty Geological Observatory, Columbia University.

Bronnimann, P., 1954. Appendix: descriptions of new species, in Todd, R. and others (eds.), Probable Occurrence of Oligocene in Saipan. American Journal of Science 252, 680.

Bronnimann, P., Resig, J., 1971. Neogene Globigerinacean biochronologic time-scale of the southwestern Pacific: DSDP Leg 7, in: Winterer, E.L., Riedel, W.R. (Eds.), Init. Repts. DSDP, 7, Pt. 2, Washington (U.S. Govt. Printing Office), pp. 1235-1470.

Brown, S.J., Elderfield, H., 1996. Variations in Mg/Ca and Sr/Ca ratios of planktonic foraminifera caused by postdepositional dissolution: Evidence of shallow Mg-dependent dissolution. Paleoceanography 11, 543-551.

Calvo, E., Pelejero, C., Pena, L.D., Cacho, I., Logan, G.A., 2011. Eastern Equatorial Pacific productivity and related-CO2 changes since the last glacial period. Proceedings of the National Academy of Sciences 108, 5537-5541.

Cane, M.A., 2005. The evolution of El Niño, past and future. Earth and Planetary Science Letters 230, 227-240.

Carpenter, W.B., Parker, W.K., Jones, T.R., 1862. Introduction to the study of foraminifera. Ray society.

Cayre, O., Lancelot, Y., Vincent, E., Hall, M.A., 1999. Paleoceanographic reconstructions from planktonic foraminifera off the Iberian Margin: temperature, salinity, and Heinrich events. Paleoceanography 14, 384-396.

Chaisson, W., d'Hondt, S., 2000. Neogene planktonic foraminifer biostratigraphy at Site 999, western Caribbean Sea, Proc. ODP, Sci. Results, pp. 19-56.

Chaisson, W., Pearson, P., 1997. Planktonic foraminifer biostratigraphy at Site 925: Middle Miocene-Pleistocene, Proceedings of the Ocean Drilling Program. Scientific results. Ocean Drilling Program, pp. 3-31.

Chaisson, W.P., Leckie, R.M., 1993. High-Resolution Neogene planktonic foraminifer biostratigraphy of Site 808, Ontong Java Plateau (western equatorial Pacific), in: Berger, W.H. (Ed.), Proceedingd of the Ocean Drilling Program, Scientific Results. Ocean Drilling Program, College Station, TX, pp. 137-178.

Chilingar, G.V., 1962. Dependence on temperature of Ca/Mg ratio of skeletal structures of organisms and direct chemical precipitates out of sea water. Bull. South. Calif. Acad. Sci 61, 45-61.

Cifelli, R.L., 1982. Early occurrences and some phylogenetic implications of spiny, honeycomb textured planktonic foraminifera. The Journal of Foraminiferal Research 12, 105-115.

Clement, A., Seager, R., Cane, M., 1999. Orbital controls on the El Nino/Southern Oscillation and the tropical climate. Paleoceanography 14, 441-456.

CLIMAP, P.M., 1976. The surface of the ice-age earth. Science (New York, NY) 191, 1131.

Coates, A.G., Collins, L.S., Aubry, M.-P., Berggren, W.A., 2004. The geology of the Darien, Panama, and the late Miocene-Pliocene collision of the Panama arc with northwestern South America. Geological Society of America Bulletin 116, 1327-1344.

Coates, A.G., Obando, J.A., 1996. The geologic evolution of the Central American Isthmus. Evolution and environment in tropical America, 21-56.

Collen, J.D., Burgess, C.J., 1979. Calcite dissolution, overgrowth and recrystallization in the benthic foraminiferal genus Notorotalia. Journal of Paleontology 53, 1343-1353.

Compton, J.S., Hodell, D.A., Garrido, J.R., Mallinson, D.J., 1993. Origin and age of phosphorite from the south-central Florida Platform: Relation of phosphogenesis to sea-level fluctuations and δ< sup> 13</sup> C excursions. Geochimica et Cosmochimica Acta 57, 131-146.

Compton, J.S., Snyder, S.W., Hodell, D.A., 1990. Phosphogenesis and weathering of shelf sediments from the southeastern United States: Implications for Miocene δ13C excursions and global cooling. Geology 18, 1227-1230.

Coxall, H.K., Wilson, P.A., Pälike, H., Lear, C.H., Backman, J., 2005. Rapid stepwise onset of Antarctic glaciation and deeper calcite compensation in the Pacific Ocean. Nature 433, 53-57.

Craig, H., 1957. Isotopic standards for carbon and oxygen and correction factors for mass-spectrometric analysis of carbon dioxide. Geochimica et Cosmochimica Acta 12, 133-149.

Craig, H., 1965. The measurement of oxygen isotopes paleotemperatures, in: Tongiorgi, E. (Ed.), Spoeto Conference on Stable Isotopes in Oceanographic Studies and Paleotemperatures, Pisa, pp. 3-24.

Cromwell, T., Montgomery, R., Stroup, E., 1954. Equatorial undercurrent in Pacific Ocean revealed by new methods. Science 119, 648-649.

Cronin, M.F., McPhaden, M.J., 1998. Upper ocean salinity balance in the western equatorial Pacific. Journal of Geophysical Research: Oceans (1978–2012) 103, 27567-27587.

Currie, B.S., Rowley, D.B., Tabor, N.J., 2005. Middle Miocene paleoaltimetry of southern Tibet: implications for the role of mantle thickening and delamination in the Himalayan orogen. Geology 33, 181-184.

Cushman, J., 1927. An outline of a re-classification of the Foraminifera. Cushman Laboratory for Foraminifera Research Special Edition 3, 1-105.

Cushman, J., Jarvis, P., 1936. Three new foraminifera from the Miocene Bowden marl of Jamaica. Contributions from the Cushman Laboratory for Foraminiferal Research 12, 3-5.

Cushman, J.A., Stainforth, R.M., 1945. The foraminifera of the Cipero marl formation of Trinidad, British West Indies.

d' Orbigny, A.D., 1826. Tableau méthodique de la classe des cephalopods. Annales des Sciences Naturelles 7, 245–314.

d' Orbigny, A.D., 1839. Foraminifères, Histoire Physique, Politique et Naturelle de l'ile de Cuba, Atlas, p. 224.

Darling, K.F., Kucera, M., Kroon, D., Wade, C.M., 2006. A resolution for the coiling direction paradox in Neogloboquadrina pachyderma. Paleoceanography 21.

Darling, K.F., Wade, C.M., Stewart, I.A., Kroon, D., Dingle, R., Brown, A.J.L., 2000. Molecular evidence for genetic mixing of Arctic and Antarctic subpolar populations of planktonic foraminifers. Nature 405, 43-47.

de Vargas, C., Norris, R., Zaninetti, L., Gibb, S.W., Pawlowski, J., 1999. Molecular evidence of cryptic speciation in planktonic foraminifers and their relation to oceanic provinces. Proceedings of the National Academy of Sciences 96, 2864-2868.

DeConto, R.M., Pollard, D., 2003. A coupled climate–ice sheet modeling approach to the early Cenozoic history of the Antarctic ice sheet. Palaeogeography, Palaeoclimatology, Palaeoecology 198, 39-52.

DeConto, R.M., Pollard, D., Wilson, P.A., Palike, H., Lear, C.H., Pagani, M., 2008. Thresholds for Cenozoic bipolar glaciation. Nature 455, 652-656.

Deuser, W., 1986. Seasonal and interannual variations in deep-water particle fluxes in the Sargasso Sea and their relation to surface hydrography. Deep Sea Research Part A. Oceanographic Research Papers 33, 225-246.

Douglas, R.G., Savin, S.M., 1978. Oxygen isotopic evidence for the depth stratification of Tertiary and Cretaceous planktic foraminifera. Marine Micropaleontology 3, 175-196.

Dowsett, H.J., Robinson, M.M., 2009. Mid-Pliocene equatorial Pacific sea surface temperature reconstruction: a multi-proxy perspective. Philosophical Transactions of the Royal Society A: Mathematical, Physical and Engineering Sciences 367, 109-125.

Edgar, K.M., Wilson, P.A., Sexton, P.F., Gibbs, S.J., Roberts, A.P., Norris, R.D., 2010. New biostratigraphic, magnetostratigraphic and isotopic insights into the Middle Eocene Climatic Optimum in low latitudes. Palaeogeography, Palaeoclimatology, Palaeoecology 297, 670-682.

Ehrenberg, C.G., 1861. Elemente des tiefen Meeresgrundes in Mexikanischen Golfstrome bei Florida; Ueber die Tiefgrund-Verhältnisse des Oceans am Eingang der Davisstrasse und bei Island. Koniglichen Preussischen Akademie der Wissenschaften zu Berlin, 275-315.

Ekart, D.D., Cerling, T.E., Montanez, I.P., Tabor, N.J., 1999. A 400 million year carbon isotope record of pedogenic carbonate: implications for paleoatmospheric carbon dioxide. American Journal of Science 299, 805-827.

Elderfield, H., Ganssen, G., 2000. Past temperature and δ18O of surface ocean waters inferred from foraminiferal Mg/Ca ratios. Nature 405, 442-445.

Elderfield, H., Vautravers, M., Cooper, M., 2002. The relationship between shell size and Mg/Ca, Sr/Ca, δ18O, and δ13C of species of planktonic foraminifera. Geochemistry, Geophysics, Geosystems 3, 1-13.

Emiliani, C., 1954. Depth habitats of some species of pelagic foraminifera as indicated by oxygen isotope ratios. American Journal of Science 252, 149-158.

Emiliani, C., 1955. Pleistocene temperatures. The Journal of Geology, 538-578.

Epstein, S., Mayeda, T., 1953. Variation of O< sup> 18</sup> content of waters from natural sources. Geochimica et Cosmochimica Acta 4, 213-224.

Erez, J., Luz, B., 1983. Experimental paleotemperature equation for planktonic foraminifera. Geochimica et Cosmochimica Acta 47, 1025-1031.

Evans, D., Müller, W., 2012. Deep time foraminifera Mg/Ca paleothermometry: Nonlinear correction for secular change in seawater Mg/Ca. Paleoceanography 27.

Fairbanks, R.G., Charles, C.D., Wright, J.D., 1992. Origin of global meltwater pulses, Radiocarbon after four decades. Springer, pp. 473-500.

Fairbanks, R.G., Evans, M.N., Rubenstone, J.L., Mortlock, R.A., Broad, K., Moore, M.D., Charles, C.D., 1997. Evaluating climate indices and their geochemical proxies measured in corals. Coral Reefs 16, S93-S100.

Fairbanks, R.G., Matthews, R.K., 1978. The marine oxygen isotope record in Pleistocene coral, Barbados, West Indies. Quaternary Research 10, 181-196.

Favre, E., François, L., Fluteau, F., Cheddadi, R., Thévenod, L., Suc, J.-P., 2007. Messinian vegetation maps of the Mediterranean region using models and interpolated pollen data. Geobios 40, 433-443.

Fedorov, A.V., Dekens, P.S., McCarthy, M., Ravelo, A.C., deMenocal, P.B., Barreiro, M., Pacanowski, R.C., Philander, S.G., 2006. The Pliocene Paradox (Mechanisms for a Permanent El Niño). Science 312, 1485-1489.

Fedorov, A.V., Philander, S.G., 2001. A stability analysis of tropical ocean-atmosphere interactions: bridging measurements and theory for El Nino. Journal of Climate 14, 3086-3101.

Finlay, H., 1940. New Zealand Foraminifera; key species in stratigraphy. Transactions of the Royal Society of New Zealand 69, 448-472.

Finlay, H., 1947. The foraminiferal evidence for Tertiary trans-Tasman correlation. Trans. R. Soc. NZ 76, 327-352.

Fleisher, R., 1974. Cenozoic planktonic foraminifera and biostratigraphy, Arabian Sea Deep Sea Drilling Project, Leg 23A, in: Whitmarsh, R.B., et al (Ed.), Initial reports Deep Sea Drilling Project. U.S. Government Printing Office, Washington, D.C, pp. 1001-1072.

Flower, B.P., Kennett, J.P., 1993. Middle Miocene ocean-climate transition: High-resolution oxygen and carbon isotopic records from Deep Sea Drilling Project Site 588A, southwest Pacific. Paleoceanography 8, 811-843.

Flower, B.P., Kennett, J.P., 1994. The middle Miocene climatic transition: East Antarctic ice sheet development, deep ocean circulation and global carbon cycling. Palaeogeography, Palaeoclimatology, Palaeoecology 108, 537-555.

Flower, B.P., Kennett, J.P., 1995. Middle Miocene deepwater paleoceanography in the southwest Pacific: Relations with East Antarctic Ice Sheet development. Paleoceanography 10, 1095-1112.

Foster, G.L., Lear, C.H., Rae, J.W., 2012. The evolution of pCO< sub> 2</sub>, ice volume and climate during the middle Miocene. Earth and Planetary Science Letters 341, 243-254.

Fox, L.R., Wade, B.S., 2013. Systematic Taxonomy of early–middle Miocene planktonic foraminifera from the equatorial Pacific Ocean: Integrated Ocean Drilling Program, Site U1338. The Journal of Foraminiferal Research 43, 374-405.

Franco-Fraguas, P., Costa, K.B., Toledo, F.A.d.L., 2011. Relationship between isotopic composition (”18O and ”13C) and plaktonic foraminifera test size in core tops from the Brazilian Continental Margin. Brazilian Journal of Oceanography 59, 327-338.

Galeotti, S., Von der Heydt, A., Huber, M., Bice, D., Dijkstra, H., Jilbert, T., Lanci, L., Reichart, G.-J., 2010. Evidence for active El Niño Southern Oscillation variability in the Late Miocene greenhouse climate. Geology 38, 419-422.

Gasperi, J., Kennett, J., 1993a. Miocene planktonic foraminifers at DSDP Site 289: depth stratification using isotopic differences, Proc. Ocean Drill. Program Sci. Results, pp. 323-332.

Gasperi, J.T., Kennett, J.P., 1993b. Vertical thermal structure evolution of Miocene surface waters: western equatorial Pacific DSDP Site 289. Marine Micropaleontology 22, 235-254.

Gill, A.E., 1980. Some simple solutions for heat-induced tropical circulation. Quarterly Journal of the Royal Meteorological Society 106, 447-462.

Gradstein, F.M., Ogg, G., Schmitz, M., 2012. The Geologic Time Scale 2012 2-Volume Set. Elsevier.

Graham, D.W., Bender, M.L., Williams, D.F., Keigwin Jr, L.D., 1982. Strontium-calcium ratios in Cenozoic planktonic foraminifera. Geochimica et Cosmochimica Acta 46, 1281-1292.

Graps, A., 1995. An introduction to wavelets. Computational Science & Engineering, IEEE 2, 50-61.

Gregory-Wodzicki, K.M., 2000. Uplift history of the Central and Northern Andes: a review. Geological Society of America Bulletin 112, 1091–1105.

Grinsted, A., Moore, J.C., Jevrejeva, S., 2004. Application of the cross wavelet transform and wavelet coherence to geophysical time series. Nonlinear Processes in Geophysics 11, 561-566.

Groeneveld, J., Nürnberg, D., Tiedemann, R., Reichart, G.J., Steph, S., Reuning, L., Crudeli, D., Mason, P., 2008. Foraminiferal Mg/Ca increase in the Caribbean during the Pliocene: Western Atlantic Warm Pool formation, salinity influence, or diagenetic overprint? Geochemistry, Geophysics, Geosystems 9.

Grossmann, A., Morlet, J., 1984. Decomposition of Hardy functions into square integrable wavelets of constant shape. SIAM journal on mathematical analysis 15, 723-736.

Hall, R., Cottam, M.A., Wilson, M.E.J., 2011. The SE Asian gateway: history and tectonics of the Australia–Asia collision. Geological Society, London, Special Publications 355, 1-6.

Hammer, Ø., Harper, D.A.T., Ryan, P.D., 2004. Past: paleontological statistics software package for education and data analysis. Palaeontologia Electronica 4.

Haq, B.U., Hardenbol, J., Vail, P.R., 1987. Chronology of fluctuating sea levels since the Triassic. Science 235, 1156-1167.

Hay, W.W., Soeding, E., DeConto, R.M., Wold, C.N., 2002. The Late Cenozoic uplift–climate change paradox. International Journal of Earth Sciences 91, 746-774.

Hays, J.D., Imbrie, J., Shackleton, N.J., 1976. Variations in the Earth's orbit: Pacemaker of the ice ages. American Association for the Advancement of Science.

Hedberg, H.D., 1937. Foraminifera of the middle Tertiary Carapita Formation of northeastern Venezuela. Journal of Paleontology, 661-697.

Hemleben, C., Spindler M., Anderson, O. R., 1989. Modern Planktonic Foraminifera. Springer Verlag, 363pp.

Henrot, A.-J., François, L., Favre, E., Butzin, M., Ouberdous, M., Munhoven, G., 2010. Effects of CO 2, continental distribution, topography and vegetation changes on the climate at the Middle Miocene: a model study. Climate of the Past 6.

Hodell, D.A., Vayavananda, A., 1993. Middle Miocene paleoceanography of the western equatorial Pacific (DSDP site 289) and the evolution ofGloborotalia (Fohsella). Marine Micropaleontology 22, 279-310.

Hofker, J., 1956. Foraminifers of Santa Cruz and Thatcher Island, Virginia Archipelago, West Indies. Copenhagen University Zoological Museum Spolia (Skrifler) 15, 9-237.

Hofker, J., 1976. Further studies on Caribbean Foraminifera. Studies of the Fauna of Curasao and other Caribbean Islands 49.

Holbourn, A., Kuhnt, W., Frank, M., Haley, B.A., 2013. Changes in Pacific Ocean circulation following the Miocene onset of permanent Antarctic ice cover. Earth and Planetary Science Letters 365, 38-50.

Holbourn, A., Kuhnt, W., Lyle, M., Schneider, L., Romero, O., Andersen, N., 2014. Middle Miocene climate cooling linked to intensification of eastern equatorial Pacific upwelling. Geology 42, 19-22.

Holbourn, A., Kuhnt, W., Schulz, M., Erlenkeuser, H., 2005. Impacts of orbital forcing and atmospheric carbon dioxide on Miocene ice-sheet expansion. Nature 438, 483-487.

Holbourn, A., Kuhnt, W., Schulz, M., Flores, J.-A., Andersen, N., 2007. Orbitally-paced climate evolution during the middle Miocene “Monterey” carbon-isotope excursion. Earth and Planetary Science Letters 261, 534-550.

Huber, B., Bijma, J., Darling, K., 2010. Cryptic speciation in the living planktonic foraminifer Globigerinella siphonifera (d'Orbigny).

Hudgins, L., Friehe, C.A., Mayer, M.E., 1993. Wavelet transforms and atmopsheric turbulence. Physical Review Letters 71, 3279.

Hüsing, S., 2008. Astrochronology of the Mediterranean Miocene. Linking Palaeoenvironmental Changes to Gateway Dynamics, Geologica Ultraiectina.

Jenkins, D., Orr, W., 1972. Planktonic foraminiferal biostratigraphy of the eastern equatorial Pacific—DSDP Leg 9. Initial reports of the deep sea drilling project 9, 1059-1193.

Jenkins, D.G., 1966. Planktonic foraminiferal datum planes in the Pacific and Trinidad Tertiary. New Zealand Journal of Geology and Geophysics 9, 424–427.

Jiménez-Moreno, G., Fauquette, S., Suc, J.P., 2008. Vegetation, climate and palaeoaltitude reconstructions of the Eastern Alps during the Miocene based on pollen records from Austria, Central Europe. Journal of Biogeography 35, 1638–1649.

John, C.M., Karner, G.D., Browning, E., Leckie, R.M., Mateo, Z., Carson, B., Lowery, C., 2011. Timing and magnitude of Miocene eustasy derived from the mixed siliciclastic-carbonate stratigraphic record of the northeastern Australian margin. Earth and Planetary Science Letters 304, 455-467.

John, C.M., Karner, G.D., Mutti, M., 2004. δ18O and Marion Plateau backstripping: Combining two approaches to constrain late middle Miocene eustatic amplitude. Geology 32, 829-832.

Karnauskas, K.B., Seager, R., Kaplan, A., Kushnir, Y., Cane, M.A., 2009. Observed strengthening of the zonal sea surface temperature gradient across the equatorial Pacific Ocean*. Journal of Climate 22, 4316-4321.

Katz, A., 1973. The interaction of magnesium with calcite during crystal growth at 25–90 C and one atmosphere. Geochimica et Cosmochimica Acta 37, 1563-1586.

Keller, G., 1981. Miocene biochronology and paleoceanography of the North Pacific. Marine Micropaleontology 6, 535-551.

Keller, G., 1985. Depth stratification of planktonic foraminifers in the Miocene ocean. Geological Society of America Memoirs 163, 177-196.

Kennett, J., Srinivasan, M., 1983. Neogene Planktonic Foraminifera: A Phylogenetic Atlas. Hutchinson Ross Publishing Co, Stroudsburg, Pennsylvania.

Kennett, J.P., 1968. Globorotalia truncatulinoides as a paleo-oceanographic index. Science 159, 1461-1463.

Kennett, J.P., Keller, G., Srinivasan, M., 1985. Miocene planktonic foraminiferal biogeography and paleoceanographic development of the Indo-Pacific region. Geological Society of America Memoir 163, 197-236.

Kessler, W.S., 2002. Is ENSO a cycle or a series of events? Geophysical Research Letters 29, 40-41-40-44.

Kessler, W.S., 2006. The circulation of the eastern tropical Pacific: A review. Progress in Oceanography 69, 181-217.

Kessler, W.S., Gourdeau, L., 2006. Wind-driven zonal jets in the South Pacific Ocean. Geophysical Research Letters 33, L03608.

Kim, S.-T., O'Neil, J.R., 1997. Equilibrium and nonequilibrium oxygen isotope effects in synthetic carbonates. Geochimica et Cosmochimica Acta 61, 3461-3475.

Knauss, J., 1963. Equatorial current systems. The sea: ideas and observations on progress in the study of the seas 2.

Knauss, J.A., 1960. Measurements of the Cromwell current. Deep Sea Research (1953) 6, 265-286.

Koch, M., 1926. Mitteltertiäre Foraminiferen aus Bulongan, Ost- Borneo. Eclogae Geologicae Helvetiae 19, 746.

Koch, M., 1935. Namensanderung einiger Tertiar--Foraminiferen aus Neiderländisch Ost-Indien. Eclogae Geologicae Helvetiae 28, 558.

Kominz, M.A., Browning, J.V., Miller, K.G., Sugarman, P.J., Mizintseva, S., Scotese, C.R., 2008. Late Cretaceous to Miocene sea-level estimates from the New Jersey and Delaware coastal plain coreholes: an error analysis. Basin Research 20, 211-226.

Koutavas, A., Lynch-Stieglitz, J., Marchitto, T.M., Sachs, J.P., 2002. El Niño-Like Pattern in Ice Age Tropical Pacific Sea Surface Temperature. Science 297, 226-230.

Kuhlemann, J., Frisch, W., Dunkl, B., Székely, B., Spiegel, C., 2001. Miocene shifts of the drainage divide of the Alps and their foreland basin. Zeitschrift für Geomorphologie, 44, 103–138.

Kuhnt, W., Holbourn, A., Hall, R., Zuvela, M., Käse, R., 2004. Neogene history of the Indonesian throughflow. Continent-ocean interactions within East Asian marginal seas, 299-320.

Kürschner, W.M., Kvacek, Z., 2009. Oligocene-Miocene CO2 fluctuations, climatic and palaeofloristic trends inferred from fossil plant assemblages in central Europe. Bulletin of Geosciences 84, 189-202.

Kürschner, W.M., Kvaček, Z., Dilcher, D.L., 2008. The impact of Miocene atmospheric carbon dioxide fluctuations on climate and the evolution of terrestrial ecosystems. Proceedings of the National Academy of Sciences 105, 449-453.

Laskar, J., 1993. Frequency analysis for multi-dimensional systems. Global dynamics and diffusion. Physica D: Nonlinear Phenomena 67, 257-281.

Laskar, J., Robutel, P., Joutel, F., Gastineau, M., Correia, A., Levrard, B., 2004. A long-term numerical solution for the insolation quantities of the Earth. Astronomy & Astrophysics 428, 261-285.

Lau, K., Weng, H., 1995. Climate signal detection using wavelet transform: How to make a time series sing. Bulletin of the American Meteorological society 76, 2391-2402.

Lea, D.W., Mashiotta, T.A., Spero, H.J., 1999. Controls on magnesium and strontium uptake in planktonic foraminifera determined by live culturing. Geochimica et Cosmochimica Acta 63, 2369-2379.

Lea, D.W., Pak, D.K., Spero, H.J., 2000. Climate impact of late Quaternary equatorial Pacific sea surface temperature variations. Science 289, 1719-1724.

Lear, C.H., Elderfield, H., Wilson, P., 2000. Cenozoic deep-sea temperatures and global ice volumes from Mg/Ca in benthic foraminiferal calcite. Science 287, 269-272.

Lear, C.H., Elderfield, H., Wilson, P., 2003. A Cenozoic seawater Sr/Ca record from benthic foraminiferal calcite and its application in determining global weathering fluxes. Earth and Planetary Science Letters 208, 69-84.

Lear, C.H., Mawbey, E.M., Rosenthal, Y., 2010. Cenozoic benthic foraminiferal Mg/Ca and Li/Ca records: Toward unlocking temperatures and saturation states. Paleoceanography 25.

Leckie, R.M., Farnham, C., Schmidt, M.G., 1993. Oligocene planktonic foraminifer biostratigraphy of Hole 803D (Ontong Java Plateau) and Hole 628A (Little Bahama Bank), and comparison with the southern high latitudes, Proceedings of the ocean drilling program, scientific results, pp. 113-136.

Lee, S.Y., Poulsen, C.J., 2005. Tropical Pacific climate response to obliquity forcing in the Pleistocene. Paleoceanography 20, PA4010.

LeRoy, L., 1939. Some small foraminifera, Ostracoda and otoliths from the Neogene ("Miocene") of the Rokan-Tapanoeli area, central Sumatra. Natuurkundig Tijdschrift voor Nederlandsch-lndie 99, 215–296.

Levitus, S., Antonov, J., Baranova, O., Boyer, T., Coleman, C., Garcia, H., Grodsky, A., Johnson, D., Locarnini, R., Mishonov, A., 2013. The World Ocean Database. Data Science Journal 12, WDS229-WDS234.

Li, Q., McGowran, B., Brunner, C.A., 2003a. Neogene planktonic foraminiferal biostratigraphy of sites 1126, 1128, 1130, 1132 and 1134, ODP Leg 182, Great Australian Bight, Proc. ODP, Sci. Results, pp. 1-65.

Li, Q., McGowran, B., Brunner, C.A., 2003b. Neogene planktonic foraminiferal biostratigraphy of sites 1126, 1128, 1130, 1132 and 1134, ODP Leg 182, Great Australian Bight, Proc. ODP Sci. Results, pp. 1-66.

Lindzen, R.S., Nigam, S., 1987. On the role of sea surface temperature gradients in forcing low-level winds and convergence in the tropics. Journal of the Atmospheric Sciences 44, 2418-2436.

Liska, R.D., 1985. The range of Globigerinoides ruber (d'Orbigny) from the Middle to Late Miocene in Trinidad and Jamaica. Micropaleontology, 372-379.

Liu, Z., Herbert, T.D., 2004. High-latitude influence on the eastern equatorial Pacific climate in the early Pleistocene epoch. Nature 427, 720-723.

Loeblich, A.R., Tappan, H., 1987. Foraminiferal Genera and Their Classification. Van Nostrand Reinhold, New York.

Loeblich, A.R., Tappan, H., 1992. Present Status of foraminiferal classification. In: Studies in Benthic Foraminifera (eds. Takayangi, Y & Saito, T). Proceedings of the Fourth International Symposium on Benthic Foraminifera, Sendai, 1990 (Benthos '90), 93-102.

Lomb, N.R., 1976. Least-squares frequency analysis of unequally spaced data. Astrophysics and space science 39, 447-462.

Lombard, F., Labeyrie, L., Michel, E., Bopp, L., Cortijo, E., Retailleau, S., Howa, H., Jorissen, F., 2011. Modelling planktic foraminifer growth and distribution using an ecophysiological multi-species approach. Biogeosciences Discussions 8, 853-873.

Lorens, R.B., Williams, D.F., Bender, M.L., 1977. The early nonstructural chemical diagenesis of foraminiferal calcite. Journal of Sedimentary Research 47, 1602-1609.

Lourens, L.J., Hilgen, F., Shackleton, N.J., Laskar, J., Wilson, G.S., 2004. The Neogene Period, in: Gradstein, F.M., Ogg, G., Smith, A.G. (Eds.), Geological Time Scale 2004. Cambridge University Press pp. 409-440.

Lyle, M., Pälike, H., Nishi, H., Raffi, I., Gamage, K., Klaus, A., 2010. The Pacific Equatorial Age Transect, IODP Expeditions 320 and 321: Building a 50-Million-Year-Long Environmental Record of the Equatorial Pacific. Scientific Drilling 9, 4-15.

Lyle, M., Raffi, I., Pälike, H., Nishi, H., Gamage, K., Klaus, A., Scientists, T.E., 2009. Pacific Equatorial AgeTransect. Integrated Ocean Drilling Program Preliminary Report. 321.

Ma, W., Tian, J., Li, Q., Wang, P., 2011. Simulation of long eccentricity (400-kyr) cycle in ocean carbon reservoir during Miocene Climate Optimum: Weathering and nutrient response to orbital change. Geophysical Research Letters 38, L10701.

Majewski, W., 2003. Water-depth distribution of Miocene planktonic foraminifera from ODP Site 744, Southern Indian Ocean. The Journal of Foraminiferal Research 33, 144-154.

Maraun, D., Kurths, J., 2004. Cross wavelet analysis: significance testing and pitfalls. Nonlinear Processes in Geophysics 11, 505-514.

Markwick, P.J., 2007. The paleogeographic and paleoclimatic significance of climate proxies for data–model comparisons, in: Williams, M., Haywood, A.M., Gregory, F.J., Schmidt, D.N. (Eds.), Deep-Time Perspectives on Climate Change: Marrying the Signal from Computer Models and Biological Proxies, The Micropaleontological Society Special Publications. The Geological Society, London, pp. 251-312.

Martin, P.A., Lea, D.W., 2002. A simple evaluation of cleaning procedures on fossil benthic foraminiferal Mg/Ca. Geochemistry, Geophysics, Geosystems 3, 8401.

Martinotti, G.M., 1990. The stratigraphic significance of Globigerinoides ruber and Globigerinoides obliquus obliquus in the Mediterranean Middle Miocene. Micropaleontology, 96-101.

McCrea, J.M., 1950. On the Isotopic Chemistry of Carbonates and a Paleotemperature Scale. The Journal of Chemical Physics 18, 849-857.

Milankovitch, M., 1941. Kanon der Erdbestrahlungen und seine Anwendung auf das Eiszeitenproblem Royal Serbian Academy. Belgrade.

Miller, K.G., Aubry, M.-P., Khan, M.J., Melillo, A., Kent, D.V., Berggren, W.A., 1985. Oligocene-Miocene biostratigraphy, magnetostratigraphy, and isotopic stratigraphy of the western North Atlantic. Geology 13, 257-261.

Miller, K.G., Fairbanks, R.G., Mountain, G.S., 1987. Tertiary oxygen isotope synthesis, sea level history, and continental margin erosion. Paleoceanography 2, 1-19.

Miller, K.G., Wright, J.D., Fairbanks, R.G., 1991. Unlocking the ice house: Oligocene-Miocene oxygen isotopes, eustasy, and margin erosion. Journal of Geophysical Research: Solid Earth (1978–2012) 96, 6829-6848.

Morimoto, M., Abe, O., Kayanne, H., Kurita, N., Matsumoto, E., Yoshida, N., 2002. Salinity records for the 1997–98 El Niño from Western Pacific corals. Geophysical Research Letters 29, 35-31-35-34.

Morlet, J., 1983. Sampling theory and wave propagation, Issues in Acoustic Signal—Image Processing and Recognition. Springer, pp. 233-261.

Morlet, J., Arens, G., Fourgeau, E., Glard, D., 1982. Wave propagation and sampling theory-Part I: Complex signal and scattering in multilayered media. Geophysics 47, 203-221.

Morris, M., Roemmich, D., Cornuelle, B., 1996. Observations of variability in the South Pacific subtropical gyre. Journal of physical oceanography 26, 2359-2380.

Mosbrugger, V., Utescher, T., Dilcher, D.L., 2005. Cenozoic continental climatic evolution of Central Europe. Proceedings of the National Academy of Sciences of the United States of America 102, 14964-14969.

Muller, R.A., MacDonald, G.J., 2002. Ice ages and astronomical causes: data, spectral analysis and mechanisms. Springer-Praxis.

Murray, J.W., 1995. Microfossil indicators of ocean water masses, circulation and climate. Geological Society, London, Special Publications 83, 245-264.

Naidu, P.D., Malmgren, B.A., 1996. Relationship between late Quaternary upwelling history and coiling properties of Neogloboquadrina pachyderma and Globigerina bulloides in the Arabian Sea. The Journal of Foraminiferal Research 26, 64-70.

Nathan, S.A., Leckie, R.M., 2003. Miocene planktonic foraminiferal biostratigraphy of sites 1143 and 1146, ODP Leg 184, South China Sea, Proc. ODP Sci. Results, pp. 1-43.

Natland, M.L., 1938. New species of foraminifera from off the west coast of North America and from the later Tertiary of the Los Angeles Basin. University of California, Scripps Institution of Oceanography Bulletin, Technical Series 4, 137–163.

Nitani, H., 1972. Beginning of the Kuroshio. Kuroshio, its physical aspects, 129-163.

Norris, R.D., 1996. Symbiosis as an evolutionary innovation in the radiation of Paleocene planktic foraminifera. Paleobiology, 461-480.

Norris, R.D., Corfield, R.M., Cartlidge, J.E., 1993. Evolution of depth ecology in the planktic foraminifera lineage Globorotalia (Fohsella). Geology 21, 975-978.

Norris, R.D., Nishi, H., 2001. Evolutionary Trends in Coiling of Tropical Paleogene Planktic Foraminifera. Paleobiology 27, 327-347.

Nürnberg, D., Bijma, J., Hemleben, C., 1996. Assessing the reliability of magnesium in foraminiferal calcite as a proxy for water mass temperatures. Geochimica et Cosmochimica Acta 60, 803-814.

O'Brien, C.L., Foster, G.L., Martinez-Boti, M.A., Abell, R., Rae, J.W.B., Pancost, R.D., 2014. High sea surface temperatures in tropical warm pools during the Pliocene. Nature Geosci 7, 606-611.

O'Neil, J.R., Clayton, R.N., Mayeda, T.K., 1969. Oxygen Isotope Fractionation in Divalent Metal Carbonates. Journal of Chemical Physics 51, 5547-5558.

Olsson, R., Hemleben, C., Berggren, W., Huber, B., 1992. Wall texture classification of planktonic Foraminifera genera in the Lower Danian. Journal of Foraminiferal Research 22, 196-213.

Olsson, R.K., 1964. Praeorbulina Olsson, a new foraminiferal genus. Journal of Palaeontology 338.

Pagani, M., Arthur, M.A., Freeman, K.H., 1999. Miocene evolution of atmospheric carbon dioxide. Paleoceanography 14, 273-292.

Pagani, M., Caldeira, K., Berner, R., Beerling, D.J., 2009. The role of terrestrial plants in limiting atmospheric CO2 decline over the past 24 million years. Nature 460, 85-88.

Pagani, M., Zachos, J.C., Freeman, K.H., Tipple, B., Bohaty, S., 2005. Marked Decline in Atmospheric Carbon Dioxide Concentrations During the Paleogene. Science 309, 600-603.

Paillard, D., 2001. Glacial cycles: toward a new paradigm. Reviews of geophysics 39, 325-346.

Pak, D.K., Kennett, J.P., 2002. A FORAMINIFERAL ISOTOPIC PROXY FOR UPPER WATER MASS STRATIFICATION. The Journal of Foraminiferal Research 32, 319-327.

Pälike, H., Nishi, H., Lyle, M., Raffi, I., Klaus, A., Gamage, K., 2010. the Expedition 320/321 Scientists, Pacific equatorial transect. Integrated Ocean Drill. Program Prelim. Rep 320, 175.

Pälike, H., Norris, R.D., Herrle, J.O., Wilson, P.A., Coxall, H.K., Lear, C.H., Shackleton, N.J., Tripati, A.K., Wade, B.S., 2006. The heartbeat of the Oligocene climate system. Science 314, 1894-1898.

Park, R., Epstein, S., 1960. Carbon isotope fractionation during photosynthesis. Geochimica et Cosmochimica Acta 21, 110-126.

Pascual, R., Jaureguizar, E.O., 1990. Evolving climates and mammalian faunas in Cenozoic South America. Journal of Human Evolution 19, 23-60.

Pearson, P., Chaisson, W., 1997. Late Paleocene to middle Miocene planktonic foraminifer biostratigraphy of the Ceara Rise, Proceedings of the Ocean Drilling Program. Scientific results. Ocean Drilling Program, pp. 33-68.

Pearson, P.N., 1995. Planktonic foraminifer biostratigraphy and the development of pelagic caps on guyots in the Marshall Island Group. In: Haggerty, JA; Premoli Silva, I; Rack, F; McNutt, MK. (eds.), Proceedings of the Ocean Drilling Program, Scientific Results 144, 38.

Pearson, P.N., Burgess, C.E., 2008. Foraminifer test preservation and diagenesis: Comparison of high latitude Eocene sites. Geological Society, London, Special Publications 303, 59-72.

Pearson, P.N., Norris, R.D., Empson, A.J., 2001. Mutabella mirabilis gen. et sp. Nov., a Miocene microperforate planktonic foraminifer with an extreme level of intraspecific variability. The Journal of Foraminiferal Research 31, 120-132.

Pearson, P.N., Olsson, R.K., Huber, B.T., Hemleben, C., Berggren, W.A., Silva, I.P., Coxall, H., Premec-Fucek, V., Wade, B., 2005. Atlas of Eocene planktonic foraminifera. Epitome 1, 274-274.

Pearson, P.N., Palmer, M.R., 2000. Atmospheric carbon dioxide concentrations over the past 60 million years. Nature 406, 695-699.

Pearson, P.N., Shackleton, N.J., Hall, M.A., 1993. Stable isotope paleoecology of middle Eocene planktonic foraminifera and multi-species isotope stratigraphy, DSDP Site 523, South Atlantic. The Journal of Foraminiferal Research 23, 123-140.

Pearson, P.N., Shackleton, N.J., Weedon, G.P., Hall, M.A., 1997. 29. Multispecies planktonic foraminifer stable isotope stratigraphy through Oligocene/Miocene boundary climatic cycles, Site 926, Proc. ODP, Sci. Results, pp. 441-449.

Pearson, P.N., van Dongen, B.E., Nicholas, C.J., Pancost, R.D., Schouten, S., Singano, J.M., Wade, B.S., 2007. Stable warm tropical climate through the Eocene Epoch. Geology 35, 211-214.

Peters, S.E., Kelly, D.C., Fraass, A.J., 2013. Oceanographic controls on the diversity and extinction of planktonic foraminifera. Nature 493, 398-401.

Potter, P.M., Szarmari, P., 2009. Global Miocene tectonics and the modern world. Earth-Science Reviews 96, 279–295.

Pound, M.J., Haywood, A.M., Salzmann, U., Riding, J.B., 2012. Global vegetation dynamics and latitudinal temperature gradients during the Mid to Late Miocene (15.97–5.33 Ma). Earth-Science Reviews 112, 1-22.

Prokoph, A., El Bilali, H., 2008. Cross-wavelet analysis: a tool for detection of relationships between paleoclimate proxy records. Math Geosci 40, 575-586.

Raffi, I., 1999. Precision and accuracy of nannofossil biostratigraphic correlation. Philosophical Transactions of the Royal Society of London. Series A: Mathematical, Physical and Engineering Sciences 357, 1975-1993.

Ramsay, A.T., Smart, C.W., Zachos, J.C., 1998. A model of early to middle Miocene deep ocean circulation for the Atlantic and Indian Oceans. Geological Society, London, Special Publications 131, 55-70.

Raymo, M., Ruddiman, W.F., 1992. Tectonic forcing of late Cenozoic climate. Nature 359, 117-122.

Raymo, M.E., 1994. The Himalayas, organic carbon burial, and climate in the Miocene. Paleoceanography 9, 399-404.

Raymo, M.E., Ruddiman, W.F., Froelich, P.N., 1988. Influence of late Cenozoic mountain building on ocean geochemical cycles. Geology 16, 649-653.

Rea, D.K., 1992. Delivery of Himalayan sediment to the northern Indian Ocean and its relation to global climate, sea level, uplift, and seawater strontium, in: Duncan, R.A., Rea, D.K., Kidd, R.B., von Rad, U., Weissel, J.K. (Eds.), Synthesis of Results from Scientific Drilling in the Indian Ocean, Geophysical Monograph. American Geophysical Union pp. 387-402.

Regenberg, M., Nürnberg, D., Schönfeld, J., Reichart, G.J., 2007. Early diagenetic overprint in Caribbean sediment cores and its effect on the geochemical composition of planktonic foraminifera. Biogeosciences 4, 957-973.

Regenberg, M., Nürnberg, D., Steph, S., Groeneveld, J., Garbe-Schönberg, D., Tiedemann, R., Dullo, W.C., 2006. Assessing the effect of dissolution on planktonic foraminiferal Mg/Ca ratios: Evidence from Caribbean core tops. Geochemistry, Geophysics, Geosystems 7.

Retallack, G.J., 1992. Middle Miocene fossil plants from Fort Ternan (Kenya) and evolution of African grasslands. Paleobiology, 383-400.

Retallack, G.J., 2009. Refining a pedogenic-carbonate CO_2 paleobarometer to quantify a middle Miocene greenhouse spike. Palaeogeography, Palaeoclimatology, Palaeoecology 281, 57-65.

Reuss, A.E., 1850. Neue Foraminiferen aus den Schichten des Österreichischen Tertiärbeckens. Denkschriften der Kaiserlichen Akadamie der Wissenschaften, Mathematisch-Naturwissenschaftliche Classe 1.

Robert, C., Stein, R., Acquaviva, 1986. Cenozoic evolution and significance of clay associations in the New Zealand region of the southwest Pacific, Leg 90, in: Kennett, J.P., von der Borch, C.C. (Eds.), Init. Rep. DSDP, pp. 1225-1238.

Rögl, F., 1999. Mediterranean and Paratethys. Facts and hypotheses of an Oligocene to Miocene paleogeography (short overview). Geologica carpathica 50, 339-349.

Rohling, E.J., Cooke, S., 2003. Stable oxygen and carbon isotopes in foraminiferal carbonate shells, Modern foraminifera. Springer, pp. 239-258.

Rosenthal, Y., Boyle, E.A., Slowey, N., 1997. Temperature control on the incorporation of magnesium, strontium, fluorine, and cadmium into benthic foraminiferal shells from Little Bahama Bank: Prospects for thermocline paleoceanography. Geochimica et Cosmochimica Acta 61, 3633-3643.

Rosenthal, Y., Lohmann, G., Lohmann, K., Sherrell, R., 2000. Incorporation and preservation of Mg in Globigerinoides sacculifer: Implications for reconstructing the temperature and 18O/16O of seawater. Paleoceanography 15, 135-145.

Royer, D.L., Wing, S.L., Beerling, D.J., Jolley, D.W., Koch, P.L., Hickey, L.J., Berner, R.A., 2001. Paleobotanical evidence for near present-day levels of atmospheric CO2 during part of the Tertiary. Science 292, 2310-2313.

Ruddiman, W., Sarnthein, M., Backman, J., Baldauf, J., Curry, W., Dupont, L., Janecek, T., Pokras, E., Raymo, M., Stabell, B., 1986. 29. Late Miocene to Pleistocene Evolution of climate in Africa and thelow-latitude Atlantic: Overview of Leg 108 Results, Proceedings of the Ocean Drilling Program: Scientific results. The Program, p. 463.

Ruddiman, W.F., 1977. Investigations of Quaternary Climate based on planktonic foraminifera. Ramsay.

Ruddiman, W.F., 2001. Earth's Climate: past and future. Macmillan.

Saito, T., 1976. Geologic significance of coiling direction in the planktonic foraminifera Pulleniatina. Geology 4, 305-309.

Scargle, J.D., 1982. Studies in astronomical time series analysis. II-Statistical aspects of spectral analysis of unevenly spaced data. The Astrophysical Journal 263, 835-853.

Schmid, M.E., 1967. Zwei neue planktonische Foraminiferen aus dem Badener Tegel von Sooß, NÖ. Annalen des Naturhistorischen Museums in Wien 71.

Schnitker, D., 1980. North Atlantic oceanography as possible cause of Antarctic glaciation and eutrophication.

Schulte, P., Alegret, L., Arenillas, I., Arz, J.A., Barton, P.J., Bown, P.R., Bralower, T.J., Christeson, G.L., Claeys, P., Cockell, C.S., Collins, G.S., Deutsch, A., Goldin, T.J., Goto, K., Grajales-Nishimura, J.M., Grieve, R.A.F., Gulick, S.P.S., Johnson, K.R., Kiessling, W., Koeberl, C., Kring, D.A., MacLeod, K.G., Matsui, T., Melosh, J., Montanari, A., Morgan, J.V., Neal, C.R., Nichols, D.J., Norris, R.D., Pierazzo, E., Ravizza, G., Rebolledo-Vieyra, M., Reimold, W.U., Robin, E., Salge, T., Speijer, R.P., Sweet, A.R., Urrutia-Fucugauchi, J., Vajda, V., Whalen, M.T., Willumsen, P.S., 2010. The Chicxulub Asteroid Impact and Mass Extinction at the Cretaceous-Paleogene Boundary. Science 327, 1214-1218.

Schulz, M., Mudelsee, M.,, 2002. REDFIT: estimating red-noise spectra directly from unevenly spaced paleoclimatic time series. Computers & Geosciences 28, 5.

Schulz, M., Stattegger, K., 1997. Spectrum: spectral analysis of unevenly spaced paleoclimatic time series. Computers & Geosciences 23, 929-945.

Schwager, C., 1866 Fossile Foraminiferen von Kar Nikobar, Reise der Österreichischen Fregatte Novara um die Erde in den Jahren 1857, 1858 und 1859, Geologischer Theil, Geologische Beobachtung, pp. 187-268.

Schwarzacher, W., 1993. Cyclostratigraphy and the Milankovitch Theory. Elsevier, Amsterdam, London, p. 225.

Shackleton, N., Kennett, J., 1975. Paleotemperature history of the Cenozoic and the initiation of Antarctic glaciation: oxygen and carbon isotope analyses in DSDP Sites 277, 279, and 281. Initial reports of the deep sea drilling project 29, 743-755.

Shevenell, A.E., Kennett, J.P., Lea, D.W., 2004. Middle Miocene Southern Ocean Cooling and Antarctic Cryosphere Expansion. Science 305, 1766-1770.

Shevenell, A.E., Kennett, J.P., Lea, D.W., 2008. Middle Miocene ice sheet dynamics, deep-sea temperatures, and carbon cycling: A Southern Ocean perspective. Geochemistry, Geophysics, Geosystems 9.

Sime, N.G., De La Rocha, C.L., Tipper, E.T., Tripati, A., Galy, A., Bickle, M.J., 2007. Interpreting the Ca isotope record of marine biogenic carbonates. Geochimica et Cosmochimica Acta 71, 3979-3989.

Smart, C.W., Thomas, E., Ramsay, A.T.S., 2007. Middle–late Miocene benthic foraminifera in a western equatorial Indian Ocean depth transect: Paleoceanographic implications. Palaeogeography, Palaeoclimatology, Palaeoecology 247, 402-420.

Spero, H.J., 1992. Do planktic foraminifera accurately record shifts in the carbon isotopic composition of seawater pCO_2. Marine Micropaleontology 19, 275-285.

Spero, H.J., Bijma, J., Lea, D.W., Bemis, B.E., 1997. Effect of seawater carbonate concentration on foraminiferal carbon and oxygen isotopes. Nature 390, 497-500.

Spero, H.J., Lea, D.W., 1993. Intraspecific stable isotope variability in the planktic foraminifera *Globigerinoides sacculifer*: Results from laboratory experiments. Marine Micropaleontology 22, 221-234.

Spero, H.J., Lerche, I., Williams, D.F., 1991. Opening the carbon isotope" vital effect" black box, 2, Quantitative model for interpreting foraminiferal carbon isotope data. Paleoceanography 6, 639-655.

Spero, H.J., Mielke, K.M., Kalve, E.M., Lea, D.W., Pak, D.K., 2003. Multispecies approach to reconstructing eastern equatorial Pacific thermocline hydrography during the past 360 kyr. Paleoceanography 18.

Spezzaferri, S., 1994. Planktonic foraminiferal biostratigraphy and taxonomy of the Oligocene and lower Miocene in the oceanic record. An overview. Palaeontographia Italica 81, 187.

Spezzaferri, S., Premoli Silva, I., 1991. Oligocene planktonic foraminiferal biostratigraphy and paleoclimatic interpretation from Hole 538A, DSDP Leg 77, Gulf of Mexico. Palaeogeography, Palaeoclimatology, Palaeoecology 83, 217-263.

Spicer, R.A., Harris, N.B., Widdowson, M., Herman, A.B., Guo, S., Valdes, P.J., Wolfe, J.A., Kelley, S.P., 2003. Constant elevation of southern Tibet over the past 15 million years. Nature 421, 622-624.

Srinivasan, M., Kennett, J., 1981. Neogene planktonic foraminiferal biostratigraphy and evolution: equatorial to subantarctic, South Pacific. Marine Micropaleontology 6, 499-533.

Stainforth, R.M., Lamb, R.J., Luterbacher, H., Beard, J.H., Jeffords, R.M., 1975. Cenozoic foraminiferal zonation and characteristics of index forms. Kansas University Paleontological Contributions, Article 62, 13–162.

Stein, R., Robert, C., 1986. Siliciclastic sediments at Sites 588, 590 and 591: Neogene and Paleogene evolution in the southwest Pacific and Australian climate. , in: Kennett, J.P., yon der Borch, C.C. (Eds.), Init. Rep. DSDP, pp. 1437-1455.

Stewart, J.A., Wilson, P.A., Edgar, K.M., Anand, P., James, R.H., 2012. Geochemical assessment of the palaeoecology, ontogeny, morphotypic variability and palaeoceanographic utility of *“Dentoglobigerina” venezuelana*. Marine Micropaleontology 84–85, 74-86.

Stoll, H.M., Schrag, D.P., 1998. Effects of Quaternary sea level cycles on strontium in seawater. Geochimica et Cosmochimica Acta 62, 1107-1118.

Stoll, H.M., Schrag, D.P., Clemens, S.C., 1999. Are seawater Sr/Ca variations preserved in Quaternary foraminifera? Geochimica et Cosmochimica Acta 63, 3535-3547.

Stott, L., Cannariato, K., Thunell, R., Haug, G.H., Koutavas, A., Lund, S., 2004. Decline of surface temperature and salinity in the western tropical Pacific Ocean in the Holocene epoch. Nature 431, 56-59.

Stults, D.Z., Wagner-Cremer, F., Axsmith, B.J., 2011. Atmospheric paleo-CO_2 estimates based on *Taxodium distichum* (Cupressaceae) fossils from the Miocene and Pliocene of Eastern North America. Palaeogeography, Palaeoclimatology, Palaeoecology 309, 327-332.

Talley, L.D., Pickard, G.L., Emery, W.J., Swift, J.H., 2011. Descriptive physical oceanography: an introduction. Access Online via Elsevier.

Thomas, D.J., Bralower, T.J., Zachos, J.C., 1999. New evidence for subtropical warming during the Late Paleocene thermal maximum: Stable isotopes from Deep Sea Drilling Project Site 527, Walvis Ridge. Paleoceanography 14, 561-570.

Tian, J., Shevenell, A., Wang, P., Zhao, Q., Li, Q., Cheng, X., 2009. Reorganization of Pacific Deep Waters linked to middle Miocene Antarctic cryosphere expansion: A perspective from the South China Sea. Palaeogeography, Palaeoclimatology, Palaeoecology 284, 375-382.

Tian, J., Wang, P., Cheng, X., 2004. Development of the East Asian monsoon and Northern Hemisphere glaciation: oxygen isotope records from the South China Sea. Quaternary Science Reviews 23, 2007-2016.

Tian, J., Yang, M., Lyle, M.W., Wilkens, R., Shackford, J.K., 2013. Obliquity and long eccentricity pacing of the Middle Miocene climate transition. Geochemistry, Geophysics, Geosystems, n/a-n/a.

Todd, R., Cloud, P.E., Low, D., Schmidt, R.G., 1954. Probable occurrence of Oligocene on Saipan. American Journal of Science 252, 673–682.

Tong, J., You, Y., Müller, R., Seton, M., 2009. Climate model sensitivity to atmospheric CO_2 concentrations for the middle Miocene. Global and Planetary Change 67, 129-140.

Torrence, C., Compo, G.P., 1998. A practical guide to wavelet analysis. Bulletin of the American Meteorological society 79, 61-78.

Trenberth, K.E., 1997. The definition of el nino. Bulletin of the American Meteorological society 78, 2771-2777.

Trenberth, K.E., Caron, J.M., 2001. Estimates of meridional atmosphere and ocean heat transports. Journal of Climate 14, 3433-3443.

Tripati, A.K., Roberts, C.D., Eagle, R.A., 2009. Coupling of CO2 and Ice Sheet Stability Over Major Climate Transitions of the Last 20 Million Years. Science 326, 1394-1397.

Turco, E., Bambini, A.M., Foresi, L., Iaccarino, S., Lirer, F., Mazzei, R., Salvatorini, G., 2002. Middle Miocene high-resolution calcareous plankton biostratigraphy at Site 926 (Leg 154, equatorial Atlantic Ocean): palaeoecological and palaeobiogeographical implications. Geobios 35, Supplement 1, 257-276.

Turk, D., McPhaden, M.J., Busalacchi, A.J., Lewis, M.R., 2001. Remotely sensed biological production in the equatorial Pacific. Science 293, 471-474.

Ujiié, Y., Asami, T., 2014. Temperature is not responsible for left-right reversal in pelagic unicellular zooplanktons. Journal of Zoology 293, 16-24.

Utescher, T., Erdei, B., François, L., Mosbrugger, V., 2007. Tree diversity in the Miocene forests of Western Eurasia. Palaeogeography, Palaeoclimatology, Palaeoecology 253, 226-250.

Verducci, M., Foresi, L.M., Scott, G.H., Tiepolo, M., Sprovieri, M., Lirer, F., 2007. East Antarctic Ice Sheet fluctuations during the Middle Miocene Climatic Transition inferred from faunal and biogeochemical data on planktonic foraminifera (Kerguelen Plateau). US Geological Survey and The National Academics; USGS OF− 2007− 1047, Short Re− search Paper 37.

Vincent, E., Berger, W.H., 1985. Carbon dioxide and polar cooling in the Miocene: The Monterey hypothesis. The Carbon Cycle and Atmospheric CO_2: Natural Variations Archean to Present, 455-468.

Vincent, E., Killingley, J., Berger, W., 1981. Stable isotope composition of benthic foraminifera from the equatorial Pacific. Nature 289, 639-643.

Vincent, E., Shackleton, N., Hall, M.A., 1991. Miocene oxygen and carbon isotope stratigraphy of planktonic foraminifers at Site 709 and 758, tropical Indian Ocean, Weissel, J., Peirce, J., Taylor, E., Alt, J., et al., Proc. ODP, Sci. Results, 121, College Station, TX (Ocean Drilling Program), pp. 241–252.

Wade, B.S., Berggren, W.A., Olsson, R.K., 2007. The biostratigraphy and paleobiology of Oligocene planktonic foraminifera from the equatorial Pacific Ocean (ODP Site 1218). Marine Micropaleontology 62, 167-179.

Wade, B.S., Pälike, H., 2004. Oligocene climate dynamics. Paleoceanography 19, PA4019.

Wade, B.S., Pearson, P.N., Berggren, W.A., Pälike, H., 2011. Review and revision of Cenozoic tropical planktonic foraminiferal biostratigraphy and calibration to the geomagnetic polarity and astronomical time scale. Earth-Science Reviews 104, 111-142.

Wagner, F., Below, R., Klerk, P., Dilcher, D.L., Joosten, H., Kürschner, W.M., Visscher, H., 1996. A natural experiment on plant acclimation: lifetime stomatal frequency response of an individual tree to annual atmospheric CO2 increase. Proceedings of the National Academy of Sciences 93, 11705-11708.

Wang, C., Deser, C., Yu, J.-Y., DiNezio, P., Clement, A., 2012. El Niño and Southern Oscillation (ENSO): A review. Coral Reefs of the Eastern Pacific, 3-19.

Wang, C., Fiedler, P.C., 2006. ENSO variability and the eastern tropical Pacific: a review. Progress in Oceanography 69, 239-266.

Wang, P., Blum, P., Nessler, S., 2000. Proceedings of the Ocean Drilling Program. Texas A & M University.

Wara, M.W., Ravelo, A.C., Delaney, M.L., 2005. Permanent El Niño-Like Conditions During the Pliocene Warm Period. Science 309, 758-761.

Watanabe, T., Suzuki, A., Minobe, S., Kawashima, T., Kameo, K., Minoshima, K., Aguilar, Y.M., Wani, R., Kawahata, H., Sowa, K., Nagai, T., Kase, T., 2011. Permanent El Nino during the Pliocene warm period not supported by coral evidence. Nature 471, 209-211.

Watkins, J.M., Mix, A.C., Wilson, J., 1996. Living planktic foraminifera: tracers of circulation and productivity regimes in the central equatorial Pacific. Deep Sea Research Part II: Topical Studies in Oceanography 43, 1257-1282.

Watkins, J.M., Mix, A.C., Wilson, J., 1998. Living planktic foraminifera in the central tropical Pacific Ocean: articulating the equatorial 'cold tongue'during La Niña, 1992. Marine Micropaleontology 33, 157-174.

Webb, S.D., 2006. The great American biotic interchange: patterns and processes. Annals of the Missouri Botanical Garden, 245-257.

Wefer, G., Berger, W., Bijma, J., Fischer, G., 1999. Clues to ocean history: a brief overview of proxies, Use of proxies in paleoceanography. Springer, pp. 1-68.

Wefer, G., Suess, E., Balzer, W., Liebezeit, G., Müller, P.J., Ungerer, C.A., Zenk, W., 1982. Fluxes of biogenic components from sediment trap deployment in circumpolar waters of the Drake Passage.

Wei, K.Y., Kennett, J.P., 1986. Taxonomic evolution of Neogene planktonic foraminifera and paleoceanographic relations. Paleoceanography 1, 67-84.

Wessels, W., 2009. Miocene rodent evolution and migration. Muroidea from Pakistan, Turkey and Northern Africa. Geologica Ultraiectina 307.

Westerhold, T., Bickert, T., Röhl, U., 2005. Middle to late Miocene oxygen isotope stratigraphy of ODP site 1085 (SE Atlantic): new constrains on Miocene climate variability and sea-level fluctuations. Palaeogeography, Palaeoclimatology, Palaeoecology 217, 205-222.

Winter, C.J., Pearson, P.N., 2001. Coiling directions in some Miocene planktonic Foraminifera. Journal of Micropalaeontology 20, 29-30.

Wolfe, J.A., 1985. Distribution of major vegetational types during the Tertiary. Geophysical Monograph Series 32, 357-375.

Woodruff, F., Douglas, R.G., 1981. Response of deep-sea benthic foraminifera to Miocene paleoclimatic events, DSDP Site 289. Marine Micropaleontology 6, 617-632.

Woodruff, F., Savin, S., 1991. Mid-Miocene isotope stratigraphy in the deep sea: High-resolution correlations, paleoclimatic cycles, and sediment preservation. Paleoceanography 6, 755-806.

Wyrtki, K., 1967. Circulation and water masses in the eastern equatorial Pacific Ocean. Int. J. Oceanol. Limnol 1, 117-147.

Xu, X., Kimoto, K., Oda, M., 1995. Predominance of left-coiling *Globorotalia truncatulinoides* (d'Orbigny) between 115,000 and 50,000 years BP: a latest foraminiferal biostratigraphic event in the western North Pacific. Quaternary Research 34, 39-47.

You, Y., 2010. Climate-model evaluation of the contribution of sea-surface temperature and carbon dioxide to the Middle Miocene Climate Optimum as a possible analogue of future climate change. Australian Journal of Earth Sciences 57, 207-219.

Zachariasse, W.J., 2012. New data on the morphology and classification pf the Oligocen-Miocene planktonic foraminifer *Paragloborotalia siakensis* (Leroy, 1939). The Journal of Foraminiferal Research 42, 156-168.

Zachos, J., Pagani, M., Sloan, L., Thomas, E., Billups, K., 2001. Trends, Rhythms, and Aberrations in Global Climate 65 Ma to Present. Science 292, 686-693.

Zachos, J.C., Dickens, G.R., Zeebe, R.E., 2008. An early Cenozoic perspective on greenhouse warming and carbon-cycle dynamics. Nature 451, 279-283.

Zeebe, R.E., Bijma, J., Wolf-Gladrow, D.A., 1999. A diffusion-reaction model of carbon isotope fractionation in foraminifera. Marine Chemistry 64, 199-227.

Zhang, Y.G., Pagani, M., Liu, Z., 2014. A 12-Million-Year Temperature History of the Tropical Pacific Ocean. Science 344, 84-87.

APPENDIX A: DATA TABLES

TABLE 1: IODP Site U1338 planktonic foraminiferal stable isotope data. MCD = Metres composite depth.

Core, section, interval (cm)	Depth (mcd)	Age (ma)	*Globigerinoides* sp.		*Globigerinoides subquadratus*		*Paragloborotalia siakensis*	
			$\delta^{18}O$	$\delta^{13}C$	$\delta^{18}O$	$\delta^{13}C$	$\delta^{18}O$	$\delta^{13}C$
B-35H-5, 50-52	350.68	13303336	-	-	-	-	-0.25	1.88
B-35H-5, 60-62	350.78	13305965	-	-	-	-	-0.10	1.84
B-35H-5, 70-72	350.88	13308595	-	-	-	-	-0.35	1.97
B-35H-5, 80-82	350.98	13311225	-	-	-	-	-0.63	1.97
B-35H-5, 90-92	351.08	13313855	-	-	-	-	-0.88	1.92
B-35H-5, 110-112	351.28	13319114	-	-	-	-	-0.93	1.56
B-35H-5, 120-122	351.38	13321744	-	-	-	-	-0.56	1.66
B-35H-5, 130-132	351.48	13324374	-	-	-	-	-0.61	1.53
B-35H-5, 140-142	351.58	13327003	-	-	-	-	-0.35	1.73
C-36H-1, 120-122	351.04	13312750	-	-	-	-	-	-
C-36H-1, 130-132	351.14	13315380	-	-	-	-	-	-
C-36H-1, 140-142	351.24	13318010	-	-	-	-	-	-
C-36H-2, 0-2	351.34	13320639	-	-	-	-	-	-
C-36H-2, 10-12	351.44	13323269	-	-	-	-	-	-
C-36H-2, 20-22	351.54	13325899	-	-	-	-	-	-
C-36H-2, 30-32	351.64	13328529	-	-	-	-	-	-
C-36H-2, 40-42	351.74	13331158	-	-	-	-	-	-
C-36H-2, 50-52	351.84	13334040	-	-	-	-	-	-
C-36H-2, 60-62	351.94	13337040	-	-	-	-	-	-
C-36H-2, 70-72	352.04	13340040	-	-	-	-	-	-
C-36H-2, 80-82	352.14	13343040	-	-	-	-	-	-
C-36H-2, 90-92	352.24	13346040	-	-	-	-	-	-
C-36H-2, 100-102	352.34	13349040	-	-	-	-	-	-
C-36H-2, 110-112	352.44	13352040	-	-	-	-	-	-
C-36H-2, 120-122	352.54	13355040	-	-	-	-	-	-
C-36H-2, 130-132	352.64	13358040	-	-	-	-	-	-
C-36H-2, 140-142	352.74	13361040	-	-	-	-	-	-
C-36H-3, 0-2	352.84	13364040	-0.83	2.52	-	-	-0.25	2.03
C-36H-3, 10-12	352.94	13367040	-0.77	3.05	-	-	-0.19	1.97
C-36H-3, 20-22	353.04	13370040	-0.92	2.71	-	-	-0.74	1.68
C-36H-3, 30-32	353.14	13372654	-1.12	2.71	-	-	-0.33	1.90
C-36H-3, 40-42	353.24	13375086	-1.14	2.70	-	-	-0.58	1.76
C-36H-3, 50-52	353.34	13377519	-	-	-	-	-0.33	1.88
C-36H-3, 60-62	353.44	13379951	-	-	-	-	-0.29	2.07
C-36H-3, 70-72	353.54	13382384	-0.90	2.70	-	-	-0.40	1.93
C-36H-3, 80-82	353.64	13384816	-	-	-	-	-0.81	1.79
C-36H-3, 90-92	353.74	13387249	-	-	-	-	-0.83	1.78

Core, section, interval (cm)	Depth (mcd)	Age (ma)	*Globigerinoides* sp.		*Globigerinoides subquadratus*		*Paragloborotalia siakensis*	
			$\delta^{18}O$	$\delta^{13}C$	$\delta^{18}O$	$\delta^{13}C$	$\delta^{18}O$	$\delta^{13}C$
C-36H-3, 100-102	353.84	13389681	-0.77	2.37	-	-	-0.72	1.69
C-36H-3, 110-112	353.94	13392114	-	-	-	-	-0.81	1.66
C-36H-3, 120-122	354.04	13394546	-0.91	2.73	-	-	-0.69	1.64
C-36H-3, 130-132	354.14	13396978	-0.77	2.58	-	-	-0.72	1.73
C-36H-3, 140-142	354.24	13399411	-0.96	2.59	-	-	-0.56	1.56
C-36H-4, 0-2	354.34	13401843	-1.18	2.42	-	-	-0.91	1.58
C-36H-4, 10-12	354.44	13404276	-1.32	2.40	-	-	-0.78	1.55
C-36H-4, 20-22	354.54	13406708	-	-	-	-	-0.57	1.80
C-36H-4, 30-32	354.64	13409141	-0.83	2.59	-	-	-0.87	1.77
C-36H-4, 40-42	354.74	13411573	-	-	-	-	-0.71	1.84
C-36H-4, 50-52	354.84	13414005	-	-	-	-	-	-
C-36H-4, 60-62	354.94	13416438	-	-	-	-	-	-
C-36H-4, 70-72	355.04	13418870	-	-	-	-	-0.48	1.74
B-36H-1, 100-102	354.94	13416414	-	-	-	-	-	-
B-36H-1, 110-112	355.04	13418846	-	-	-	-	-	-
B-36H-1, 120-122	355.14	13421278	-1.87	2.20	-	-	-0.98	1.88
B-36H-1, 130-132	355.24	13423711	-	-	-	-	-1.37	1.54
B-36H-1, 140-142	355.34	13426191	-0.99	2.59	-	-	-0.59	1.79
B-36H-2, 0-2	355.44	13428724	-	-	-	-	-0.94	1.58
B-36H-2, 10-12	355.54	13431257	-	-	-	-	-	-
B-36H-2, 20-22	355.64	13433791	-	-	-	-	-1.06	1.45
B-36H-2, 30-32	355.74	13436324	-1.28	2.56	-	-	-0.84	1.59
B-36H-2, 40-42	355.84	13438857	-0.77	2.59	-	-	-0.85	1.81
B-36H-2, 50-52	355.94	13441391	-	-	-	-	-0.60	1.81
B-36H-2, 60-62	356.04	13443924	-	-	-	-	-	-
B-36H-2, 70-72	356.14	13446457	-1.12	2.58	-	-	-	-
B-36H-2, 80-82	356.24	13448991	-	-	-	-	-0.58	1.77
B-36H-2, 90-92	356.34	13451524	-	-	-	-	-	-
B-36H-2, 100-102	356.44	13454057	-1.12	3.01	-	-	-0.75	1.51
B-36H-2, 110-112	356.54	13456591	-0.68	2.71	-	-	-0.53	1.97
B-36H-2, 120-122	356.64	13459124	-0.85	2.75	-	-	-	-
B-36H-2, 130-132	356.74	13461657	-0.49	2.59	-	-	-0.77	1.84
B-36H-2, 140-142	356.84	13464191	-1.03	2.83	-	-	-1.08	1.66
B-36H-3, 0-2	356.94	13466724	-0.77	2.76	-	-	-1.02	1.71
B-36H-3, 10-12	357.04	13469257	-0.95	2.73	-	-	-0.58	1.83
B-36H-3, 20-22	357.14	13471791	-1.07	2.40	-	-	-0.44	1.81
B-36H-3, 30-32	357.24	13474324	-0.77	2.75	-	-	-0.47	1.96
B-36H-3, 40-42	357.34	13476857	-0.82	2.51	-	-	-	-
B-36H-3, 50-52	357.44	13479391	-	-	-	-	-0.25	1.83
B-36H-3, 60-62	357.54	13481924	-0.72	2.69	-	-	-	-
B-36H-3, 70-72	357.64	13484457	-1.04	2.93	-	-	-	-
B-36H-3, 80-82	357.74	13486991	-0.90	2.78	-	-	-0.38	2.00
B-36H-3, 90-92	357.84	13489524	-0.78	2.67	-	-	-0.54	1.90

Core, section, interval (cm)	**Depth (mcd)**	**Age (ma)**	***Globigerinoides* sp.**		***Globigerinoides subquadratus***		***Paragloborotalia siakensis***	
			$\delta^{18}O$	**$\delta^{13}C$**	**$\delta^{18}O$**	**$\delta^{13}C$**	**$\delta^{18}O$**	**$\delta^{13}C$**
B-36H-3, 100-102	357.94	13492057	-0.98	2.67	-	-	-0.83	1.74
B-36H-3, 110-112	358.04	13494591	-0.74	2.52	-	-	-0.49	1.78
B-36H-3, 120-122	358.14	13497124	-0.92	2.63	-	-	-0.51	1.78
B-36H-3, 130-132	358.24	13499657	-0.90	2.49	-	-	-	-
B-36H-3, 140-142	358.34	13502446	-	-	-	-	-	-
B-36H-4, 0-2	358.44	13505523	-1.20	2.66	-	-	-0.64	1.50
B-36H-4, 10-12	358.54	13508600	-	-	-	-	-	-
B-36H-4, 20-22	358.64	13511677	-1.17	2.33	-	-	-1.01	1.57
B-36H-4, 30-32	358.74	13514754	-	-	-	-	-1.02	1.91
B-36H-4, 40-42	358.84	13517831	-1.39	2.65	-	-	-1.08	1.47
B-36H-4, 50-52	358.94	13520908	-1.28	2.57	-	-	-1.15	1.23
B-36H-4, 60-62	359.04	13523985	-1.44	2.36	-	-	-1.34	0.95
B-36H-4, 70-72	359.14	13527062	-	-	-	-	-	-
B-36H-4, 80-82	359.24	13530138	-1.20	2.41	-	-	-0.76	1.95
B-36H-4, 90-92	359.34	13533215	-1.13	2.77	-	-	-0.72	1.83
B-36H-4, 100-102	359.44	13536292	-1.08	2.62	-	-	-0.53	1.83
B-36H-4, 110-112	359.54	13539369	-1.00	2.04	-	-	-0.83	1.50
B-36H-4, 120-122	359.64	13542277	-	-	-	-	-1.00	1.34
B-36H-4, 130-132	359.74	13544995	-	-	-	-	-1.15	1.29
B-36H-4, 140-142	359.84	13547713	-0.54	2.03	-	-	-	-
B-36H-5, 0-2	359.94	13550431	-0.72	2.86	-	-	-0.56	1.59
B-36H-5, 10-12	360.04	13553149	-	-	-	-	-	-
B-36H-5, 20-22	360.14	13555867	-0.59	2.77	-	-	-	-
B-36H-5, 30-32	360.24	13558585	-1.43	2.58	-	-	-	-
B-36H-5, 40-42	360.34	13561303	-0.37	2.77	-	-	-	-
B-36H-5, 50-52	360.44	13564021	-0.78	3.04	-	-	-	-
B-36H-5, 60-62	360.54	13566739	-0.66	2.92	-	-	-	-
B-36H-5, 70-72	360.64	13569457	-0.59	3.06	-	-	-	-
B-36H-5, 80-82	360.74	13572175	-0.82	3.09	-	-	-0.37	1.67
B-36H-5, 90-92	360.84	13574893	-0.98	3.01	-	-	-	-
B-36H-5, 100-102	360.94	13577611	-0.84	2.86	-	-	-0.60	1.39
B-36H-5, 110-112	361.04	13580329	-1.07	2.65	-	-	-	-
B-36H-5, 120-122	361.14	13583047	-0.72	2.76	-	-	-0.41	1.44
B-36H-5, 130-132	361.24	13585765	-0.67	2.69	-	-	-0.75	0.74
B-36H-5, 140-142	361.34	13588483	-0.70	2.76	-	-	-0.37	1.49
B-36H-5, 150-152	361.44	13591201	-0.68	2.57	-	-	-0.41	1.39
B-36H-6, 0-2	361.44	13591201	-1.04	2.69	-	-	-0.81	0.99
B-36H-6, 10-12	361.54	13594000	-0.09	2.18	-	-	-	-
B-36H-6, 20-22	361.64	13597861	-1.04	2.78	-	-	-	-
B-36H-6, 30-32	361.74	13601842	-0.62	2.77	-	-	-0.58	1.36
C-37H-1, 80-82	361.77	13603036	-0.56	3.01	-	-	-4.25	-0.66
B-36H-6, 40-42	361.84	13605822	-	-	-	-	-0.35	1.51
C-37H-1, 90-92	361.87	13607017	-	-	-	-	-0.49	1.44

Core, section, interval (cm)	Depth (mcd)	Age (ma)	*Globigerinoides* sp.		*Globigerinoides subquadratus*		*Paragloborotalia siakensis*	
			$\delta^{18}O$	$\delta^{13}C$	$\delta^{18}O$	$\delta^{13}C$	$\delta^{18}O$	$\delta^{13}C$
C-37H-1, 100-102	361.97	13610997	-	-	-	-	-	-
C-37H-1, 110-112	362.07	13614978	-	-	-	-	-	-
C-37H-1, 120-122	362.17	13618958	-	-	-	-	-	-
C-37H-1, 130-132	362.27	13622939	-	-	-	-	-0.53	1.61
C-37H-1, 140-142	362.37	13626919	-	-	-	-	-	-
C-37H-2, 0-2	362.47	13630900	-0.75	3.11	-	-	-	-
C-37H-2, 10-12	362.57	13635000	-0.96	3.17	-	-	-	-
C-37H-2, 20-22	362.67	13637832	-	-	-	-	-	-
C-37H-2, 30-32	362.77	13640752	-0.51	3.06	-	-	-	-
C-37H-2, 40-42	362.87	13643672	-0.62	3.14	-	-	-0.61	1.34
C-37H-2, 50-52	362.97	13646592	-0.57	3.03	-	-	-0.60	1.35
C-37H-2, 60-62	363.07	13649512	-0.77	3.08	-	-	-0.49	1.44
C-37H-2, 70-72	363.17	13652432	-0.72	3.11	-	-	-0.53	1.45
C-37H-2, 80-82	363.27	13655352	-0.87	3.19	-	-	-	-
C-37H-2, 90-92	363.37	13658272	-0.76	3.17	-	-	-0.53	2.05
C-37H-2, 100-102	363.47	13661192	-0.86	3.32	-	-	-	-
C-37H-2, 110-112	363.57	13664112	-1.07	3.55	-	-	-0.96	1.95
C-37H-2, 120-122	363.67	13667032	-0.73	3.21	-	-	-	-
C-37H-2, 130-132	363.77	13669952	-0.33	3.11	-	-	-	-
C-37H-2, 140-142	363.87	13672872	-0.46	2.92	-	-	-0.27	2.11
C-37H-3, 0-2	363.97	13675792	-0.59	3.20	-	-	0.05	2.11
C-37H-3, 10-12	364.07	13678712	-0.60	3.07	-	-	-0.48	2.13
C-37H-3, 20-22	364.17	13681632	-0.81	3.24	-	-	-0.91	1.97
C-37H-3, 30-32	364.27	13684552	-0.75	2.95	-	-	-0.10	2.10
C-37H-3, 40-42	364.37	13687472	-0.84	2.91	-	-	-0.29	1.90
C-37H-3, 50-52	364.47	13690392	-0.60	3.07	-	-	-0.81	2.08
C-37H-3, 60-62	364.57	13693312	-0.93	3.16	-	-	-0.97	1.96
C-37H-3, 70-72	364.67	13696232	-0.95	3.31	-	-	-	-
C-37H-3, 80-82	364.77	13699152	-0.85	3.14	-	-	-	-
C-37H-3, 90-92	364.87	13702072	-	-	-	-	-	-
C-37H-3, 100-102	364.97	13704992	-0.81	3.24	-	-	-0.63	2.10
C-37H-3, 110-112	365.07	13708000	-0.72	3.12	-	-	-1.04	2.02
C-37H-3, 120-122	365.17	13709863	-0.92	3.15	-	-	-0.45	2.15
C-37H-3, 130-132	365.27	13711783	-0.81	2.74	-	-	-0.67	1.90
C-37H-3, 140-142	365.37	13713703	-0.95	3.22	-	-	-1.35	1.89
C-37H-4, 0-2	365.48	13715816	-	-	-	-	-0.80	1.78
C-37H-4, 10-12	365.58	13717736	-0.82	3.19	-	-	-0.64	1.98
C-37H-4, 20-22	365.68	13719656	-0.59	3.02	-	-	-0.70	2.07
C-37H-4, 30-32	365.78	13721576	-0.71	3.18	-	-	-0.68	2.34
C-37H-4, 40-42	365.88	13723497	-0.77	3.15	-	-	0.18	2.43
C-37H-4, 50-52	365.98	13725417	-0.53	3.09	-	-	-0.47	2.33
C-37H-4, 60-62	366.08	13727337	-	-	-	-	-0.74	2.17
C-37H-4, 70-72	366.18	13729258	-1.03	3.17	-	-	-0.76	2.09

Core, section, interval (cm)	Depth (mcd)	Age (ma)	*Globigerinoides* sp.		*Globigerinoides subquadratus*		*Paragloborotalia siakensis*	
			$\delta^{18}O$	$\delta^{13}C$	$\delta^{18}O$	$\delta^{13}C$	$\delta^{18}O$	$\delta^{13}C$
C-37H-4, 80-82	366.28	13731178	-1.19	3.46	-	-	-0.84	2.01
C-37H-4, 90-92	366.38	13733098	-	-	-	-	-0.60	2.06
C-37H-4, 100-102	366.48	13735018	-0.83	3.00	-	-	-	-
C-37H-4, 110-112	366.58	13736939	-0.82	2.96	-	-	-0.01	2.31
C-37H-4, 120-122	366.68	13738859	-0.74	2.86	-	-	-0.06	2.06
C-37H-4, 130-132	366.78	13740779	-0.84	3.12	-	-	-0.33	2.03
C-37H-4, 140-142	366.88	13742700	-0.43	3.03	-	-	-0.33	1.92
C-37H-5, 0-2	366.98	13744620	-0.98	2.93	-	-	-0.40	2.03
C-37H-5, 10-12	367.08	13746540	-0.49	3.02	-	-	-0.31	2.04
B-37H-2, 110-112	366.98	13744697	-0.69	3.12	-	-	-0.17	2.10
B-37H-2, 120-122	367.08	13746617	-0.40	2.97	-	-	-0.17	2.20
B-37H-2, 130-132	367.18	13748537	-0.40	3.23	-	-	-0.12	2.16
B-37H-2, 140-142	367.28	13750458	-0.97	3.09	-	-	-0.62	2.02
B-37H-2, 150-152	367.33	13751399	-0.12	3.41	-	-	-0.60	2.14
B-37H-3, 0-2	367.38	13752378	-0.92	3.21	-	-	-0.48	2.06
B-37H-3, 10-12	367.48	13754298	-5.28	0.82	-	-	-	-
B-37H-3, 20-22	367.58	13756218	-1.11	3.20	-	-	-0.89	2.00
B-37H-3, 30-32	367.68	13758139	-0.67	3.01	-	-	-0.35	2.13
B-37H-3, 40-42	367.78	13760059	-0.73	2.99	-	-	0.11	2.15
B-37H-3, 50-52	367.88	13762046	-0.85	2.93	-	-	0.02	2.08
B-37H-3, 60-62	367.98	13764096	-0.87	3.35	-	-	-0.33	2.04
B-37H-3, 70-72	368.08	13766146	-0.97	3.22	-	-	-0.52	2.07
B-37H-3, 80-82	368.18	13768196	-0.71	3.07	-	-	-0.46	2.07
B-37H-3, 90-92	368.28	13770246	-1.08	3.36	-	-	-	-
B-37H-3, 100-102	368.38	13772296	-0.82	3.09	-	-	0.02	2.08
B-37H-3, 110-112	368.48	13774346	-0.85	3.02	-	-	-0.33	2.04
B-37H-3, 120-122	368.58	13776396	-1.02	3.07	-	-	-0.52	2.07
B-37H-3, 130-132	368.68	13778446	-0.82	2.71	-	-	-0.46	2.07
B-37H-3, 140-142	368.78	13780496	-0.75	3.00	-	-	-0.58	1.90
B-37H-4, 0-2	368.88	13782546	-0.92	2.92	-	-	-0.53	1.95
B-37H-4, 10-12	368.98	13784596	-		-	-	-0.28	2.01
B-37H-4, 20-22	369.08	13786646	-0.90	2.59	-	-	0.25	2.01
B-37H-4, 30-32	369.18	13788696	-0.88	2.91	-	-	-0.39	1.83
B-37H-4, 40-42	369.28	13790746	-		-	-	-0.33	1.65
B-37H-4, 50-52	369.38	13792796	-0.79	2.61	-	-	-0.32	1.79
B-37H-4, 60-62	369.48	13794846	-0.82	2.89	-	-	-0.80	1.64
B-37H-4, 70-72	369.58	13796896	-1.24	2.58	-	-	-0.55	1.87
B-37H-4, 80-82	369.68	13798946	-1.10	2.90	-	-	-	-
B-37H-4, 90-92	369.78	13800996	-0.87	2.69	-	-	-0.65	1.79
B-37H-4, 100-102	369.88	13803046	-1.06	2.73	-	-	-0.88	1.87
B-37H-4, 110-112	369.98	13805096	-0.70	2.98	-	-	-0.25	1.81
B-37H-4, 120-122	370.08	13807146	-0.47	2.82	-	-	-0.22	1.85
B-37H-4, 130-132	370.18	13809196	-0.83	2.92	-	-	-	-

Core, section, interval (cm)	Depth (mcd)	Age (ma)	*Globigerinoides* sp.		*Globigerinoides subquadratus*		*Paragloborotalia siakensis*	
			$\delta^{18}O$	$\delta^{13}C$	$\delta^{18}O$	$\delta^{13}C$	$\delta^{18}O$	$\delta^{13}C$
B-37H-4, 140-142	370.28	13811246	-1.00	2.80	-	-	-0.47	1.73
B-37H-5, 0-2	370.38	13813296	-	-	-	-	-	-
B-37H-5, 10-12	370.48	13815346	-	-	-	-	-	-
B-37H-5, 20-22	370.58	13817396	-	-	-	-	-	-
B-37H-5, 30-32	370.68	13819446	-	-	-	-	-	-
B-37H-5, 40-42	370.78	13821496	-	-	-	-	-	-
B-37H-5, 50-52	370.88	13823546	-	-	-	-	-	-
B-37H-5, 60-62	370.98	13825596	-	-	-	-	-	-
B-37H-5, 70-72	371.08	13827646	-	-	-	-	-	-
B-37H-5, 80-82	371.18	13829696	-	-	-	-	-	-
B37H05, 85-88	371.23	13830721	-0.66	2.76	-	-	-	-
B-37H-5, 90-92	371.28	13831746	-	-	-	-	-	-
B37H05, 95-97	371.33	13832771	-0.55	2.93	-	-	-	-
B-37H-5, 100-102	371.38	13833796	-	-	-	-	-0.52	1.81
B37H05, 105-107	371.43	13834821	-0.81	2.57	-	-	-	-
B-37H-5, 110-112	371.48	13835846	-	-	-	-	-0.02	1.82
B-37H-5, 120-122	371.58	13837896	-	-	-	-	-0.63	1.81
B37H05, 125-127	371.63	13838921	-0.07	2.94	-	-	-	-
B-37H-5, 130-132	371.68	13839946	-	-	-	-	-0.31	1.80
B37H05, 135-137	371.73	13840971	-0.89	2.63	-	-	-	-
B-37H-5, 140-142	371.78	13841996	-	-	-	-	-	-
B37H05, 145-147	371.83	13843000	-0.89	2.52	-	-	-	-
B-37H-6, 0-2	371.88	13845391	-	-	-	-	-0.17	1.82
B37H06, 5-7	371.93	13847734	-0.91	2.46	-	-	-	-
B-37H-6, 10-12	371.98	13850078	-	-	-	-	-0.15	1.52
B37H06, 15-17	372.03	13852422	-0.74	2.45	-	-	-	-
B-37H-6, 20-22	372.08	13854766	-	-	-	-	-	-
B37H06, 25-27	372.13	13857109	-0.97	2.60	-	-	-	-
B-37H-6, 30-32	372.18	13859453	-	-	-	-	-	-
B37H06, 35-37	372.19	13859641	-0.93	2.68	-	-	-	-
C-38H-1, 120-122	372.19	13859828	-0.86	2.84	-	-	-0.45	1.50
C-38H-1, 130-132	372.29	13864516	-0.99	3.03	-	-	-0.49	1.83
C-38H-1, 140-142	372.39	13869203	-0.67	2.81	-	-	-	-
C-38H-2, 0-2	372.49	13873891	-1.13	2.72	-	-	-	-
C-38H-2, 10-12	372.59	13878578	-1.30	2.67	-	-	-	-
C-38H-2, 20-22	372.69	13883266	-0.25	2.29	-	-	-	-
C-38H-2, 30-32	372.79	13888000	-0.87	2.73	-	-	-	-
C-38H-2, 40-42	372.89	13893148	-0.93	2.71	-	-	-	-
C-38H-2, 50-52	372.99	13898348	-1.12	2.62	-	-	-	-
C-38H-2, 60-62	373.09	13902784	-	-	-	-	-	-
C-38H-2, 70-72	373.19	13906424	-0.72	2.74	-	-	-	-
C-38H-2, 80-82	373.29	13910064	-1.02	2.72	-	-	-	-
C-38H-2, 90-92	373.39	13913704	-1.37	2.85	-	-	-	-

Core, section, interval (cm)	Depth (mcd)	Age (ma)	*Globigerinoides* sp.		*Globigerinoides subquadratus*		*Paragloborotalia siakensis*	
			$\delta^{18}O$	$\delta^{13}C$	$\delta^{18}O$	$\delta^{13}C$	$\delta^{18}O$	$\delta^{13}C$
C-38H-2, 100-102	373.49	13917344	-0.61	2.62	-	-	-	-
C-38H-2, 110-112	373.59	13920984	-1.34	2.47	-	-	-	-
C-38H-2, 120-122	373.69	13924624	-1.44	2.55	-	-	-	-
C-38H-2, 130-132	373.79	13928264	-	-	-	-	-	-
C-38H-2, 140-142	373.89	13931904	-1.38	2.76	-	-	-	-
C-38H-3, 0-2	373.99	13935544	-1.37	2.84	-	-	-	-
C-38H-3, 10-12	374.09	13939184	-	-	-	-	-	-
C-38H-3, 20-22	374.19	13942824	-1.11	2.95	-	-	-	-
C-38H-3, 30-32	374.29	13946464	-1.17	2.85	-	-	-	-
C-38H-3, 40-42	374.39	13950104	-0.97	2.69	-	-	-	-
C-38H-3, 50-52	374.49	13953744	-1.05	2.64	-	-	-	-
C-38H-3, 60-62	374.59	13968072	-1.04	2.59	-	-	-	-
C-38H-3, 70-72	374.69	13970588	-	-	-	-	-	-
C-38H-3, 80-82	374.79	13973104	-	-	-	-	-	-
C-38H-3, 90-92	374.89	13975620	-	-	-	-	-	-
C-38H-3, 100-102	374.99	13978136	-	-	-	-	-	-
C-38H-3, 110-112	375.09	13980652	-	-	-	-	-	-
C-38H-3, 120-122	375.19	13983168	-	-	-	-	-	-
C-38H-3, 130-132	375.29	13985685	-	-	-	-	-	-
C-38H-3, 140-142	375.39	13988201	-	-	-	-	-	-
C-38H-4, 0-2	375.49	13990717	-1.07	2.90	-	-	-	-
C-38H-4, 10-12	375.59	13993233	-1.38	2.85	-	-	-	-
C-38H-4, 20-22	375.69	13995749	-	-	-	-	-	-
C-38H-4, 30-32	375.79	13998265	-	-	-	-	-	-
C-38H-4, 40-42	375.89	14000781	-1.28	2.88	-	-	-	-
C-38H-4, 50-52	375.99	14003297	-1.50	2.78	-	-	-	-
C-38H-4, 60-62	376.09	14005814	-	-	-	-	-	-
C-38H-4, 70-72	376.19	14008330	-	-	-	-	-	-
C-38H-4, 80-82	376.29	14010846	-1.38	2.76	-	-	-	-
C-38H-4, 90-92	376.39	14013362	-	-	-	-	-	-
C-38H-4, 100-102	376.49	14015878	-	-	-	-	-	-
C-38H-4, 110-112	376.59	14018394	-1.41	2.87	-	-	-	-
C-38H-4, 120-122	376.69	14020910	-1.48	3.08	-	-	-	-
C-38H-4, 130-132	376.79	14023426	-1.60	2.95	-	-	-	-
C-38H-4, 140-142	376.89	14025943	-1.35	2.94	-	-	-	-
C-38H-5, 0-2	376.99	14028459	-1.14	2.64	-	-	-	-
C-38H-5, 10-12	377.09	14031000	-1.31	2.57	-	-	-	-
C-38H-5, 20-22	377.19	14034481	-	-	-	-	-	-
C-38H-5, 30-32	377.29	14037997	-0.99	2.84	-	-	-	-
C-38H-5, 40-42	377.39	14041513	-1.06	2.86	-	-	-	-
C-38H-5, 50-52	377.49	14045029	-	-	-	-	-	-
C-38H-5, 60-62	377.59	14048545	-0.84	3.05	-	-	-	-
C-38H-5, 70-72	377.69	14052061	-0.87	3.19	-	-	-	-

Core, section, interval (cm)	**Depth (mcd)**	**Age (ma)**	***Globigerinoides* sp.**		***Globigerinoides subquadratus***		***Paragloborotalia siakensis***	
			$\delta^{18}O$	**$\delta^{13}C$**	**$\delta^{18}O$**	**$\delta^{13}C$**	**$\delta^{18}O$**	**$\delta^{13}C$**
C-38H-5, 80-82	377.79	14055577	-0.94	3.09	-	-	-	-
C-38H-5, 90-92	377.89	14059093	-1.00	3.30	-	-	-	-
C-38H-5, 100-102	377.99	14062609	-	-	-	-	-	-
B-38H-2, 60-62	377.88	14058882	-	-	-	-	-	-
B-38H-2, 70-72	377.98	14062398	-0.89	3.03	-	-	-	-
B-38H-2, 80-82	378.08	14065914	-0.82	3.13	-	-	-	-
B-38H-2, 90-92	378.18	14069430	-1.23	2.83	-	-	-	-
B-38H-2, 100-102	378.28	14072946	-1.01	2.83	-	-	-	-
B-38H-2, 110-112	378.38	14076462	-1.40	3.10	-	-	-	-
B-38H-2, 120-122	378.48	14079978	-	-	-	-	-	-
B-38H-2, 130-132	378.58	14083494	-1.10	2.86	-	-	-0.23	2.15
B-38H-2, 140-142	378.68	14087010	-1.10	3.05	-	-	-	-
B-38H-3, 0-2	378.78	14090526	-0.82	3.00	-	-	-	-
B-38H-3, 10-12	378.88	14094042	-0.94	3.16	-	-	-	-
B-38H-3, 20-22	378.98	14097558	-0.91	2.98	-	-	-	-
B-38H-3, 30-32	379.08	14101074	-2.58	3.05	-	-	-	-
B-38H-3, 40-42	379.18	14104589	-1.40	3.08	-	-	-	-
B-38H-3, 50-52	379.28	14108000	-0.89	3.03	-	-	-	-
B-38H-3, 60-62	379.38	14111208	-0.83	2.73	-	-	-	-
B-38H-3, 70-72	379.48	14114323	-1.11	2.60	-	-	-	-
B-38H-3, 80-82	379.58	14117438	-0.86	2.70	-	-	-	-
B-38H-3, 90-92	379.68	14120552	-1.06	2.61	-	-	-	-
B-38H-3, 100-102	379.78	14123667	-0.91	2.59	-	-	-	-
B-38H-3, 110-112	379.88	14126782	-0.83	2.82	-	-	-0.47	1.84
B-38H-3, 120-122	379.98	14129897	-1.03	2.88	-	-	-	-
B-38H-3, 130-132	380.08	14133011	-1.02	2.85	-	-	-	-
B-38H-3, 140-142	380.18	14136126	-1.06	2.91	-	-	-	-
B-38H-4, 0-2	380.28	14139241	-1.05	2.84	-	-	-0.11	2.05
B-38H-4, 10-12	380.38	14142356	-0.86	2.69	-	-	-	-
B-38H-4, 20-22	380.48	14145470	-0.76	2.76	-	-	-	-
B-38H-4, 30-32	380.58	14149454	-1.35	2.76	-	-	-	-
B-38H-4, 40-42	380.68	14153615	-0.75	2.44	-	-	-	-
B-38H-4, 50-52	380.78	14157776	-1.16	2.29	-	-	-	-
B-38H-4, 60-62	380.88	14161938	-1.11	2.69	-	-	-	-
B-38H-4, 70-72	380.98	14166099	-1.16	2.60	-	-	-	-
B-38H-4, 80-82	381.08	14170260	-0.68	2.41	-	-	-	-
B-38H-4, 90-92	381.18	14174422	-0.83	2.83	-	-	-	-
B-38H-4, 100-102	381.28	14178583	-1.21	2.83	-	-	-	-
B-38H-4, 110-112	381.38	14182744	-1.04	2.48	-	-	-	-
B-38H-4, 120-122	381.48	14186905	-1.14	2.70	-	-	-	-
B-38H-4, 130-132	381.58	14191067	-1.08	2.95	-	-	-	-
B-38H-4, 140-142	381.68	14195228	-0.83	2.74	-	-	-	-
B-38H-5, 0-2	381.78	14199389	-0.92	2.63	-	-	-	-

Core, section, interval (cm)	**Depth (mcd)**	**Age (ma)**	***Globigerinoides* sp.**		***Globigerinoides subquadratus***		***Paragloborotalia siakensis***	
			$\delta^{18}O$	**$\delta^{13}C$**	**$\delta^{18}O$**	**$\delta^{13}C$**	**$\delta^{18}O$**	**$\delta^{13}C$**
B-38H-5, 10-12	381.88	14203551	-0.99	2.89	-	-	-	-
B-38H-5, 20-22	381.98	14207712	-1.04	2.89	-	-	-	-
B-38H-5, 30-32	382.08	14211873	-0.95	2.68	-	-	-	-
B-38H-5, 40-42	382.18	14216035	-0.96	2.59	-	-	-	-
B-38H-5, 50-52	382.28	14220196	-0.89	2.51	-	-	-	-
B-38H-5, 60-62	382.38	14224357	-1.21	2.81	-	-	-	-
B-38H-5, 70-72	382.48	14228518	-1.16	2.55	-	-	-	-
B-38H-5, 80-82	382.58	14232680	-1.77	2.90	-	-	-	-
C-39H-2, 30-32	382.80	14241793	-1.24	2.64	-	-	-	-
C-39H-2, 40-42	382.90	14245954	-0.97	2.41	-	-	-	-
C-39H-2, 50-52	383.00	14250115	-1.11	2.64	-	-	-	-
C-39H-2, 60-62	383.10	14254277	-1.17	2.86	-	-	-	-
C-39H-2, 70-72	383.20	14258438	-0.63	2.71	-	-	-	-
C-39H-2, 80-82	383.30	14262599	-0.94	2.86	-	-	-0.54	2.41
C-39H-2, 90-92	383.40	14266761	-1.29	2.91	-	-	-	-
C-39H-2, 100-102	383.50	14270922	-1.33	2.96	-	-	-0.60	2.10
C-39H-2, 110-112	383.60	14275000	-1.50	2.84	-	-	-	-
C-39H-2, 120-122	383.70	14277817	-1.42	2.55	-	-	-0.59	2.05
C-39H-2, 130-132	383.80	14280579	-0.98	2.55	-	-	-	-
C-39H-2, 140-142	383.90	14283341	-0.95	2.58	-	-	-	-
C-39H-3, 0-2	384.00	14286103	-1.09	2.72	-	-	-	-
C-39H-3, 10-12	384.10	14288865	-1.11	2.75	-	-	-	-
C-39H-3, 20-22	384.20	14291627	-1.14	2.70	-	-	-	-
C-39H-3, 30-32	384.30	14294389	-1.02	2.74	-	-	-0.79	2.04
C-39H-3, 40-42	384.40	14297150	-0.84	2.70	-	-	-	-
C-39H-3, 50-52	384.50	14299912	-1.12	2.81	-	-	-	-
C-39H-3, 60-62	384.60	14302674	-1.31	2.79	-	-	-	-
C-39H-3, 90-92	384.90	14313632	-1.24	3.02	-	-	-	-
C-39H-3, 100-102	385.00	14317454	-1.17	2.69	-	-	-	-
C-39H-3, 110-112	385.10	14321276	-1.25	2.63	-	-	-	-
C-39H-3, 120-122	385.20	14325099	-1.10	2.51	-	-	-	-
C-39H-3, 140-142	385.40	14332743	-1.36	2.72	-	-	-	-
C-39H-4, 0-2	385.50	14336565	-0.82	2.67	-	-	-	-
C-39H-4, 10-12	385.60	14340388	-1.17	2.70	-	-	-	-
C-39H-4, 30-32	385.80	14348032	-1.06	2.88	-	-	-	-
C-39H-4, 40-42	385.90	14351854	-0.83	2.75	-	-	-	-
C-39H-4, 50-52	386.00	14355676	-0.89	2.78	-	-	-	-
C-39H-4, 60-62	386.10	14359499	-1.19	2.80	-	-	-	-
C-39H-4, 70-72	386.20	14363321	-1.47	2.51	-	-	-	-
C-39H-4, 80-82	386.30	14367143	-1.12	2.47	-	-	-	-
C-39H-4, 110-112	386.60	14378610	-1.37	2.44	-	-	-	-
C-39H-4, 120-122	386.70	14382432	-1.66	2.90	-	-	-	-
C-39H-4, 130-132	386.80	14386254	-1.12	2.61	-	-	-	-

Core, section, interval (cm)	**Depth (mcd)**	**Age (ma)**	***Globigerinoides* sp.**		***Globigerinoides subquadratus***		***Paragloborotalia siakensis***	
			δ^{18}O	**δ^{13}C**	**δ^{18}O**	**δ^{13}C**	**δ^{18}O**	**δ^{13}C**
C-39H-4, 140-142	386.90	14390000	-1.35	2.76	-	-	-	-
C-39H-5, 0-2	387.00	14393910	-0.74	2.78	-	-	-	-
C-39H-5, 10-12	387.10	14397743	-0.52	2.80	-	-	-	-
C-39H-5, 20-22	387.20	14401577	-0.59	2.93	-	-	-	-
C-39H-5, 30-32	387.30	14405410	-0.97	2.75	-	-	-	-
C-39H-5, 40-42	387.40	14409243	-0.92	2.85	-	-	-	-
C-39H-5, 50-52	387.50	14413077	-1.15	2.77	-	-	-	-
C-39H-5, 80-82	387.80	14424577	-0.88	3.23	-	-	-	-
C-39H-5, 90-92	387.90	14428410	-	-	-	-	-	-
C-39H-5, 100-102	388.00	14432243	-1.39	3.00	-	-	-	-
C-39H-5, 110-112	388.10	14436000	-1.34	2.82	-	-	-	-
C-39H-5, 120-122	388.20	14438318	-	-	-	-	-	-
C-39H-5, 130-132	388.30	14440591	-1.08	2.79	-	-	-	-
C-39H-5, 140-142	388.40	14442864	-0.89	2.91	-	-	-	-
C-39H-6, 0-2	388.50	14445136	-0.86	2.72	-	-	-	-
C-39H-6, 10-12	388.60	14447409	-0.99	2.75	-	-	-	-
C-39H-6, 20-22	388.70	14449682	-0.74	2.96	-	-	-	-
C-39H-6, 30-32	388.80	14451955	-0.72	2.77	-	-	-	-
C-39H-6, 40-42	388.90	14454227	-1.01	2.85	-	-	-	-
C-39H-6, 60-62	389.10	14458773	-1.03	2.92	-	-	-	-
C-39H-6, 70-72	389.20	14461045	-1.24	3.30	-	-	-	-
C-39H-6, 80-82	389.30	14463318	-1.00	3.05	-	-	-	-
C-39H-6, 90-92	389.40	14465591	-0.96	3.08	-	-	-	-
C-39H-6, 100-102	389.50	14467864	-1.07	2.89	-	-	-	-
C-39H-6, 110-112	389.60	14470136	-1.62	2.64	-	-	-	-
C-39H-6, 120-122	389.70	14472409	-1.55	2.49	-	-	-	-
C-39H-6, 130-132	389.80	14474682	-1.69	2.92	-	-	-	-
C-39H-6, 140-142	389.90	14476955	-1.37	2.44	-	-	-	-
C-39H-7, 20-22	390.20	14483773	-1.16	2.87	-	-	-	-
C-39H-7, 30-32	390.30	14486045	-1.07	2.94	-	-	-	-
C-39H-7, 50-52	390.50	14490591	-1.10	2.92	-	-	-	-
C-39H-7, 60-62	390.60	14492864	-1.49	2.51	-	-	-	-
C-39H-7, 70-72	390.70	14495136	-1.29	2.24	-	-	-	-
C-40H-1, 10-12	390.98	14501500	-1.19	2.98	-	-	-	-
C-40H-1, 20-22	391.08	14503773	-0.89	2.65	-	-	-	-
C-40H-1, 30-32	391.18	14506000	-0.99	2.40	-	-	-	-
C-40H-1, 40-42	391.28	14508720	-1.38	2.71	-	-	-	-
C-40H-1, 50-52	391.38	14511387	-0.87	2.43	-	-	-	-
C-40H-1, 60-62	391.48	14514053	-	-	-	-	-	-
C-40H-1, 70-72	391.58	14516720	-	-	-	-	-	-
C-40H-1, 80-82	391.68	14519387	-0.85	2.13	-	-	-	-
C-40H-1, 90-92	391.78	14522053	-0.89	2.49	-	-	-	-
C-40H-1, 100-102	391.88	14524720	-0.58	2.36	-	-	-	-

Core, section, interval (cm)	**Depth (mcd)**	**Age (ma)**	***Globigerinoides* sp.**		***Globigerinoides subquadratus***		***Paragloborotalia siakensis***	
			$\delta^{18}O$	**$\delta^{13}C$**	**$\delta^{18}O$**	**$\delta^{13}C$**	**$\delta^{18}O$**	**$\delta^{13}C$**
C-40H-1, 110-112	391.98	14527387	-0.65	2.55	-	-	-	-
C-40H-1, 120-122	392.08	14530053	-0.56	2.56	-	-	-	-
C-40H-1, 130-132	392.18	14532720	-0.64	2.40	-	-	-	-
C-40H-1, 140-142	392.28	14535387	-0.55	2.44	-	-	-	-
C-40H-2, 0-2	392.38	14538053	-0.93	2.57	-	-	-	-
C-40H-2, 10-12	392.48	14540720	-	-	-	-	-	-
C-40H-2, 20-22	392.58	14543387	-0.62	2.51	-	-	-	-
C-40H-2, 30-32	392.68	14546053	-1.47	2.99	-	-	-	-
C-40H-2, 40-42	392.78	14548720	-1.18	3.32	-	-	-	-
C-40H-2, 50-52	392.88	14551308	-	-	-	-	-	-
C-40H-2, 60-62	392.98	14553825	-1.15	3.11	-	-	-	-
C-40H-2, 70-72	393.08	14556341	-1.33	3.34	-	-	-	-
C-40H-2, 80-82	393.18	14558857	-1.26	2.99	-	-	-	-
C-40H-2, 90-92	393.28	14561373	-1.40	2.92	-	-	-	-
C-40H-2, 100-102	393.38	14563889	-1.46	3.03	-	-	-	-
C-40H-2, 110-112	393.48	14566405	-1.01	2.84	-	-	-	-
C-40H-2, 120-122	393.58	14568921	-1.11	2.77	-	-	-	-
C-40H-2, 130-132	393.68	14571437	-1.28	2.90	-	-	-	-
C-40H-2, 140-142	393.78	14573954	-0.53	2.74	-	-	-	-
C-40H-3, 0-2	393.88	14576470	-1.05	2.99	-	-	-	-
C-40H-3, 10-12	393.98	14578986	-0.90	3.12	-	-	-	-
C-40H-3, 20-22	394.08	14581502	-1.27	3.22	-	-	-	-
C-40H-3, 30-32	394.18	14584018	-1.19	3.02	-	-	-	-
C-40H-3, 40-42	394.28	14586534	-1.33	2.98	-	-	-	-
C-40H-3, 50-52	394.38	14589000	-0.94	2.87	-	-	-	-
C-40H-3, 60-62	394.48	14592551	-1.16	3.11	-	-	-	-
C-40H-3, 70-72	394.58	14596033	-1.21	3.04	-	-	-0.61	2.29
C-40H-3, 80-82	394.68	14599514	-0.73	2.80	-	-	-	-
C-40H-3, 90-92	394.78	14602996	-0.91	2.76	-	-	-0.42	2.11
C-40H-3, 100-102	394.88	14606477	-0.53	2.91	-	-	-	-
C-40H-3, 110-112	394.98	14609959	-0.66	2.65	-	-	-0.42	2.02
C-40H-3, 120-122	395.08	14613440	-0.63	2.99	-	-	-	-
C-40H-3, 130-132	395.18	14616921	-0.90	3.25	-	-	-1.03	2.09
C-40H-3, 140-142	395.28	14620403	-0.96	3.16	-	-	-	-
C-40H-4, 0-2	395.38	14623884	-0.93	2.82	-	-	-	-
C-40H-4, 10-12	395.48	14627366	-1.09	3.22	-	-	-	-
C-40H-4, 20-22	395.58	14630847	-1.06	3.46	-	-	-0.82	2.28
C-40H-4, 30-32	395.68	14634329	-0.71	3.28	-	-	-	-
C-40H-4, 40-42	395.78	14637810	-0.60	3.22	-	-	-0.52	2.41
C-40H-4, 50-52	395.88	14641292	-0.51	3.04	-	-	-	-
C-40H-4, 60-62	395.98	14644773	-0.80	2.92	-	-	0.24	2.40
C-40H-4, 70-72	396.08	14648255	-	-	-	-	-	-
C-40H-4, 80-82	396.18	14651736	-	-	-	-	-0.08	2.27

Core, section, interval (cm)	Depth (mcd)	Age (ma)	*Globigerinoides* sp.		*Globigerinoides subquadratus*		*Paragloborotalia siakensis*	
			$\delta^{18}O$	$\delta^{13}C$	$\delta^{18}O$	$\delta^{13}C$	$\delta^{18}O$	$\delta^{13}C$
C-40H-4, 90-92	396.28	14655218	-	-	-	-	-	-
C-40H-4, 100-102	396.38	14658699	-	-	-	-	-0.06	2.20
C-40H-4, 110-112	396.48	14662181	-	-	-	-	-	-
C-40H-4, 120-122	396.58	14665662	-	-	-	-	2.27	2.44
C-40H-4, 130-132	396.68	14669144	-	-	-	-	-	-
C-40H-4, 140-142	396.78	14672625	-	-	-	-	1.12	2.53
C-40H-5, 0-2	396.88	14676107	-	-	-	-	-	-
C-40H-5, 10-12	396.98	14679588	-0.58	2.80	-	-	-	-
C-40H-5, 20-22	397.08	14683070	-1.10	2.66	-	-	-	-
C-40H-5, 30-32	397.18	14686551	-0.85	2.66	-	-	-	-
C-40H-5, 40-42	397.28	14690033	-0.74	2.84	-	-	-	-
C-40H-5, 50-52	397.38	14693514	-1.14	2.82	-	-	-	-
C-40H-5, 60-62	397.48	14696996	-0.92	2.76	-	-	-	-
C-40H-5, 70-72	397.58	14700477	-1.02	2.88	-	-	-	-
C-40H-5, 80-82	397.68	14703959	-0.79	2.60	-	-	-	-
C-40H-5, 90-92	397.78	14707440	-1.17	2.91	-	-	-	-
C-40H-5, 100-102	397.88	14710921	-1.10	2.81	-1.02	2.81	-	-
C-40H-5, 110-112	397.98	14714403	-0.98	2.71	-1.03	2.76	-	-
C-40H-5, 120-122	398.08	14717884	-1.19	2.65	-0.90	2.72	-	-
C-40H-5, 130-132	398.18	14721366	-1.23	2.49	-1.08	2.80	-	-
C-40H-5, 140-142	398.28	14724847	-1.35	2.99	-0.88	2.67	-	-
C-40H-6, 0-2	398.38	14728329	-1.28	2.97	-1.33	2.85	-	-
C-40H-6, 10-12	398.48	14731810	-0.73	2.38	-0.99	2.86	-	-
C-40H-6, 20-22	398.58	14735292	-	-	-1.08	2.79	-	-
C-40H-6, 30-32	398.68	14738773	-	-	-0.79	2.84	-	-
C-40H-6, 40-42	398.78	14742255	-1.23	2.38	-0.75	2.61	-	-
C-40H-6, 50-52	398.88	14745736	-0.87	2.65	-0.98	2.68	-	-
C-40H-6, 60-62	398.98	14749218	-1.62	2.81	-1.04	2.50	-	-
C-40H-6, 70-72	399.08	14752699	-	-	-1.04	2.59	-	-
C-40H-6, 80-82	399.18	14756181	-0.92	2.96	-	-	-	-
C-40H-6, 90-92	399.28	14759662	-0.80	2.81	-1.25	3.02	-	-
C-40H-6, 100-102	399.38	14763144	-0.94	2.88	-1.25	3.00	-	-
C-40H-6, 110-112	399.48	14766625	-	-	-1.29	2.84	-	-
C-40H-7, 0-2	399.48	14766625	-0.93	2.49	-	-	-	-
C-40H-6, 120-122	399.58	14770107	-	-	-	-	-	-
C-40H-7, 10-12	399.58	14770107	-1.20	2.70	-	-	-	-
B-40H-6, 130-132	399.68	14773588	-	-	-	-	-	-
B-40H-7, 20-22	399.68	14773588	-1.09	2.61	-	-	-	-
B-40H-6, 140-142	399.78	14777000	-	-	-	-	-	-
B-40H-7, 30-32	399.78	14777076	-	-	-	-	-	-
B-40H-7, 40-42	399.88	14780892	-0.92	2.39	-	-	-	-
B-40H-7, 50-52	399.98	14784708	-1.07	2.34	-1.33	2.94	-	-
B-40H-1, 0-2	400.10	14789058	-0.80	2.44	-	-	-	-

Core, section, interval (cm)	**Depth (mcd)**	**Age (ma)**	***Globigerinoides* sp.**		***Globigerinoides subquadratus***		***Paragloborotalia siakensis***	
			$\delta^{18}O$	**$\delta^{13}C$**	**$\delta^{18}O$**	**$\delta^{13}C$**	**$\delta^{18}O$**	**$\delta^{13}C$**
B-40H-1, 10-12	400.20	14792874	-0.89	2.31	-	-	-	-
B-40H-1, 20-22	400.30	14796689	-1.19	2.67	-	-	-	-
B-40H-1, 30-32	400.40	14800505	-1.24	2.45	-1.07	2.77	-	-
B-40H-1, 40-42	400.50	14804321	-0.76	2.84	-	-	-	-
B-40H-1, 50-52	400.60	14808137	-1.04	2.92	-0.93	2.60	-	-
B-40H-1, 60-62	400.70	14811953	-1.14	3.01	-	-	-	-
B-40H-1, 70-72	400.80	14815768	-1.11	2.87	-	-	-	-
B-40H-1, 80-82	400.90	14819584	-	-	-	-	-	-
B-40H-1, 90-92	401.00	14823400	-	-	-	-	-	-
B-40H-1, 100-102	401.10	14827216	-1.02	2.83	-0.84	2.65	-	-
B-40H-1, 110-112	401.20	14831032	-1.21	2.70	-1.12	2.55	-	-
B-40H-1, 120-122	401.30	14835000	-1.38	2.57	-1.23	2.76	-	-
B-40H-1, 130-132	401.40	14837124	-	-	-	-	-	-
B-40H-1, 140-142	401.50	14839336	-1.33	2.69	-	-	-	-
B-40H-2, 0-2	401.60	14841549	-1.32	3.11	-1.24	2.91	-	-
C-40H-2, 10-12	401.70	14843761	-1.02	2.91	-	-	-	-
C-40H-2, 20-22	401.80	14845973	-0.74	2.91	-	-	-	-
C-40H-2, 30-32	401.90	14848186	-0.87	2.84	-	-	-	-
C-40H-2, 40-42	402.00	14850398	-0.83	2.83	-	-	-	-
C-40H-2, 50-52	402.10	14852611	-0.69	2.56	-1.24	3.11	-	-
C-40H-2, 60-62	402.20	14854823	-1.13	2.71	-1.21	2.73	-	-
C-41H-1, 80-82	402.09	14852522	-	-	-1.54	2.81	-	-
C-41H-1, 90-92	402.19	14854735	-1.02	2.99	-	-	-	-
C-41H-1, 100-102	402.29	14856947	-	-	-	-	-	-
C-41H-1, 110-112	402.39	14859159	-1.07	2.66	-	-	-	-
C-41H-1, 120-122	402.49	14861372			-0.93	3.04	-	-
C-41H-1, 130-132	402.59	14863584	-1.06	2.67	-0.79	2.99	-	-
C-41H-1, 140-142	402.69	14865796	-	-	-0.87	2.95	-	-
C-41H-2, 0-2	402.79	14868009	-	-	-1.06	2.94	-	-
C-41H-2, 10-12	402.89	14870221	-0.45	2.59	-0.81	2.70	-	-
C-41H-2, 20-22	402.99	14872434	-	-	-0.84	2.69	-	-
C-41H-2, 30-32	403.09	14874646	-0.83	2.84	-0.89	2.88	-	-
C-41H-2, 40-42	403.19	14876858	-	-	-1.12	2.92	-	-
C-41H-2, 50-52	403.29	14879071	-0.76	2.86	-1.00	2.76	-	-
C-41H-2, 60-62	403.39	14881283	-	-	-1.00	2.70	-	-
C-41H-2, 70-72	403.49	14883496	-0.67	2.75	-0.61	2.66	-	-
C-41H-2, 80-82	403.59	14885708	-	-	-1.07	2.54	-	-
C-41H-2, 90-92	403.69	14887920	-0.96	2.77	-1.14	2.68	-	-
C-41H-2, 100-102	403.79	14890133	-0.73	2.63	-1.10	2.65	-	-
C-41H-2, 110-112	403.89	14892345	-0.98	2.81	-1.24	2.31	-	-
C-41H-2, 120-122	403.99	14894558	-0.86	2.60	-1.06	2.87	-	-
C-41H-2, 130-132	404.09	14896770	-0.85	2.71	-0.89	2.97	-	-
C-41H-2, 140-142	404.19	14898982	-0.82	2.59	-0.97	2.71	-	-

Core, section, interval (cm)	Depth (mcd)	Age (ma)	*Globigerinoides* sp.		*Globigerinoides subquadratus*		*Paragloborotalia siakensis*	
			$\delta^{18}O$	$\delta^{13}C$	$\delta^{18}O$	$\delta^{13}C$	$\delta^{18}O$	$\delta^{13}C$
C-41H-3, 0-2	404.19	14898982	-0.80	2.52	-0.97	2.92	-	-
C-41H-3, 10-12	404.39	14903407	-0.68	2.71	-0.68	2.79	-	-
C-41H-3, 20-22	404.49	14905619	-1.02	2.85	-0.97	2.83	-	-
C-41H-3, 30-32	404.59	14907832	-0.94	2.78	-0.48	2.57	-	-
C-41H-3, 40-42	404.69	14910000	-0.86	2.69	-1.07	2.73	-	-
C-41H-3, 50-52	404.79	14913978	-1.33	2.71	-0.88	2.85	-	-
C-41H-3, 60-62	404.89	14917878	-1.13	2.91	-1.12	2.86	-	-
C-41H-3, 70-72	404.99	14921778	-1.11	2.89	-0.90	2.70	-	-
C-41H-3, 80-82	405.09	14925678	-1.02	2.78	-1.14	2.85	-	-
C-41H-3, 90-92	405.19	14929578	-1.39	2.62	-0.54	2.55	-	-
C-41H-3, 100-102	405.29	14933478	-1.23	2.48	-0.88	2.64	-	-
C-41H-3, 110-112	405.39	14937378	-1.22	2.58	-0.91	2.65	-	-
C-41H-3, 120-122	405.49	14941278	-	-	-1.11	2.64	-	-
C-41H-3, 130-132	405.59	14945178	-0.80	2.82	-0.95	2.75	-	-
C-41H-3, 140-142	405.69	14949000	-1.17	3.03	-1.10	2.67	-	-
C-41H-4, 0-2	405.79	14952918	-1.33	2.88	-1.08	2.77	-	-
C-41H-4, 10-12	405.89	14956760	-1.33	2.86	-	-	-	-
C-41H-4, 20-22	405.99	14960602	-0.81	2.81	-1.27	2.84	-	-
C-41H-4, 30-32	406.09	14964443	-0.93	2.99	-	-	-	-
C-41H-4, 40-42	406.19	14968285	-1.15	2.87	-0.83	2.63	-	-
C-41H-4, 50-52	406.29	14972127	-0.95	2.90	-	-	-	-
C-41H-4, 60-62	406.39	14975968	-1.01	2.84	-1.26	2.53	-	-
C-41H-4, 70-72	406.49	14979810	-0.80	2.80	-	-	-	-
C-41H-4, 80-82	406.59	14983652	-0.81	2.91	-0.72	2.84	-	-
C-41H-4, 90-92	406.69	14987493	-0.81	2.63	-1.24	2.87	-	-
C-41H-4, 100-102	406.79	14991335	-0.99	2.55	-1.37	2.80	-	-
C-41H-4, 110-112	406.89	14995177	-0.86	2.73	-0.91	2.65	-	-
C-41H-4, 120-122	406.99	14999018	-	-	-1.04	2.91	-	-
C-41H-4, 130-132	407.09	15002860	-0.88	2.76	-0.70	2.89	-	-
C-41H-4, 140-142	407.19	15006701	-0.99	2.88	-0.88	2.98	-	-
C-41H-5, 0-2	407.29	15010543	-1.22	2.82	-0.88	2.99	-	-
C-41H-5, 10-12	407.39	15014385	-1.67	2.41	-1.16	2.94	-	-
C-41H-5, 20-22	407.49	15018226	-0.99	2.69	-0.88	2.80	-	-
C-41H-5, 30-32	407.59	15022068	-1.05	2.53	-0.62	2.69	-	-
C-41H-5, 40-42	407.69	15025910	-1.05	2.55	-0.75	2.85	-	-
C-41H-5, 50-52	407.79	15029751	-0.86	2.59	-1.18	2.80	-	-
C-41H-5, 60-62	407.89	15033593	-1.26	2.67	-1.00	2.82	-	-
C-41H-5, 70-72	407.99	15037435	-1.60	1.98	-0.68	2.68	-	-
C-41H-5, 80-82	408.09	15041276	-1.27	2.66	-0.97	2.91	-	-
C-41H-5, 90-92	408.19	15045118	-1.26	2.80	-0.63	2.86	-	-
C-41H-5, 100-102	408.29	15048960	-0.82	2.61	-0.89	2.65	-	-
C-41H-5, 110-112	408.39	15052801	-1.03	2.76	-0.88	2.63	-	-
C-41H-5, 120-122	408.49	15056643	-1.33	2.65	-0.87	2.84	-	-

Core, section, interval (cm)	Depth (mcd)	Age (ma)	*Globigerinoides* sp.		*Globigerinoides subquadratus*		*Paragloborotalia siakensis*	
			δ18O	δ13C	δ18O	δ13C	δ18O	δ13C
C-41H-5, 130-132	408.59	15060484	-1.18	2.80	-0.88	2.65	-	-
C-41H-5, 140-142	408.69	15064326	-1.17	2.88	-1.01	2.89	-	-
C-41H-6, 0-2	408.80	15068552	-1.28	2.82	-1.10	2.71	-	-
C-41H-6, 10-12	408.90	15072394	-	-	-1.08	2.84	-	-
C-41H-6, 20-22	409.00	15076235	-	-	-0.97	2.49	-	-
C-41H-6, 30-32	409.10	15080000	-	-	-1.13	2.67	-	-
C-41H-6, 40-42	409.20	15083978	-	-	-1.13	2.95	-	-
C-41H-6, 50-52	409.30	15087878	-1.28	2.63	-1.03	2.82	-	-
C-41H-6, 60-62	409.40	15091778	-1.06	2.57	-1.43	2.63	-	-
C-41H-6, 70-72	409.50	15095678	-	-	-1.05	2.52	-	-
C-41H-6, 80-82	409.60	15099578	-	-	-1.10	2.75	-	-
C-41H-6, 90-92	409.70	15103478	-	-	-	-	-	-
C-41H-6, 100-102	409.80	15107378	-	-	-	-	-	-
C-41H-6, 110-112	409.90	15111278	-	-	-	-	-	-
C-41H-6, 120-122	410.00	15115178	-	-	-	-	-	-
C-41H-6, 130-132	410.10	15119000	-	-	-	-	-	-
C-41H-6, 140-142	410.20	15122370	-	-	-	-	-	-
C-41H-7, 0-2	410.31	15126004	-	-	-1.14	2.73	-	-
C-41H-7, 10-12	410.41	15129308	-	-	-1.18	2.63	-	-
B-41H-7, 20-22	410.51	15132612	-	-	-	-	-	-
B-41H-7, 30-32	410.61	15135916	-	-	-	-	-	-
B-41H-7, 40-42	410.71	15139220	-	-	-	-	-	-
B-41H-7, 50-52	410.81	15142524	-	-	-0.83	2.41	-	-
B-41H-7, 60-62	410.91	15145828	-	-	-1.12	2.60	-	-
B-41H-7, 70-72	411.01	15149132	-	-	-1.39	2.88	-	-
B-41H-1, 0-2	410.87	15144341	-	-	-	-	-	-
B-41H-1, 10-12	410.97	15147645	-	-	-1.16	2.92	-	-
B-41H-1, 20-22	411.07	15150949	-	-	-1.34	2.75	-	-
B-41H-1, 30-32	411.17	15154253	-	-	-1.09	3.01	-	-
B-41H-1, 40-42	411.27	15157557	-	-	-1.53	2.86	-	-
B-41H-1, 50-52	411.37	15160861	-	-	-1.09	2.84	-	-
B-41H-1, 60-62	411.47	15164165	-	-	-0.93	3.01	-	-
B-41H-1, 70-72	411.57	15167469	-	-	-1.40	2.94	-	-
B-41H-1, 80-82	411.67	15170773	-	-	-1.10	2.85	-	-
B-41H-1, 90-92	411.77	15174077	-	-	-1.43	2.85	-	-
B-41H-1, 100-102	411.87	15177381	-	-	-1.77	2.73	-	-
B-41H-1, 110-112	411.97	15180685	-	-	-1.42	2.99	-	-
B-41H-1, 120-122	412.07	15183989	-	-	-1.01	3.09	-	-
B-41H-1, 130-132	412.17	15187293	-	-	-1.02	2.63	-	-
B-41H-1, 140-142	412.27	15190597	-	-	-0.95	2.80	-	-
B-41H-2, 0-2	412.37	15194000	-	-	-1.11	2.94	-	-
B-41H-2, 10-12	412.47	15199543	-	-	-0.90	2.86	-	-
B-41H-2, 20-22	412.57	15205257	-	-	-	-	-	-

Core, section, interval (cm)	Depth (mcd)	Age (ma)	*Globigerinoides* sp.		*Globigerinoides subquadratus*		*Paragloborotalia siakensis*	
			$\delta^{18}O$	$\delta^{13}C$	$\delta^{18}O$	$\delta^{13}C$	$\delta^{18}O$	$\delta^{13}C$
B-41H-2, 30-32	412.67	15210971	-	-	-0.64	2.51	-	-
B-41H-2, 40-42	412.77	15216686	-	-	-1.25	2.81	-	-
B-41H-2, 50-52	412.87	15222400	-	-	-1.02	2.77	-	-
B-41H-2, 60-62	412.97	15228114	-	-	-1.51	2.45	-	-
B-41H-2, 70-72	413.07	15234000	-	-	-1.18	2.53	-	-
B-41H-2, 80-82	413.17	15239604	-	-	-1.40	2.50	-	-
B-41H-2, 90-92	413.27	15245382	-	-	-1.41	2.76	-	-
B-41H-2, 100-102	413.37	15251160	-	-	-1.65	2.76	-	-
B-41H-2, 110-112	413.47	15256938	-	-	-1.40	2.86	-	-
B-41H-2, 120-122	413.57	15262716	-	-	-	-	-	-
B-41H-2, 130-132	413.67	15268493	-	-	-1.13	2.66	-	-
B-41H-2, 140-142	413.77	15274271	-	-	-1.18	2.62	-	-
B-41H-3, 0-2	413.87	15280049	-	-	-1.45	2.69	-	-
B-41H-3, 10-12	413.97	15286000	-	-	-	-	-	-
B-41H-3, 20-22	414.07	15290203	-	-	-1.34	2.79	-	-
B-41H-3, 30-32	414.17	15294537	-	-	-0.68	2.68	-	-
B-41H-3, 40-42	414.27	15298870	-	-	-0.77	2.96	-	-
B-41H-3, 50-52	414.37	15303203	-	-	-1.02	3.10	-	-
B-41H-3, 60-62	414.47	15307537	-	-	-1.23	2.97	-	-
B-41H-3, 70-72	414.57	15311870	-	-	-0.94	2.92	-	-
B-41H-3, 80-82	414.67	15316203	-	-	-0.86	2.88	-	-
B-41H-3, 90-92	414.77	15320537	-	-	-1.00	2.99	-	-
B-41H-3, 100-102	414.87	15325000	-	-	-	-	-	-
B-41H-3, 110-112	414.97	15327656	-	-	-1.57	2.83	-	-
B-41H-3, 120-122	415.07	15330394	-	-	-1.20	3.06	-	-
B-41H-3, 130-132	415.17	15333132	-	-	-1.25	2.92	-	-
B-41H-3, 140-142	415.27	15335870	-	-	-1.27	2.89	-	-
B-41H-4, 0-2	415.37	15338608	-	-	-1.22	2.76	-	-
B-41H-4, 10-12	415.47	15341346	-	-	-1.67	2.65	-	-
B-41H-4, 20-22	415.57	15344085	-	-	-1.51	2.76	-	-
B-41H-4, 30-32	415.67	15346823	-	-	-1.23	3.15	-	-
B-41H-4, 40-42	415.77	15349561	-	-	-1.24	3.01	-	-
B-41H-4, 50-52	415.87	15352299	-	-	-1.48	3.21	-	-
B-41H-4, 60-62	415.97	15355037	-	-	-1.14	3.11	-	-
B-41H-4, 70-72	416.07	15357775	-	-	-1.17	3.16	-	-
B-41H-4, 80-82	416.17	15360513	-	-	-0.99	3.26	-	-
B-41H-4, 90-92	416.27	15363251	-	-	-	-	-	-
B-41H-4, 100-102	416.37	15365989	-	-	-0.87	2.94	-	-
B-41H-4, 110-112	416.47	15368727	-	-	-1.01	3.07	-	-
B-41H-4, 120-122	416.57	15371465	-	-	-0.94	2.96	-	-
B-41H-4, 130-132	416.67	15374204	-	-	-0.90	2.90	-	-
B-41H-4, 140-142	416.77	15376942	-	-	-1.21	3.03	-	-
B-41H-5, 0-2	416.87	15379680	-	-	-1.14	3.16	-	-

Core, section, interval (cm)	Depth (mcd)	Age (ma)	*Globigerinoides* sp.		*Globigerinoides subquadratus*		*Paragloborotalia siakensis*	
			$\delta^{18}O$	$\delta^{13}C$	$\delta^{18}O$	$\delta^{13}C$	$\delta^{18}O$	$\delta^{13}C$
B-41H-5, 10-12	416.97	15382418	-	-	-1.19	3.06	-	-
B-41H-5, 20-22	417.07	15385156	-	-	-	-	-	-
B-41H-5, 30-32	417.17	15387894	-	-	-	-	-	-
B-41H-5, 40-42	417.27	15390632	-	-	-1.14	3.13	-	-
B-41H-5, 50-52	417.37	15393370	-	-	-1.02	2.96	-	-
B-41H-5, 60-62	417.47	15396108	-	-	-1.05	3.05	-	-
B-41H-5, 70-72	417.57	15398846	-	-	-1.23	2.97	-	-
B-41H-5, 80-82	417.67	15401585	-	-	-	-	-	-
B-41H-5, 90-92	417.77	15404323	-	-	-1.04	2.87	-	-
B-41H-5, 100-102	417.87	15407061	-	-	-1.06	2.78	-	-
B-41H-5, 110-112	417.97	15409799	-	-	-1.02	2.87	-	-
B-41H-5, 120-122	418.07	15412537	-	-	-1.96	2.70	-	-
B-41H-5, 130-132	418.17	15415275	-	-	-1.29	2.97	-	-
B-41H-5, 140-142	418.27	15418013	-	-	-1.43	3.02	-	-
B-41H-6, 0-2	418.37	15420751	-	-	-1.30	3.18	-	-
B-41H-6, 10-12	418.47	15423489	-	-	-1.80	2.79	-	-
B-41H-6, 20-22	418.57	15426227	-	-	-0.71	3.19	-	-
C-41H-6, 30-32	418.67	15428965	-	-	-1.08	3.10	-	-
C-41H-6, 40-42	418.77	15431704	-	-	-0.85	2.92	-	-
C-41H-6, 50-52	418.87	15434442	-	-	-1.22	2.90	-	-
C-41H-6, 60-62	418.97	15437180	-	-	-1.10	2.70	-	-
C-41H-6, 70-72	419.07	15440000	-	-	-0.92	2.84	-	-
C-41H-6, 80-82	419.17	15444003	-	-	-0.81	2.84	-	-
C-43H-1, 130-132	418.95	15435130	-	-	-0.99	2.89	-	-
C-43H-1, 140-142	419.05	15439257	-	-	-0.89	2.86	-	-
C-43H-2, 0-2	419.15	15443384	-	-	-0.76	2.76	-	-
C-43H-2, 10-12	419.25	15447511	-	-	-1.06	3.00	-	-
C-43H-2, 20-22	419.35	15451638	-	-	-	-	-	-
C-43H-2, 30-32	419.45	15455765	-	-	-0.90	2.98	-	-
C-43H-2, 40-42	419.55	15459892	-	-	-0.99	3.07	-	-
C-43H-2, 50-52	419.65	15464019	-	-	-	-	-	-
C-43H-2, 60-62	419.75	15468146	-	-	-1.34	2.89	-	-
C-43H-2, 70-72	419.85	15472273	-	-	-1.15	2.76	-	-
C-43H-2, 80-82	419.95	15476400	-	-	-	-	-	-
C-43H-2, 90-92	420.05	15480527	-	-	-0.94	2.72	-	-
C-43H-2, 100-102	420.15	15484654	-	-	-0.88	3.06	-	-
C-43H-2, 110-112	420.25	15488781	-	-	-1.11	3.11	-	-
C-43H-2, 120-122	420.35	15492908	-	-	-1.24	2.93	-	-
C-43H-2, 130-132	420.45	15497035	-	-	-1.02	3.09	-	-
C-43H-2, 140-142	420.55	15501162	-	-	-0.82	3.10	-	-
C-43H-3, 0-2	420.66	15505702	-	-	-1.00	3.19	-	-
C-43H-3, 10-12	420.76	15509829	-	-	-0.93	3.08	-	-
C-43H-3, 20-22	420.86	15513956	-	-	-0.96	2.98	-	-

Core, section, interval (cm)	Depth (mcd)	Age (ma)	*Globigerinoides* sp.		*Globigerinoides subquadratus*		*Paragloborotalia siakensis*	
			$\delta^{18}O$	$\delta^{13}C$	$\delta^{18}O$	$\delta^{13}C$	$\delta^{18}O$	$\delta^{13}C$
C-43H-3, 30-32	420.96	15518000	-	-	-1.22	3.05	-	-
C-43H-3, 40-42	421.06	15519780	-	-	-1.11	2.78	-	-
C-43H-3, 50-52	421.16	15521525	-	-	-1.32	2.87	-	-
C-43H-3, 60-62	421.26	15523270	-	-	-1.03	3.02	-	-
C-43H-3, 70-72	421.36	15525015	-	-	-1.22	2.98	-	-
C-43H-3, 80-82	421.46	15526760	-	-	-0.96	2.77	-	-
C-43H-3, 90-92	421.56	15528505	-	-	-1.74	2.68	-	-
C-43H-3, 100-102	421.66	15530250	-	-	-1.17	2.93	-	-
C-43H-3, 110-112	421.76	15531995	-	-	-0.92	3.08	-	-
C-43H-3, 120-122	421.86	15533740	-	-	-0.87	3.00	-	-
C-43H-3, 130-132	421.96	15535485	-	-	-1.03	3.02	-	-
C-43H-3, 140-142	422.06	15537230	-	-	-1.06	2.87	-	-
C-43H-4, 0-2	422.17	15539149	-	-	-1.02	2.89	-	-
C-43H-4, 10-12	422.27	15540894	-	-	-1.16	2.92	-	-
C-43H-4, 20-22	422.37	15542639	-	-	-1.16	2.84	-	-
C-43H-4, 30-32	422.47	15544384	-	-	-1.12	2.81	-	-
C-43H-4, 40-42	422.57	15546129	-	-	-0.93	2.74	-	-
B-43H-4, 50-52	422.67	15547874	-	-	-0.90	2.98	-	-
B-43H-4, 60-62	422.77	15549619	-	-	-0.79	3.01	-	-
B-43H-4, 70-72	422.87	15551364	-	-	-0.99	3.03	-	-
B-43H-4, 80-82	422.97	15553109	-	-	-1.00	2.96	-	-
B-43H-4, 90-92	423.07	15554854	-	-	-	-	-	-
B-43H-4, 100-102	423.17	15556599	-	-	-0.94	3.09	-	-
B-42H-2, 40-42	423.04	15554295	-	-	-0.71	3.04	-	-
B-42H-2, 40-42	423.04	15554295	-	-	-0.89	3.13	-	-
B-42H-2, 50-52	423.14	15556040	-	-	-0.86	3.00	-	-
B-42H-2, 60-62	423.24	15557785	-	-	-1.02	2.88	-	-
B-42H-2, 70-72	423.34	15559530	-	-	-1.01	2.87	-	-
B-42H-2, 80-82	423.44	15561275	-	-	-0.78	2.76	-	-
C-42H-2, 90-92	423.54	15563020	-	-	-0.90	2.92	-	-
C-42H-2, 100-102	423.64	15564765	-	-	-0.82	2.85	-	-
C-42H-2, 110-112	423.74	15566510	-	-	-0.70	2.65	-	-
C-42H-2, 120-122	423.84	15568255	-	-	-1.28	2.43	-	-
C-42H-2, 130-132	423.94	15570000	-	-	-1.11	2.60	-	-
C-42H-2, 140-142	424.04	15575000	-	-	-1.06	2.73	-	-
C-44H-1, 30-32	428.11	15728795	-	-	-1.16	2.78	-	-
C-44H-1, 40-42	428.21	15732547	-	-	-1.13	2.68	-	-
C-44H-1, 50-52	428.31	15736300	-	-	-1.20	2.67	-	-
C-44H-1, 60-62	428.41	15740052	-	-	-1.21	2.74	-	-
C-44H-1, 70-72	428.51	15743805	-	-	-1.34	2.78	-	-
C-44H-1, 80-82	428.61	15747557	-	-	-1.18	2.81	-	-
C-44H-1, 90-92	428.71	15751309	-	-	-1.15	2.61	-	-
C-44H-1, 100-102	428.81	15755062	-	-	-1.29	2.78	-	-

Core, section, interval (cm)	**Depth (mcd)**	**Age (ma)**	***Globigerinoides* sp.**			***Globigerinoides subquadratus***			***Paragloborotalia siakensis***	
			δ^{18}O	**δ^{13}C**		**δ^{18}O**	**δ^{13}C**		**δ^{18}O**	**δ^{13}C**
C-44H-1, 110-112	428.91	15758814	-	-		-1.54	2.65		-	-
C-44H-1, 120-122	429.01	15762567	-	-		-	-		-	-

TABLE X: IODP Site U1338 multispecies planktonic foraminiferal stable isotope data. MCD = Metres composite depth.

Core, section, interval (cm)	Depth (mcd)	Age (ma)	Species	Size fraction (μm)	$\delta^{18}O$	$\delta^{13}C$
B-36H-4, 40-42	361.84	13605822	*D. altispira*	*315*	2.12	-0.65
B-36H-4, 40-42	361.84	13605822	*D. altispira*	*250*	2.23	-0.37
B-36H-4, 40-42	361.84	13605822	*D. altispira*	*150*	2.22	-0.46
B-36H-4, 40-42	361.84	13605822	*S. disjuncta*	*315*	2.25	-0.07
B-36H-4, 40-42	361.84	13605822	*S. disjuncta*	*250*	1.99	0.16
B-36H-4, 40-42	361.84	13605822	*D. venezuelana*	*315*	1.65	0.57
B-36H-4, 40-42	361.84	13605822	*D. venezuelana*	*250*	1.84	0.37
B-36H-4, 40-42	361.84	13605822	*D. venezuelana*	*150*	1.77	-0.33
B-36H-4, 40-42	361.84	13605822	*G. quadrilobatus*	*315*	3.07	-1.09
B-36H-4, 40-42	361.84	13605822	*G. quadrilobatus*	*250*	-	-
B-36H-4, 40-42	361.84	13605822	*G. quadrilobatus*	*150*	2.23	-0.83
B-36H-4, 40-42	361.84	13605822	*fohsella* sp.	*250*	1.54	1.19
B-36H-4, 40-42	361.84	13605822	*fohsella* sp.	*150*	1.60	0.65
B-36H-5, 130-132	361.24	13585765	*fohsella* sp.	*250*	1.83	1.44
B-36H-5, 130-132	361.24	13585765	*fohsella* sp.	*150*	1.64	0.20
B-36H-5, 130-132	361.24	13585765	*D. venezuelana*	*315*	1.55	0.52
B-36H-5, 130-132	361.24	13585765	*D. venezuelana*	*250*	1.68	0.36
B-36H-5, 130-132	361.24	13585765	*D. venezuelana*	*150*	-	-
B-36H-5, 130-132	361.24	13585765	*D. altispira*	*315*	2.74	-0.38
B-36H-5, 130-132	361.24	13585765	*D. altispira*	*250*	2.60	-0.34
B-36H-5, 130-132	361.24	13585765	*D. altispira*	*150*	2.23	-0.30
B-36H-5, 130-132	361.24	13585765	*G. quadrilobatus*	*315*	-	-
B-36H-5, 130-132	361.24	13585765	*G. quadrilobatus*	*250*	2.57	-0.84
B-36H-5, 130-132	361.24	13585765	*G. quadrilobatus*	*150*	2.27	-0.75
B-36H-5, 130-132	361.24	13585765	*S. disjuncta*	*315*	2.37	-0.39
B-36H-5, 130-132	361.24	13585765	*S. disjuncta*	*250*	2.06	-0.36
B-36H-5, 130-132	361.24	13585765	*S. disjuncta*	*150*	1.78	-0.10
C-40H-4, 40-42	395.78	14637810	*G. quadrilobatus*	*315*	3.53	-1.07
C-40H-4, 40-42	395.78	14637810	*G. quadrilobatus*	*250*	3.11	-0.63
C-40H-4, 40-42	395.78	14637810	*G. quadrilobatus*	*150*	2.65	-0.74
C-40H-4, 40-42	395.78	14637810	*D. altispira*	*315*	3.97	-0.95
C-40H-4, 40-42	395.78	14637810	*D. altispira*	*250*	3.18	-0.32
C-40H-4, 40-42	395.78	14637810	*D. altispira*	*150*	2.90	-0.21
C-40H-4, 40-42	395.78	14637810	*D. venezuelana*	*315*	2.21	0.57
C-40H-4, 40-42	395.78	14637810	*D. venezuelana*	*250*	2.93	-0.35
C-40H-4, 40-42	395.78	14637810	*D. venezuelana*	*150*	2.32	-0.18

TABLE 2: IODP Site U1338 stable isotope data from planktonic foraminifera *Clavatroella bermudezi*. MCD = Metres composite depth.

Core, section, interval (cm)	Depth (mcd)	Age (ma)	*Clavatorella bermudezi*	
			$\delta^{13}C$	**$\delta^{18}O$**
B-37H-4, 110-112	369.98	13805096	1.68	2.09
B-37H-4, 120-122	370.08	13807146	2.03	4.06
B-37H-4, 130-132	370.18	13809196	1.81	3.65
B-37H-5, 100-102	371.38	13833796	2.43	9.73
B-37H-5, 110-112	371.48	13835846	1.70	3.19
B-37H-5, 120-122	371.58	13837896	1.71	2.07
B-37H-5, 130-132	371.68	13839946	1.67	2.27
B-37H-6, 0-2	371.88	13845391	2.00	5.24
B-37H-6, 10-12	371.98	13850078	1.78	2.3
C-38H-1, 120-122	372.19	13859828	1.66	3.53
C-38H-1, 140-142	372.39	13869203	1.62	2.15
C-38H-2, 0-2	372.49	13873891	2.05	6.01
C-38H-3, 30-32	374.29	13946464	1.95	2.92
C-38H-4, 140-142	376.89	14025943	1.94	2.65
C-38H-5, 10-12	377.09	14031000	1.54	2.02
C-38H-5, 50-52	377.49	14045029	2.10	5.14
C-38H-5, 70-72	377.69	14052061	1.88	2.73
B-38H-3, 60-62	379.38	14111208	2.20	2.84
B-38H-3, 90-92	379.68	14120552	1.64	1.44
B-38H-3, 110-112	379.88	14126782	1.65	1.93
C-39H-3, 30-32	384.3	14294389	1.68	2.1
C-39H-4, 20-22	385.7	14344210	1.97	1.88
C-39H-4, 40-42	385.9	14351854	1.93	1.66
C-39H-4, 60-62	386.1	14359499	1.38	0.81
C-39H-4, 70-72	386.4	14370965	1.70	1.56

TABLE 3: IODP Site U1338 planktonic foraminiferal trace metal data and SST estimates. MCD = Metres composite depth.

Core, section, interval (cm)	Depth (mcd)	Age (Ma)	Species	Spec no.	Total (mg)	Mg/Ca	Temp.	Sr/Ca
C36H03, 20-22	353.04	13370040	*G. quadrilobatus*	25	-	2.76	22.03	1.23
C36H03, 80-82	353.64	13384816	*G. quadrilobatus*	27	0.31	2.48	20.84	1.29
C36H03, 140-142	354.24	13399411	*G. quadrilobatus*	28	0.30	2.95	22.76	1.33
B36H02, 110-132	356.54	13456591	*G. quadrilobatus*	21	0.20	2.56	21.21	1.22
B36H03, 10-32	357.04	13469257	*G. quadrilobatus*	14	0.15	4.00	26.15	1.19
B36H05, 0-2	359.94	13550431	*G. quadrilobatus*	28	0.33	3.48	24.59	1.26
B36H05, 70-92	360.64	13572175	*G. quadrilobatus*	29	0.31	2.84	22.36	1.25
B36H05, 130-132	361.24	13585765	*G. quadrilobatus*	30	0.35	2.99	22.92	1.22
B36H06, 40-42	361.84	13605822	*G. quadrilobatus*	25	0.37	2.88	22.49	1.24
C37H01, 90-92	361.87	13607017	*G. quadrilobatus*	26	0.28	2.99	22.91	1.28
C37H02, 40-42	362.87	13643672	*G. quadrilobatus*	24	0.28	3.09	23.29	1.22
C37H02, 140-142	363.87	13672872	*G. quadrilobatus*	30	0.33	2.91	22.60	1.17
C37H03, 50-52	364.47	13690392	*G. quadrilobatus*	34	0.37	3.11	23.36	1.22
C37H04, 10-12	365.58	13717736	*G. quadrilobatus*	24	0.27	3.06	23.17	1.22
C37H04, 60-72	366.08	13727337	*G. quadrilobatus*	21	0.22	3.00	22.95	1.28
C37H05, 0-2	366.98	13744620	*G. quadrilobatus*	28	0.32	3.28	23.96	1.26
B37H02, 130-132	367.18	13748537	*G. quadrilobatus*	29	2.32	3.38	24.29	0.94
B37H03, 30-42	367.68	13758139	*G. quadrilobatus*	24	0.24	3.65	25.15	1.32
B37H03, 80-82	368.18	13768196	*G. quadrilobatus*	20	0.24	3.75	25.44	1.25
B37H03, 120-122	368.58	13776396	*G. quadrilobatus*	30	0.33	3.45	24.50	1.36
B37H04, 20-22	369.08	13786646	*G. quadrilobatus*	30	0.33	2.94	22.73	1.29
B37H04, 70-72	369.58	13796896	*G. quadrilobatus*	26	0.29	3.17	23.57	1.24
B37H04, 140-142	370.28	13811246	*G. quadrilobatus*	30	0.36	3.15	23.51	1.24
B37H05, 80-82	371.18	13829696	*G. quadrilobatus*	24	0.29	3.83	25.68	1.26
C38H02, 10-42	372.59	13878578	*G. quadrilobatus*	28	0.30	3.44	24.48	1.24
B37H05 130-142	371.68	13839946	*G. quadrilobatus*	27	0.31	3.54	24.80	1.17
B37H06 20-32	372.08	13854766	*G. quadrilobatus*	32	0.38	3.19	23.64	1.26
C38H01 120-132	372.19	13859828	*G. quadrilobatus*	28	0.34	2.89	22.55	1.25
C38H03 30-42	374.29	13946464	*G. quadrilobatus*	28	0.32	3.26	23.88	1.23
C38H04 140-142	376.89	14025943	*G. quadrilobatus*	28	0.29	3.30	24.00	1.27
C38H05 30-32	377.29	14037997	*G. quadrilobatus*	29	0.36	3.14	23.47	1.27
B38H02 70-92	377.69	14065914	*G. quadrilobatus*	27	0.33	3.35	24.20	1.21
B38H02 130-142	378.58	14083494	*G. quadrilobatus*	26	0.29	3.09	23.28	1.25
B38H03 50-62	379.28	14108000	*G. quadrilobatus*	23	0.26	3.09	23.27	1.26
B38H02, 80-82	379.58	14117438	*G. quadrilobatus*	32	0.17	3.05	23.14	1.30
B38H03 100-102	379.78	14123667	*G. quadrilobatus*	30	0.32	3.41	24.38	1.39
B38H03 140-142	380.18	14136126	*G. quadrilobatus*	28	0.29	3.02	23.04	1.30
B38H04 40-52	380.68	14153615	*G. quadrilobatus*	22	0.23	3.03	23.07	1.23
B38H04, 80-92	381.08	14170260	*G. quadrilobatus*	25	0.29	2.90	22.60	1.25
B38H04,120-142	381.48	14191067	*G. quadrilobatus*	20	0.20	3.17	23.57	1.25

Core, section, interval (cm)	**Depth (mcd)**	**Age (Ma)**	**Species**	**Spec no.**	**Total (mg)**	**Mg/Ca**	**Temp.**	**Sr/Ca**
B38H05 40-52	382.18	14216035	*G. quadrilobatus*	26	0.28	3.73	25.37	1.22
B38H05, 50-52	382.28	14220196	*G. quadrilobatus*	30	0.21	3.19	23.65	1.24
C39H02 0-12	382.50	14228518	*G. quadrilobatus*	35	0.41	3.28	23.95	1.28
C39H02 60-72	383.10	14302674	*G. quadrilobatus*	28	0.36	3.13	23.43	1.17
C39H02 140-142	383.90	14283341	*G. quadrilobatus*	32	0.36	3.08	23.23	1.21
C39H03 130-142	385.30	14332743	*G. quadrilobatus*	18	0.16	3.73	25.38	1.32
C39H04 50-72	386.00	14359499	*G. quadrilobatus*	23	0.26	3.62	25.05	1.21
C39H04 120-142	386.70	14386254	*G. quadrilobatus*	23	0.26	3.12	23.41	1.24
C39H05 90-112	387.90	14432243	*G. quadrilobatus*	23	0.25	3.22	23.74	1.22
C39H06 0-22	388.50	14447409	*G. quadrilobatus*	23	0.28	3.00	22.97	1.22
C39H06 80-102	389.30	14465591	*G. quadrilobatus*	32	0.34	3.15	23.51	1.22
C39H06 140-142	389.90	14476955	*G. quadrilobatus*	21	0.20	3.18	23.60	1.29
C39H07 50-62	390.50	14490591	*G. quadrilobatus*	24	0.25	3.21	23.71	1.24
C40H01 20-32	391.08	14503773	*G. quadrilobatus*	28	0.33	3.11	23.37	1.23
C40H01 100-112	391.88	14524720	*G. quadrilobatus*	29	0.33	3.33	24.10	1.20
C40H01 130-142	392.18	14532720	*G. quadrilobatus*	24	0.34	2.99	22.92	1.19
C40H02 60-72	392.98	14553825	*G. quadrilobatus*	28	0.31	3.02	23.03	1.20
C40H02 120-132	393.58	14568921	*G. quadrilobatus*	15	0.14	3.65	25.15	1.25
C40H03 40-52	394.28	14586534	*G. quadrilobatus*	28	0.28	3.25	23.84	1.19
C40H03 100-112	391.88	14606477	*G. quadrilobatus*	25	0.30	2.88	22.51	1.22
C40H04 0-12	394.88	14623884	*G. quadrilobatus*	26	0.30	3.07	23.22	1.20
C40H04 70-82	395.38	14648255	*G. quadrilobatus*	34	0.38	2.99	22.93	1.21
C40H04, 140-142	396.78	14672625	*G. quadrilobatus*	31	0.55	3.05	23.15	1.24
C40H05, 60-62	397.48	14696996	*G. quadrilobatus*	27	0.30	2.96	22.80	1.26
C40H05, 60-62	397.48	14696996	*G. quadrilobatus*	31	0.49	3.24	23.80	1.25
C40H06 0-12	398.38	14728329	*G. quadrilobatus*	27	0.28	3.10	23.32	1.20
C40H06 80-92	399.18	14756181	*G. quadrilobatus*	27	0.27	3.06	23.19	1.20
B40H01 0-22	400.10	14792874	*G. quadrilobatus*	28	0.34	3.18	23.61	1.22
B40H01, 100-102	401.10	14827216	*G. quadrilobatus*	29	0.37	3.44	24.47	1.21
B40H01 100-112	401.10	14827216	*G. quadrilobatus*	22	0.24	3.81	25.60	1.20
C41H01 90-102	402.19	14854735	*G. quadrilobatus*	21	0.25	3.24	23.81	1.21
C41H02 50-52	403.29	14879071	*G. quadrilobatus*	25	0.25	3.20	23.68	1.28
C41H04, 20-22	405.99	14960602	*G. quadrilobatus*	19	0.21	2.79	22.15	1.18
C41H04 20-32	405.99	14964443	*G. quadrilobatus*	24	0.32	3.57	24.90	1.18
C41H04 80-92	406.59	14983652	*G. quadrilobatus*	23	0.27	3.14	23.48	1.20
C41H04 130-142	407.09	15002860	*G. quadrilobatus*	25	0.28	3.06	23.19	1.24
C41H05 40-52	407.69	15025910	*G. quadrilobatus*	30	0.36	3.13	23.44	1.21
C41H05 90-102	408.19	15041276	*G. quadrilobatus*	26	0.30	3.19	23.65	1.35
C41H06, 60-62	409.40	15091778	*G. quadrilobatus*	27	0.32	3.10	23.33	1.20
B41H01, 20-22	411.07	15150949	*G. quadrilobatus*	29	0.43	2.87	22.46	1.24
B41H03, 120-122	415.07	15330394	*G. quadrilobatus*	29	0.40	3.35	24.17	1.25
B41H03, 130-132	415.17	15333132	*G. quadrilobatus*	32	0.28	3.55	24.83	1.28
B41H04, 110-112	416.47	15368727	*G. quadrilobatus*	19	0.20	3.43	24.45	1.26

Core, section, interval (cm)	Depth (mcd)	Age (Ma)	Species	Spec no.	Total (mg)	Mg/Ca	Temp.	Sr/Ca
B41H05, 50-52	417.37	15393370	*G. quadrilobatus*	25	0.37	1.83	17.46	n.d
C43H02, 110-112	420.25	15488781	*G. quadrilobatus*	27	0.45	2.94	22.75	n.d
C43H03, 10-12	420.76	15509829	*G. quadrilobatus*	27	0.20	3.28	23.96	1.21
C43H03, 80-82	421.46	15526760	*G. quadrilobatus*	20	0.36	4.58	27.66	n.d
C40H05, 0-12	396.88	14679588	*G. subquadratus*	32	0.35	3.48	24.59	1.25
C40H05, 50-62	397.38	14693514	*G. subquadratus*	40	0.47	3.72	25.35	1.24
C40H05, 100-112	397.88	14710921	*G. subquadratus*	28	0.31	3.45	24.50	1.22
B40H01, 0-22	400.10	14789058	*G. subquadratus*	32	0.35	3.86	25.76	1.25
B40H02, 20-32	401.80	14845973	*G. subquadratus*	30	0.28	3.63	25.07	1.22
C41H01, 90-102	402.19	14854735	*G. subquadratus*	40	0.42	3.62	25.06	1.21
C41H02, 40-52	403.19	14879071	*G. subquadratus*	28	0.29	3.64	25.10	1.21
C41H02, 100-122	403.79	14892345	*G. subquadratus*	35	0.38	3.96	26.05	1.23
C41H03, 0-12	404.19	14898982	*G. subquadratus*	36	0.38	3.75	25.43	1.21
C41H04, 20-32	405.99	14960602	*G. subquadratus*	29	0.36	3.68	25.22	1.21
C41H04, 80-92	406.59	14983652	*G. subquadratus*	31	0.39	3.78	25.52	1.24
C41H05, 30-42	407.59	15022068	*G. subquadratus*	28	0.30	3.58	24.93	1.23
C41H07, 10-22	410.41	15129308	*G. subquadratus*	30	0.31	3.77	25.49	1.25
B41H01, 10-22	410.97	15147645	*G. subquadratus*	28	0.30	3.91	25.89	1.28
B41H02, 30-32	412.67	15210971	*G. subquadratus*	32	0.42	4.07	26.35	1.18
B41H02, 40-42	412.77	15216686	*G. subquadratus*	34	0.44	4.19	26.66	1.26
B41H02, 50-52	412.87	15222400	*G. subquadratus*	33	0.41	4.55	27.60	1.28
B41H02, 70-72	413.07	15234000	*G. subquadratus*	30	0.36	4.00	26.14	1.27
B41H02, 80-82	413.17	15239604	*G. subquadratus*	31	2.35	4.42	27.26	1.20
B41H02, 90-92	413.27	15245382	*G. subquadratus*	33	0.46	3.94	26.00	1.26
B41H02, 100-102	413.37	15251160	*G. subquadratus*	30	0.34	3.87	25.79	1.28
B41H02, 110-112	413.47	15256938	*G. subquadratus*	32	0.33	3.92	25.93	1.27
B41H02, 120-132	413.57	15262716	*G. subquadratus*	24	0.27	3.74	25.41	1.25
B41H02, 140-142	413.77	15274271	*G. subquadratus*	27	0.24	4.26	26.86	1.20
B41H03, 0-2	413.87	15280049	*G. subquadratus*	25	0.34	4.02	26.22	1.28
B41H03, 20-22	414.07	15290203	*G. subquadratus*	24	0.29	4.24	26.80	1.29
B41H03, 30-32	414.17	15294537	*G. subquadratus*	35	0.37	5.33	29.35	1.16
B41H03, 40-42	414.27	15298870	*G. subquadratus*	31	0.34	3.93	25.95	1.25
B41H03, 50-52	414.37	15303203	*G. subquadratus*	28	0.31	4.00	26.14	1.24
B41H03, 80-82	414.67	15316203	*G. subquadratus*	35	0.41	3.92	25.93	1.24
B41H03, 90-92	414.77	15320537	*G. subquadratus*	29	0.23	3.76	25.48	1.26
B41H03, 100-102	414.87	15325000	*G. subquadratus*	30	0.35	4.06	26.32	1.33
B41H03, 110-112	414.97	15327656	*G. subquadratus*	28	0.31	3.84	25.69	1.28
B41H03, 120-132	415.07	15330394	*G. subquadratus*	25	0.33	3.92	25.92	1.26
B41H03, 140-142	415.27	15335870	*G. subquadratus*	35	0.26	3.87	25.78	1.29
B41H04, 0-2	415.37	15338608	*G. subquadratus*	35	0.39	3.98	26.11	1.31
B41H04, 10-12	415.47	15341346	*G. subquadratus*	34	0.42	3.93	25.96	1.30
B41H04, 20-22	415.57	15344085	*G. subquadratus*	30	0.41	3.91	25.91	1.30
B41H04, 50-52	415.87	15352299	*G. subquadratus*	30	0.44	3.80	25.59	1.28

Core, section, interval (cm)	Depth (mcd)	Age (Ma)	Species	Spec no.	Total (mg)	Mg/Ca	Temp.	Sr/Ca
B41H04, 60-62	415.97	15355037	*G. subquadratus*	32	0.46	3.61	25.00	1.28
B41H04, 70-72	416.07	15357775	*G. subquadratus*	33	0.46	3.74	25.42	1.29
B41H04, 80-82	416.17	15360513	*G. subquadratus*	27	0.53	3.84	25.69	1.29
B41H04, 90-92	416.27	15363251	*G. subquadratus*	34	0.60	3.72	25.35	n.d.
B41H04, 100-102	416.37	15365989	*G. subquadratus*	33	0.36	4.02	26.20	1.31
B41H04, 110-112	416.47	15368727	*G. subquadratus*	35	0.59	3.89	25.85	1.21
B41H04, 110-112	416.47	15368727	*G. subquadratus*	30	0.34	3.66	25.16	1.27
B41H04, 120-122	416.57	15371465	*G. subquadratus*	29	0.16	3.96	26.05	1.30
B41H04, 140-142	416.77	15376942	*G. subquadratus*	34	0.32	3.77	25.50	1.30
B41H05, 0-2	416.87	15379680	*G. subquadratus*	30	0.47	3.67	25.21	1.34
B41H05, 10-12	416.97	15382418	*G. subquadratus*	34	0.40	3.68	25.22	1.25
B41H05, 50-62	417.37	15393370	*G. subquadratus*	32	0.40	3.62	25.03	1.27
B41H06, 20-42	418.57	15426227	*G. subquadratus*	33	0.43	3.70	25.28	1.24
C43H01, 130-142	418.95	15435130	*G. subquadratus*	37	0.38	3.82	25.66	1.22
C43H02, 110-122	420.25	15488781	*G. subquadratus*	29	0.30	3.91	25.91	1.23
C43H03, 10-22	420.76	15509829	*G. subquadratus*	35	0.36	3.94	25.97	1.20
C43H03, 80-92	421.46	15526760	*G. subquadratus*	27	0.28	4.21	26.71	1.26
C43H04, 0-12	422.17	15539149	*G. subquadratus*	23	0.29	4.24	26.81	1.25
C43H04, 80-92	422.97	15553109	*G. subquadratus*	36	0.37	3.87	25.79	1.27
C41H04, 30-32	406.09	14964443	*D. altispira*	17	0.181	2.95	22.77	1.10
B41H01, 20-22	411.07	15150949	*D. altispira*	18	0.160	3.18	23.61	1.17
B41H03, 120-122	415.07	15330394	*D. altispira*	26	0.517	3.21	23.71	1.13
B41H03, 130-132	415.17	15333132	*D. altispira*	20	0.282	3.06	23.17	1.17
B41H04, 30-32	415.67	15346823	*D. altispira*	19	0.305	2.88	22.49	n.d.
B41H04, 110-112	416.47	15368727	*D. altispira*	25	0.214	3.14	23.46	1.17
C43H01, 130-132	418.95	15435130	*D. altispira*	24	0.248	1.40	14.49	n.d.
C43H02, 110-112	420.25	15488781	*D. altispira*	21	0.256	3.22	23.75	n.d.
C43H03, 10-12	420.76	15509829	*D. altispira*	21	0.262	3.03	23.06	1.10
C43H03, 80-82	421.46	15526760	*D. altispira*	33	0.305	3.20	23.68	1.16
C41H04, 30-32	406.09	14964443	*D. venezuelana*	18	0.268	2.66	21.62	1.13
B41H01, 20-22	411.07	15150949	*D. venezuelana*	21	0.320	3.61	25.02	1.04
B41H03, 120-122	415.07	15330394	*D. venezuelana*	21	0.236	2.81	22.25	1.16
B41H03, 130-132	415.17	15333132	*D. venezuelana*	24	0.419	2.75	21.99	1.20
B41H04, 30-32	415.67	15346823	*D. venezuelana*	30	0.415	2.92	22.64	1.16
B41H04, 110-112	416.47	15368727	*D. venezuelana*	33	0.291	3.75	25.44	n.d.
B41H05, 50-52	417.37	15393370	*D. venezuelana*	30	0.330	2.77	22.07	1.12
B41H06, 20-22	418.57	15426227	*D. venezuelana*	26	0.494	4.35	27.09	n.d.
C43H01, 130-132	418.95	15435130	*D. venezuelana*	27	0.428	4.15	26.56	n.d.
C43H02, 110-112	420.25	15488781	*D. venezuelana*	28	0.399	3.70	25.28	n.d.
C43H03, 10-12	420.76	15509829	*D. venezuelana*	32	0.342	3.10	23.31	1.13
C43H03, 80-82	421.46	15526760	*D. venezuelana*	28	0.264	3.18	23.61	1.14

TABLE 4: IODP Site U1338 planktonic foraminiferal trace metal data. MCD = Metres composite depth.

Core, section, interval (cm)	Depth (mcd)	Age (Ma)	Species	Mg/Ca	Sr/Ca	Fe/Ca	Al/Ca	Mn/Ca	Fe/Mg
C-36H-03, 20-22	353.04	13370040	*G. quadrilobatus*	2.76	1.23	0.17	0.23	1.25	0.06
C-36H-03, 80-82	353.64	13384816	*G. quadrilobatus*	2.48	1.29	0.19	0.56	1.11	0.08
C-36H-03, 140-142	354.24	13399411	*G. quadrilobatus*	2.95	1.33	0.13	0.62	0.93	0.04
B-36H-05, 0-2	359.94	13550431	*G. quadrilobatus*	3.48	1.26	0.59	0.25	0.90	0.17
B-36H-05, 70-92	360.64	13572175	*G. quadrilobatus*	2.84	1.25	0.16	0.05	1.22	0.06
B-36H-05, 130-132	361.24	13585765	*G. quadrilobatus*	2.99	1.22	0.22	0.09	1.36	0.08
B-36H-06, 40-42	361.84	13605822	*G. quadrilobatus*	2.88	1.24	0.19	0.19	1.20	0.07
C-37H-01, 90-92	361.87	13607017	*G. quadrilobatus*	2.99	1.28	0.28	0.12	0.97	0.09
C-37H-02, 40-42	362.87	13643672	*G. quadrilobatus*	3.09	1.22	0.20	0.17	1.25	0.07
C-37H-02, 140-142	363.87	13672872	*G. quadrilobatus*	2.91	1.17	0.24	0.14	1.54	0.08
C-37H-03, 50-52	364.47	13690392	*G. quadrilobatus*	3.11	1.22	0.19	0.13	1.18	0.06
C-37H-04, 10-12	365.58	13717736	*G. quadrilobatus*	3.06	1.22	0.27	0.31	1.22	0.09
C-37H-04, 60-72	366.08	13727337	*G. quadrilobatus*	3.00	1.28	0.27	0.46	1.05	0.09
C-37H-05, 0-2	366.98	13744620	*G. quadrilobatus*	3.28	1.26	0.18	0.18	1.11	0.05
B-37H-02, 130-132	367.18	13748537	*G. quadrilobatus*	3.38	0.94	0.55	0.62	0.58	0.07
B-37H-03, 30-42	367.68	13758139	*G. quadrilobatus*	3.65	1.32	0.89	2.68	0.30	0.21
B-37H-03, 80-82	368.18	13768196	*G. quadrilobatus*	3.75	1.25	0.47	2.07	0.52	0.11
B-37H-03, 120-122	368.58	13776396	*G. quadrilobatus*	3.45	1.36	0.23	2.02	0.40	0.06
B-37H-04, 20-22	369.08	13786646	*G. quadrilobatus*	2.94	1.29	0.29	0.73	0.96	0.10
B-37H-04, 70-72	369.58	13796896	*G. quadrilobatus*	3.17	1.24	0.19	0.26	1.31	0.06
B-37H-04, 140-142	370.28	13811246	*G. quadrilobatus*	3.15	1.24	0.22	0.23	1.07	0.07
B-37H-05, 80-82	371.18	13829696	*G. quadrilobatus*	3.83	1.26	0.02	2.61	0.88	0.00
B-37H-05, 130-142	371.68	13839946	*G. quadrilobatus*	3.54	1.17	0.34	2.03	0.70	0.08
B-37H-06, 20-32	372.08	13854766	*G. quadrilobatus*	3.19	1.26	0.21	0.63	0.92	0.06
C-38H-01, 120-132	372.19	13859828	*G. quadrilobatus*	2.89	1.25	0.21	0.48	0.95	0.07
C-38H-03, 30-42	374.29	13946464	*G. quadrilobatus*	3.26	1.23	0.30	0.41	1.05	0.09
C-38H-04, 140-142	376.89	14025943	*G. quadrilobatus*	3.30	1.27	0.36	0.43	0.94	0.11
C-38H-05, 30-32	377.29	14037997	*G. quadrilobatus*	3.14	1.27	0.47	0.76	0.91	0.14
B-38H-02, 70-92	377.69	14065914	*G. quadrilobatus*	3.35	1.21	0.33	0.49	0.69	0.10
B-38H-02, 130-142	378.58	14083494	*G. quadrilobatus*	3.09	1.25	0.19	0.10	0.96	0.06
B-38H-03, 50-62	379.28	14108000	*G. quadrilobatus*	3.09	1.26	0.33	0.03	0.96	0.11
B-38H-03, 100-102	379.78	14123667	*G. quadrilobatus*	3.41	1.39	1.29	4.94	0.10	0.27
B-38H-03, 140-142	380.18	14136126	*G. quadrilobatus*	3.02	1.30	0.36	0.44	1.00	0.12
B-38H-04, 40-52	380.68	14153615	*G. quadrilobatus*	3.03	1.23	0.28	0.25	1.00	0.09
B-38H-04,120-142	381.48	14191067	*G. quadrilobatus*	3.17	1.25	0.20	0.15	1.00	0.06
B-38H-05, 40-52	382.18	14216035	*G. quadrilobatus*	3.73	1.22	0.24	0.04	1.18	0.07
C-39H-02, 0-12	382.5	14228518	*G. quadrilobatus*	3.28	1.28	0.40	0.47	0.88	0.12
C-39H-02, 60-72	383.1	14302674	*G. quadrilobatus*	3.13	1.17	0.20	0.13	1.00	0.06
C-39H-02, 140-142	383.9	14283341	*G. quadrilobatus*	3.08	1.21	0.21	0.20	0.90	0.07
C-39H-03, 130-142	385.3	14332743	*G. quadrilobatus*	3.73	1.32	1.22	1.13	0.42	0.30

Core, section, interval (cm)	Depth (mcd)	Age (Ma)	Species	Mg/Ca	Sr/Ca	Fe/Ca	Al/Ca	Mn/Ca	Fe/Mg
C-39H-04, 50-72	386	14359499	*G. quadrilobatus*	3.62	1.21	0.36	0.35	0.78	0.10
C-39H-04, 120-142	386.7	14386254	*G. quadrilobatus*	3.12	1.24	0.51	0.52	0.55	0.16
C-39H-05, 90-112	387.9	14432243	*G. quadrilobatus*	3.22	1.22	0.24	0.35	0.76	0.08
C-39H-06, 0-22	388.5	14447409	*G. quadrilobatus*	3.00	1.22	0.19	0.43	0.64	0.06
C-39H-06, 80-102	389.3	14465591	*G. quadrilobatus*	3.15	1.22	0.18	0.08	0.93	0.06
C-39H-06, 140-142	389.9	14476955	*G. quadrilobatus*	3.18	1.29	0.29	0.33	0.64	0.09
C-39H-07, 50-62	390.5	14490591	*G. quadrilobatus*	3.21	1.24	0.29	0.25	0.60	0.09
C-40H-01, 20-32	391.08	14503773	*G. quadrilobatus*	3.11	1.23	0.04	0.39	0.63	0.01
C-40H-01, 100-112	391.88	14524720	*G. quadrilobatus*	3.33	1.20	0.31	0.25	0.87	0.09
C-40H-01, 130-142	392.18	14532720	*G. quadrilobatus*	2.99	1.19	0.18	0.10	0.83	0.06
C-40H-02, 60-72	392.98	14553825	*G. quadrilobatus*	3.02	1.20	0.18	0.12	0.69	0.06
C-40H-02, 120-132	393.58	14568921	*G. quadrilobatus*	3.65	1.25	0.18	0.13	0.63	0.05
C-40H-03, 40-52	394.28	14586534	*G. quadrilobatus*	3.25	1.19	0.19	0.08	0.60	0.06
C-40H-03, 100-112	391.88	14606477	*G. quadrilobatus*	2.88	1.22	0.16	0.15	0.56	0.06
C-40H-04, 0-12	394.88	14623884	*G. quadrilobatus*	3.07	1.20	0.18	0.13	0.59	0.06
C-40H-04, 70-82	395.38	14648255	*G. quadrilobatus*	2.99	1.21	0.19	0.11	0.69	0.07
C-40H-06, 0-12	398.38	14728329	*G. quadrilobatus*	3.10	1.20	0.03	0.24	0.01	0.01
C-40H-06, 80-92	399.18	14756181	*G. quadrilobatus*	3.06	1.20	0.16	0.24	0.53	0.05
B-40H-01, 0-22	400.1	14792874	*G. quadrilobatus*	3.18	1.22	0.16	0.14	0.66	0.05
B-40H-01, 100-112	401.1	14827216	*G. quadrilobatus*	3.81	1.20	0.20	0.08	0.75	0.05
C-41 H-01, 90-102	402.19	14854735	*G. quadrilobatus*	3.24	1.21	0.23	0.19	0.58	0.07
C-41H-02, 50-52	403.29	14879071	*G. quadrilobatus*	3.20	1.28	0.36	0.92	0.60	0.10
C-41H-03, 80-92	406.59	14983652	*G. quadrilobatus*	n.d.	1.23	0.40	1.23	0.51	0.00
C-41H-04, 20-32	405.99	14964443	*G. quadrilobatus*	3.57	1.18	0.25	0.10	0.59	0.07
C-41H-04, 80-92	406.59	14983652	*G. quadrilobatus*	3.14	1.20	0.19	0.15	0.59	0.06
C-41H-04, 130-142	407.09	15002860	*G. quadrilobatus*	3.06	1.24	0.26	0.23	0.64	0.09
C-41H-05, 40-52	407.69	15025910	*G. quadrilobatus*	3.13	1.21	0.17	0.17	0.61	0.06
C-41H-05, 90-102	408.19	15041276	*G. quadrilobatus*	3.19	1.35	0.65	2.12	0.30	0.17
C-40H-05, 0-12	396.88	14679588	*G. subquadratus*	3.48	1.25	0.31	0.35	0.76	0.09
C-40H-05, 50-62	397.38	14693514	*G. subquadratus*	3.72	1.24	0.19	0.06	0.83	0.05
C-40H-05, 100-112	397.88	14710921	*G. subquadratus*	3.45	1.22	0.22	0.19	0.99	0.06
B-40H-01, 0-22	400.1	14789058	*G. subquadratus*	3.86	1.25	0.25	0.25	0.94	0.07
B-40H-02, 20-32	401.8	14845973	*G. subquadratus*	3.63	1.22	0.28	0.53	0.83	0.08
C-41H-01, 90-102	402.19	14854735	*G. subquadratus*	3.62	1.21	0.18	0.02	0.84	0.05
C-41H-02, 40-52	403.19	14879071	*G. subquadratus*	3.64	1.21	0.19	0.11	0.84	0.05
C-41H-02, 100-122	403.79	14892345	*G. subquadratus*	3.96	1.23	0.23	0.15	0.96	0.06
C-41H-03, 0-12	404.19	14898982	*G. subquadratus*	3.75	1.21	0.25	0.08	1.08	0.07
C-41H-04, 20-32	405.99	14960602	*G. subquadratus*	3.68	1.21	0.27	0.29	0.71	0.07
C-41H-04, 80-92	406.59	14983652	*G. subquadratus*	3.78	1.24	0.19	0.14	0.83	0.05
C-41H-05, 30-42	407.59	15022068	*G. subquadratus*	3.58	1.23	0.24	0.26	0.90	0.07
C-41H-07, 10-22	410.41	15129308	*G. subquadratus*	3.77	1.25	0.19	0.33	0.96	0.05
B-41H-01, 10-22	410.97	15147645	*G. subquadratus*	3.91	1.28	0.22	0.20	0.77	0.06
B-41H-02, 120-132	413.57	15262716	*G. subquadratus*	3.74	1.25	0.17	0.10	0.89	0.05
B-41H-03, 120-132	415.07	15330394	*G. subquadratus*	3.92	1.26	0.18	0.10	0.78	0.05

Core, section, interval (cm)	Depth (mcd)	Age (Ma)	Species	Mg/Ca	Sr/Ca	Fe/Ca	Al/Ca	Mn/Ca	Fe/Mg
B-41H-04, 110-112	416.47	15368727	*G. subquadratus*	3.72	1.24	0.15	0.06	0.97	0.04
B-41H-04, 110-112	416.47	15368727	*G. subquadratus*	3.66	1.27	0.14	0.05	0.90	0.04
B-41H-05, 50-62	417.37	15393370	*G. subquadratus*	3.62	1.27	0.16	0.13	0.72	0.05
B-41H-06, 20-42	418.57	15426227	*G. subquadratus*	3.70	1.24	0.15	0.06	0.77	0.04
C-43H-01, 130-142	418.95	15435130	*G. subquadratus*	3.82	1.22	0.14	0.06	0.99	0.04
C-43H-02, 110-122	420.25	15488781	*G. subquadratus*	3.91	1.23	0.16	0.07	0.98	0.04
C-43H-03, 10-22	420.76	15509829	*G. subquadratus*	3.94	1.20	0.18	0.06	1.01	0.05
C-43H-03, 80-92	421.46	15526760	*G. subquadratus*	4.21	1.26	0.20	0.49	0.90	0.05
C-43H-04, 0-12	422.17	15539149	*G. subquadratus*	4.24	1.25	0.40	0.05	0.91	0.09
C-43H-04, 80-92	422.97	15553109	*G. subquadratus*	3.87	1.27	0.29	0.71	0.98	0.07

TABLE 5: *Paragloborotalia siakensis* coiling data from IODP Site U1338.

Core, section, interval (cm)	Depth (mcd)	Age (ma)	*Paragloborotalia siakensis*		Total	% sinistral
			sinistral	dextral		
B-35H-5, 50-52	350.68	13303336	56	1	57	**98**
B-35H-5, 60-62	350.78	13305965	51	0	51	**100**
B-35H-5, 70-72	350.88	13308595	72	1	73	**99**
B-35H-5, 80-82	350.98	13311225	195	3	198	**98**
B-35H-5, 90-92	351.08	13313855	50	0	50	**100**
B-35H-5, 110-112	351.28	13319114	80	0	80	**100**
B-35H-5, 120-122	351.38	13321744	56	1	57	**98**
B-35H-5, 130-132	351.48	13324374	31	2	33	**94**
B-35H-5, 140-142	351.58	13327003	17	0	17	**100**
C-36H-3, 0-2	352.84	13364040	64	0	64	**100**
C-36H-3, 10-12	352.94	13367040	134	1	135	**99**
C-36H-3, 20-22	353.04	13370040	98	3	101	**97**
C-36H-3, 30-32	353.14	13372654	261	7	268	**97**
C-36H-3, 40-42	353.24	13375086	60	5	65	**92**
C-36H-3, 50-52	353.34	13377519	122	2	124	**98**
C-36H-3, 60-62	353.44	13379951	165	2	167	**99**
C-36H-3, 70-72	353.54	13382384	30	0	30	**100**
C-36H-3, 80-82	353.64	13384816	30	0	30	**100**
C-36H-3, 90-92	353.74	13387249	29	1	30	**97**
C-36H-3, 100-102	353.84	13389681	29	1	30	**97**
C-36H-3, 110-112	353.94	13392114	30	0	30	**100**
C-36H-3, 120-122	354.04	13394546	29	1	30	**97**
C-36H-3, 130-132	354.14	13396978	30	0	30	**100**
C-36H-3, 140-142	354.24	13399411	29	1	30	**97**
C-36H-4, 0-2	354.34	13401843	37	1	38	**97**
C-36H-4, 10-12	354.44	13404276	19	2	21	**90**
C-36H-4, 20-22	354.54	13406708	16	0	16	**100**
C-36H-4, 30-32	354.64	13409141	23	1	24	**96**
C-36H-4, 40-42	354.74	13411573	11	0	11	**100**
C-36H-4, 50-52	354.84	13414005	5	0	5	**100**
C-36H-4, 60-62	354.94	13416438	5	0	5	**100**
B-36H-1, 100-102	354.94	13416414	18	1	19	**95**
B-36H-1, 110-112	355.04	13418846	1	0	1	**100**
B-36H-1, 120-122	355.14	13421278	9	0	9	**100**
B-36H-1, 130-132	355.24	13423711	12	0	12	**100**
B-36H-1, 140-142	355.34	13426191	17	1	18	**94**
B-36H-2, 0-2	355.44	13428724	10	0	10	**100**
B-36H-2, 10-12	355.54	13431257	1	0	1	**100**
B-36H-2, 20-22	355.64	13433791	8	0	8	**100**
B-36H-2, 30-32	355.74	13436324	9	0	9	**100**
B-36H-2, 40-42	355.84	13438857	79	0	79	**100**

Core, section, interval (cm)	Depth (mcd)	Age (ma)	*Paragloborotalia siakensis*		Total	% sinistral
			sinistral	dextral		
B-36H-2, 50-52	355.94	13441391	46	1	47	**98**
B-36H-2, 60-62	356.04	13443924	2	0	2	**100**
B-36H-2, 70-72	356.14	13446457	4	0	4	**100**
B-36H-2, 80-82	356.24	13448991	10	0	10	**100**
B-36H-2, 90-92	356.34	13451524	2	0	2	**100**
B-36H-2, 100-102	356.44	13454057	8	1	9	**89**
B-36H-2, 110-112	356.54	13456591	136	1	137	**99**
B-36H-2, 120-122	356.64	13459124	41	1	42	**98**
B-36H-2, 130-132	356.74	13461657	85	2	87	**98**
B-36H-2, 140-142	356.84	13464191	10	1	11	**91**
B-36H-3, 0-2	356.94	13466724	56	3	59	**95**
B-36H-3, 10-12	357.04	13469257	76	5	81	**94**
B-36H-3, 20-22	357.14	13471791	102	5	107	**95**
B-36H-3, 30-32	357.24	13474324	13	0	13	**100**
B-36H-3, 40-42	357.34	13476857	3	0	3	**100**
B-36H-3, 50-52	357.44	13479391	6	0	6	**100**
B-36H-3, 60-62	357.54	13481924	2	0	2	**100**
B-36H-3, 70-72	357.64	13484457	54	4	58	**93**
B-36H-3, 80-82	357.74	13486991	59	3	62	**95**
B-36H-3, 90-92	357.84	13489524	28	1	29	**97**
B-36H-3, 100-102	357.94	13492057	6	1	7	**86**
B-36H-3, 110-112	358.04	13494591	30	1	31	**97**
B-36H-3, 120-122	358.14	13497124	46	2	48	**96**
B-36H-3, 130-132	358.24	13499657	10	0	10	**100**
B-36H-3, 140-142	358.34	13502446	1	0	1	**100**
B-36H-4, 0-2	358.44	13505523	8	0	8	**100**
B-36H-4, 10-12	358.54	13508600	12	0	12	**100**
B-36H-4, 20-22	358.64	13511677	11	3	14	**79**
B-36H-4, 30-32	358.74	13514754	4	0	4	**100**
B-36H-4, 40-42	358.84	13517831	10	0	10	**100**
B-36H-4, 50-52	358.94	13520908	21	0	21	**100**
B-36H-4, 60-62	359.04	13523985	7	0	7	**100**
B-36H-4, 80-82	359.24	13530138	13	1	14	**93**
B-36H-4, 90-92	359.34	13533215	9	0	9	**100**
B-36H-4, 100-102	359.44	13536292	38	2	40	**95**
B-36H-4, 110-112	359.54	13539369	19	0	19	**100**
B-36H-4, 120-122	359.64	13542277	5	0	5	**100**
B-36H-4, 130-132	359.74	13544995	21	0	21	**100**
B-36H-4, 140-142	359.84	13547713	4	0	4	**100**
B-36H-5, 0-2	359.94	13550431	38	0	38	**100**
B-36H-5, 10-12	360.04	13553149	2	0	2	**100**
B-36H-5, 20-22	360.14	13555867	2	2	4	**50**
B-36H-5, 30-32	360.24	13558585	2	1	3	**67**

Core, section, interval (cm)	Depth (mcd)	Age (ma)	*Paragloborotalia siakensis*		Total	% sinistral
			sinistral	dextral		
B-36H-5, 50-52	360.44	13564021	12	0	12	**100**
B-36H-5, 60-62	360.54	13566739	7	1	8	**88**
B-36H-5, 70-72	360.64	13569457	9	1	10	**90**
B-36H-5, 80-82	360.74	13572175	19	0	19	**100**
B-36H-5, 90-92	360.84	13574893	14	0	14	**100**
B-36H-5, 100-102	360.94	13577611	24	0	24	**100**
B-36H-5, 110-112	361.04	13580329	11	0	11	**100**
B-36H-5, 120-122	361.14	13583047	7	2	9	**78**
B-36H-5, 130-132	361.24	13585765	90	3	93	**97**
B-36H-5, 140-142	361.34	13588483	60	4	64	**94**
B-36H-5, 150-152	361.44	13591201	0	0	0	
B-36H-6, 0-2	361.44	13591201	11	2	13	**85**
B-36H-6, 10-12	361.54	13594000	4	0	4	**100**
B-36H-6, 20-22	361.64	13597861	1	0	1	**100**
B-36H-6, 30-32	361.74	13601842	46	2	48	**96**
C-37H-1, 80-82	361.77	13603036	20	0	20	**100**
B-36H-6, 40-42	361.84	13605822	79	7	86	**92**
C-37H-1, 90-92	361.87	13607017	28	3	31	**90**
C-37H-1, 100-102	361.97	13610997	2	0	2	**100**
C-37H-1, 110-112	362.07	13614978	3	0	3	**100**
C-37H-1, 130-132	362.27	13622939	24	2	26	**92**
C-37H-1, 140-142	362.37	13626919	4	0	4	**100**
C-37H-2, 10-12	362.57	13635000	2	0	2	**100**
C-37H-2, 20-22	362.67	13637832	2	0	2	**100**
C-37H-2, 30-32	362.77	13640752	1	0	1	**100**
C-37H-2, 40-42	362.87	13643672	17	5	22	**77**
C-37H-2, 50-52	362.97	13646592	16	2	18	**89**
C-37H-2, 60-62	363.07	13649512	13	1	14	**93**
C-37H-2, 70-72	363.17	13652432	10	2	12	**83**
C-37H-2, 80-82	363.27	13655352	9	1	10	**90**
C-37H-2, 90-92	363.37	13658272	6	1	7	**86**
C-37H-2, 100-102	363.47	13661192	4	0	4	**100**
C-37H-2, 110-112	363.57	13664112	10	1	11	**91**
C-37H-2, 120-122	363.67	13667032	2	1	3	**67**
C-37H-2, 130-132	363.77	13669952	6	0	6	**100**
C-37H-2, 140-142	363.87	13672872	55	5	60	**92**
C-37H-3, 0-2	363.97	13675792	6	1	7	**86**
C-37H-3, 10-12	364.07	13678712	11	7	18	**61**
C-37H-3, 20-22	364.17	13681632	4	5	9	**44**
C-37H-3, 30-32	364.27	13684552	4	5	9	**44**
C-37H-3, 40-42	364.37	13687472	19	3	22	**86**
C-37H-3, 50-52	364.47	13690392	27	1	28	**96**
C-37H-3, 60-62	364.57	13693312	21	4	25	**84**

Core, section, interval (cm)	Depth (mcd)	Age (ma)	*Paragloborotalia siakensis*		Total	% sinistral
			sinistral	dextral		
C-37H-3, 70-72	364.67	13696232	3	0	3	**100**
C-37H-3, 80-82	364.77	13699152	15	3	18	**83**
C-37H-3, 90-92	364.87	13702072	6	0	6	**100**
C-37H-3, 100-102	364.97	13704992	14	1	15	**93**
C-37H-3, 110-112	365.07	13708000	65	6	71	**92**
C-37H-3, 120-122	365.17	13709863	20	3	23	**87**
C-37H-3, 130-132	365.27	13711783	6	1	7	**86**
C-37H-3, 140-142	365.37	13713703	14	2	16	**88**
C-37H-4, 0-2	365.48	13715816	6	6	12	**50**
C-37H-4, 10-12	365.58	13717736	6	7	13	**46**
C-37H-4, 20-22	365.68	13719656	34	11	45	**76**
C-37H-4, 30-32	365.78	13721576	22	2	24	**92**
C-37H-4, 40-42	365.88	13723497	24	2	26	**92**
C-37H-4, 50-52	365.98	13725417	44	4	48	**92**
C-37H-4, 60-62	366.08	13727337	27	4	31	**87**
C-37H-4, 70-72	366.18	13729258	12	0	12	**100**
C-37H-4, 80-82	366.28	13731178	10	0	10	**100**
C-37H-4, 90-92	366.38	13733098	50	7	57	**88**
C-37H-4, 100-102	366.48	13735018	110	10	120	**92**
C-37H-4, 110-112	366.58	13736939	40	3	43	**93**
C-37H-4, 120-122	366.68	13738859	85	7	92	**92**
C-37H-4, 130-132	366.78	13740779	51	3	54	**94**
C-37H-4, 140-142	366.88	13742700	24	8	32	**75**
C-37H-5, 0-2	366.98	13744620	27	20	47	**57**
C-37H-5, 10-12	367.08	13746540	49	5	54	**91**
B-37H-2, 110-112	366.98	13744697	45	6	51	**88**
B-37H-2, 120-122	367.08	13746617	77	12	89	**87**
B-37H-2, 130-132	367.18	13748537	116	13	129	**90**
B-37H-2, 140-142	367.28	13750458	22	18	40	**55**
B-37H-2, 150-152	367.33	13751399	13	10	23	**57**
B-37H-3, 0-2	367.38	13752378	14	16	30	**47**
B-37H-3, 10-12	367.48	13754298	1	3	4	**25**
B-37H-3, 20-22	367.58	13756218	6	8	14	**43**
B-37H-3, 30-32	367.68	13758139	20	4	24	**83**
B-37H-3, 40-42	367.78	13760059	184	17	201	**92**
B-37H-3, 50-52	367.88	13762046	51	5	56	**91**
B-37H-3, 60-62	367.98	13764096	28	2	30	**93**
B-37H-3, 70-72	368.08	13766146	28	3	31	**90**
B-37H-3, 80-82	368.18	13768196	6	5	11	**55**
B-37H-3, 90-92	368.28	13770246	0	1	1	**0**
B-37H-3, 100-102	368.38	13772296	33	2	35	**94**
B-37H-3, 110-112	368.48	13774346	120	16	136	**88**
B-37H-3, 120-122	368.58	13776396	123	10	133	**92**

Core, section, interval (cm)	Depth (mcd)	Age (ma)	*Paragloborotalia siakensis*		Total	% sinistral
			sinistral	dextral		
B-37H-3, 130-132	368.68	13778446	29	1	30	**97**
B-37H-3, 140-142	368.78	13780496	10	0	10	**100**
B-37H-4, 0-2	368.88	13782546	8	0	8	**100**
B-37H-4, 10-12	368.98	13784596	117	10	127	**92**
B-37H-4, 20-22	369.08	13786646	27	3	30	**90**
B-37H-4, 30-32	369.18	13788696	41	3	44	**93**
B-37H-4, 40-42	369.28	13790746	7	0	7	**100**
B-37H-4, 50-52	369.38	13792796	130	3	133	**98**
B-37H-4, 60-62	369.48	13794846	29	1	30	**97**
B-37H-4, 70-72	369.58	13796896	82	2	84	**98**
B-37H-4, 80-82	369.68	13798946	6	0	6	**100**
B-37H-4, 90-92	369.78	13800996	22	1	23	**96**
B-37H-4, 100-102	369.88	13803046	6	0	6	**100**
B-37H-4, 110-112	369.98	13805096	79	8	87	**91**
B-37H-4, 120-122	370.08	13807146	29	1	30	**97**
B-37H-4, 130-132	370.18	13809196	40	4	44	**91**
B-37H-4, 140-142	370.28	13811246	10	0	10	**100**
B-37H-5, 40-42	370.78	13821496	1	0	1	**100**
B-37H-5, 60-62	370.98	13825596	2	0	2	**100**
B-37H-5, 100-102	371.38	13833796	28	1	29	**97**
B-37H-5, 110-112	371.48	13835846	10	0	10	**100**
B-37H-5, 120-122	371.58	13837896	49	7	56	**88**
B-37H-5, 130-132	371.68	13839946	31	6	37	**84**
B-37H-5, 140-142	371.78	13841996	2	0	2	**100**
B-37H-6, 0-2	371.88	13845391	36	1	37	**97**
B-37H-6, 10-12	371.98	13850078	16	0	16	**100**
C-38H-1, 120-122	372.19	13859828	10	1	11	**91**
C-38H-1, 140-142	372.39	13869203	20	0	20	**100**
C-38H-2, 0-2	372.49	13873891	3	0	3	**100**
C-38H-2, 20-22	372.69	13883266	1	0	1	**100**
C-38H-2, 40-42	372.89	13893148	2	1	3	**67**
C-38H-2, 120-122	373.69	13924624	11	2	13	**85**
C-38H-3, 0-2	373.99	13935544	1	0	1	**100**
C-38H-3, 30-32	374.29	13946464	3	0	3	**100**
C-38H-4, 20-22	375.69	13995749	3	0	3	**100**
C-38H-5, 10-12	377.09	14031000	4	0	4	**100**
C-38H-5, 50-52	377.49	14045029	1	0	1	**100**
C-38H-5, 70-72	377.69	14052061	2	0	2	**100**
B-38H-2, 120-122	378.48	14079978	8	0	8	**100**
B-38H-2, 140-142	378.68	14087010	1	0	1	**100**
B-38H-3, 90-92	379.68	14120552	1	0	1	**100**
B-38H-3, 110-112	379.88	14126782	7	0	7	**100**
B-38H-4, 0-2	380.28	14139241	9	1	10	**90**

Core, section, interval (cm)	**Depth (mcd)**	**Age (ma)**	***Paragloborotalia siakensis***		**Total**	**% sinistral**
			sinistral	**dextral**		
B-38H-4, 20-22	380.48	14145470	3	0	3	**100**
B-38H-4, 30-32	380.58	14149454	3	0	3	**100**
C-40H-4, 0-2	395.38	14623884	5	0	5	**100**
C-40H-4, 20-22	395.58	14630847	10	1	11	**91**
C-40H-4, 40-42	395.78	14637810	21	4	25	**84**
C-40H-4, 60-62	395.98	14644773	16	2	18	**89**
C-40H-4, 80-82	396.18	14651736	14	2	16	**88**
C-40H-4, 100-102	396.38	14658699	13	4	17	**76**
C-40H-4, 120-122	396.58	14665662	22	2	24	**92**
C-40H-4, 140-142	396.78	14672625	28	5	33	**85**
C-40H-5, 10-12	396.98	14679588	38	2	40	**95**
C-40H-5, 30-32	397.18	14686551	14	1	15	**93**
C-40H-5, 50-52	397.38	14693514	24	0	24	**100**
C-40H-5, 70-72	397.58	14700477	8	0	8	**100**
C-40H-5, 90-92	397.78	14707440	22	2	24	**92**
C-40H-5, 110-112	397.98	14714403	4	1	5	**80**
C-40H-6, 0-2	398.38	14728329	4	0	4	**100**
C-41H-3, 70-72	404.99	14921778	3	0	3	**100**
C-41H-3, 90-92	405.19	14929578	5	1	6	**83**
C-41H-3, 110-112	405.39	14937378	1	0	1	**100**
C-41H-4, 0-2	405.79	14952918	1	0	1	**100**
C-41H-4, 20-22	405.99	14960602	1	0	1	**100**
C-41H-4, 40-42	406.19	14968285	2	2	4	**50**
C-41H-4, 60-62	406.39	14975968	2	1	3	**67**
C-41H-4, 80-82	406.59	14983652	3	0	3	**100**
C-41H-4, 100-102	406.79	14991335	1	0	1	**100**
C-41H-4, 120-122	406.99	14999018	2	0	2	**100**
C-41H-4, 140-142	407.19	15006701	7	0	7	**100**
C-41H-5, 10-12	407.39	15014385	8	0	8	**100**
C-41H-5, 30-32	407.59	15022068	6	0	6	**100**
C-41H-5, 50-52	407.79	15029751	5	0	5	**100**
C-41H-5, 90-92	408.19	15045118	4	1	5	**80**
C-41H-5, 110-112	408.39	15052801	1	0	1	**100**
C-41H-5, 130-132	408.59	15060484	5	0	5	**100**
C-41H-6, 0-2	408.80	15068552	1	0	1	**100**
C-41H-6, 60-62	409.40	15091778	5	1	6	**83**
B-41H-1, 20-22	411.07	15150949	12	0	12	**100**
B-41H-1, 30-32	411.17	15154253	14	3	17	**82**
B-41H-1, 50-52	411.37	15160861	12	2	14	**86**
B-41H-1, 70-72	411.57	15167469	10	1	11	**91**
B-41H-1, 90-92	411.77	15174077	5	0	5	**100**
B-41H-1, 130-132	412.17	15187293	16	2	18	**89**
B-41H-2, 0-2	412.37	15194000	2	0	2	**100**

Core, section, interval (cm)	Depth (mcd)	Age (ma)	*Paragloborotalia siakensis*		Total	% sinistral
			sinistral	dextral		
B-41H-2, 20-22	412.57	15205257	22	5	27	**81**
B-41H-2, 40-42	412.77	15216686	21	3	24	**88**
B-41H-2, 100-102	413.37	15251160	0	2	2	**0**
B-41H-2, 120-122	413.57	15262716	4	1	5	**80**
B-41H-2, 140-142	413.77	15274271	21	9	30	**70**
B-41H-3, 30-32	414.17	15294537	21	5	26	**81**
B-41H-3, 50-52	414.37	15303203	19	1	20	**95**
B-41H-3, 70-72	414.57	15311870	6	2	8	**75**
B-41H-3, 90-92	414.77	15320537	5	2	7	**71**
B-41H-3, 130-132	415.17	15333132	6	1	7	**86**
B-41H-4, 20-22	415.57	15344085	10	1	11	**91**
B-41H-4, 80-82	416.17	15360513	1	0	1	**100**
B-41H-4, 90-92	416.27	15363251	1	0	1	**100**
B-41H-4, 100-102	416.37	15365989	4	1	5	**80**
B-41H-4, 110-112	416.47	15368727	20	25	45	**44**
B-41H-4, 120-122	416.57	15371465	0	1	1	**0**
B-41H-4, 130-132	416.67	15374204	5	8	13	**38**
B-41H-4, 140-142	416.77	15376942	4	2	6	**67**
B-41H-5, 0-2	416.87	15379680	1	1	2	**50**
B-41H-5, 20-22	417.07	15385156	2	1	3	**67**
B-41H-5, 60-62	417.47	15396108	2	0	2	**100**
B-41H-5, 80-82	417.67	15401585	6	10	16	**38**
B-41H-5, 100-102	417.87	15407061	5	7	12	**42**
B-41H-5, 120-122	418.07	15412537	6	1	7	**86**
B-41H-6, 10-12	418.47	15423489	1	0	1	**100**
C-41H-6, 30-32	418.67	15428965	7	1	8	**88**
C-41H-6, 40-42	418.77	15431704	3	5	8	**38**
C-41H-6, 60-62	418.97	15437180	2	1	3	**67**
C-41H-6, 80-82	419.17	15444003	9	5	14	**64**
C-43H-1, 140-142	419.05	15439257	2	0	2	**100**
C-43H-2, 10-12	419.25	15447511	0	1	1	**0**
C-43H-2, 30-32	419.45	15455765	1	0	1	**100**
C-43H-2, 50-52	419.65	15464019	1	4	5	**20**
C-43H-2, 70-72	419.85	15472273	1	0	1	**100**
C-43H-2, 90-92	420.05	15480527	0	1	1	**0**
C-43H-2, 110-112	420.25	15488781	1	1	2	**50**
C-43H-2, 130-132	420.45	15497035	5	8	13	**38**
C-43H-3, 0-2	420.66	15505702	10	12	22	**45**
C-43H-3, 20-22	420.86	15513956	0	1	1	**0**
C-43H-3, 40-42	421.06	15519780	2	2	4	**50**
C-43H-3, 60-62	421.26	15523270	2	5	7	**29**
C-43H-3, 80-82	421.46	15526760	3	1	4	**75**
C-43H-3, 100-102	421.66	15530250	5	10	15	**33**

Core, section, interval (cm)	Depth (mcd)	Age (ma)	*Paragloborotalia siakensis*		Total	% sinistral
			sinistral	dextral		
C-43H-3, 120-122	421.86	15533740	8	12	20	**40**
C-43H-3, 140-142	422.06	15537230	6	9	15	**40**
C-43H-4, 10-12	422.27	15540894	10	14	24	**42**
C-42H-2, 90-92	423.54	15563020	5	6	11	**45**
C-42H-2, 110-112	423.74	15566510	6	6	10	**60**
C-42H-2, 130-132	423.94	15570000	3	2	5	**60**

APPENDIX B: SUPPLEMENTARY FIGURES

APPENDIX 1: IODP Site U1338 and ODP Site 1146 location map

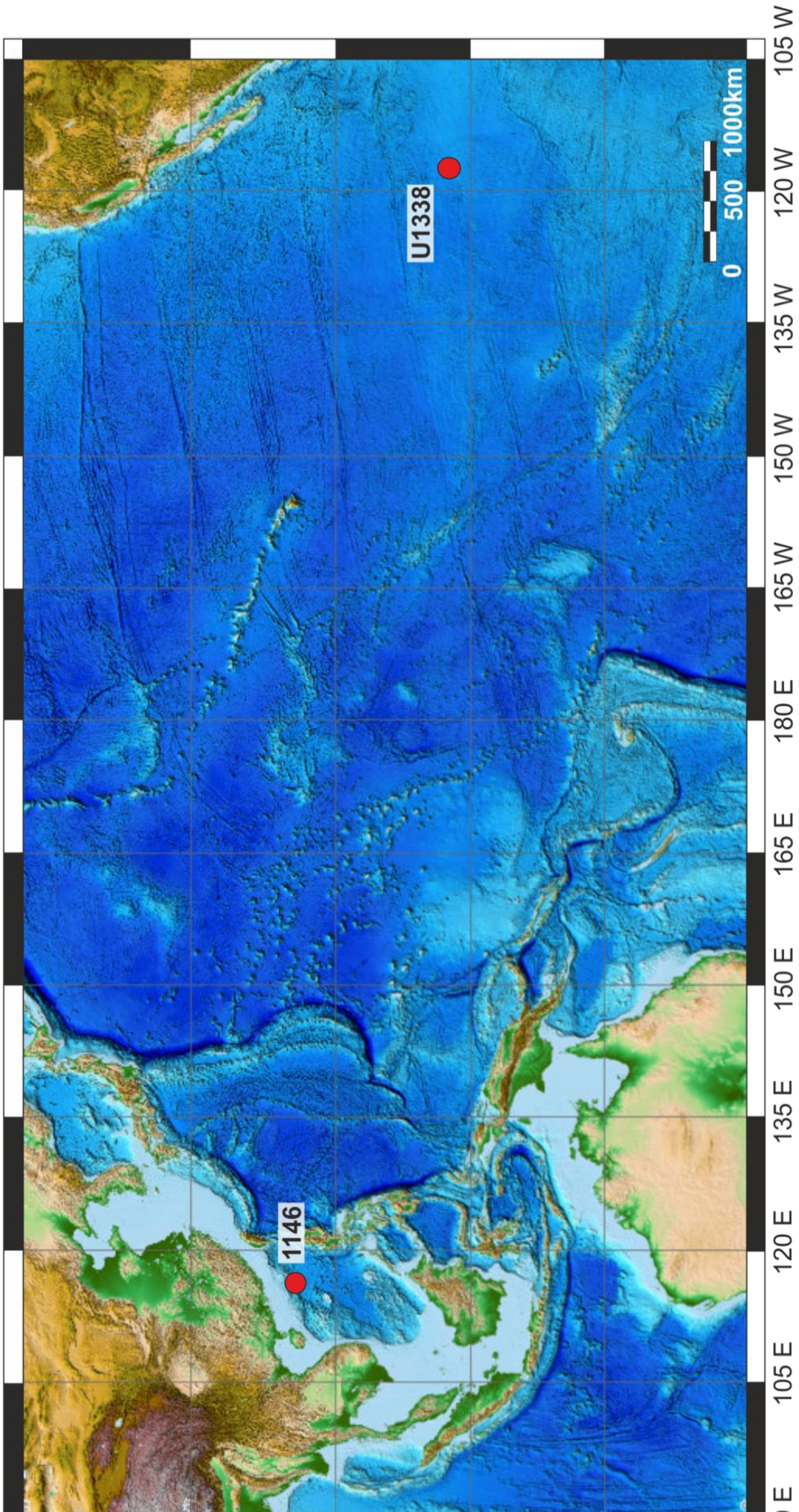

APPENDIX 2: IODP Site U1338 planktonic foraminiferal trace metal data

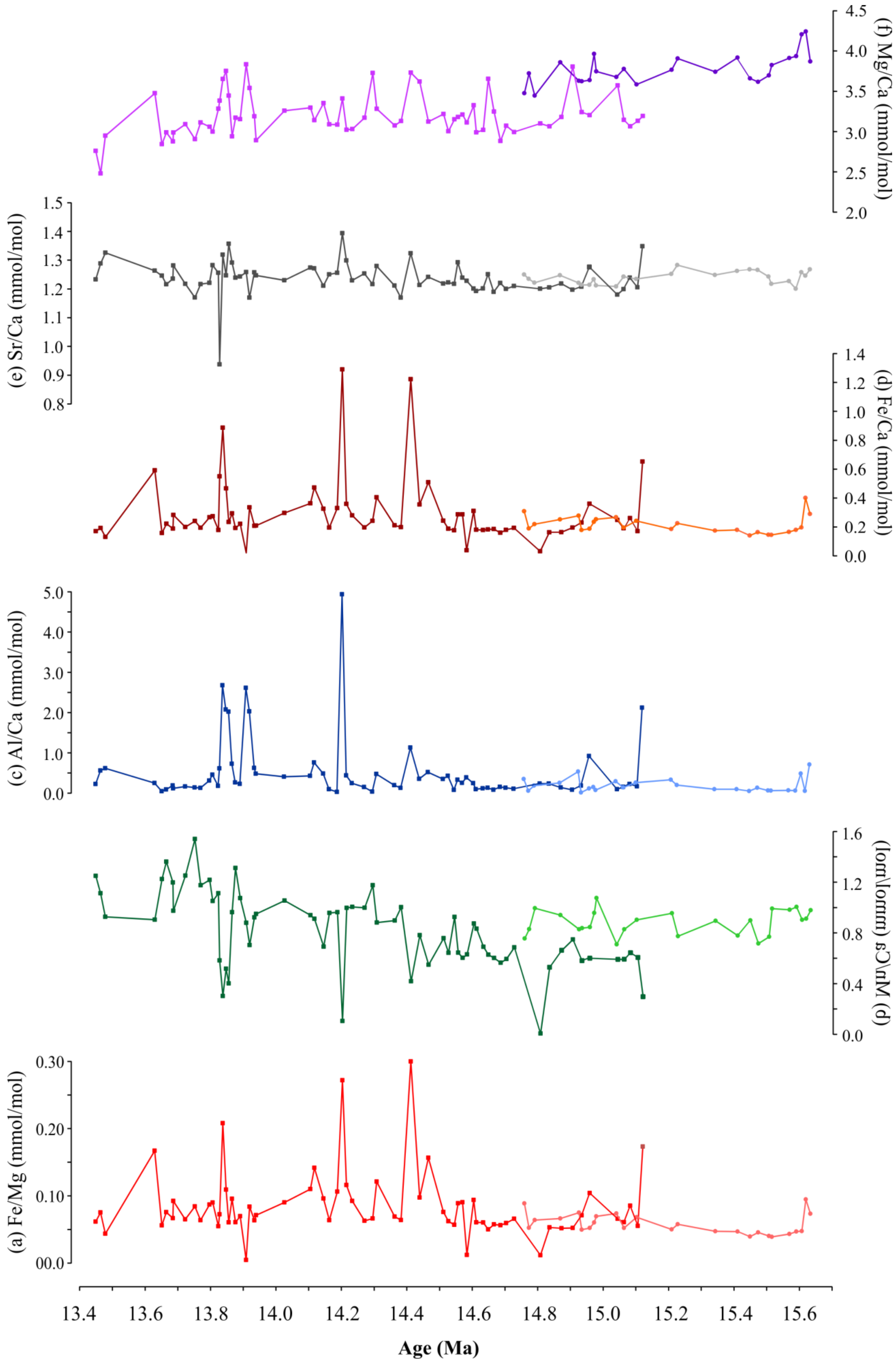

APPENDIX 3: IODP Site U1338 unedited *P. siakensis* coiling direction data

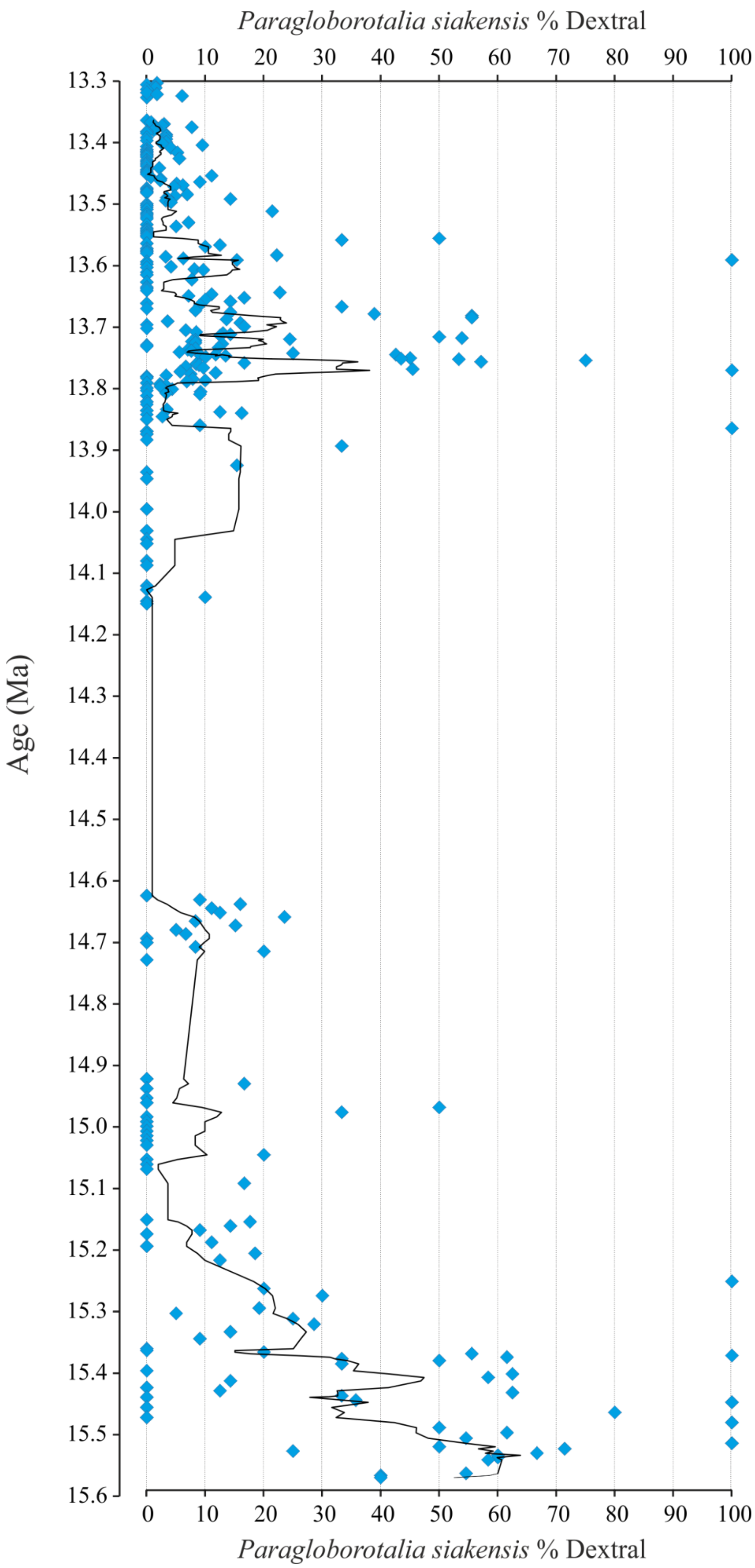

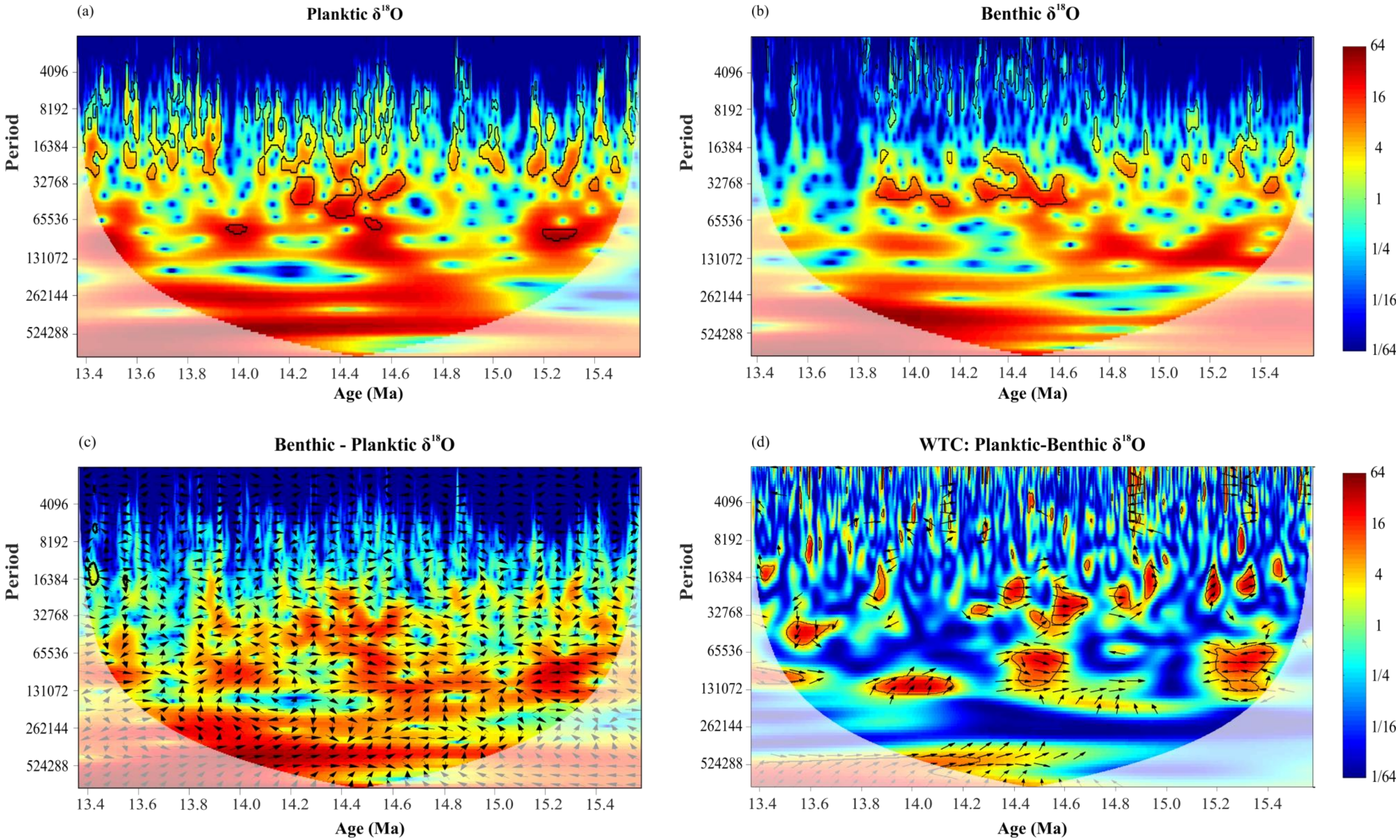

Appendix 4: IODP Site U1338 Wavelet Analyses of planktonic and benthic $\delta^{18}O$ data.

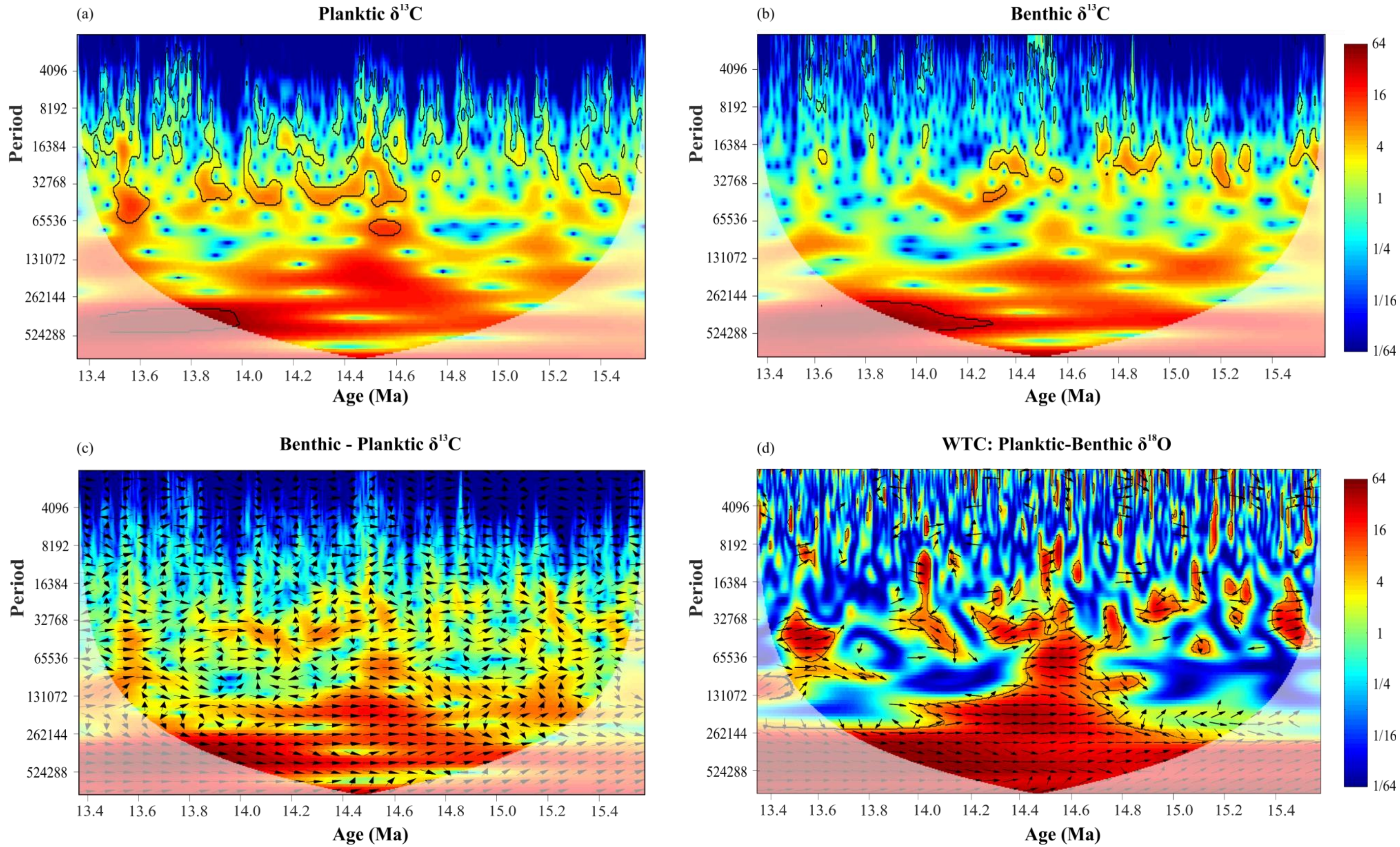

APPENDIX 5: IODP Site U1338 Wavelet Analyses of planktonic and benthic $\delta^{13}C$ data.

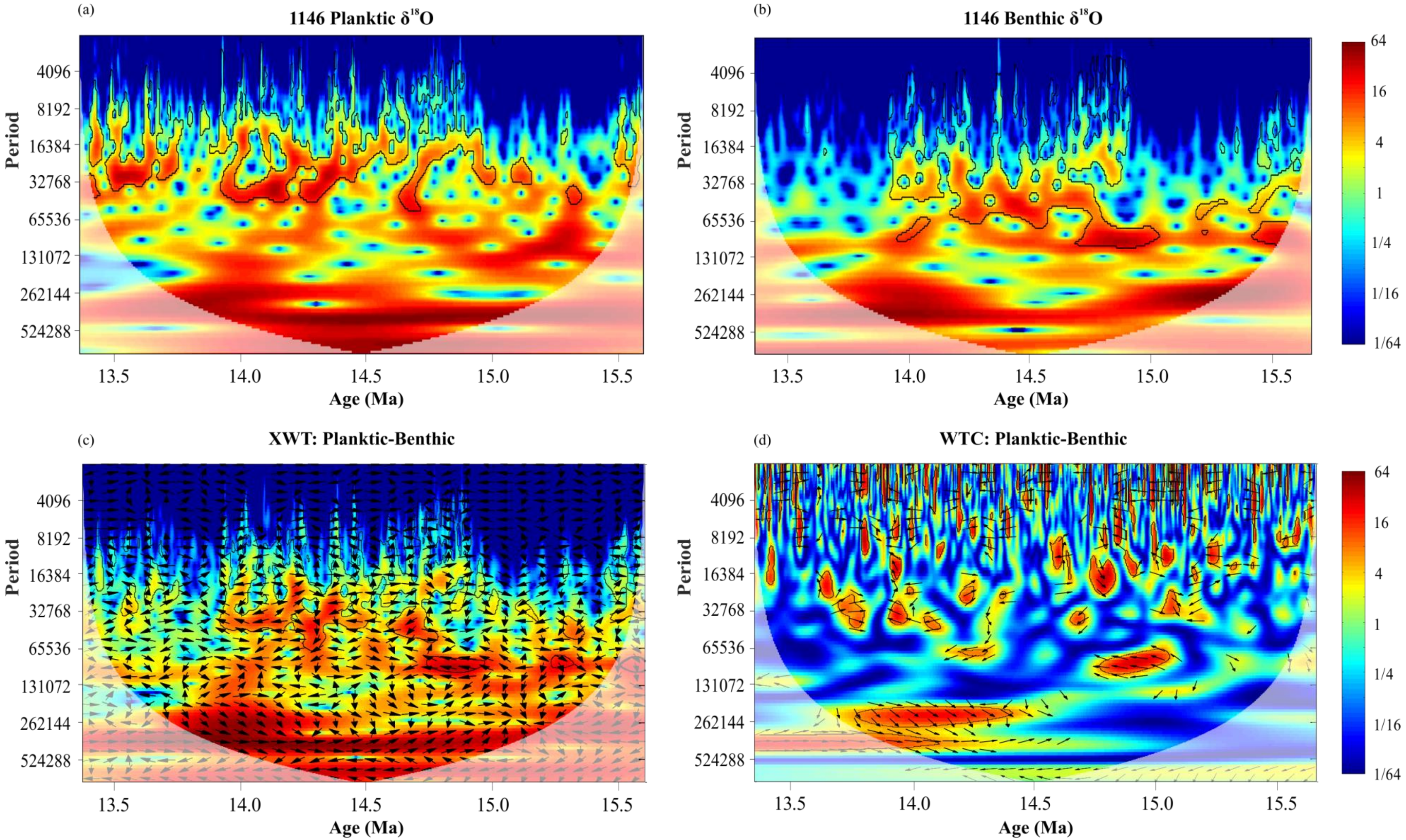

APPENDIX 6: IODP Site 1146 Wavelet Analyses of planktonic and benthic $\delta^{18}O$ data.

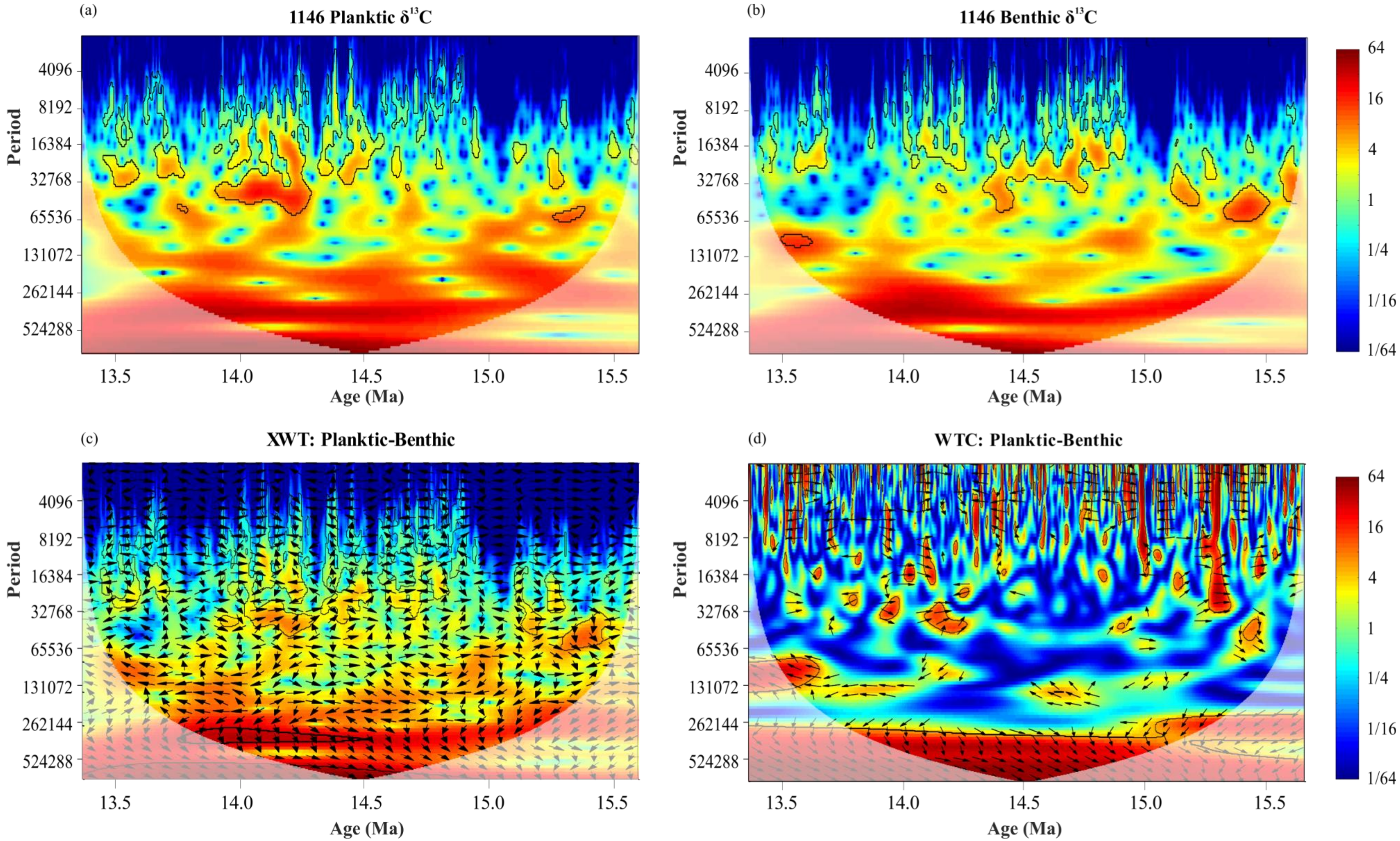

APPENDIX 7: IODP Site 1146 Wavelet Analyses of planktonic and benthic $\delta^{13}C$ data.

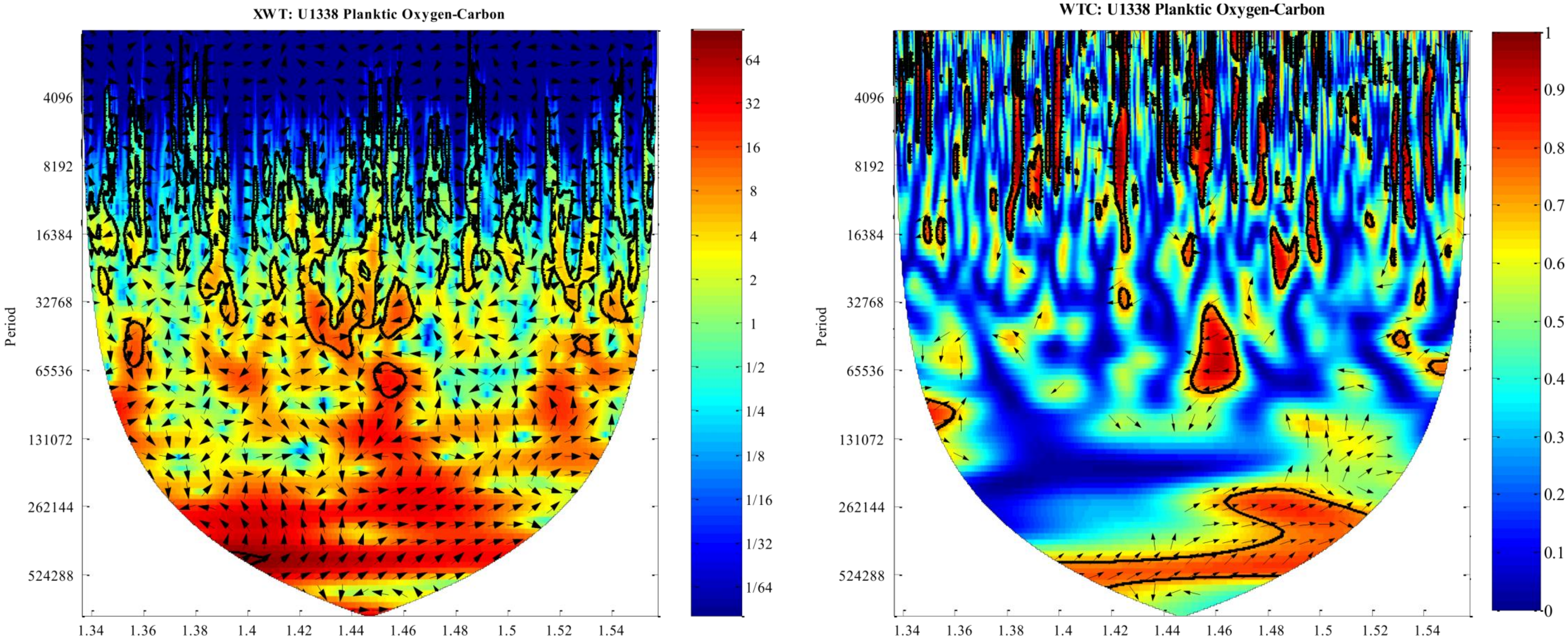

APPENDIX 8: IODP Site U1336 Cross Wavelet Transfer planktonic $\delta^{18}O$ and $\delta^{13}C$ data.

"IT WAS the best of times, it was the worst of times, it was the age of wisdom, it was the age of foolishness, it was the epoch of belief, it was the epoch of incredulity, it was the season of Light, it was the season of Darkness, it was the spring of hope, it was the winter of despair, we had everything before us, we had nothing before us, we were all going direct to Heaven, we were all going direct the other way- in short, the period was so far like the present period, that some of its noisiest authorities insisted on its being received, for good or for evil, in the superlative degree of comparison only."

-Charles Dickens